PORE SIZE DISTRIBUTION AND ITS EFFECT ON THE BEHAVIOR OF A COMPACTED CLAY

SEPT. 1971 - NUMBER 16

BY

SYED AHMED

JHRP

JOINT HIGHWAY RESEARCH PROJECT

PURDUE UNIVERSITY AND
INDIANA STATE HIGHWAY COMMISSION

Progress Report

PORE SIZE DISTRIBUTION AND ITS EFFECT ON THE BEHAVIOR OF A COMPACTED CLAY

TO: J. F. McLaughlin, Director
Joint Highway Research Project

September 28, 1971

Project: C-36-5H

FROM: H. L. Michael, Associate Director
Joint Highway Research Project

File: 6-6-8

The report attached is a Progress Report on the HPR Part II research project titled "Pore Size Distribution and Its Effect on Behavior of Compacted Clayey Soils". The report is titled "Pore Size Distribution and Its Effect on the Behavior of a Compacted Clay" by Mr. Syed Ahmed, a Graduate Assistant in Research on our staff. Professors C. W. Lovell and Sidney Diamond directed the research.

The report contains results of extensive measurements of the sizes of pores and the distribution of porosity in compacted samples of the commercially available illite clay called Grundite. Pore size distribution was found to be strongly influenced by the molding water content and was significantly influenced by the method of compacting. The results of correlating pore size distribution with mechanical properties are discussed.

The report is submitted as partial fulfillment of the objectives of this project and for acceptance. The report will also be submitted to the ISHC and the FHWA for their review, comment and approval.

Sincerely,

Harold L. Michael
Associate Director

HLM:ms

cc: F. L. Ashbaucher, W. L. Dolch, W. H. Goetz, M. L. Grecco, M. J. Gutzwiller, G. K. Hallock, M. E. Harr, R. H. Harrell, M. L. Hayes, R. D. Miles, J. V. Miller, C. F. Scholer, M. B. Scott, W. T. Spencer, J. A. Spooner, N. W. Steinkamp, H. R. J. Walsh, K. B. Woods, E. J. Yoder

Progress Report

PORE SIZE DISTRIBUTION AND ITS EFFECT ON THE BEHAVIOR OF A COMPACTED CLAY

by

Syed Ahmed
Graduate Assistant in Research

Joint Highway Research Project

Project No.: C-36-5H
File No.: 6-6-8

Prepared as Part of an Investigation

Conducted by

Joint Highway Research Project
Engineering Experiment Station
Purdue University

in cooperation with the

Indiana State Highway Commission

and the

U.S. Department of Transportation
Federal Highway Administration

Purdue University
Lafayette, Indiana
September 28, 1971

ACKNOWLEDGMENTS

The writer is deeply indebted to his major professors, Dr. Sidney Diamond and Dr. C. W. Lovell, Jr. for their guidance, inspiration and assistance during the course of this research and in the preparation of this thesis.

The author wishes to express his appreciation and thanks to his friends and all those persons who helped in this investigation and in the preparation of this thesis. Thanks are also due to Mr. D. N. Winslow and Mr. J. R. Hooper for their assistance in the experimental work.

Sincere thanks are due to Mrs. Marjorie Shoaf and Miss Mary Kerkhoff for their skillful typing of the manuscript.

This research was supported by the Indiana State Highway Commission and the Federal Highway Administration, U. S. Department of Transportation and was administered through the Joint Highway Research Project.

Finally, this author wishes to thank his parents, Mr. M. J. Ahmed and Mrs. Masooda Ahmed for their understanding and encouragement.

TABLE OF CONTENTS

TABLE OF CONTENTS (CON'T)

LIST OF TABLES

LIST OF TABLES (CON'T)

LIST OF TABLES (CON'T)

LIST OF FIGURES

LIST OF FIGURES (CON'T)

LIST OF FIGURES (CON'T)

LIST OF FIGURES (CON'T)

LIST OF FIGURES (CON'T)

LIST OF SYMBOLS AND ABBREVIATIONS

Symbol	Description
AD	Air Drying
D_{50}	Mean Pore Diameter
E_T	Tangent Modulus
E_{q_u}	Secant Modulus at Peak Strength
$E_{q_{u/2}}$	Secant Modulus at Half Peak Strength
e	Void Ratio
e_{AC}	Void Ratio As Compacted
FD	Freeze Drying
G_s	Specific Gravity of Solids
HM	Harvard Miniature (Kneading Compaction)
MAFD	Measurements by Micrometer After Freeze Drying
MBFD	Measurements by Micrometer Before Freeze Drying
MAOD	Measurements by Micrometer After Oven Drying
MBOD	Measurements by Micrometer Before Oven Drying
n	Porosity
n_{AC}	Porosity As Compacted
PAFD	Measurements in Penetrometer After Freeze Drying
PAOD	Measurements in Penetrometer After Freeze Drying
r	Pore Radius
S	Degree of Saturation
SP	Standard Proctor
OD	Oven Drying

LIST OF SYMBOLS AND ABBREVIATIONS (CON'T)

Symbol	Description
ST	Static Compaction
V	Total Volume
V_a	Volume of Air
V_s	Volume of Solids
V_w	Volume of Water
W_s	Weight of Solids
w	Water Content
w_{PD}	Water Content Obtained by Freeze Drying
w_{GAC}	Gross As Compacted Water Content
γ_d	Dry Unit Weight
γ_w	Unit Weight of Water
θ	Contact Angle of Mercury
σ	Surface Tension of Mercury
μ,μm	Micron or Micrometer
Å	Angstrom

ABSTRACT

Ahmed, Syed. M.S.C.E., Purdue University, June 1971. Pore Size Distribution and its Effect on the Behavior of a Compacted Clay. Major Professors: Sidney Diamond and C. W. Lovell, Jr.

This investigation deals with the measurement of the sizes of the pores and the distribution of the porosity in compacted samples of a clay. The primary independent variables studied were molding water content and type of laboratory compaction. In addition to compaction characteristics and pore size distributions, undrained strength data were also obtained and interpreted in the light of pore size distributions.

The clay used was the commercially available illite clay called Grundite. The methods of compaction were impact, kneading and static.

The pore size distribution measures require dry samples. Conventional oven drying is unsuitable since the pore size distribution is modified by the shrinkage caused by the evaporative drying. Removal of the water at essentially constant volume is possible by freeze drying, and suitable equipment and techniques for this process were developed.

Pore size distributions were obtained by mercury porosimetry. Pore volume is measured by the quantity of mercury intruded under each of a series of increments of pressure, while the pore diameters are calculated from the Washburn equation (48) for each of the pressures. The mercury porosimetry technique is thought to be a reliable, fast and simple procedure for obtaining the pore size distributions.

Pore size distribution curves were obtained for a diameter range of

about 600 μ to about 0.016 μ. They indicate a strong influence of the molding water content, but only a secondary influence of the method of compacting to a given moisture-unit weight condition. Samples possessing the same total porosity but compacted at two different water contents would usually have different pore size distributions.

Unconfined compression tests were performed and correlated with the pore size distribution. Samples compacted on the dry side showed brittle failure at low strains, apparently due in part to the breakdown of large pores, which are present in large numbers in dry side compacted samples. Samples compacted on the wet side of optimum continue to deform at high strains without apparent fracture.

INTRODUCTION

Clayey soils find frequent use in compacted highway subgrades and embankments. The load deformation and water transmission characteristics of these compacted clays are recognized to be dependent upon the packing and arrangement of the particulate units. Gross measures are effected by the bulk porosity (or average unit weight), and these afford many useful correlations with performance.

Since a particular unit weight can be achieved with a variety of particulate arrangements, additional correlation has been achieved with postulated soil structure or fabric.

The examination of the distribution of non-solid space is a slightly different approach, and one which may add a significant new dimension to the understanding and prediction of soil behavior. The first approach would logically be the measurement of pore size distributions achieved under different levels of moisture content, compactive effort, and compactive type, and correlation of changes in pore size distribution with changes in dependent variables like compacted unit weight, strength, stiffness and the like.

After due consideration of the large number of potentially important variables, the independent variables to be studied were narrowed down to the method of compaction, the compactive effort, and the molding water content. Only one clay was used, viz., the commercially available Grundite, but a pilot study conducted on Georgia Kaolinite and Leda Clay

showed that corresponding relationships can be obtained for other soils as well. Three methods of compaction, viz., impact (Standard Proctor), kneading, and static were used. The compactive effort level was held constant for only the Standard Proctor compaction. For other compactive types, the energy was varied to produce the predetermined moisture-unit weight relationship given by the Standard Proctor curve. Water contents were chosen to cover the total practical range of laboratory compaction.

The dependent variable of compacted unit weight defines the total porosity within which the pore size distribution occurs. Undrained, unconfined stress-strain and strength characteristics were chosen for measurement, as they are both simple to measure and relatively descriptive of the engineering performance of the as-compacted soil.

Pore size distributions were obtained by mercury porosimetry. A review of previous experience with this procedure gave a preliminary indication of its suitability for this research. This method has been successfully used by Winslow and Diamond (52)[1] and Diamond (9). Although, on the average, only eighty percent of the total pore space could be penetrated by the available equipment, this portion of the distribution was an adequate descriptor. In this study pores varying in diameter over five orders of magnitude were measured. Comparisons among pore size distributions are made by relative shapes and positions of cumulative frequency distribution curves.

An essential requirement for measuring the sizes of the pores is that the pores must be empty. Conventional oven or air drying increases surface tension forces in the pore water. The induced stresses act on

---

[1] Numbers in parentheses refer to the references cited in Bibliography.

the particulate soil units and may modify their arrangement. Constant volume drying is desired, and a freeze-dry technique was selected. In the freezing step, the cooling rate must be very rapid to minimize moisture migration under gradients induced in the vicinity of ice nucleation. The samples used in this research were small in dimension and were rapidly cooled in liquid nitrogen at about -196°C. Volume changes induced by the freeze drying varied with other test variables, but in all cases the shrinkage was small.

The molding water content was found to be an extremely important variable with respect to pore size distribution, peak strength and stress-strain ratios in the unconfined compression test. The type of compaction used to achieve a particular moisture-unit weight condition had relatively little effect on the pore size distribution.

LITERATURE REVIEW

Structure and Engineering Behavior of Compacted Clay

A pioneering attempt to explain the structure and the engineering behavior of compacted clay on a semi-quantitative basis was made by Lambe (20,21). In a series of two papers he discussed the arrangement and orientations of particles caused by the compaction process, and dealt with the factors affecting the permeability, shrinkage and swelling, and shear strength of compacted clays. His basic reasoning regarding the structure of the clay stems from the principles of colloid chemistry and crystal chemistry. Making use of the Gouy-Chapman double layer theory he inferred that if the potential energy is reduced when adjacent clay particles approach each other, they will so approach and flocculate as to form aggregates. If the energy of the system increases when the particles approach each other, they will move apart or disperse. The variables which affect the stability or change the energy of the soil-water system include electrolyte concentration, ion valence, dielectric constant, temperature, size of hydrated ion, pH, and anion adsorption.

It should however, be appreciated that a soil water system is different from the dilute suspensions of colloids for which the colloid theory was developed. Important differences occur in the particle size and shape, soil concentration, interparticle spacing, and applied forces. Nonetheless, understanding of the double layer theory was thought to be helpful in understanding the compaction process as the water content is varied.

Lambe (20) asserted that on the dry side of optimum there is not sufficient water for the diffuse double layers of the soil colloids to develop fully. The small amount of water present depresses the double layer, reducing the interparticle repulsion, and thereby causing a tendency toward flocculation of the colloids. Flocculation was said to result in a low degree of particle orientation and low unit weight. As the water is increased to near optimum for a given compactive effort and type the double layers around the soil particles were thought to expand, and the electrolyte concentration is reduced. The resulting reduced degree of flocculation was said to permit a more orderly arrangement of particles and a higher unit weight. When water is increased past the optimum, expansion of the double layer, i.e., a continued reduction in the net attractive forces between particles, takes place. Even though a more orderly arrangement of particles was thought to exist on the wet side compared with that at optimum, the unit weight on the wet side is lower because the added water has diluted the soil particle concentration.

Because of the water deficiency, the water present in compacted soil is subject to tension, which decreases as the water content is increased from the dry to the wet side of optimum. Increased compactive energy aligns the clay particles more nearly parallel, giving higher unit weight. However, at high molding water content, increased compactive effort may merely align particles without significantly altering the particle spacing.

Lambe (20) cites the work of Mitchell and Pacey who made direct microscopic measurements of particulate orientation and assigned numbers to the fabric of several clays. The limitation of microscope resolution

prevented reliable determinations of orientation in zones smaller than 10 microns wide. It was assumed that the orientations measured within regions 10 microns and larger in size existed between individual particles.

Since such direct measurements of particle orientation are difficult and time-consuming, Lambe (20) suggests that the amount of shrinkage upon drying be used as a measure of average orientation. A soil with parallel particulate orientation is reasoned to undergo more volume reduction upon drying than the same soil with units in a random array.

In a subsequent paper Lambe (21) presented physical explanations of shear strength, one dimensional compression, permeability, etc., in the light of his hypothesis. Dealing with the factors responsible for the volume change of the compacted clays he concluded that changes in size of the soil micelle, i.e., soil mineral particle plus double layer water, is an important contributor to compression upon application of pressure, and is almost the sole cause of rebound upon load reduction.

Seed and Chan (42) contributed an important paper which detailed the structure and strength characteristics of compacted clays. Their results on shrinkage supplemented the conclusions drawn earlier by Lambe (21). Their results on the swelling characteristics indicated that samples compacted dry of optimum exhibit higher swelling characteristics and swell to higher water contents than do samples of the same unit weight compacted wet of optimum. This led them to conclude that flocculated structures have a greater swelling tendency compared with the dispersed structures. These authors drew the following conclusions about the strength and deformation characteristics of compacted soils:

(1) The more flocculated samples have much steeper stress-strain curves and develop their maximum strengths at low strains in

undrained strength testing; the more dispersed samples have much flatter stress-strain curves and continue to increase in strength even at very high strains.

(2) At low strains the pore water pressures in the samples compacted wet of optimum are considerably greater than those in the samples compacted dry of optimum, even though both samples had the same water content during the test (on account of soaking). At high strains however, both types of samples exhibited approximately the same pore-water pressures.

(3) For samples compacted dry of optimum and wet of optimum and soaked to the same moisture content, the rates of mobilization of strength for the two samples, in terms of effective stresses, are for all practical purposes the same; although these samples exhibited quite different stress-strain relationships when loaded to failure in undrained tests.

(4) The influence of soil structure on strength is limited to the influence on pore-water pressures. Thus strength variations due to differences in structure can be explained equally satisfactorily in terms of corresponding differences in pore-water pressures. While the explanation in terms of soil structure is probably the more fundamental, it suffers from the severe disadvantage that structure cannot be measured directly and therefore the influence can only be evaluated qualitatively. Hence, although pore-water pressure is a less fundamental predictor it is the best available for quantitative evaluation.

Seed and Chan (42) contended that the shear strain during compaction plays an important part in producing an increased dispersion of the clay particles; and that in many cases it is the progressive increase in shear deformation (for a constant compactive effort), as the water content is increased, which is largely responsible for the progressive increase in the degree of orientation of the clay particles. This consideration of shear strains during compaction adds a new dimension to the hypothesis earlier presented by Lambe (20). Seed and Chan (42) ran several tests in order to understand the differences among the various compaction methods. Their interpretation follows:

a) For samples prepared dry of optimum, all methods of compaction produce no appreciable shear deformations, and consequently, essentially similar flocculated structures are developed, and the method of compaction has no appreciable effect on the strength characteristics.

b) For samples of the same composition prepared wet of optimum:

1. Kneading compaction causes the largest shear strains during compaction and, therefore, the highest degree of dispersion. It also produces the highest pore-water pressures and the lowest strengths at low strains, and the highest shrinkage.

2. Impact compaction causes slightly less shear strain during compaction and consequently the degree of dispersion is not quite so great as for kneading compaction. The strengths at low strains are slightly higher and the shrinkage is slightly less.

3. Static compaction causes little shear strain during compaction, resulting in a relatively flocculated structure, the lowest pore-water pressures and highest strengths at low strains, and the least shrinkage.

Pore Size Distribution Studies

Although the idea of forcing mercury into capillaries to determine their sizes was put forward some fifty years ago (48), the refinement of methods to determine the distribution of pore sizes, by intruding mercury under pressure into porous media, is relatively recent. Therefore, the literature available for review is quite limited.

Washburn (48) proposed the equation,

$$p = \frac{-2\sigma \cos\theta}{r}$$

where

p is the pressure required to intrude mercury

r is the radius of the circular capillary pore intruded at pressure p

σ is the surface tension of the mercury

θ is the contact angle of mercury with the capillary wall.

He postulated that it would be feasible to determine the distribution of effective pore radii in a porous material; and mentioned that corrections for mercury compressibility and expansion of the pressure bomb would be required.

Development of Apparatus and Technique

Drake and Ritter (12,37) were the first to put the scheme of Washburn (48) to practical use. They used a mercury dilatometer, filling pistol, and a high-pressure bomb (10,000 psi maximum pressure) for the complete operation. The dilatometer was filled with sample through its open bottom, sealed off, and placed in the filling pistol. The dilatometer was first evacuated, and then filled with mercury at atmospheric pressure. Finally, the dilatometer was placed in a high-pressure bomb where pressure was applied, first by nitrogen and then by forcing oil into the bomb, up to the maximum working value. The volume changes were measured electrically. They successfully used this apparatus for obtaining the pore size distribution curves of diatomaceous earth, activated clay, pelleted gel, activated carbon and various other materials.

Winslow and Shapiro (51) developed a compact device for mercury porosimetry. Their instrument consisted of a penetrometer, a filling device, and a porosimeter. Pressure was applied hydraulically, and controlled, stepwise pressuring was obtained by means of a hand-operated pressure generator. The instrument could be operated at low pressure and the determination of pore sizes as large as 100 microns was possible. The lower pore limit was 0.3 micron. The penetration was determined directly by volumetric readings. Winslow and Shapiro (51) successfully used their instrument to obtain the pore spectra of various materials.

They also attempted to obtain a pore spectrum for a reference standard sample of known pore sizes, thus permitting an estimate of the errors resulting from their several assumptions. The reference standard consisted of a block of nickel, perforated by small drills of known diameter. Unfortunately, their results were not precise enough to permit definite conclusions.

Presentation of Results and Treatment of Data

The pioneering work of Drake and Ritter (12,37) introduced two important ways of presenting the pore size distributions: plotting the cumulative voids per gram vs. pore diameter, i.e., the cumulative distribution function, and alternatively, drawing the differential distribution function D(r) vs. pore radius. The differential distribution function is derived from the following equation.

$$D(r) = \frac{p}{r} \frac{d(V_o - V)}{dp}$$

where

p is pressure

r is pore radius

V_o is total pore volume

V is volume of pores smaller than r. The factor $\frac{d(V_o - V)}{dp}$ in this function was obtained by graphical differentiation. These authors attempted to fit standard distributions to their curves; the modified Maxwellian distribution and displaced Gaussian distribution were tried, as well. They also proposed numerical integration procedures for obtaining the average pore radius ($\bar{r}$) according to the following equation.

$$\bar{r} = \int_0^\infty r\, D(r)\, dr/V_o$$

Hiltrop and Lemish (15) found it advantageous to plot pore radius vs. the normalized differential distribution function d(r), given by the equation,

$$d(r) = \frac{p}{rV_o} \frac{d(V_o - V)}{dp}$$

Use of d(r) produces an area under the curve of unity and the plots can be easily compared by their shapes.

Orr (35) also found the plotting of differential distribution functions to be useful. He also discussed the possibility of obtaining the specific surface area from pressure penetration volume curves, provided sufficiently high pressures are applied to force mercury into the smallest pores, and provided there are no pores with entrance regions smaller than their dimensions elsewhere. The values of specific surface areas obtained by Orr, from the pore size distributions, were in close agreement with those obtained by low temperature gas adsorption. He gave the following equation for obtaining the average pore radius (r_a),

$$r_a = 2 \frac{V_t}{S}$$

where V_t is total pore volume, expressed in cubic centimeter per gram, and S is the specific surface area of the material in square meters per gram. He also introduced an analysis for calculating the particle size distribution for irregular particles of uniform size.

Rootare (38) made a survey of pore size distribution studies. He pointed out that the comparison of pore areas, as obtained by Orr (35),

with the surface areas obtained by nitrogen adsorption (B.E.T. method) has been fair, when the pore size distribution is symmetrical. However, it becomes poor when curves are skewed and more complex, e.g., in the case of bimodal distributions. Rootare (38) described the work of Rootare and Prenzlow, who obtained surface areas from mercury intrusion, with no assumption of any particular pore geometry. The problem was approached from the point of view that work is required to force mercury into the pores, measured as pV work. This could be directly related to the total area of the sample immersed in mercury. The relationship obtained was:

$$A = \frac{\int_{V_o}^{V_m} p\,dV}{\sigma \cos\theta}$$

where

A is the surface area

p is the pressure applied

V is the volume intruded

σ is the surface tension of mercury

θ is the contact angle of mercury

Limitations and Errors

Drake and Ritter (12,37) critically assessed the limitations and the sources of error in pore size distribution determinations. They pointed out that the assumption of circular pore cross sections enters through the ratio (2/r) of perimeter to area. For a non-circular cross section this ratio can still be viewed as the reciprocal of some average radius, although the constant may not necessarily be 2. The result will be a change by a constant factor in the value of the radius corresponding to a

given pressure. The shape of the distribution curve, and the order of magnitude of the calculated radii should not be appreciably different, regardless of the shape chosen. These authors also considered that the value of the contact angle was not certain, but they demonstrated that the error due to an incorrect contact angle value is less serious than the assumption of cylindrical pores, and that it operates in the same manner in its ultimate effect on the distribution curve. They emphasized the distinction between the 'average' size of a pore and the size of its entrance. The pore radius calculated from mercury porosimetry is the radius of the largest available opening to the pore. If pores exist with radii which are considerably larger than the largest entrances to them, these pores will be measured incorrectly as being of the size of the largest opening. This was shown by de-intrusion experiments. Drake and Ritter observed that upon reducing the pressure from 10,000 psi, the desorption curve did not follow the intrusion curve, and in addition the appearance of the sample after the test was changed. They concluded that:

> "If the pores of these materials were either uniform in diameter or V-shaped, one would expect the mercury to flow out when the applied pressure is released. If however, there are pores with small mouths, the so-called ink-bottle pores, they would not be expected to empty when the pressure is released."

In a subsequent paper by Drake (11) the phenomenon of hysteresis is studied in further detail. All the catalyst samples exhibited retention of mercury upon depressuring. Drake (11) modified the earlier method of Drake and Ritter (12,37) to permit coverage of the high pressure range (up to 60,000 psi), beyond the 'macropore-size' range. He also observed that at most pressures mercury intrusion equilibrium is reached within a very few minutes. In the steep section of the pressuring plot

however, the rate of penetration of mercury is relatively slow. He also defined the ultimate limit of pore diameter amenable to the method as 35 Å, corresponding to about 60,000 psi. As a matter of fact, 60,000 psi pressure is more than normally required for intruding pores in many systems.

Orr (35) contended that the fact that all the mercury is not spontaneously de-intruded when the pressure is returned to zero proves the existence of at least some 'ink-bottle' pores. He presented pressuring and depressuring curves with hysteresis. Orr also made some estimates of the sizes of enlarged interior cavities from the pressuring and depressuring data.

Watson, May and Butterworth (49) studied pore size distributions in bricks. Six different methods for obtaining distributions were listed by these authors. However, they submitted that except for mercury porosimetry, none of the methods was capable of measuring the required range of pore sizes. Their explanation of the phenomenon of mercury retention is different from the ink-bottle concept. They suggest that since in a system of inter-connecting pores the majority of the mercury columns entering a specimen coalesce, the menisci which oppose the entry of the mercury disappear, and the force that might otherwise cause its ejection is removed, thus causing the retention of mercury. This hypothesis is not yet supported by experimental evidence.

Rootare (38) presents an extensive survey, with a bibliography of some fifty seven references, on mercury porosimetry. He notes that pore size distribution curves are frequently biased towards the small pore sizes because of the hysteresis effect caused by the 'ink-bottle'

type pores. His conclusions on sources of errors are summarized below.

(1) Corrections for compressibility of mercury with pressure should be made.

(2) Compressibility of solids in the intruded medium may introduce error.

(3) Entrapped air is a source of error in intruded volume measurement.

(4) A kinetic hysteresis effect, viz., the finite time required for the equilibrium of mercury intrusion, may shift the distribution curve.

(5) A volume hysteresis effect, i.e., retention of mercury after depressuring,seems to indicate that opening of the pores rather than pores themselves are intruded.

(6) The cylindrical pore shape model may be too approximate.

(7) The surface tension of mercury is affected to some extent by temperature but to a greater extent by purity.

(8) The largest source of error comes from the assumption of a constant value for the contact angle θ for all samples.

(9) The breakdown of porous materials, especially those having constricted opening may be a source of error at high pressure.

Sarakhov (41) suspected that the mercury would become contaminated through contact with the intruded media surfaces and the gases and vapors adsorbed on them. Consequently its surface tension and contact angle may change during a run. On the basis of his experience, the author states that the angle of contact after an experiment may be appreciably lower than the initial angle, and that in certain cases almost complete wetting may be attained. He estimates that the overall error in determining the pore dimensions by mercury porosimetry, due to incorrect estimation of the values of surface tension and contact angle of mercury, or their variation during the experiment, may be 30 to 40% or more. He noted however, that for most practical problems, one can take

$\sigma = 480$ dyne cm^{-1} and $\theta = 140°$.

With respect to breakdown of larger pores, his opinion is similar to that of Rootare (38). Sarakhov stated that at the maximum pressure all the pores with narrow inlets are either already filled with mercury or broken down, or their strength is such that they withstand the external pressure, but are not filled with mercury because of the smallness of their orifices.

Recently Hill (16) contributed a paper aimed at improving the method of interpreting mercury penetration data. He employed an apparatus which could provide a maximum pressure of 20,000 psi. In addition to the normal readings of volume entering pores at each step of increasing pressure, he also took readings of the volume remaining in the pores in each of a series of steps of reducing pressure. Hill made his studies on fired kaolinite, illite, and montmorillonite (fired at different temperatures), brick samples, and others prepared artifically. Tests on the artifically porous samples showed that ejection occurs from cylindrical pores only when the pressure is dropped from 1/2 to 1/3 of the penetration pressure. He learned that as the pressure is reduced, the instability of the mercury column in the capillary need not result in ejection of the mercury when the critical pressure is reached, unless there is some discontinuity in the surface of the capillary or a sharp change in its radius of curvature from which a break in the column of mercury can be initiated. He has hypothesized that mercury will be ejected from a pore if the energy conditions are favorable, i.e., when the change in surface energy is greater than the work done against external pressure. On this basis he presented an analysis which showed that the penetration pressure, for mercury in a

cylindrical pore, is just twice the critical pressure below which mercury should be ejected from the pore. Therefore, in a completely filled cylindrical pore the mercury will be ejected when the pressure has fallen to half the value of the penetration pressure (practically this ratio is 1/2 to 1/3). Once the critical ejection pressure is reached, mercury is likely to be ejected from a filled pore of varying diameter along which the diameter does not vary by a factor of more than two to one, because the external pressure will be lower than the penetration pressure for the largest part of the pore. Hence, if mercury is retained in a filled cylindrical pore, even when the pressure has fallen to half of the penetration pressure, it should be in unstable equilibrium. The case of incompletely filled pores is different; the mercury will commence to be emptied from the pore as soon as pressure is reduced below the penetration pressure, but only for that part of the pore at which the free surface is located. Isolated pockets of mercury will be retained in the pores containing constrictions, enlargements and other irregularities because the ejection pressure will be higher than the penetration pressure. This author has introduced the term 'Retention Factor', which is the ratio of volume of pores remaining filled at atmospheric pressure to the volume filled at the maximum pressure. Obviously, when the pore skeleton consists mainly of enlargements greater in size than the largest pore leading into them, the Retention Factor is likely to be high. Thus the Retention Factor is an indication of the inaccuracy in the conventional distribution. Hill obtained the corrected curve by three different procedures, involving respectively, ejection data, re-entry data, and conventional curves multiplied by (1 - Retention Factor). These corrected distributions were used

to calculate specific surface areas, and were compared with the areas obtained from gas-sorption data. He noticed that on the whole, the best agreement with the gas sorption estimates is obtained when the curve is corrected by the third method. Hill therefore stated that the conventional pore size distribution curves should be corrected by multiplying it by (1 - Retention Factor), which, he believes, allows a more accurate comparison of the nature of the pore space in different bodies.

Applications of Pore Size Distribution

Pore size distribution has found application in several fields. Some of the applications have been mentioned briefly in the earlier sections. Several more recent studies are summarized below.

Hiltrop and Lemish (15) studied the relationship of pore size distribution and other rock properties to serviceability of some carbonate aggregates. They considered that pore space characteristics are important because of their direct influence on other physical and chemical properties. Pore characteristics determine the flow of moisture into and out of an aggregate, the water retentivity of the aggregate, and the development of pressure during freezing and thawing cycles. Moreover, the interior surface of the pores provides an area on which surface-chemical reactions can proceed between mobile substances and the constituents of the rock.

They used a mercury capillary pressure apparatus which provided a pressure range from 20 to 2,000 psi. They concluded that pore size distribution alone is not closely related to freezing, thawing or service record; but when combined with certain other variables it appears to be

a determining factor.

The significance of pore size distribution in predicting the frost susceptibility of soils was recognized by Csathy and Townsend (7). They contended that every essential factor in the mechanism of frost action is intimately related to pore size. They gave the following specific examples:

> (1) It governs freezing point depression in as much as it constitutes the size restriction for the growing ice crystals.
>
> (2) It reflects pressure effects, and it is a measure of the relative proximity of particle surfaces.
>
> (3) The possibility of localized ice formation is determined by the relative distribution of pore sizes.
>
> (4) The retardation of the ice front is essentially governed by the pore size restrictions.
>
> (5) The ratio of free to bound water during freezing, and the drainage and stability condition upon thawing depend on the sizes and distribution of pores.
>
> (6) All the potential components induced by freezing (capillary, suction, thermal, vapor-pressure, electrical and osmotic) appear closely related to pore sizes.
>
> (7) It is the governing factor in the supercooling theory, considering either the nucleation temperature aspect or the relative freezing point depression.
>
> (8) In the electro-osmotic theory, pore size indirectly controls the facility with which the double layers are recharged, and thus the electro-osmotic activity of the system.
>
> (9) The basic soil properties apparently influencing the nature of frost action such as: suction, capillarity and permeability are probably direct functions of the distribution of pore sizes, even though these relationships cannot be presently expressed mathematically.

These authors also referred to Schofield's idea of interpreting suction and possibly capillary moisture profile curves in terms of pore size distribution.

As a result of experimental work, Csathy and Townsend (7) concluded that pore size distribution could constitute a suitable criterion for rating the frost susceptibility of soils; a criterion superior to current grain-size distribution guides.

Kun and Kunin (19) used mercury porosimetry for studying the pore structure of macroreticular ion exchange resins. They characterized the distributions by the pore diameter at 50% of the total porosity, and the pore diameter at the point of inflection of distribution curves.

Winslow and Diamond (52) used mercury porosimetry to measure pores in Portland cement paste with diameters between 1000 μ and 0.0085 μ. They employed a new macro-pore porosimeter and assessed such factors as the difference between theoretical and effective mercury compressibility and heating due to compression.

Pore size distribution data have also been used to predict permeability (6,18). Klock and Boersma (18) propose that the contribution of each pore size class be estimated and combined to obtain the total flow rate. These authors measured permeabilities with a constant head permeameter. The intrinsic permeability was calculated by the empirical equation advanced by Milligan and Quark.

Pore size distributions in soil were studied by Diamond (9), who collected information about a number of reference clay minerals, naturally occurring subsoils, and sedimented and compacted commercial clays. Most of the work was on oven dried samples, but he also presented curves for samples dried by both freeze drying and critical region drying. The question of accurate contact angle has been debated in the literature. Diamond (9) set out to actually measure the contact angle by the heights

of sessile drops method. He found an angle of 147° for kaolinite and illite and 139° for montmorillonite clay. He was particularly interested in differences in pore size distribution demonstrated by the different clays.

The Fithian illite exhibited an extremely 'tight' microstructure, with much pore volume at diameters less than 300 Å. This fineness is believed to be a consequence of both small particle size and the geological consolidation of the clay. For the Clay Spur montmorillonite and the Garfield nontronite X-ray basal spacing dropped from 12.6 Å to 9.7 Å after oven drying. This is indicative of a 25% loss in volume within 'particles', yet this loss was not translated into any significant loss of pore space within the microstructure of the aggregate of particles constituting the sample. Most of the pore space in selected Indiana soils was found to be in pores of equivalent diameter greater than 1 μ, and a significant porosity was found in pores greater than 100 μ for two of the soils. In contrast, practically all the porosity in the reference clays was in pores smaller than 3000 Å (0.3 μ). Another feature of the natural clays was that essentially all the pore space was intrudable at pressures below 15,000 psi.

Diamond also obtained pore size distributions for dispersed and salt-flocculated sedimented specimens of kaolinite and illite. Each curve has distinctive features, with the condition of sedimentation being a more or less common denominator. He has also presented pore size distributions for kaolinite and illite compacted by an impact procedure. He found that all the samples compacted at optimum or on the wet side of the optimum moisture content displayed identical pore-size distribution

characteristics on oven drying. Diamond postulates that

> ".... there are two basic microstructures generated in compacting the kaolinite; if compaction is carried out at low moisture contents or with insufficient compactive effort for the moisture content present, a microstructure is produced which does not shrink appreciably on oven drying and in which there is retained a significant content of relatively-large diameter pores, ranging up to several microns. If kaolinite is compacted either at optimum moisture or above optimum moisture, very significant shrinkage takes place on oven drying, and the resultant dried clay has pores only of equivalent diameters less than 2000 Å. These results are consistent with the notion that the former samples have retained much of the structure of the individual, more-or-less spherical aggregates of particles formed in the mixing process, while the more effective compaction in the latter case has brought the clay particles into a more nearly homogeneous, quasi-parallel arrangement".

Diamond also examined the pore structure of a quick clay from Canada by comparing the pore size distributions after ovendrying and after critical region drying and concluded that the procedures of freeze drying or critical region drying are more satisfactory.

Recently, Sridharan, Altschaeffl and Diamond (44) made pore size distribution studies of statically compacted Georgia kaolin, Grundite and a naturally occurring soil, the 'Boston Blue Clay'. Some of their deductions are noted below:

> (1) Statically compacted kaolinite samples were observed to undergo no significant shrinkage as a result of air drying and oven drying.
>
> (2) Inspection of pore size distribution curves of a series of kaolinite samples, mixed at the same water content, but statically compacted to different void ratios, suggests that the curves are quite similar to each other. They appear to have four more-or-less distinct portions of reasonably constant slope, viz., a 'gross pore region', a 'coarse pore region', a 'fine pore region' and a 'very fine pore region'.
>
> (3) The major differential effect of the compaction process on kaolinite is to decrease the content of gross and coarse pores. Increasing compaction (decreasing void ratio) results in a linear decrease of the average pore diameter. On the other hand, the pore system less than 0.14 μ, i.e., fine and very fine region, is almost independent of the degree of compaction.

(4) Initial compaction of kaolinite reduces the maximum size and the amount of gross pores, but as long as this process is incomplete, the rest of the pores are unaffected. When the gross pores have been essentially eliminated, further compaction is at the expense of the range of pore sizes in the coarse pore region. Even at the maximum level of compaction there is no reduction in the volume of the fine and very fine pores. In fact, higher degree of compaction tends to increase this volume slightly.

(5) Pore size distribution curves of the illite and Boston Blue Clays were grossly different from the pore size distribution curves of kaolinite. Undoubtedly, the particle size distribution, particle shape, particle stiffness, and degree of local aggregation at the start of compaction all influence the pore size distribution attained with a given soil.

In summary, in this section, development of apparatus and technique, presentation of results and treatment of data, limitations and errors, and applications of pore size distribution have been discussed. Mercury porosimeters, available commercially, enable the measurement of pore sizes over several orders of magnitude. The results, when presented in a suitable form, give valuable information and provide an insight into the nature of the porous structure of the specimen under study.

By far the most critical assumption is that of cylindrical pores. Many researchers have discussed the presence of the so called 'ink-bottle' or 'ink-well' pores; most of this discussion is qualitative. Actually, the pore structure should be expected to be quite complex and quite variable from one material to another; with small pores built into the large pores, the pores having several entries, and so on. The existence of ink-bottle pores is one explanation of the kinetic hysteresis and retention of mercury, but it is not the only explanation. The selection of the correct values for contact angle and surface tension of mercury should be given careful consideration. Proper attention is also required in making the various corrections, viz., compressibility, entrapped air, etc.

Hill's (16) correction may improve the estimate of the pore size distribution, but its validity is as yet unproven.

Pore size distributions have been used in studying the characteristics of mineral aggregates, in examining the pore structure of cement pastes, and in predicting the flow characteristics of porous materials. Diamond, et. al. obtained pore size distributions of several natural occurring and compacted soils. There is a clear indication that this method can be successfully employed in studying the structure of compacted clays.

Freeze Drying

The freeze drying technique was used in this study for extracting the water of the compacted samples without disturbing their structure. It is a well known technique in the disciplines of biological, medical and food sciences. It is employed where morphology, solubility and chemical integrity of the material is to be perserved. The majority of the literature reviewed in this section has come from the above disciplines, and relates to substances quite different from soils. Therefore the conclusions drawn in these studies are not necessarily directly applicable to the present study. However, this review is intended to help in gaining an understanding of the various factors involved and in making the concepts clear.

Freeze drying is different from normal oven or air drying in that it substitutes liquid-solid and solid-gas interfaces for the liquid gas front of normal drying. As the name implies, freeze drying is a two part process, and will be so discussed.

Freezing

The freezing phase of the process is probably the more complex, and least understood in detail. There is a considerable discussion and a wide spectrum of opinion in the literature on the forms of ice[1] which are developed at the various rates of temperature change and for the various temperature-pressure combinations. Since it is of importance in the freeze drying of soils, a fairly extensive summary of the conflicting results secured by various workers is included here.

An X-ray analysis of rapidly frozen gelatin gels led Merryman (33) to conclude that in rapid freezing an incomplete crystalline structure is developed, which then undergoes subsequent recrystallization on exposure to higher temperature. Rosenquist (39) has emphasized the importance of distinction between the characteristics of pure water and water of a two phase system. On the basis of his freezing experiments on a normal illite clay, he contends that the clay water at low temperature (approximately -185°C) is kept in a metastable state of higher energy compared with normal ice at the same temperature.

Dowell and Reinfret (10) report that they were able to produce vitreous ice by condensation of water vapor on a surface maintained below -160°C. This ice is reported to undergo a partial and irreversible change to cubic ice at temperatures above -160°C, with the rate of transformation strongly dependent on temperature. They have further claimed that the mixed cubic-vitreous phase undergoes an irreversible transformation to hexagonal ice I at temperatures above -130°C, again with the rate being dependent on temperature. They describe unsuccessful attempts

---

1. For a review of the forms of ice, the reader is referred to references 2, 27, 28 and 30.

to produce vitreous ice from liquid water by spraying it on a substrate held at -190°C, and by plunging films of water on metal foils into liquid nitrogen. This was not too unexpected in the light of Luyet's (30) prediction that a cooling rate of 20,000°C per sec. would be required to vitrify liquid water.

The X-ray diffraction patterns obtained by the authors showed that the structure of vitreous ice was different from that of water at ordinary temperatures, being composed partly of small particles of crystalline ice, and partly of ice with a random network type of structure. They concluded:

> "In vitreous ice domains exist in which there is a tendency toward the same layer structure present in the crystalline phases, although with random distribution of molecules within the layers. Those domains having very nearly the same layer spacing as the crystalline phases are apparently quite stable, but those having greater disorder are unstable. At temperatures above -160°C, crystallization to the cubic phase begins spontaneously at a few sites in the unstable zones, and the crystallization at each site quickly grows to about 400 Å, where further growth is hindered by more stable zones. Further crystallization takes place at new sites in the unstable domains, the process continuing until all such areas have crystallized. This state is now stable at all temperatures below -130°C. Above -130°C both the cubic and the remaining vitreous ice begin to show conversion to the stable hexagonal phase. The individual sizes growing to moderate sizes, probably near 10 μ. The ultimate size of the crystallites will depend on the highest temperature to which the sample is exposed for a given time."

There is a considerable disagreement on the exact nature of cubic ice. Luyet, Tanner and Rapatz (29), in a later X-ray diffraction study concluded that cubic ice did not exist.

Luyet (28) presented a concise review of ice formation and sublimation drying in physical systems. He drew the following conclusions:

> (1) Ice patterns in aqueous solutions can be classified into four types: the hexagonal forms, the irregular dendrites, the coarse spherulites and the evanescent spherulites.

(2) The type which will develop in a particular condition depends primarily on the cooling rates. Rapidly cooled solutions may have very complex structures in which various types of ice formations are intimately mixed with each other and with the amorphous phase. The rate of cooling determines the degree to which the crystallization is hindered or inhibited, a complete inhibition resulting in the preservation of the amorphous state.

(3) One of the four types, the evanescent spherulite, is apparently in a state of incomplete crystallization. Upon rewarming the specimen, crystallization goes to completion in a form of 'recrystallization' designated as 'irruptive'.

(4) Other types of ice formations, usually produced in rapid freezing also contain material which undergoes irruptive recrystallization. Thus, the study of the effects of rapid freezing, in general, is essentially a study of incompletely crystallized and of amorphous material, which completes its crystallization upon being rewarmed.

(5) Since the material subjected to freeze drying contains an amorphous portion (bound water which does not crystallize at any temperature), and a portion in which the crystallization has been partly impeded by rapid cooling, there is always a fraction, often important, which has never been frozen and is not freeze dried but is merely dried at low temperatures in so-called 'pseudo freeze drying'.

Experimenting with bentonite gels, Ahlrichs and White (1) found that both quick freezing and sublimation alter the original gel structure. They observed that during quick freezing with liquid nitrogen all but two molecular layers of water moved from between the crystals of saturated gels, and that water molecules migrated to ice crystals formed near the clay crystals.

Anderson and Hoekstra (2) made an X-ray diffraction study of frozen pastes of various clay minerals. They observed that spontaneous nucleation occurred at about -5°C. They are convinced that the adsorbed water collected at nucleation sites, where in spite of adsorption forces, it crystallized in normal hexagonal configurations. Their determinations

at higher water contents and lower temperatures gave results which were attributable to hexagonal ice. They postulated that the orientation of the clay particles determined the orientation of the ice crystals in the frozen clays. Clay particles act as effective ice-nucleating agents, and the c-axis of the microcrystals of ice tend to lie in planes perpendicular to the c-axis of the platey clay crystals. These authors note that a completely amorphous form of ice may appear when water vapor at a pressure of about 10^{-5} torr condenses on a substrate at or below -100°C. A vitreous form, stable at higher temperatures, is also acknowledged. Therefore, in their judgement, a form of ice in frozen clay different from the normal tridymite structure should not be surprising.

They also propose the existence of an unfrozen, submicroscopic structural layer of water separating the clay surface from the ice. Although the nature and distribution of the two phases is not well understood, it is thought that the unfrozen water and ice are in equilibrium. The migration of particles and other foreign bodies ahead of an advancing freezing front is the result of this unfrozen layer.

Lovell (27) concluded that very substantial proportions of the total soil moisture of fine-grained soils remains unfrozen at temperatures as cold as -25°C. The more clayey the soil, the greater the quantity of unfrozen moisture.

In a recent paper Delsemme and Wenger (8) describe a new allotropic form of ice with a density of 2.32 ± 0.15 gram per cc which may form at very low temperature and pressures. They vaporized distilled, outgassed water in a vacuum chamber maintained at 10^{-4} mm of mercury. This was then condensed on a copper core, cooled with refrigerating liquids,

pressure being maintained at 6 to 8×10^{-3} mm of mercury. They found that at temperatures near or below -173°C a new form of ice with very high density was produced. They varied the temperature and condensing rate and found out that the condensing rate is not critical but that the temperature was critical; no glassy high-density ice being produced at temperatures higher than -175°C.

Drying

The drying of frozen material takes place when the partial pressure of water vapor at the frozen surface exceeds that of the surroundings. The evaporating molecules collide with the surrounding air, causing retardation of the evaporation and an accumulation of water molecules in the region of the boundary between the solid and the air. Apparently, the higher the concentration of water vapor, the greater the probability of a return. This may cause complete cessation of drying in a closed system, if the vapors become saturated throughout the enclosure and the temperature difference between the evaporating source and the ambient air disappears. The speed of diffusion of the vapor through the enveloping air, to the moisture-removing agent can be enhanced by two methods (40):

a) Scavenging action of a stream of dry air or gas, at atmospheric or reduced pressure, flowing over the surface of evaporation.

b) Maintenance of a low pressure of air above the surface with or without vapor-removing agent.

Merryman (32) has given an splendid explanation of the mechanism of vacuum drying. He divides the sublimation process into three parts:

1) the introduction of heat to supply the energy necessary for sublimation;

2) the transfer of water vapor from the sublimating ice crystal through the already dried shell of the specimens;

3) the removal of water vapor that reaches the surface of the specimen.

These three steps are briefly described below.

According to the kinetic theory of gases, the temperature of a substance is a function of the average speed of its molecules. The transition from the solid to the vapor is a transition from a restricted to a relatively unrestricted state. Molecules having the highest speed normal to a surface of evaporation are those which are most likely to escape. When evaporation takes place, the average speed of the remaining molecules is lowered, and the temperature of the aggregate is reduced. In other words, energy in the form of latent heat of sublimation is acquired by each molecule which transfers its state. This energy is primarily derived from the environment, the process resulting in a fall of temperature. Thus, in the ideal condition when all the sublimating molecules have been promptly removed from the system, and unless loss of heat energy is compensated from without, the temperature will fall to such a degree that sublimation cannot take place. In practice however, as sublimation proceeds, an increasing concentration of water vapor develops in the space around the ice. Hence there is a strong probability of water vapor molecules recondensing after sublimation, should they happen to strike a site with the proper energy and orientation. In the final analysis therefore, specimen temperature is determined by the rate of heat input and the rate of vapor transfer away from the drying boundary.

Sublimation takes place from the surface towards the center of the specimen. A growing shell of dried material develops as the drying

boundary progresses into the specimen. Water vapor transfer should take place, by diffusion away from the drying boundary through this barrier of increasing thickness. As the concentration of water vapor molecules develops at the drying boundary, diffusion toward an area of lesser concentration will take place. The resistance to diffusion is generally very high. The only force that drives water vapor from the drying boundary to the specimen surface is a concentration gradient. An external vacuum does not 'suck' water out, it merely reduces the concentration of gas molecules present in the pores and thus reduces the resistance to water vapor flow.

The removal of water vapor that reaches the surface of the specimen is the last leg of the sublimation process. Since a concentration gradient is the motivating force for vapor transfer, a steep concentration gradient between the specimen surface and the condenser is necessary for the removal of water vapor from the specimen. This can be effected by raising the concentration at the boundary, but this may be limited by the highest temperature tolerable, since vapor pressure is related to temperature. An alternate way would be to reduce the vapor pressure by lowering the temperature on the condensing surface. Most designs make use of this second approach. The function of the vacuum system is to provide a long mean free path, so that the transfer of water vapor away from the specimen surface is as efficient as practical, i.e., with the minimum number of collisions en route.

In the light of the above discussion, a drying system should be designed such that:

(1) Means are provided for the introduction of heat, keeping the drying boundary at the maximum permissible temperature, i.e.,

maximum vapor pressure for a good concentration gradient. Ideally, the specimen would be suspended and would receive heat by radiation uniformly on all sides.

(2) Easy vapor transfer through the dried shell should be able to take place. Since this depends basically on the nature of porous material, measures such as reducing the thickness of the specimen and punching of holes is about all that can be done.

(3) An evacuated space should be available, in which collisions are minimal, providing long mean free paths.

(4) A condensing surface, maintained at very low temperature and vapor pressure, should be furnished. Ideally the condensing surface should surround the specimen.

Rosenqvist (39) and Rice, Kaesberg and Stahmann (36) have noted that a drying agent, such as phosphorous pentaoxide is also helpful. There is also some discussion about the possible advantage of a diffusion pump over a mechanical vacuum pump. Results of Rice, Kaesberg and Stahmann (36) have shown that no great advantage is obtained with a diffusion pump until sublimation temperatures of about -40°C are approached. But at low temperatures (less than -50°C), the vapor pressure of ice is less than the usual vacuum produced by mechanical pumps, so that a diffusion pump is essential. A similar observation was made by Rowe (40).

Freeze Drying and the Behavior of Clay

Norrish and Rausell-Colom (34) investigated the effects of freezing on the swelling of clay minerals in the form of gels in which the solids content was small compared to the water content. They used gel specimens of Wyoming bentonite, nontronite, and vermiculite, and obtained diffraction traces in a low range of 2θ from 0.5° to 2° and in a high range of 3.5° to 10°. Then they froze the samples with a stream of cold carbon dioxide and obtained the diffraction patterns. Finally, samples were

allowed to thaw and diffraction traces were again obtained. By examining these traces they concluded that the expanded interlayer structure of the swollen specimen collapses upon freezing, and on thawing the gel returns to its original state. Comparison of orientation curves showed that there was a decrease in orientation on freezing, and that this effect is reversible; the original orientation being restored on thawing. They have speculated on the mechanism of collapse, stating that apparently no major change occurs during cooling until ice is observed to form. If it is assumed that ice crystals nucleate at random through the gel, then, as these crystals grow, water will migrate to their surfaces and at the same time pressure will be exerted on the silicate layer, causing local collapse. This may disrupt the preferred orientation of clay particles as well. They think that after thawing, diffuse ionic double layers, which were destroyed on freezing, will be re-established and the resulting osmotic repulsion will restore the clay to its original condition. These authors make a subtle remark that a small collapse may occur on drying. It is interesting to note here that the assumption of ice nucleation by these authors is not different from the deductions of Ahlrichs and White (1), who postulated that the ice nuclei are formed in the more normal water in the larger pores between stacks of clay minerals referred to as 'domains' rather than between the clay crystals within a domain.

It is profitable to examine volume changes incurred by 'normal' freezing. Hamilton (13) compacted five Alberta clay soils by an impact compaction procedure, insulated them on the sides and bottom and effected a unidirectional freezing from the ambient to -37°F. He noted that

during the freezing process shrinkage of the drier samples occurred, and blisters of air became trapped between the sides of the samples and the rubber membranes, and between the top of the samples and the endcaps. He did not observe bubbles in those samples which expanded upon freezing. In all cases, freezing resulted in a decrease of sample diameter, while the sample length increased or decreased depending upon the compaction moisture content and unit weight, viz., talking in general of samples compacted on the dry side of optimum moisture shrank while those compacted on the wet side expanded. Further, a large portion of the total dimension change occurred immediately upon freezing, over the temperature range of $+30^{\circ}F$ to $+20^{\circ}F$.

He also performed cyclic freezing and thawing and found that at the end of the first and second freeze-thaw cycles, sample volumes were greater than the as-compacted volumes, regardless of whether the samples expanded or shrunk upon freezing. This was more pronounced in the more plastic soils. By increasing the compactive effort from Standard AASHO to Modified AASHO maximum, the measured shrinkage decreased and the degree of saturation for maximum shrinkage increased. This author found it reasonable to explain the shrinkage phenomenon on the basis of the Powers and Helmuth theory for freezing of cement pastes. With reductions in temperature, but above the soil water freezing point, a small decrease in bulk volume of partly saturated soils will take place due to thermal contraction of the individual components. Upon freezing, an expansionary tendency is created due to soil water freezing. At the same time shrinkage forces are also present, since freezing of the soil water reduces the thickness of adsorbed water films around individual soil particles

and packets of soil particles, and increases soil suction in a manner similar to drying. He records that in general the swelling tendency is associated with high degrees of saturation and shrinkage with low degrees of saturation. At very low degrees of saturation shrinkage is limited by the very large attractive forces exerted by the clay particles on the adsorbed water, which prevents freezing except at very low temperatures.

In summary, the review of literature on freezing of water of a two phase system indicates that the exact nature of the ice developed is hard to ascertain. The form of ice developed is mainly dependent on the freezing rate or in other words on the rate of removal of heat, which is governed by the thermal conductivity of the sample. It would perhaps not be quite correct to state that at sufficiently high freezing rates all the ice developed is amorphous in nature. However, it appears reasonable to believe that at high freezing rates the nucleation sites are numerous and therefore, the crystallites are smaller in size, are located in the voids, and are separated from the mineral particle surfaces.

The phenomena of heating and sublimation is nicely summarized by Merryman (32) in the following words:

> "Assume a frozen specimen at very low temperature contained in any proper freeze-drying apparatus. As heat is supplied, the surface temperature of the specimen rises, and sublimation begins. A temperature is approached at which the sublimation rate will be comparable to the rate of heat input. However, as drying progresses, a layer of dried material develops, and an increasing resistance to vapour flow is introduced. This situation leads to an increasing concentration of vapour at the drying boundary, with an increasing amount of vapour returning to the ice crystal and giving up its latent heat. This effect reduces the net amount of heat utilized, and the available excess heat produces a rise in temperature, both increasing temperature. The sublimation rate increases, a high vapour pressure develops at the drying boundary, the diffusion gradient to the surface steepens, and vapour

diffuses to the specimen surface at a higher rate, until the rate of vapour removed corresponds again to the rate of heat input. During subsequent drying an equilibrium is constantly being approached between heat input, sublimation rate, recondensation rate, vapour pressure and vapour flow. In the last analysis it will be the vapour flow that limits the rate of drying."

APPARATUS AND EXPERIMENTAL PROCEDURES

Mixing and Curing

Soil was mixed in a Liquid-Solid Blender made by the Patterson-Kelley Company, Inc. of East Stroudsburg, Pennsylvania. This blender, shown in Figure 1, consists of twin shells which rotate on the horizontal axis. Water is supplied from a graduated cylinder to a pressure sprinkler tube inside the shells. The inside rotor is provided with projections for mixing the soil. Both the inside rotor and the shells are rotated by an electric motor.

Preliminary trials revealed two things concerning the operation of this device. First, the blender is at its best when about 3000 grams is used as a batch. Second, there is a loss of water which depends on certain details of the procedure. A correction curve was developed and is included in Figure C1, Appendix C. In operation, a batch of 3000 grams of Grundite as received from the factory was placed in the shells, and the shell covers were placed and tightened. The corrected amount of water was placed in the graduated cylinder. The shell and the rotor were rotated, and water was introduced in small installments. The mixing was interrupted two or three times, in a given run, to scrape away soil sticking to the walls of the blender in order to obtain a more homogeneous mix. The total mixing time was 20, 25 and 18 minutes for batches mixed dry of, wet of, and approximately at the Standard Proctor optimum moisture.

After mixing, the soil was sealed inside a polyethylene bag, which

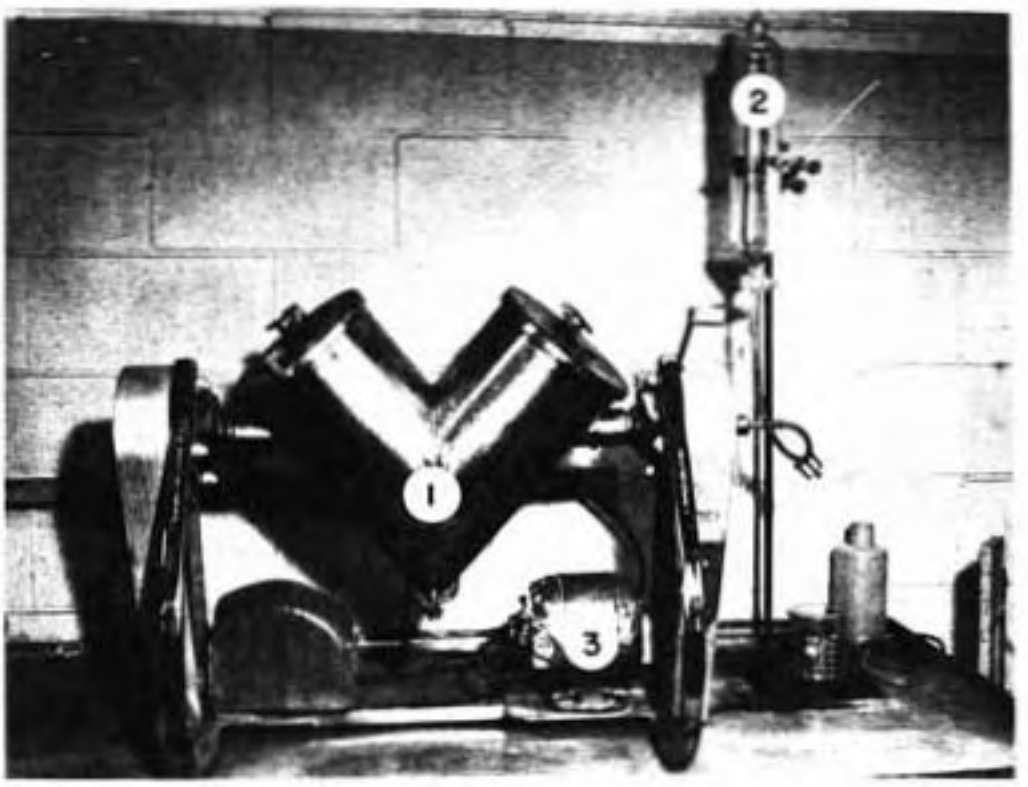

1. Twin Shells
2. Graduated Cylinder
3. Electric Motor

Figure 1 - Liquid - Solid Blender

was, in turn, sealed inside a larger polyethylene bag. The bagged samples were stored in a room of high humidity (to allow the moisture in the sample to equilibrate with the soil) for at least 5 days. The maximum time of storage was about 36 days.

It was observed that as a result of the mixing process, the original dry powder became a collection of roughly spherical aggregations.

Compaction Procedures and Protection of Compacted Samples

Three compactive types were used in this study, namely, impact, kneading and static. These procedures are described here individually.

Impact Compaction

The Standard Proctor compaction procedure (22) was followed in substance. Once the compaction curve had been defined, three moisture contents were selected, viz., one somewhat dry of the optimum, one wet of the optimum and one approximately equal to the optimum. The moisture-density relationship is shown in Figure C2, Appendix C. Soil batches were then mixed in the blender to the preselected moisture contents. The mixed soil was cured for 25 days in the high humidity room. Before compaction, the mixed soil was sieved over the No. 4 U.S. Standard sieve and the retained portion discarded. By wasting a small quantity of the aggregates it was felt that a more homogeneous mixture was achieved. Wherever the plus No. 4 material was a substantial part of the total, the separation was not made. Moisture content checks were made for all the batches of the material passing and retained on the No. 4 sieve and larger aggregates were found to have a higher moisture content than the smaller ones.

The soil was compacted in three layers, and the surfaces of the interior layers were roughened in order to blend them together.

Kneading Compaction

Wilson (50) described a compaction device popularly known as the 'Harvard Miniature Compaction Apparatus'. The compaction mold is 1/454 cu. ft. in volume, which means that the weight of a compacted specimen in grams is numerically equal to the unit weight in lbs./cu. ft. The device is shown in Figure 2. There are three notable advantages of this method of compaction: (1) material quantities are small and previously unused soil can be used for each moisture content; (2) the compacting action is a more realistic simulation of field compaction than that of the Proctor type of test; and (3) the extruded sample is a convenient size for strength testing.

The soil was given the same precompaction treatment as was stated for the Standard Proctor. The compaction process was mechanized, using the device shown in Figure 3. The electric motor of this device turns an eccentric cam mounted horizontally. Through a system of pulleys the motion of the cam is translated to an up and down motion of a vertical rod on which the compactor (item 4, Figure 2) can be mounted. Push and release are then controlled by the motion of the cam, and the compactor is simply a vertical rigid member. The pressure exerted can be varied by varying the amount of weight on the loading frame. The counterpart of the spring in the manual device is a spring supported platform for the compaction mold.

The action of the mechanized device is obviously slightly different than that of the manual one. However, control of compaction effort is a

1. Mold
2. Collar
3. Base
4. Spring Tamper
5. Mold Holding Device

Figure 2 - Harvard Miniature Compaction Apparatus (Manual)

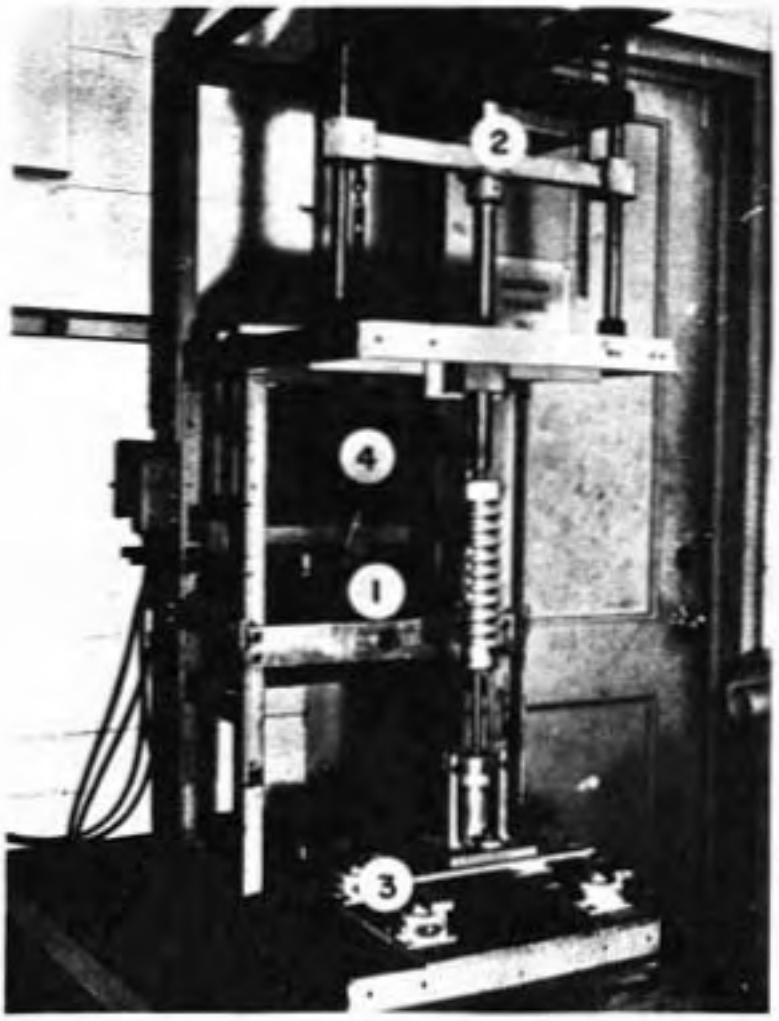

1. Cam
2. Loading Frame
3. Spring Supported Platform
4. Balancing Loads

Figure 3 - Kneading Compaction Apparatus (Mechanized)

chronic problem with the manual device, and the mechanization achieves such control quite nicely.

The compaction effort used in this method of compaction was adjusted by changing the number of tamps and the tamping pressure in order to fit a moisture-unit weight combination on the Standard Proctor curve. Sample calculations are shown in Appendix C.

Static Compaction

The static procedure is not standardized and can be implemented in a variety of ways. A major problem in the procedure is non-uniformity of unit weight. To combat the latter problem, the mold and technique of Sridharan (44) were employed. The mold is 2 inches high and has an inside diameter of 1 inch. As shown in Figure 4, it is used with six extension pieces with lengths of 1/16 in., 1/8 in., 3/16 in., 1/4 in., 3/8 in. and 1 in. Compaction is begun with the largest extension and proceeds in steps until the predetermined sample length is attained.

In this case, the effort was varied to permit a fitting of moisture-unit weight conditions to the Standard Proctor curve. Sample calculations are shown in Appendix C. Two extension pieces were used in each of the six stages of compaction. In every stage compaction was from the top; the mold was turned upside down to permit compaction from both the ends. The compaction plunger was pushed by a manually operated hydraulic press. The successive thicknesses of the sample at each stage were 3 in., 2-3/8 in., 2-1/4 in., 2-3/16 in., 2-1/8 in., 2-1/16 in. and finally 2 in. After compaction the sample was extruded with the same device used for the Harvard Miniature samples.

Figure 4 - Static Compaction Mold

The compacted cylinders prepared by all the above methods were sealed in a polyethylene bag. A wet towel was wrapped around the bag, and this combination was sealed in a second polyethylene bag. All such samples were kept in capped 1-lb coffee cans. Moisture content checks confirmed the effectiveness of this procedure for times up to 30 days.

Preparation of Samples for Freeze Drying and Pore Size Determination

Preparation of samples for freeze drying and subsequent pore size determination underwent four stages of improvement in the course of experimental investigations. Initially it was thought that since the minimum dimension of the sample controls the rate of freeze drying, that disc-shaped samples 8 mm in diameter but only 1 mm thick were appropriate. However, it was soon obvious that nearly all of the sample volume was disturbed by the trimming process. Next, samples were obtained by cutting a small bulky piece from the compacted soil. It was desired to know the 'as-trimmed' void ratio or porosity so that comparisons could be made with the gross as-compacted values, as well as with the values which obtained after freeze drying. Volume measures of as-trimmed samples obtained by mercury displacement, in a filling device, were not consistent, and could not be viewed with confidence.

It was reasoned that a part of the problem of volume measure was the irregular shape of the sample, and accordingly, in the third stage, samples of geometric shape were cut out of the compacted sample. To this end, brass cork borers were used. The penetrating edge was sharpened, the inside walls were lubricated, and the samples were obtained by simply pushing the cutter into the compacted soil cylinder. After

the required length was penetrated, the cross section was sheared by rotating the handle. The sample was ejected from the cutter by means of a rubber tipped rod. These samples were an improvement over the previous ones, but the brass was too soft a material and the wall thickness of the cutter was too great for the consistent acquisition of a relatively undisturbed sample.

Finally, a more sophisticated sampler was designed adhering to the concepts of thin-walled tubes for minimal soil disturbance [Hvorslev (17)]. This sampler was of stainless steel and was tempered at a high temperature. Details of the sampler are shown in Figure 5. The sample size was constrained by the size of the porosimeter (described later). This sampler was named the 'miniature tube sampler'. The sampler and the accessories are shown in Figure 6.

Compacted soil cylinders prepared by kneading or static process were held in the split cylinder shown in Figure 7. The tube sampler was pushed in for the required length, sheared by rotating the handle, and pulled out. The tube was placed in the miter and held firmly by screws. A teflon tipped extruder was used to remove the soil from the tube. First, a very small length was extruded and the end squared by a sharp razor. This was followed by the ejection of the whole sample; the upper end did not always need squaring since the compacted surface was smooth at the start.

Sampling of the Proctor compacted soils was similar except that a quarter of the compacted soil cylinder was placed in the slotted cylinder shown in Figure 7. It was held in place by wooden blocks that filled the remainder of the space, and tube sampled.

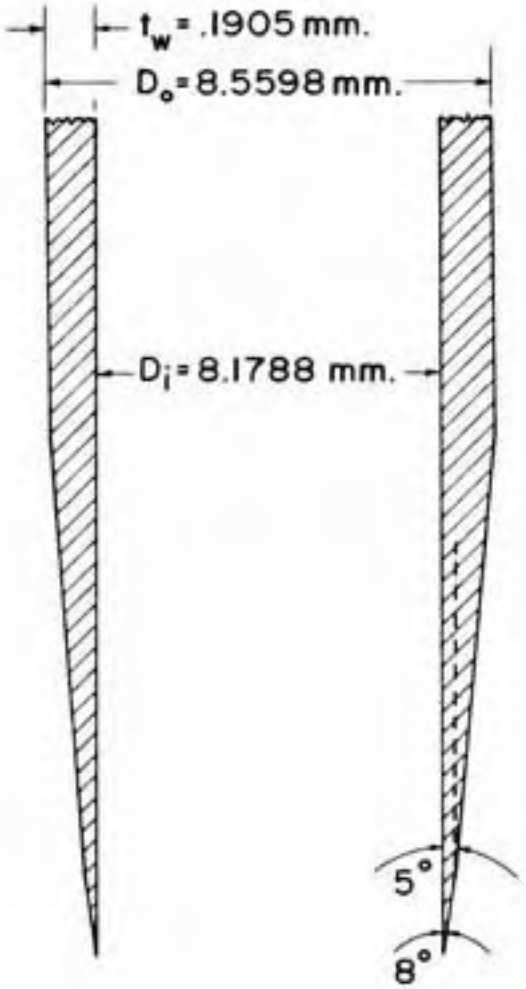

$$\text{Area Ratio} = \frac{D_o^2 - D_i^2}{D_o^2} = 8.70\ \%$$

Figure 5 - Miniature Tube Sampler (Not to Scale)

1. Extruder
2. Holding Jaw
3. The Sampler
4. Teflon Cap

Figure 6 - Miniature Tube Sampler and Accessories

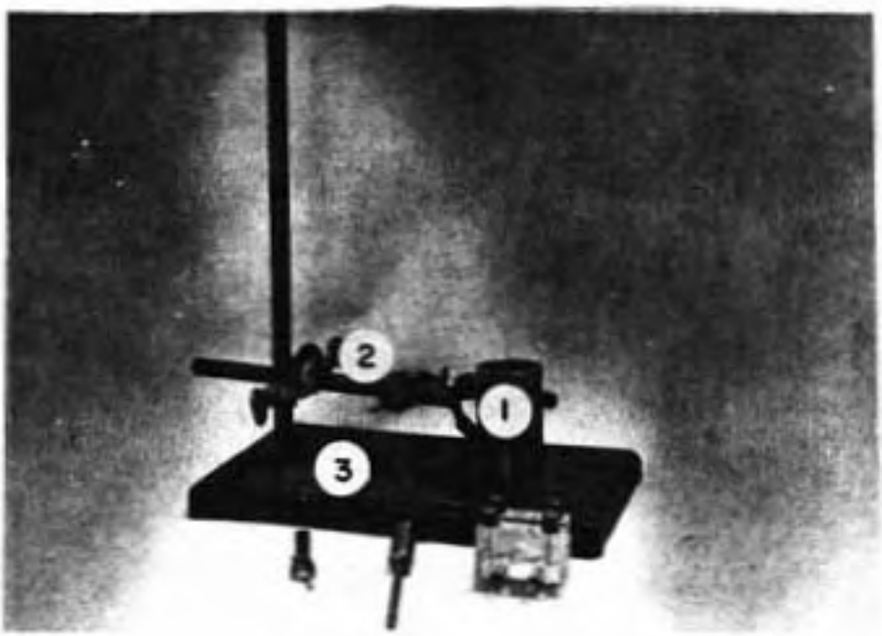

1. Split Cylinder
2. Clamps
3. Stand

Figure 7- Set - Up for Sampling

These processes worked well for all samples except those significantly dry of Standard Proctor optimum. Such materials were best sampled by cutting out small roughly geometric chunks with a sharp razor blade.

Calculation of Sample Conditions

As shown in Figure 8, if weight, volume, water content and apparent specific gravity of solids are known with respect to a sample condition, all other volumetric and gravimetric quantities, as well as ratios thereof, can be calculated. Of particular interest are the void ratio (e) and the porosity (n). Whereas weights can be measured with precision, volumes, particularly volumes of irregular shapes, are much more difficult to determine precisely. Initially, volumes of the irregular samples were obtained by mercury displacement in a device in which mercury is drawn in by applying a differential pressure. But it was learned that this procedure underestimates the volumes, because surface irregularities and the larger pores are filled with mercury at the ambient atmospheric pressure. It was concluded that wherever possible, volumetric measurements should be made by a precision micrometer.

As noted before, the miniature tube sampler gave satisfactory service except for 'dry side' samples. In the latter case, appreciable disturbance was signaled by the difficulty of penetrating the sampler and of extruding the sample. The analysis presented in Appendix C gives the details of sampling disturbance.

It was intuitively thought that razor-cut samples of strong dry-side material would be fairly undisturbed. To check the hypothesis, several of the razor-cut samples were coated by a mixture of wax and vaseline, and their volumes were determined in the filling device (described later).

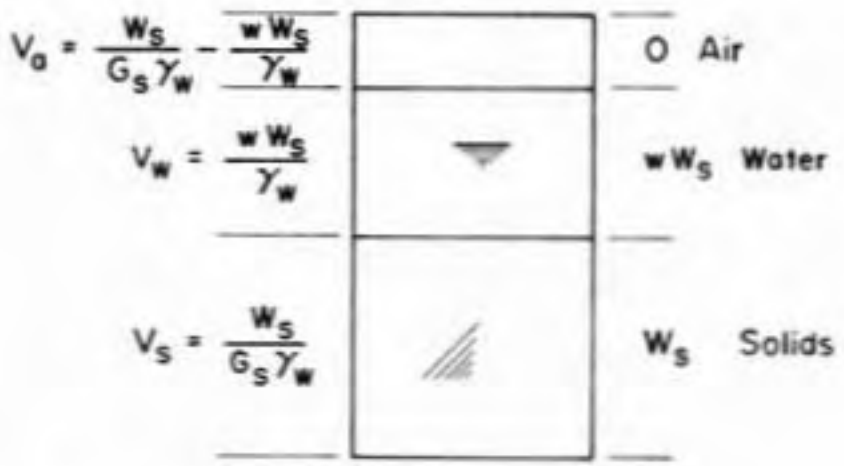

$$G_s = \frac{W_s}{V_s \gamma_w} \qquad w = \frac{W_w}{W_s}$$

Knowns = G_s, w, W, V

Required = V_v, e, n

$$W = W_s(1 + w)$$

$$\therefore \; W_s = W \div (1 + w)$$

$$\therefore \; V_v = V - \frac{W}{(1 + w)\, G_s \gamma_w}$$

$$e = \frac{V_v}{V_s} = \frac{V - \dfrac{W}{(1 + w)\, G_s \gamma_w}}{\dfrac{W}{(1 + w)\, G_s \gamma_w}} = \frac{V(1 + w)\, G_s \gamma_w}{W} - 1$$

$$n\ (cm^3/gm) = \frac{V_v}{W_s} = \frac{V - \dfrac{W}{(1 + w) G_s \gamma_w}}{\dfrac{W}{(1 + w)}} = \frac{V\, G_s \gamma_w}{\dfrac{W}{(1 + w)}} - 1$$

Figure 8 - Sample Conditions

These samples gave a porosity which was 98% of the gross as-compacted porosity. With this success it was concluded that the razor trimmed dry side samples were reasonably undisturbed.

The above procedure of porosity determination is time consuming, and after the determinations in the filling device it is not convenient to recover the same sample for freeze drying and pore size determination. Accordingly, it was not routinely used to calculate trimmed volumes.

Freeze Drying

The samples were held in buckets which consisted of a porous stone base and walls made of foil, which formed three or four individual compartments. The compartment walls had holes to admit the freezing liquid. The samples were placed in the compartments with a pair of tweezers, and the buckets were lowered quickly into the container of freezing liquid. The freezing liquid reached the specimens from all sides, and hopefully froze them almost instantaneously. Freezing was accompanied by a bubbling induced by the loss of heat from the samples. Frozen specimens were kept immersed in the freezing liquid until ready to be transferred to the sublimation unit.

The four bay sublimation unit is shown in Figures 9 and 10. It consists basically of a glass sample container which is surrounded by a slush contained in a Dewar flask. The sample container is connected by glass tubing to a condensing tube which is surrounded by the condensing liquid. On the top are stopcocks which connect the bays with the vacuum pump. Bleeder valves are also provided for introducing air. The whole assembly is mounted on a rigid frame.

Freeze drying is a batch process, involving first, freezing of

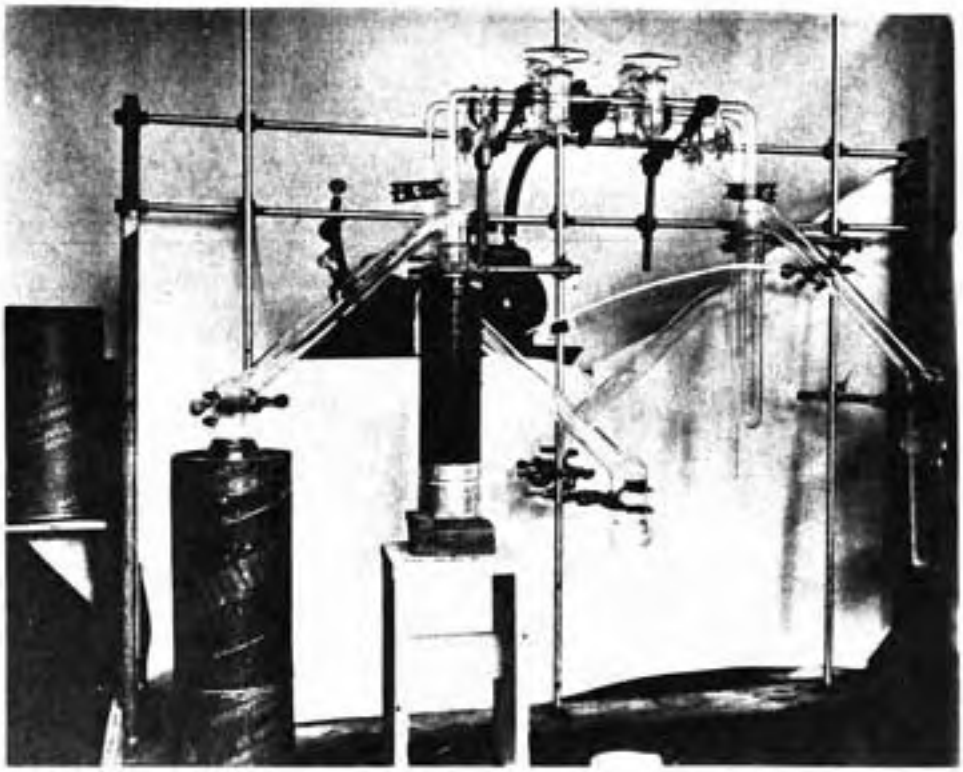

Figure 9 - Sublimation Unit

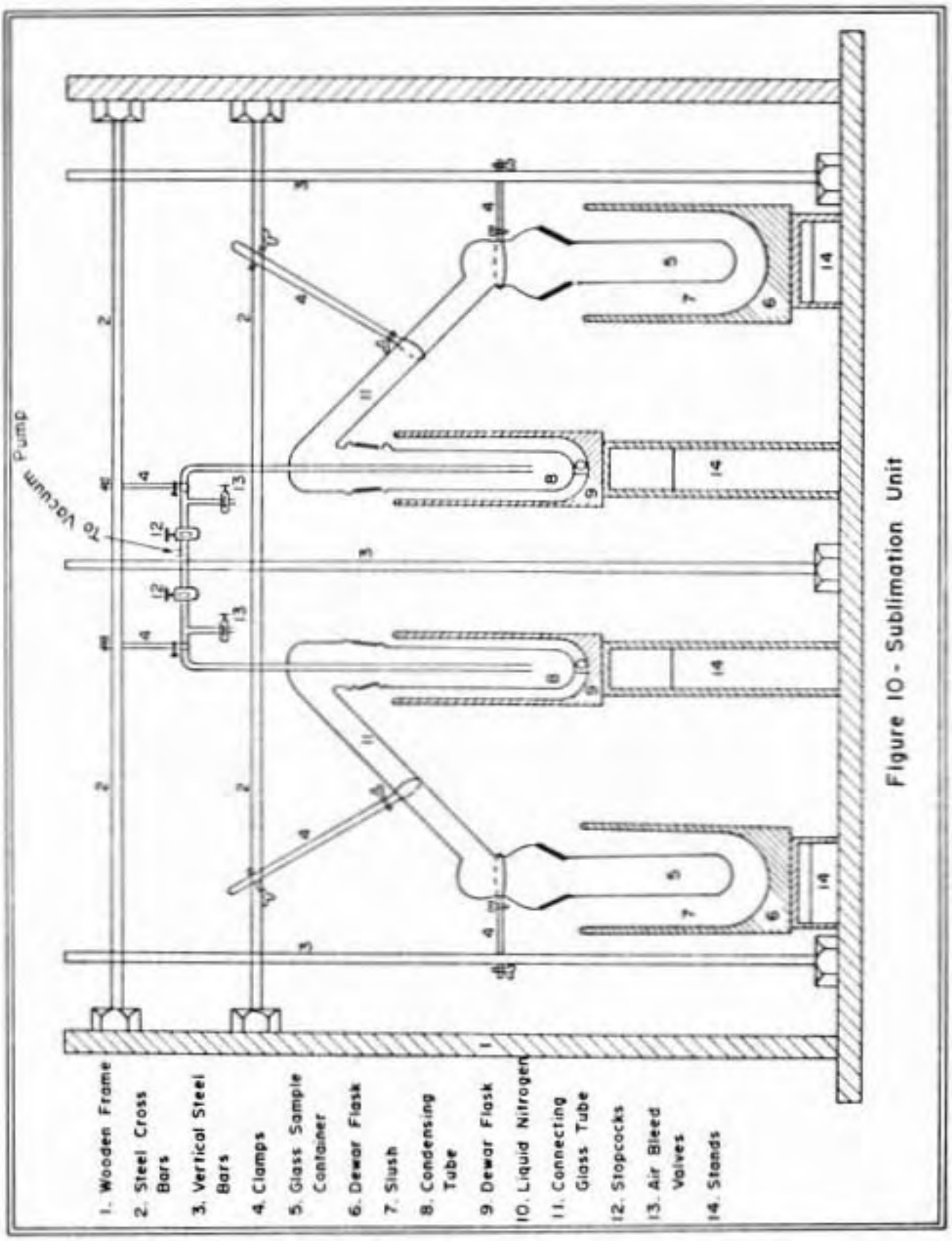

Figure 10 - Sublimation Unit

samples in the liquid nitrogen, then transfer to the sublimation unit, and finally, sublimation. The sublimation process proceeds in the following manner. An ice-water slush is placed in a Dewar flask and the glass sample container is placed in it. After the container has achieved temperature equilibrium with the slush, the frozen samples are placed within it. The temperature of the slush is maintained such that the samples remain frozen and do not melt during the sublimation process. The container, with the slush surrounding it, is then hooked in the unit and a Dewar filled with liquid nitrogen is raised to chill the condensing tube. Timing of the actions is critical, viz., raising of the liquid nitrogen Dewar should immediately follow the connecting of the sample container to the apparatus. Otherwise, moisture may condense in the sample container or on the samples. A vacuum is applied by opening the stopcock of the bay. Finally, the bleeder valve is closed. Liquid nitrogen is added at intervals to replace the portion converted into gas. The slush temperature is checked periodically, since it tends to increase with time.

In the initial stages of the research, the slush bath was prepared by mixing crushed dry ice in trichlorethylene. This mixture could be maintained in the vicinity of -65°C. The samples used in those initial stages were very thin and could be dried in a period of 24 to 48 hours. Later, when thicker samples were chosen the drying process was considerably slower. The reason for the slow freeze drying was the very low vapor pressure and vapor pressure gradient produced when this -65°C slush was used. To avert this problem, different slush baths were tried which could provide a temperature,

a) low enough to keep all soil water frozen,

b) high enough to produce a vapor pressure resulting in drying in a reasonable span of time.

In the final selection process, two slush baths were chosen. The first was prepared by partially freezing m-xylene with liquid nitrogen; this gave a temperature in the vicinity of -40°C. The second was prepared by mixing magnesium chloride with crushed ice: this gave a temperature of about -21°C. However, this temperature rose quickly due to the melting of ice and it was necessary to add chunks of dry ice to originate ice nucleation and compensate for the melting. This technique maintained the bath between the temperatures of -24 to -30°C for a reasonable period of time (about 10 hours). Both of these slush baths served satisfactorily. Xylene is inflammable; $MgCl_2$ is messy but less hazardous. At these higher temperatures and consequently higher vapor pressures, the samples could be dried in an average period of 12 to 18 hours. The slush bath was removed and an equilibration time of a few hours was allowed before the samples were finally removed from the apparatus. Sample weights before and after freeze drying defined the amount of water removed.

Pore Size Determination

The Apparatus

The three main units of apparatus used in pore size determinations are shown in Figures 11, 12, and 13. Figure 11 shows the penetrometer, which consists of a bulb of about 6.0 ml. volume and a capillary stem graduated from 0.000 to 0.200 ml., in divisions of 0.002 ml. The diameter of the bore is 1.300 mm. A steel cap and a teflon screw are used to close the mouth of the bulb.

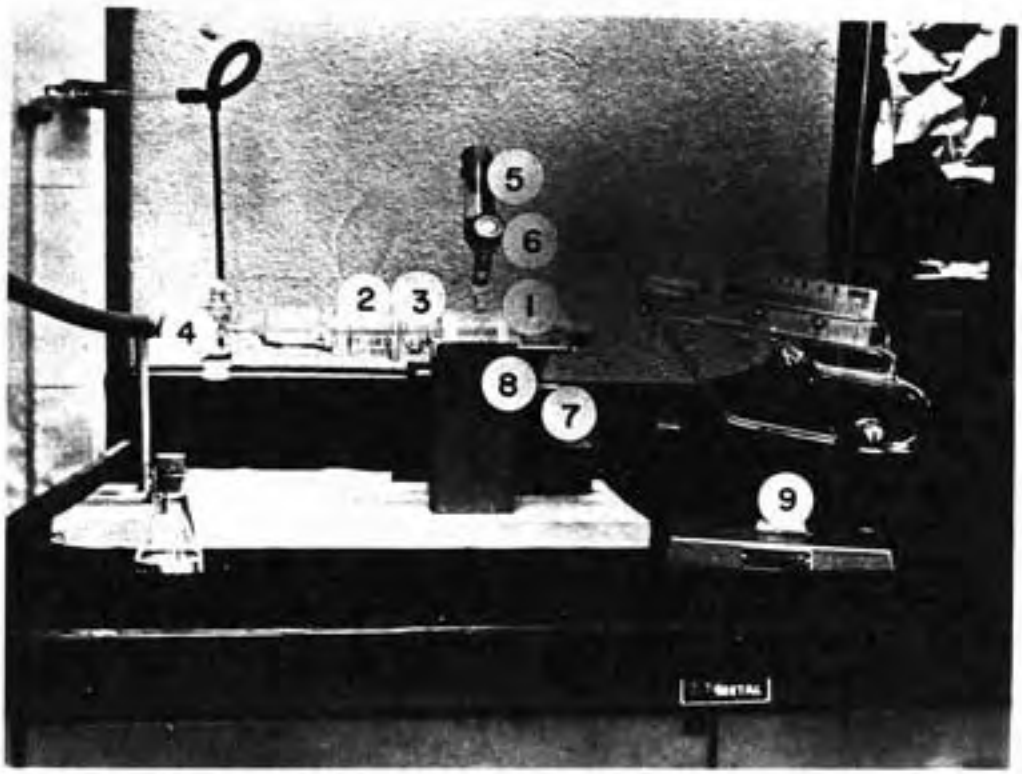

1. Glass Chamber
2. Ground Glass Joint
3. Constriction
4. Stopcock
5. Mercury Reservoir
6. Teflon Stopcock
7. Wooden Blocks
8. Side Arm
9. Mc Leod Gage

Figure 12 (A) - The Filling Device

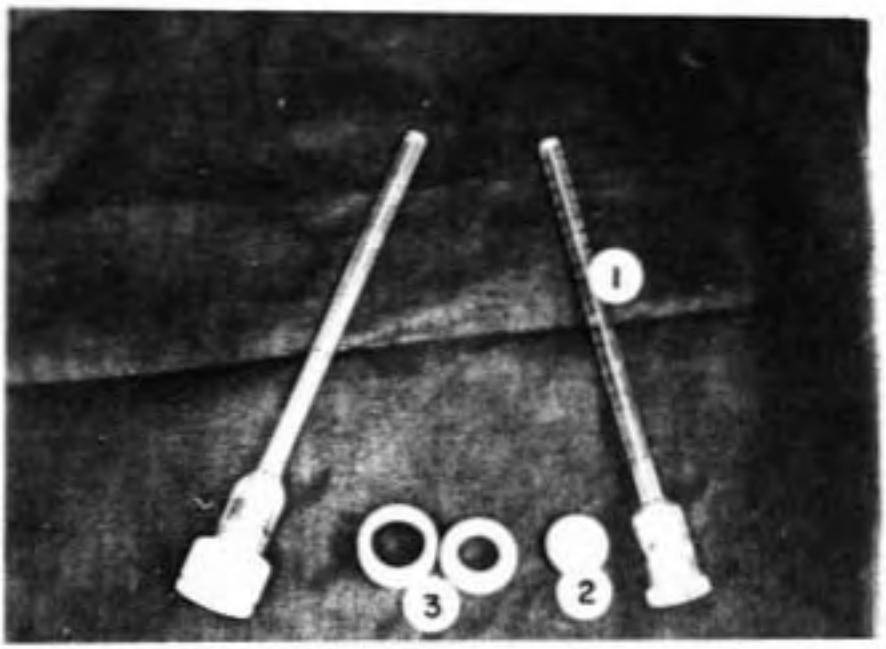

Penetrometer
2. Steel Cap
3. Teflon Screw

Figure 11- Penetrometer and Assembly

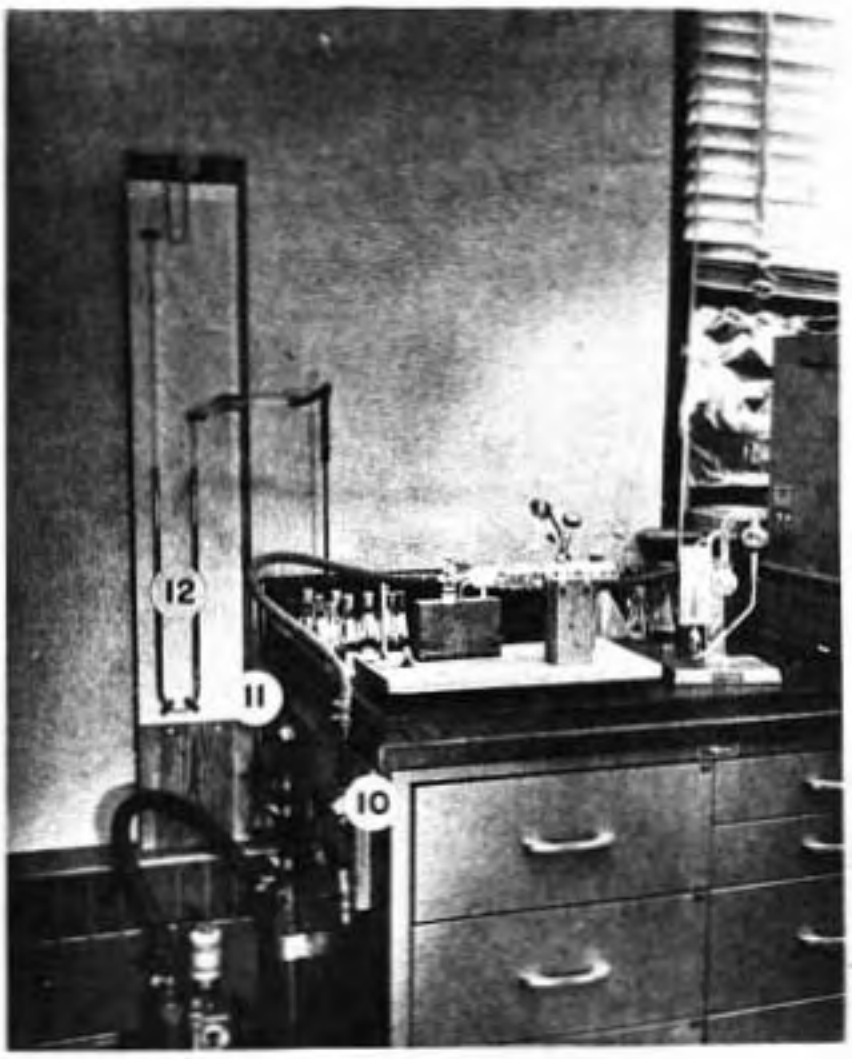

10. Bleeder Valve
11. Valve Connection to Vacuum Pump
12. Mercury Manometer

Figure 12 (B) - Filling Device, Vacuum Manifold and Manometer

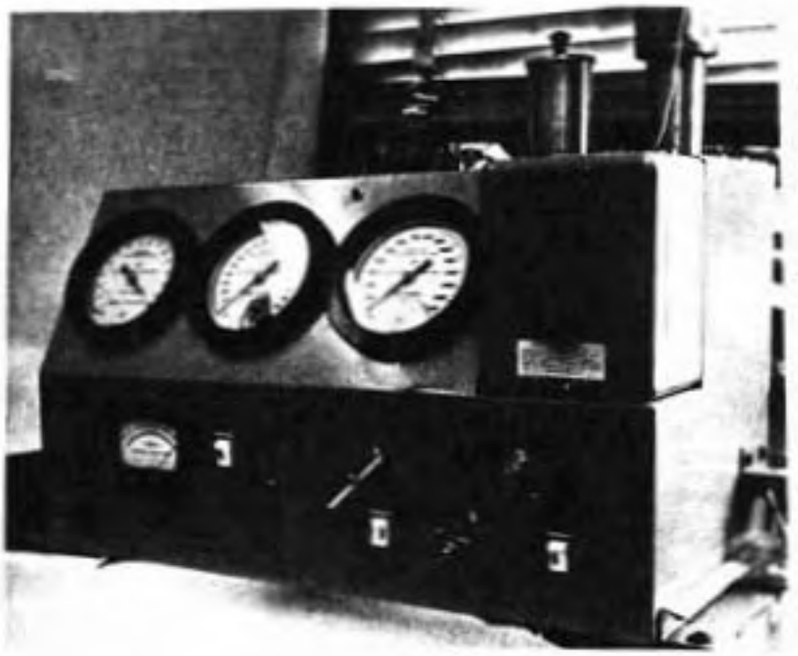

Figure 13 - The Porosimeter

Figure 12 shows the filling device[1] with its accessories. The main features of the filling device are:

(1) A glass chamber having a bullet nose in which the stem of the penetrometer rests with the mercury surface touching underside.

(2) A ground glass joint which connects the second part of the chamber with the first. This contains a wad of glass wool which presses against the head of the penetrometer.

(3) A constriction, in which a tapered teflon stopper, having a slit, is mounted on the penetrometer stem to hold the penetrometer in horizontal alignment.

(4) A stopcock, which connects the filling device with the vacuum manifold and the mercury manometer.

(5) A reservoir to hold mercury.

(6) An ungreased teflon stopcock.

(7) Wooden blocks.

(8) Side arm for adjusting the level of mercury in the chamber, (1) above.

In Figure 12B a number of parts are identified by numbers, i.e., No. 10 is a bleeder valve, No. 11 is a valve connection to the vacuum pump and No. 12 is the mercury manometer. The vacuum pressure is measured by the McLeod Gage (No. 9). This device can be rotated on a horizontal axis.

An Aminco Porosimeter, shown in Figure 13, was used for intruding mercury at pressures higher than atmospheric. Several improvements were effected on the commercial model (52). The apparatus as used had two Bourdon tube gages with capacities of 1000 psi and 15,000 psi. The smallest increments on the gages were 5 psi and 100 psi, respectively. The pressure was generated by an electrically driven hydraulic pump. Intrusion of

---

1. U.S. Patent Application 583, 838, Prado Laboratories, Inc., Cleveland, Ohio.

mercury is sensed by a stainless steel needle which follows the position of the meniscus of the mercury in the capillary stem of the penetrometer. As the needle advances, its linear movement is digitally recorded on a counter in terms of volume of mercury intruded. The smallest volume change which can be registered is 0.00005 ml.

The Technique

Except for the samples compacted on the dry side of the optimum, void volumes were within the range of the instrument (<0.2 ml). First, the sample was weighed on an analytical balance to 0.0001 gram. Then the sample was placed in the bulb of the penetrometer, light grease was applied to the glass periphery at the mouth, the smooth end of the steel cap was placed on the mouth and rotated to spread the grease, and the teflon screw was tightened. The assembly was then weighed and placed in the filling device. The vacuum pump was started and the system was connected to it by opening the vacuum valve. With the side arm (No. 8 in Figure 12A) resting on both the wooden blocks, mercury was introduced from the reservoir (No. 5 in Figure 12A) by opening the teflon stopcock (No. 6) until it just touched the underside of the stem. This quantity of mercury was just sufficient to fill the penetrometer. Evacuation continued until the pressure, measured by the McLeod gage, dropped below ten microns; in most of the tests the evacuation pressure was equal to or less than five microns. The side arm (No. 8 in Figure 12A) was then tipped up and rested on a wooden block. With manipulation, the bullet side of the mercury chamber was filled and the opening of the capillary was blocked. When the vacuum valve was closed and the filling pressure was applied by opening the bleeder valve, mercury flowed through the stem

filling the penetrometer and enveloping the sample. The side arm was then rotated back to the original position, breaking the mercury column at or near the opening of the stem of the penetrometer. The filling pressure and the initial reading on the stem were then recorded. For these tests, the filling pressure was kept constant at 20 millimeters of mercury. This pressure corresponds to a pore diameter of about 600 microns, which means that diameters larger than this were not included in the measurements. The pressure was increased in steps and mercury penetration was read on the stem after equilibration following each pressure increment. This continued until the atmospheric pressure was reached. Then the penetrometer filled with mercury was removed from the filling device and weighed to obtain the weight of the mercury present in the unit.

The assembly was then placed, stem down, in the pressure chamber of the porosimeter, the socket tightened, and the chamber completely filled with the pressuring fluid (alcohol). The pressure is applied in increments and intrusion of mercury is noted by the digital readout after equilibrium at each increment. Thirty to forty steps were enough to give reasonably spaced points on the pore distribution curve. In each step the pressure was held constant until the probe movement had practically ceased. It was found that after a swift intrusion for low pressures, very little increase in intruded volume takes place with time. However, for pressures beyond 8,000 psi, the equilibration time was increased. The highest pressure which could be attained varied between 13,900 and 14,500 psi.

Reduction of Data

The data recorded in the filling device operation are the weight of the sample, weight of sample and penetrometer, evacuation pressure, filling pressure, stem reading and weight of sample penetrometer after filling with mercury. The pressure and the stem reading are noted for every pressure step. In the porosimeter operation, gage pressure and probe readings are recorded at each step. To obtain the absolute pressure on the sample, one atmosphere of pressure must be added, i.e., the dial gage reads zero at one atmosphere, and a negative head of mercury must be subtracted, since the penetrometer was held vertically with the stem down. The net correction was an addition of 11 psi to the gage pressure.

A number of other corrections were effected, as follows.

(a) The effect of compression of air entrapped at the filling pressure was deducted at each step from the gross intrusions recorded, Boyle's Law being used to calculate the reduction in volume of the gas at each pressure step. This correction was usually very small and its significance disappeared at a pressure below one atmosphere.

(b) The measured volume of mercury intruded was also corrected for the compressibility of mercury at high pressures. A plot (shown in Appendix C) of decrease of volume of mercury with pressure was obtained by loading the penetrometer with mercury only and pressuring. The measured change in volume thus obtained was the net effective change, since compression of mercury was accompanied and partly offset by the effect of compression on the glass sample holder.

The data and the corrections became programmed input for calculation of sample characteristics and indices. The Programma, a program desk calculator manufactured by Olivetti Underwood was used. A typical set of these calculations is present in Appendix C.

Preparing Samples for Strength Testing

Cylinders compacted by the Standard Proctor procedure were cut into four quarters by a metal band saw. The compacted soil cylinder was placed in a specially fabricated steel cylinder, provided with four vertical slots and tightening nuts (Figure 14). The assembly was then mounted on the bed of the saw and clamped. The saw blade was lowered slowly and gently until the full thickness of the cylinder head had been cut. Intermittently the blade was raised and cleaned. Gentle handling was necessary to avoid cleavage at the interlayer compaction planes.

Two of the sample quarters were sawed for pore size determinations. The other two were used to produce strength-test cylinders with the electrically driven soil lathe shown in Figure 15. Coarse cutting was done with a knife before using the lathe. After the desired diameter (1.312 inch) was attained, the sample was transferred to the hollow cylinder or miter box shown in Figure 16. As shown, extension pieces of varying thicknesses can be combined in any desired manner and number. The final length of 2.62 in. was achieved with the aid of sufficient extension pieces to avoid cantilever-action stresses in the samples during end trimming. This process of preparing the samples for strength testing from Standard Proctor cylinders was one of the most delicate parts of the experimentation.

Statically compacted samples were of appropriate size for the testing.

Samples compacted by kneading compaction were cut to a length twice the diameter using the device shown in Figure 16.

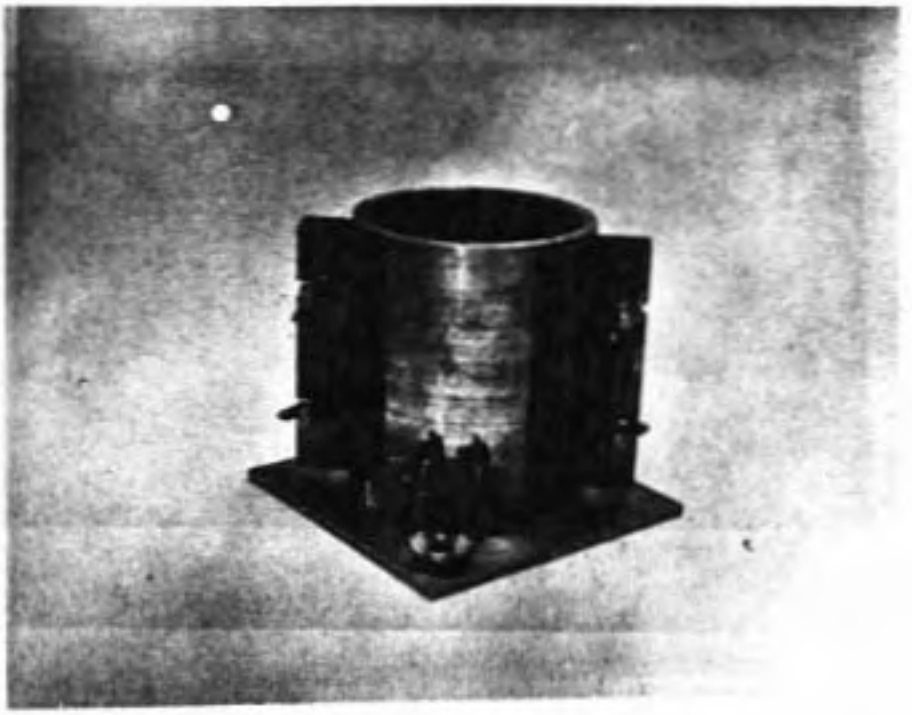

Figure 14 - Slotted Steel Cylinder

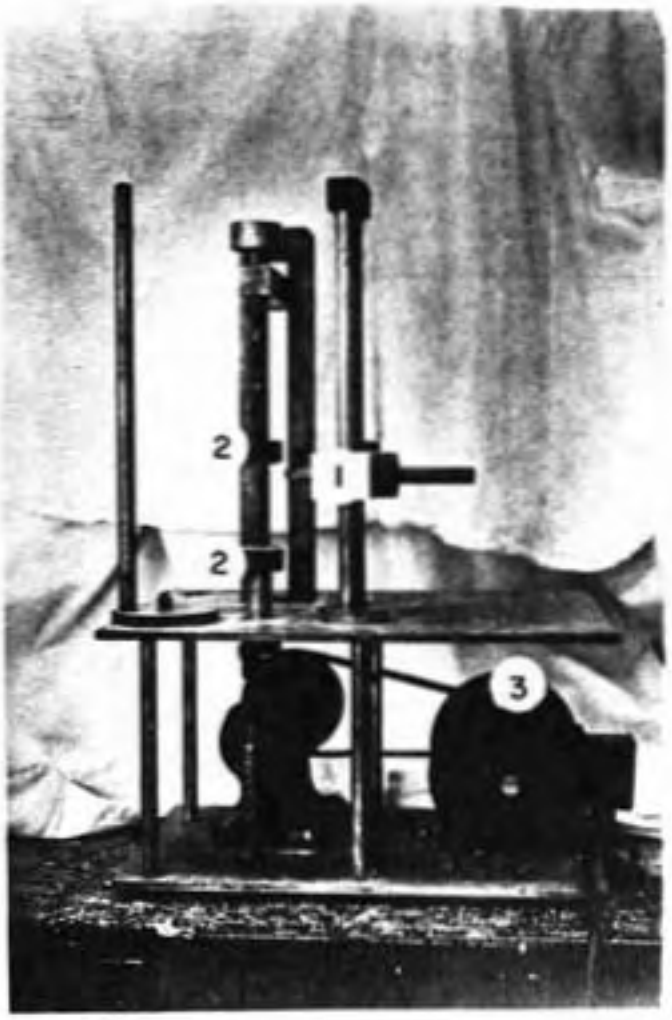

1. Steel Tool
2. Top and Bottom Heads
3. Electric Motor

Figure 15 - Lathe for Preparing Specimen for Strength Testing

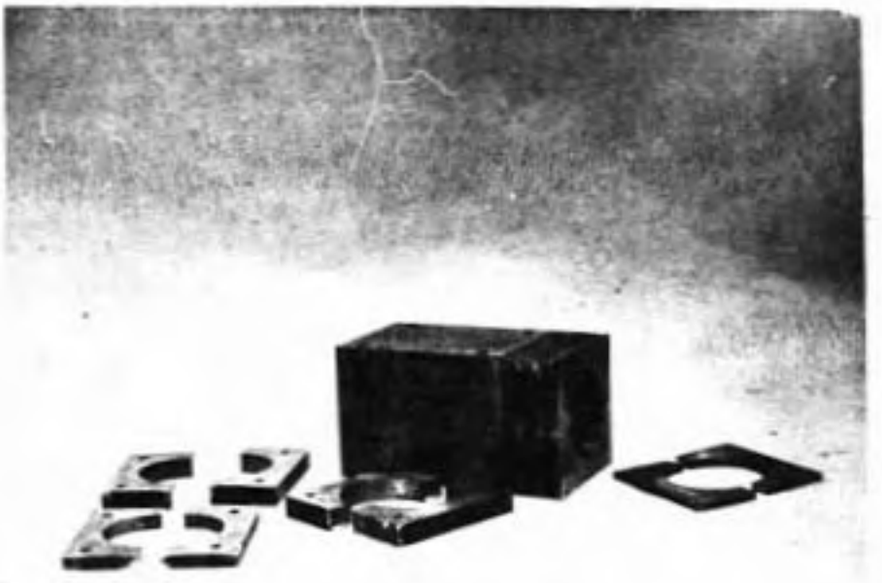

Figure 16 - Miter Box

Unconfined Compression Testing

The Model 56 compression device of Wykeham-Farrance Ltd. was used in the unconfined compression testing (Figure 17). This machine is run by an electric motor at a constant strain rate, and has a capacity of 10,000 pounds. A 300-lb proving ring recorded the load, and a deflection dial with a minimum division of 0.001 inch registered the axial deflection. Two modifications were made to the routine test.

1) To achieve improved homogeneity of stress in the samples the end-loading conditions were altered.[1]

2) To obtain a better definition of stress level than would be afforded by a constant volume assumption, the actual diameter changes were measured at the mid-height of the sample. The sensor was a LVDT and it was connected to a time chart for continuous recording.

Even though the testing was accomplished without confining pressure, the sample was tested inside a triaxial cell, without a membrane. The use of the triaxial cell also diminished the moisture loss. All tests were run at a constant strain rate of about one percent per minute. Typical data and calculations are presented in Appendix C.

---

1. Oversized aluminum top and bottom platens were machined and their surfaces were given a polished finish (see Figure 18). Dry lubricant (MS-122, Miller Stephenson Chemical Co., Inc., Chicago) was applied to these plates for lubrication.

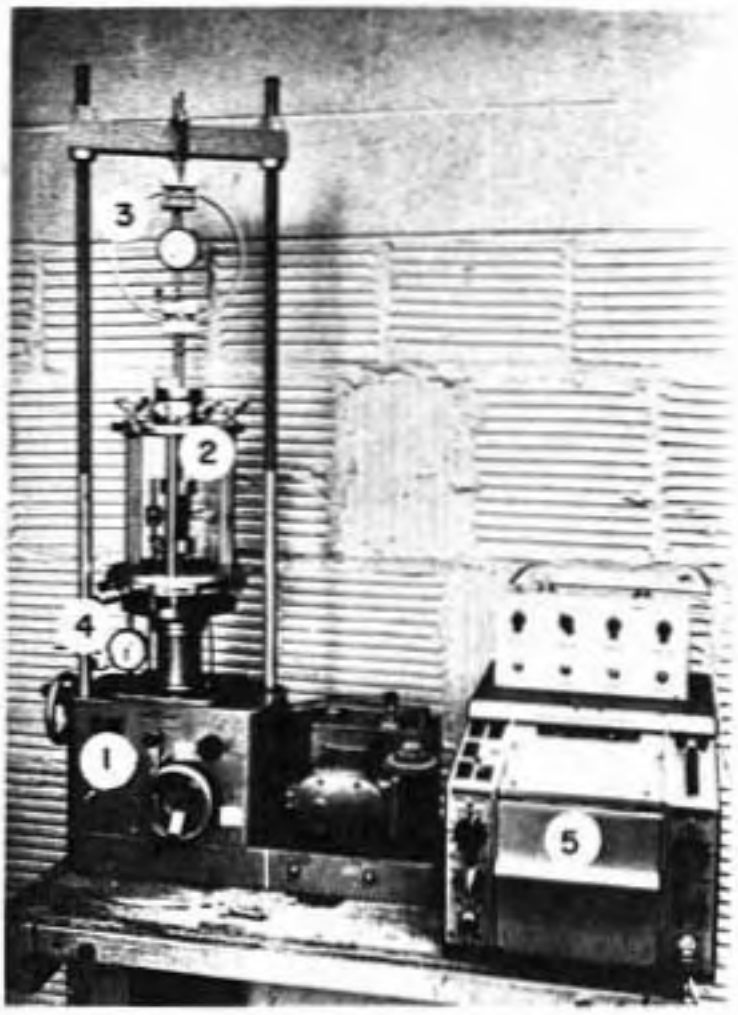

1. Model 56 Compression Device
2. Triaxial Cell
3. Proving Ring
4. Deflection Dial
5. Recorder

Figure 17 - Set-Up for Unconfined Compression Tests

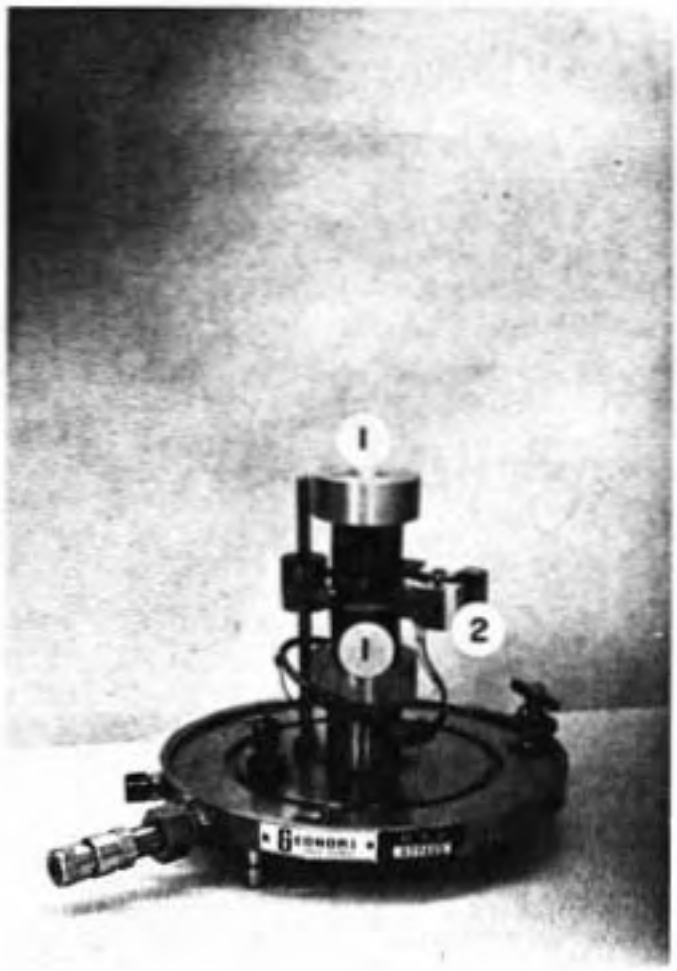

1. End Platens
2. LVDT

Figure 18 - Sample Assembly on Triaxial Cell Base

RESULTS AND DISCUSSION OF RESULTS

Compaction Results

A summary of compaction results is presented in Table 1. The moisture-unit weight relationship obtained by the Standard Proctor method was taken as the control curve, i.e., the effort level was adjusted in the static and kneading compaction to 'fit' the Standard Proctor unit weight at the compaction water content. A single batch of soil was used for all the compaction tests. Some variability in water content was unavoidable. Examination of Table 1 shows that except for Cylinder No. 2 of the kneading compaction, unit weight variation was within one pound per cubic foot of that desired. The variation of water content was not more than one percent of water content. Values of void ratio and porosity shown in the table were rounded to the second decimal place.

The expression for degree of saturation is $S = \frac{\gamma_d \, w \, G_s}{G_s \gamma_w - \gamma_d}$. It is clear from this relationship that a relatively low moisture content in combination with a relatively high unit weight can produce a relatively high degree of saturation.

Effects of Sampling

Compaction cylinders prepared at and beyond the Standard Proctor optimum moisture content were sampled with the miniature tube sampler (Figure 5). These are Nos. 3 and 4 and some of the No. 2's of Table 1. In Tables 2, 3 and 4 are presented sample characteristics for the top

TABLE 1

Properties of the Compacted Samples Used in Freeze Drying and Pore Size Determinations

STANDARD PROCTOR (SP)

PROPERTY \ COMPACTION CYLINDER NO.	1 (Dry)	2 (Near Optimum)	3 (Optimum)	4 (Wet)
Water Content (w) %	15.6	20.2	21.5	26.0
Dry Unit Weight (γ_d) pcf	96.0	99.6	100.1	96.4
Void Ratio (e)	0.80	0.74	0.73	0.79
Porosity (n) cm^3/gm	0.29	0.26	0.26	0.29
Degree of Saturation (S) %	54.1	75.9	81.5	91.0

KNEADING COMPACTION (KM)

PROPERTY \ COMPACTION CYLINDER NO.	1 (Dry)	2 (Near Optimum)	3 (Optimum)	4 (Wet)
Water Content (w) %	16.2	19.8	21.4	26.2
Dry Unit Weight (γ_d) pcf	96.0	102.7	99.5	96.3
Void Ratio (e)	0.80	0.68	0.74	0.80
Porosity (n) cm^3/gm	0.29	0.25	0.27	0.29
Degree of Saturation (S) %	55.9	80.0	80.0	90.1
Pressure on Tamper (lbs)	39.5	39.5	30.7	21.9
No. of Tamps for each of five layers	13	10	15	20

STATIC COMPACTION (ST)

PROPERTY \ COMPACTION CYLINDER NO.	1 (Dry)	2 (Near Optimum)	3 (Optimum)	4 (Wet)
Water Content (w) %	15.6	19.4	21.4	26.1
Dry Unit Weight (γ_d) pcf	96.1	99.8	100.2	96.5
Void Ratio (e)	0.80	0.73	0.73	0.79
Porosity (n) cm^3/gm	0.29	0.27	0.26	0.29
Degree of Saturation (S) %	50.9	72.9	81.5	90.5

and next to the top compaction layers in Cylinder No. 3 (kneading type).

In Table 2 void ratios, porosities, etc., were calculated on the basis of sampling tube dimensions. The weight of solids was obtained assuming that the sample water content was equal to that of the compacted cylinder. Sample porosities (or void ratios) were 99.5 to 115.7 percent of the cylinder values. Penetration of a sampling tube can produce either sample volume increase or decrease, depending upon the initial soil condition and the sampling details. An increase (positive dilation) is clearly indicated here.

The data of Table 3 are based upon measurements of the samples after extrusion from the sampling tube. Again, the sample could show volume increase or decrease, depending upon the soil condition and details of the extrusion process. In these examples, the net effect of sampling and extrusion is an apparent reduction in volume with respect to the as-compacted values.

The net reductions in porosity and void ratio are given in Table 4. These reductions are the sum of many effects. They also depend upon the variability of these two index properties within the compaction cylinder. To restate the point, it is not feasible to assess the degree of sampling disturbance more closely, since the initial (unsampled) condition is not precisely known at the sampling location. The apparent reduction in porosity due to sample procurement ranged from 3 to 12% even when the best available equipment and most careful procedures were used.

TABLE 2

Effect of Sample Intrusion into the Sampler

Remarks:
Height given here is the height of cylinders in the sampler before extrusion. Diameter is inside dia. of the sampler.

As Compacted Properties (AC)

w	γ_d	e	n	S
21.43	99.47	0.74	0.27	80

	TOP LAYER					NEXT TO TOP LAYER				
SAMPLE NO.	1C*	2E	3C	4E	5E	6C	7E	8E	9E	10E
DIAMETER mm	8.18	8.18	8.18	8.18	8.18	8.18	8.18	8.18	8.18	8.18
HEIGHT mm	6.07	6.47	5.88	5.53	7.32	10.55	5.73	7.78	8.68	8.38
WET WEIGHT gm	0.6190	0.6405	0.5769	0.5562	0.7190	1.0063	0.5645	0.8157	0.8822	0.8400
SAMPLE VOL cm^3	0.319	0.340	0.309	0.290	0.385	0.554	0.301	0.409	0.456	0.440
VOID VOL cm^3	0.125	0.150	0.138	0.125	0.171	0.255	0.133	0.166	0.194	0.191
VOID RATIO (e)	0.734	0.786	0.802	0.758	0.800	0.854	0.794	0.686	0.740	0.764
$\frac{e}{e_{AC}}$ %	99.5	106.5	108.7	102.7	108.4	115.7	107.7	93.0	100.2	103.5
POROSITY (n) cm^3/gm	0.265	0.284	0.290	0.274	0.289	0.308	0.287	0.248	0.267	0.276
$\frac{n}{n_{AC}}$ %	99.5	106.5	108.7	102.7	108.4	115.7	107.7	93.0	100.2	103.5

*C indicates that the sample was taken from the zone near the center

E indicates that the sample was taken from the zone near the edges

TABLE 3

Effect of Sample Extrusion from the Sampler

Remarks:
Height and dia. given here were measured after extrusion. Teflon extruder was used.

As Compacted Properties (AC)

w	γ_d	e	n	S
21.43	99.47	0.74	0.27	80

	TOP LAYER					NEXT TO TOP LAYER				
SAMPLE NO.	1C*	2E	3C	4E	5E	6C	7E	8C	9E	10E
DIAMETER mm	8.06	8.15	8.10	8.15	8.15	8.11	8.06	8.19	8.12	8.05
HEIGHT mm	5.93	6.37	5.73	5.47	7.26	10.40	5.64	7.65	8.67	8.28
WET WEIGHT gm	0.6190	0.6405	0.5769	0.5562	0.7190	1.0063	0.5645	0.8157	0.8822	0.8400
SAMPLE VOL cm^3	0.303	0.332	0.295	0.278	0.379	0.537	0.288	0.403	0.449	0.422
VOID VOL cm^3	0.119	0.142	0.124	0.113	0.165	0.238	0.120	0.161	0.187	0.172
VOID RATIO (e)	0.644	0.745	0.722	0.684	0.772	0.796	0.715	0.662	0.712	0.688
$\frac{e}{e_{AC}}$ %	87.3	101.1	97.9	92.7	104.70	107.9	96.9	89.81	96.5	93.2
POROSITY (n) cm^3/gm	0.233	0.269	0.261	0.247	0.279	0.287	0.258	0.239	0.257	0.248
$\frac{n}{n_{AC}}$ %	87.3	101.0	97.8	92.7	104.7	107.9	96.9	89.8	96.5	93.2

*C indicates that the sample was taken from the zone near the center

E indicates that the sample was taken from the zone near the edges

TABLE 4

Cumulative Losses

	TOP LAYER					NEXT TO TOP LAYER				
Sample No.	1C*	2E*	3C	4E	5E	6C	7E	8C	9E	10E
DIA. LOSS mm	0.10	0.03	0.08	0.13	0.03	0.07	0.12	0.01	0.06	0.13
DIA. LOSS AS PERCENT OF ORIGINAL %	1.47	0.37	0.98	1.59	0.37	0.86	1.47	0.12	0.73	1.59
HEIGHT LOSS mm	0.14	0.10	0.15	0.06	0.06	0.15	0.09	0.13	0.01	0.10
HEIGHT LOSS AS PERCENT OF ORIGINAL %	2.31	1.55	2.55	1.08	0.82	1.42	1.57	1.67	0.12	1.19
WEIGHT LOSS gm	None	None	None	None	None	None	None	None	None	None
SAMPLE VOL. LOSS cm^3	0.016	0.008	0.014	0.012	0.006	0.017	0.013	0.006	0.007	0.019
SAMPLE VOL. LOSS AS PERCENT OF ORIGINAL %	5.14	2.29	4.43	4.21	1.53	3.10	4.45	1.42	1.58	4.29
VOID VOL. LOSS cm^3	0.016	0.008	0.014	0.012	0.006	0.017	0.013	0.006	0.007	0.019
VOID VOL. LOSS AS PERCENT OF ORIGINAL %	10.1	5.1	10.0	9.7	3.5	6.7	10.0	3.5	3.7	10.0
VOID RATIO LOSS	0.089	0.041	0.080	0.074	0.028	0.056	0.080	0.024	0.027	0.076
$\frac{e}{e_{AC}}$ LOSS %	12.1	5.48	10.9	10.0	3.8	7.8	10.8	3.3	3.7	10.3
POROSITY LOSS cm^3/gm	0.032	0.015	0.029	0.027	0.010	0.021	0.029	0.009	0.010	0.027
$\frac{n}{n_{AC}}$ LOSS %	12.1	5.5	10.9	10.0	3.8	7.8	10.8	3.3	3.7	10.3

*C indicates that the sample was taken from the zone near the center
E indicates that the sample was taken from the zone near the edges

Quality Control

Table 5 presents a typical set of data of the samples obtained by the Standard Proctor compaction (compaction cylinder No. 3, Table 1). The heights and diameters recorded in this table are the average values of two or three measurements obtained after extrusion from the sampler. It was assumed, for these preliminary computations, that the water content of the samples was the same as that of the cylinder at the time of compaction. Samples with a void ratio equal to or greater than 90 percent expressed as percent of the as-compacted void ratio of the cylinder were selected for freeze drying. At least one sample from each layer was oven dried at 105°C for at least 24 hours, to obtain a water content closely approximating that of the companion sample from that layer which entered the freeze drying. Samples Nos. 1, 13, 21 and 26 gave water contents of 19.1%, 17.7%, 18.2% and 19.5%, respectively. These water contents were used to obtain the weights of solids of the individual samples from the respective layers, and subsequently the properties of the samples as they entered freeze drying. In addition, soil trimmed in the vicinity of the sampling area from all the layers was dried at 105°C to obtain the average water content of the sampling region and the comparable values of 'as trimmed' void ratio and porosity used in Table 6. Also in this Table are the final values of the samples as they entered the freeze-drying process. In general, water content of the individual samples is found to be lower than the gross water content of the compacted cylinder. The as trimmed water content from the sampling region is also found to be lower than the compacted water content of the cylinder.

It is also observed that the samples from the top layer were

TABLE 5

Preliminary Computations for Selection of Samples

As Compacted Properties (AC)

e	n	w	γ_d
0.73	0.26	21.37	100.11

SAMPLE NO.	DIAMETER mm	HEIGHT mm	SAMPLE WT. gm	SAMPLE VOL. cm^3	VOID VOL. cm^3	VOID RATIO (e)	$\frac{e}{e_{AC}}$ %	POROSITY cm^3/gm	$\frac{n}{n_{AC}}$ %	SELECTED FOR
1C	6.14	9.73	1.0346	0.538	0.193	0.645	88.5	0.232	88.6	OD*
2E	6.11	8.64	0.8492	0.446	0.156	0.776	106.8	0.280	106.9	FD
3C	6.19	8.52	0.9457	0.451	0.181	0.726	99.3	0.261	99.4	FD
4E	6.17	9.55	0.9758	0.500	0.204	0.814	111.8	0.294	112.4	FD
5C	6.04	8.59	0.8763	0.457	0.175	0.672	92.4	0.242	92.5	AD
6E	6.06	7.38	0.6734	0.477	0.171	0.855	117.6	0.308	117.8	FD
7C	6.10	8.74	0.8803	0.458	0.168	0.734	98.6	0.259	98.7	FD
8C	6.12	8.64	0.8446	0.450	0.164	0.691	95.1	0.249	95.2	AD
9A	6.14	6.60	0.6518	0.345	0.125	0.737	100.3	0.264	100.5	FD
10C	6.13	7.40	0.7336	0.384	0.140	0.734	104.0	0.273	104.2	FD
11E	6.12	8.90	0.8812	0.464	0.169	0.733	101.7	0.272	103.8	FD
12C	6.15	8.37	0.8312	0.438	0.154	0.741	102.0	0.265	102.1	FD
13E	6.15	8.84	0.8803	0.463	0.170	0.750	103.4	0.271	103.5	FD
14C	6.14	8.39	0.8362	0.437	0.160	0.734	104.0	0.273	104.1	FD
15E	6.15	8.94	0.9181	0.466	0.171	0.708	97.4	0.256	97.6	FD
16C	6.11	7.40	0.7346	0.385	0.141	0.644	88.5	0.231	88.3	FD
17E	6.16	8.44	0.9030	0.441	0.173	0.644	88.4	0.232	88.7	FD
18C	6.22	8.32	0.9079	0.473	0.175	0.662	91.0	0.239	91.6	FD
19E	6.19	9.15	0.9908	0.480	0.183	0.713	97.1	0.258	97.2	AD
20E	6.17	8.79	0.9607	0.464	0.167	0.623	85.8	0.225	85.9	AD
21C	6.15	9.76	1.0452	0.509	0.174	0.607	83.4	0.219	83.7	OD
22E	6.21	10.55	1.1517	0.559	0.201	0.665	91.6	0.240	86.1	FD
23E	6.17	9.86	1.0791	0.517	0.194	0.611	84.0	0.220	84.1	AD
24C	6.19	8.52	0.9150	0.438	0.166	0.611	84.0	0.220	84.1	AD
25C	6.19	11.43	1.2269	0.607	0.233	0.633	87.1	0.228	87.2	AD
26C	6.20	11.57	1.2707	0.611	1.1.1	0.617	84.9	0.223	85.0	OD
27E	6.20	11.12	1.1951	0.587	0.201	0.666	91.7	0.241	91.8	FD
28E	6.23	10.56	1.1440	0.561	0.200	0.647	89.1	0.234	89.2	FD
29E	6.22	10.19	1.0954	0.541	0.194	0.655	90.2	0.237	90.3	FD

* OD stands for oven drying
FD stands for freeze drying
AD stands for air drying

TABLE 6

Samples Entering Freeze-Drying

As Compacted Properties (AC)

e	n	w	γ_d
0.71	0.25	20.29	101.00

SAMPLE NO.	DIAMETER mm	HEIGHT mm	SAMPLE WT. gm	SAMPLE VOL. cm^3	VOID VOL. cm^3	VOID RATIO (e)	$\frac{e}{e_{AC}}$ %	POROSITY cm^3/gm	$\frac{n}{n_{AC}}$ %	SELECTED FOR
1C	6.14	9.73	1.0346	0.506	0.193	0.614	86.4	0.222	88.5	OD*
2E	6.13	8.64	0.9497	0.449	0.191	0.747	104.4	0.268	104.5	FD
3C	6.19	8.20	0.8457	0.433	0.177	0.659	96.9	0.249	97.0	FD
4E	6.17	9.55	0.9258	0.500	0.220	0.784	110.2	0.283	110.4	FD
5C	6.04	8.59	0.8763	0.436	0.170	0.638	89.7	0.230	89.8	AD
6E	6.06	7.28	0.6734	0.372	0.167	0.810	115.2	0.296	115.4	FD
7C	6.10	8.74	0.8853	0.450	0.183	0.684	96.2	0.247	96.3	FD
8C	6.12	8.69	0.8949	0.450	0.175	0.639	89.8	0.231	89.9	AD
9E	6.14	6.65	0.6911	0.346	0.146	0.732	103.0	0.264	103.1	FD
10C	6.13	7.40	0.7350	0.384	0.156	0.704	98.7	0.253	98.8	FD
11E	6.12	8.90	0.9239	0.461	0.190	0.699	98.3	0.252	98.5	FD
12C	6.11	8.27	0.8331	0.431	0.170	0.688	96.7	0.248	96.8	FD
13E	6.13	8.84	0.8853	0.461	0.180	0.699	98.1	0.252	98.2	FD
14C	6.14	8.30	0.8362	0.437	0.181	0.704	98.9	0.254	99.0	FD
15E	6.15	8.94	0.9181	0.466	0.185	0.656	92.2	0.237	92.3	FD
16C	6.11	7.46	0.7596	0.389	0.144	0.599	84.2	0.216	84.3	FD
17E	6.16	8.44	0.8830	0.441	0.166	0.601	84.5	0.217	84.6	FD
18C	6.12	8.92	0.9574	0.473	0.181	0.619	87.0	0.223	87.1	FD
19E	6.19	9.15	0.9426	0.482	0.179	0.591	83.0	0.213	83.1	AD
20E	6.17	8.94	0.9360	0.477	0.168	0.569	80.0	0.205	80.1	AD
21C	6.15	9.76	1.0057	0.509	0.194	0.566	79.6	0.204	79.7	OD
22E	6.21	10.55	1.0557	0.535	0.196	0.583	82.0	0.211	82.1	FD
23C	6.17	9.08	1.0731	0.517	0.186	0.569	80.0	0.205	80.1	AD
24C	6.19	9.34	0.9915	0.496	0.177	0.550	80.4	0.210	80.5	AD
25C	6.19	11.43	1.2399	0.632	0.228	0.608	85.5	0.219	85.6	AD
26C	6.20	11.37	1.2797	0.644	0.237	0.582	81.8	0.214	81.9	OD
27E	6.20	11.12	1.1851	0.597	0.214	0.641	90.1	0.231	90.2	FD
28E	6.22	10.56	1.1440	0.565	0.214	0.602	87.3	0.225	87.4	FD
29E	6.22	10.19	1.0484	0.541	0.210	0.630	88.6	0.226	88.7	FD

* OD stands for oven drying
FD stands for freeze drying
AD stands for air drying

generally denser than the samples recovered from the other two layers.

Cumulative Pore Size Distributions

Figure 19 shows a typical 'average' cumulative pore size distribution obtained by mercury porosimetry after freeze drying. Individual curves were obtained from replicate samples representing all the methods of compaction, and for all of the moisture content levels. The average cumulative curves were obtained from the 'band' of the replicate curves for a given condition. A typical band of curves, that for the average curve of Figure 19, is shown in Figure 20.

The procedure of obtaining the average cumulative curve from such a band of curves was as follows. Every curve was divided into various diameter groups, the number of groups ranging from 21 to 32 depending upon the nature of the slope of the curves. The increase in penetration ('Δ penetration') was obtained for each run as the curve advanced from the upper to the lower boundary of the diameter group. The Δ penetration for all the replicate runs was then averaged. The average cumulative penetration for the lower boundary of a particular diameter group was obtained by simply adding the average cumulative penetration for the preceding diameter; the average cumulative penetration for the lower boundary of the first diameter group was the Δ penetration for that group.

The largest diameter penetrated was defined by the filling pressure of 20 mm of mercury. This limited the largest measurable pore diameter to approximately 600 microns. The existence of porosity in such high diameter ranges is indicated by the data of Table 7 for the samples of kneading compaction at 21.4% water content. In these runs, mercury was filled at a pressure of 10 mm of mercury. Filling of mercury at low

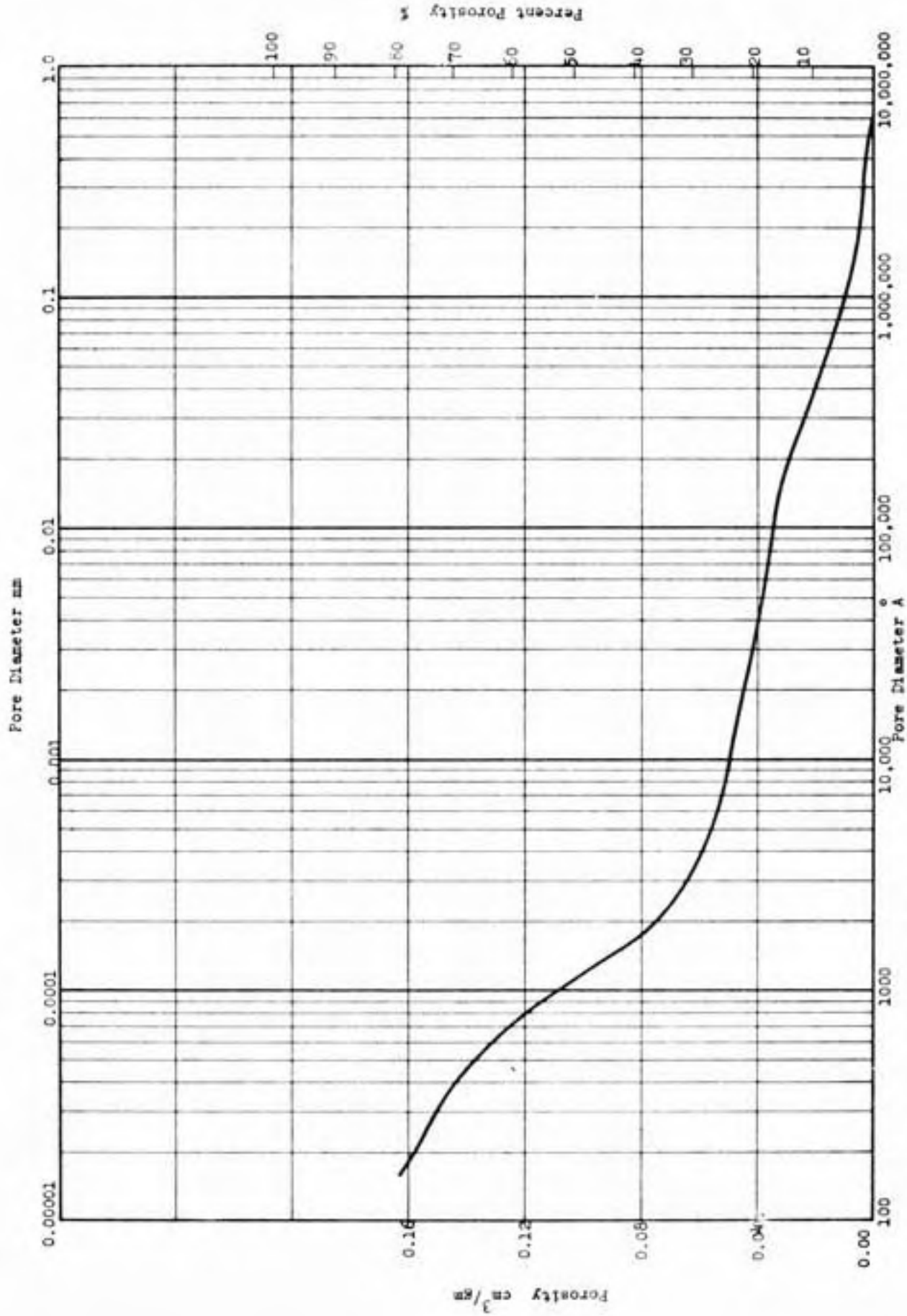

Figure 19 - Average Cumulative Pore Size Distribution

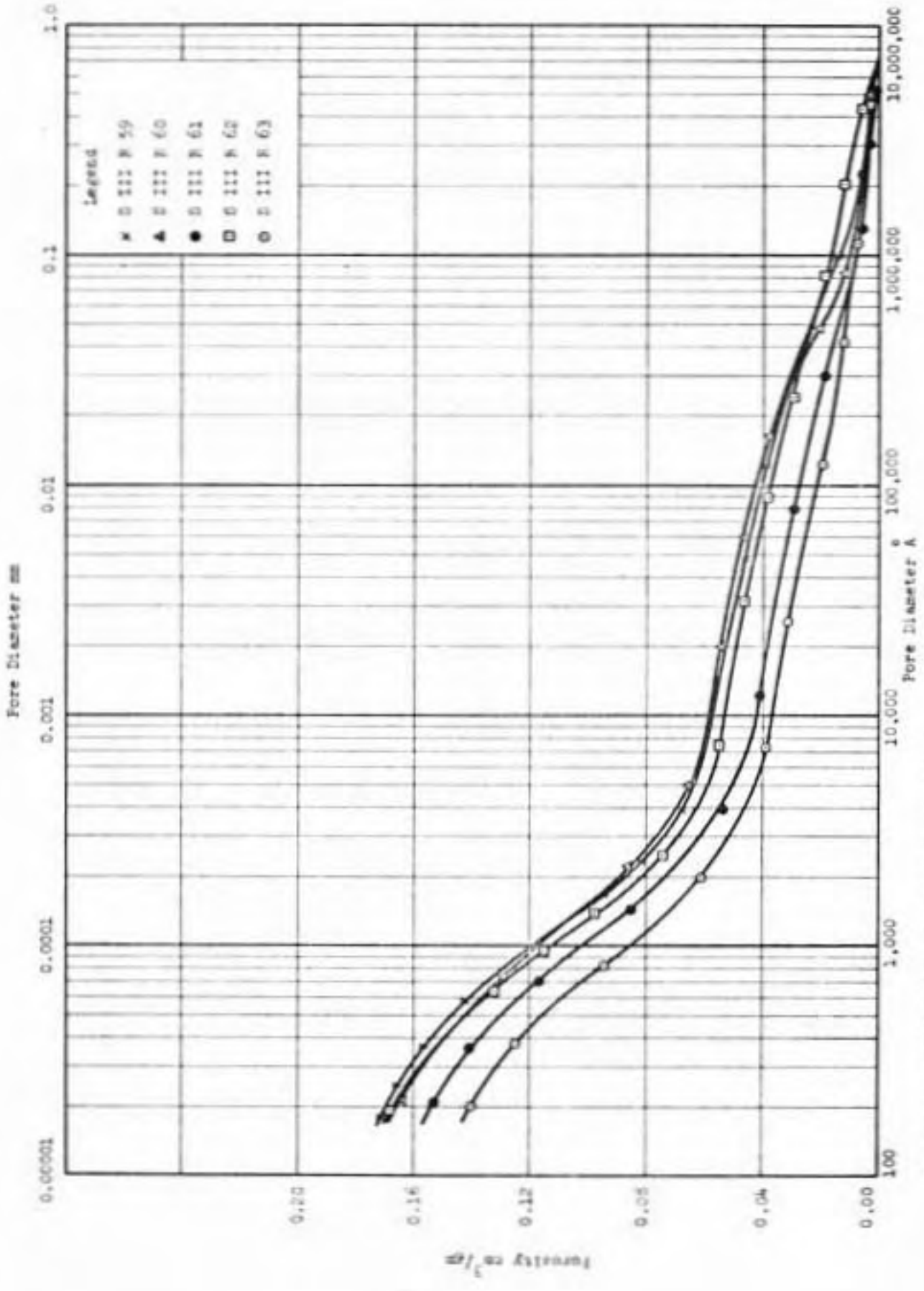

Figure 20 - Typical Pore Size Distribution Band

TABLE 7

Porosity in Very Large Pores

Filling Pressure = 10 mm Hg

PROPERTY SAMPLE AND RUN NUMBER	BOUNDING PORE DIAMETERS μ	POROSITY cm^3/gm	PERCENT POROSITY %
SIII R49	1218	-	-
	609	0.0020	1.1
SIII R50	1218	-	-
	609	0.0087	4.1
SIII R51	1218	-	-
	609	0.0014	0.2
SIII R52	1218	-	-
	609	0.0068	4.3

pressure requires a very high vacuum to be present initially in the penetrometer, otherwise the correction for trapped air becomes large. The smallest diameter measured depended on the highest pressure attainable by the porosimeter, this diameter being about 160 Å. It can be seen from Figures 19 and 20 that only about eighty percent of the cumulative voids were penetrated in the pressure range of the equipment available. Nevertheless, the method was adequate to produce a distribution covering five orders of magnitude of pore diameter.

Measurements of Porosity

Total porosity was obtained in the penetrometer after freeze drying as part of the pore size determinations. Such values of porosity are referred to by the abbreviation PAFD. In addition, porosity was independently obtained from weight and volume measurements before and after freeze drying, micrometer measurements being used to obtain the volume of the samples. These values of porosity are referred to by the abbreviations MBFD and MAFD for the before and after freeze drying conditions respectively. Tables 8 through 19 give the various measurements of porosity.

Examination of the Tables shows that the ratio of PAFD to MBFD values for the samples of regular geometric shapes (Tables 14 through 19) was always less than the ratio of MAFD to MBFD values. In one extreme case, the discrepancy is of the order of 10%. The major reason for this discrepancy is presumably the existence of pore diameters large enough to be penetrated at the lowest filling pressure.

The porosity associated with such large pores would be masked by

the filling operation of the penetrometer and thus the porosity measured by the penetrometer would be underestimated. Table 7 gives results of using a filling pressure of half the value used for all the runs reported in Tables 14 through 19. If the ratio of PAFD to the gross as-compacted (AC) porosity is assumed similar to the ratio of PAFD to MBFD, then one may infer that the maximum percentage of the pores larger than the smallest measurable at the filling pressure is obtained at different compaction moisture contents for the different methods of compaction. The apparent maximum amount of inferred 'large' pores is not always obtained on the dry side. Note that the assumption may not be good when absolute magnitudes are in question, because small cylindrical samples, several orders of magnitude smaller than the large compacted cylinders depart in their porosity from that of the gross as-compacted porosity. However, for purely relative comparisons, the assumption should not be too erroneous. It is found that the lowest ratio of PAFD to AC, i.e., largest percentage of the inferred large pores, was obtained at the driest compaction water content (15.6%), for the Standard Proctor compaction, but at the optimum water content (21.4%) for the kneading compaction, and on the wet side of optimum (26.1%) for the static compaction. When these ratios are plotted (Figure 21) the trend for the kneading and the Standard Proctor compaction seem to be alike, but static compaction differs from both. This indication that the statically compacted samples behave differently is intensified when the ratios of porosity before and after freeze drying (both obtained by micrometer measurements) are plotted. Thus, the content of large pores (larger than 609 microns) that is inferred to be present varies differently with moisture content

TABLE 8

Measurements of Porosity

Standard Proctor (Dry Side)

w = 12.9%
FD
w = 15.6%
GAC

SERIES NO.	RUN No.	POROSITY (n) PAFD cm^3/gm	POROSITY (n) PAFD ÷ AC %
S III	R 77	0.24	83
S III	R 78	0.27	93
S III	R 79	0.20	69
S III	R 82	0.22	76
S III	R 89	0.24	83
S III	R 90	0.22	76
AVG.		0.23	80

TABLE 9

Measurements of Porosity

Kneading Compaction (Dry Side)

w = 15.3%
FD
w = 16.2%
GAC

SERIES NO.	RUN NO.	POROSITY (n) PAFD cm^3/gm	POROSITY (n) PAFD ÷ AC %
S III	R 70	0.26	90
S III	R 71	0.25	86
S III	R 72	0.25	86
S III	R 73	0.26	90
S III	R 74	0.22	76
S III	R 81	0.22	76
AVG.		0.24	84

TABLE 10

Measurements of Porosity

Static Compaction (Dry Side)

w = 15.5%
FD
w = 15.6%
CAC

SERIES NO.	RUN NO.	POROSITY (n) PAFD cm^3/gm	POROSITY (n) PAFD ÷ AC %
S III	R 64	0.26	90
S III	R 65	0.27	93
S III	R 66	0.24	83
S III	R 67	0.25	86
S III	R 68	0.25	86
S III	R 69	0.24	83
AVG.		0.25	87

TABLE 11

Measurements of Porosity

Standard Proctor (Near OMC)

w = 20.2%

GAC

SERIES NO.	RUN NO.	POROSITY (n) PAFD cm^3/gm	POROSITY (n) PAFD ÷ AC %
S II	R 26	0.25	95
S II	R 34	0.26	98
S II	R 17	0.22	84
S II	R 18	0.22	85
S II	R 19	0.23	87
S II	R 20	0.23	87
S II	R 61	0.24	92
S II	R 62	0.22	85
AVG.		0.24	89

TABLE 12

Measurements of Porosity

Kneading Compaction (Near OMC)

w = 19.4%

GAC

SERIES NO.	RUN NO.	POROSITY (n) PAFD cm^3/gm	POROSITY (n) PAFD ÷ AC %
S II	R 24	0.22	89
S II	R 25	0.20	81
S II	R 33	0.21	84
S II	R 31	0.23	94
S II	R 32	0.23	95
AVG.		0.22	89

TABLE 13

Measurements of Porosity

Static Compaction (Near OMC)

w = 19.4%

GAC

SERIES NO.	RUN NO.	POROSITY (n) PAFD cm^3/gm	POROSITY (n) PAFD ÷ AC %
S II	R 23	0.22	86
S II	R 27	0.23	87
S II	R 28	0.22	84
S II	R 29	0.22	89
S II	R 30	0.22	84
AVG.		0.22	85

Measurements of Porosity

TABLE 14

Standard Proctor (OMC)

w = 17.27%
FD

w = 21.37%
GAC

SERIES & RUN NO.	MBPD cm^3/gm	MAPD cm^3/gm	PAPD cm^3/gm	MAPD : MBPD %	PAPD : MBPD %
S III R 43	0.25	0.21	0.19	84	76
S III R 44	0.27	0.24	0.21	89	78
S III R 45	0.25	0.22	0.21	88	84
S III R 46	0.25	0.24	0.22	96	88
S III R 47	0.22	0.20	0.18	91	82
AVG.	0.25	0.22	0.20	90	82

TABLE 15

Kneading Compaction (OMC)

w = 17.35%
FD

w = 21.43%
GAC

SERIES & RUN NO.	MBPD cm^3/gm	MAPD cm^3/gm	PAPD cm^3/gm	MAPD : MBPD %	PAPD : MBPD %
S III R 51	0.29	0.20	0.18	69	62
S III R 53	0.24	0.21	0.20	88	74
S III R 54	0.25	0.23	0.20	92	80
S III R 55	0.24	0.21	0.19	88	79
S III R 56	0.25	0.22	0.20	88	80
S III R 57	0.26	0.24	0.20	92	77
S III R 58	0.27	0.24	0.22	89	81
AVG.	0.26	0.22	0.20	86	76

TABLE 16

Static Compaction (OMC)

w = 17.64%
FD

w = 21.38%
GAC

SERIES & RUN NO.	MBPD cm^3/gm	MAPD cm^3/gm	PAPD cm^3/gm	MAPD : MBPD %	PAPD : MBPD %
S III R 59	0.25	0.23	0.22	92	88
S III R 60	0.25	0.23	0.22	92	88
S III R 61	0.26	0.23	0.21	88	81
S III R 62	0.26	0.24	0.22	92	85
S III R 63	0.25	0.23	0.19	92	76
AVG.	0.25	0.23	0.21	91	83

Measurements of Porosity

TABLE 17

Standard Proctor (Wet Side)

w = 22.05% FD

w = 26.05% GAC

SERIES & RUN No.	POROSITY (n)				
	MBFD cm^3/gm	MAFD cm^3/gm	PAFD cm^3/gm	MAFD ÷ MBFD %	PAFD ÷ MBFD %
S III R 6	0.26	0.24	0.23	92	88
S III R 7	0.25	0.25	0.23	100	92
S III R 8	0.26	0.25	0.23	96	88
S III R 9	0.27	0.25	0.23	93	85
S III R 10	0.27	0.24	0.23	89	85
S III R 11	0.27	0.25	0.23	93	85
AVG.	0.2	0.25	0.23	94	87

TABLE 18

Kneading Compaction (Wet Side)

w = 21.36% FD

w = 26.23% GAC

SERIES & RUN NO.	POROSITY (n)				
	MBFD cm^3/gm	MAFD cm^3/gm	PAFD cm^3/gm	MAFD ÷ MBFD %	PAFD ÷ MBFD %
S III R 19	0.26	0.22	0.23	85	88
S III R 20	0.27	0.26	0.24	96	89
S III R 24	0.27	0.24	0.23	89	85
S III R 25	0.26	0.23	0.23	88	88
S III R 26	0.24	0.23	0.22	92	92
AVG.	0.26	0.24	0.23	90	89

TABLE 19

Static Compaction (Wet Side)

w = 22.58% FD

w = 26.05% GAC

SERIES & RUN NO.	POROSITY (n)				
	MBFD cm^3/gm	MAFD cm^3/gm	PAFD cm^3/gm	MAFD ÷ MBFD %	PAFD ÷ MBFD %
S III R 12	0.29	0.27	0.25	86	86
S III R 13	0.29	0.25	0.23	93	79
S III R 14	0.29	0.27	0.23	86	79
S III R 15	0.26	0.23	0.23	88	88
S III R 16	0.29	0.24	0.23	83	79
AVG.	0.28	0.25	0.23	87	82

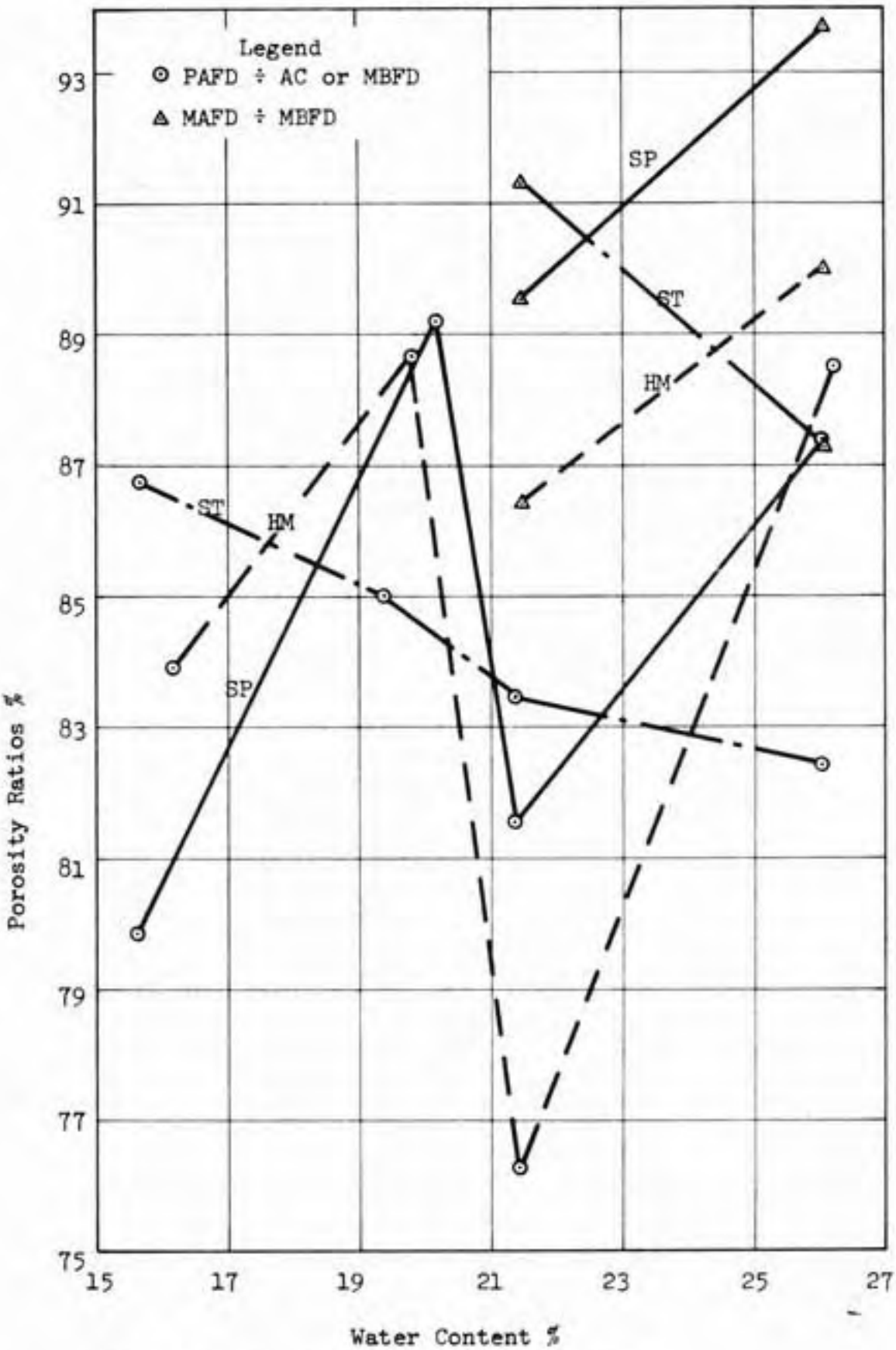

Figure 21 - Variation of Porosity Ratios

for various methods of compaction, i.e., the static compaction differing considerably from the Standard Proctor and kneading compaction methods.

Examination of average values of porosity obtained by micrometer measurements before and after freeze drying indicates that, apparently some shrinkage has been produced by the freeze drying, but it is small enough to be tolerated.

Influence of Molding Water Content on Pore Size Distribution

Average cumulative pore size distribution curves are plotted in Figures 22, 23 and 24 for the Standard Proctor, kneading and static compactions at four different molding water contents. These water contents are 'dry', 'near optimum', 'at optimum' and 'wet of optimum' as defined by the Standard Proctor method (Table 1). It is seen from Table 1 that for all the methods of compaction the total porosity for wet of optimum is the same as dry of optimum. However, it is seen from the above Figures that the distribution of the porosity for the two moisture conditions is sharply different. The distribution of porosity seems to be affected by as little as a 2% difference in the water content, even though the total porosity does not change more than 0.02 $cm^3/gm.$, e.g., compare the distribution for the near optimum and optimum water contents of Table 1.

It is convenient to study these curves in terms of three arbitrary diameter ranges: coarse, from 609 μ to 50 μ; medium, 50 μ to 0.5 μ; fine, 0.5 μ to 0.016 μ. It is found that the pore size distribution curves of the samples compacted by different methods, at one molding water content, show similar characteristics. The observations that

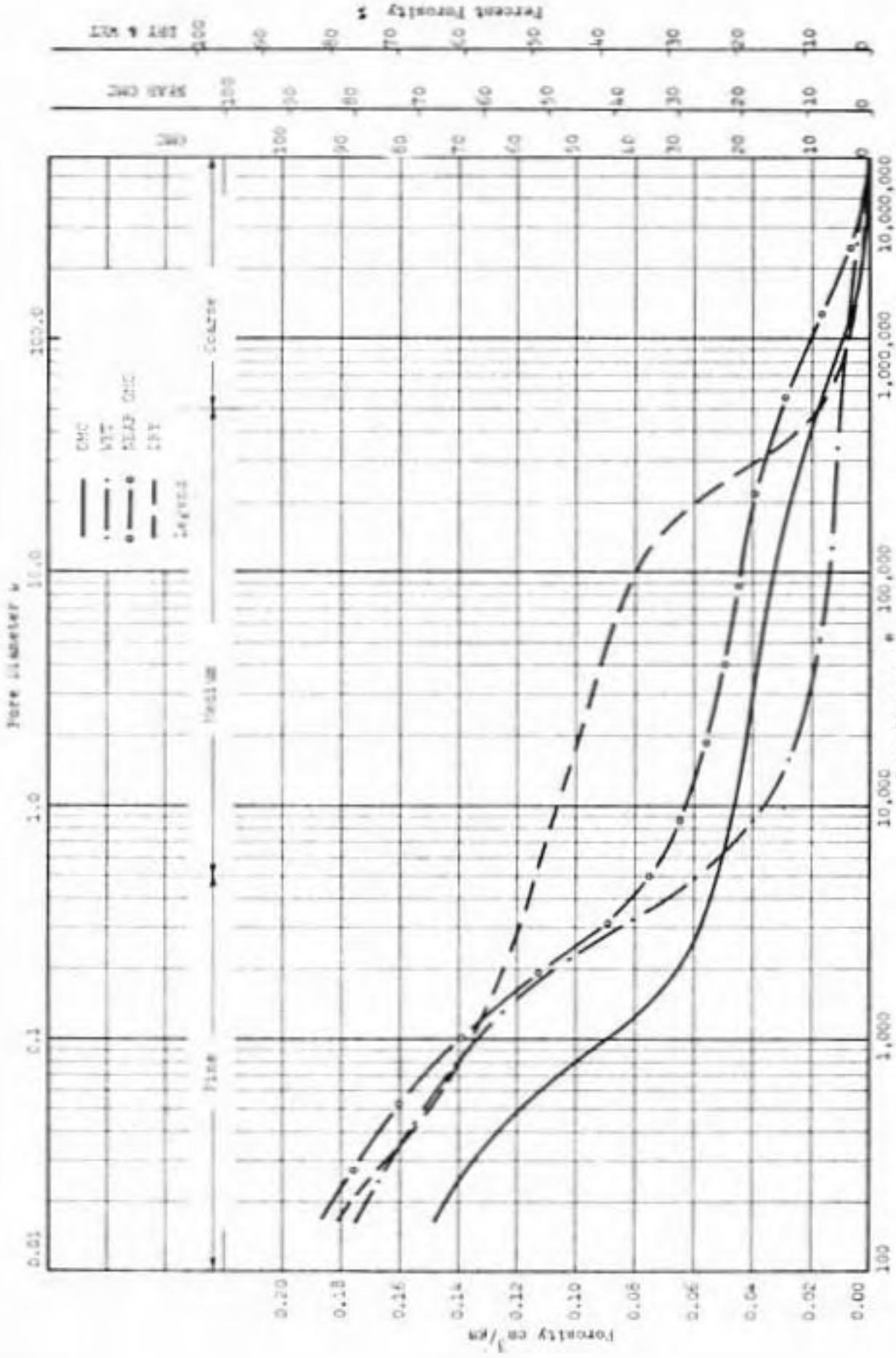

Figure 22 - Pore Size Distributions of Samples Compacted by Standard Proctor (SP) at Various Water Contents

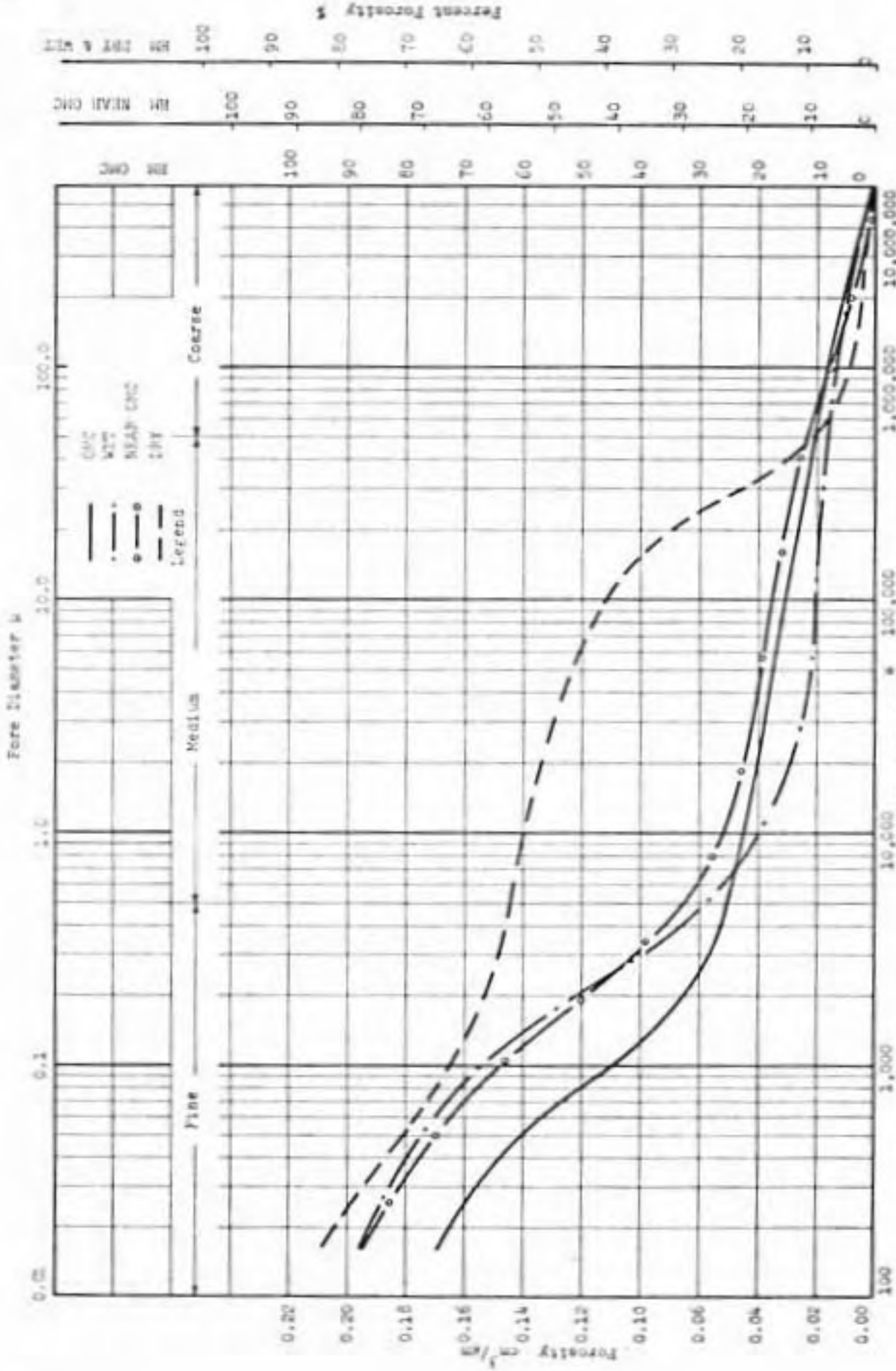

Figure 23 - Pore Size Distributions of Samples Compacted by Kneading Compaction (RM) at Various Water Contents

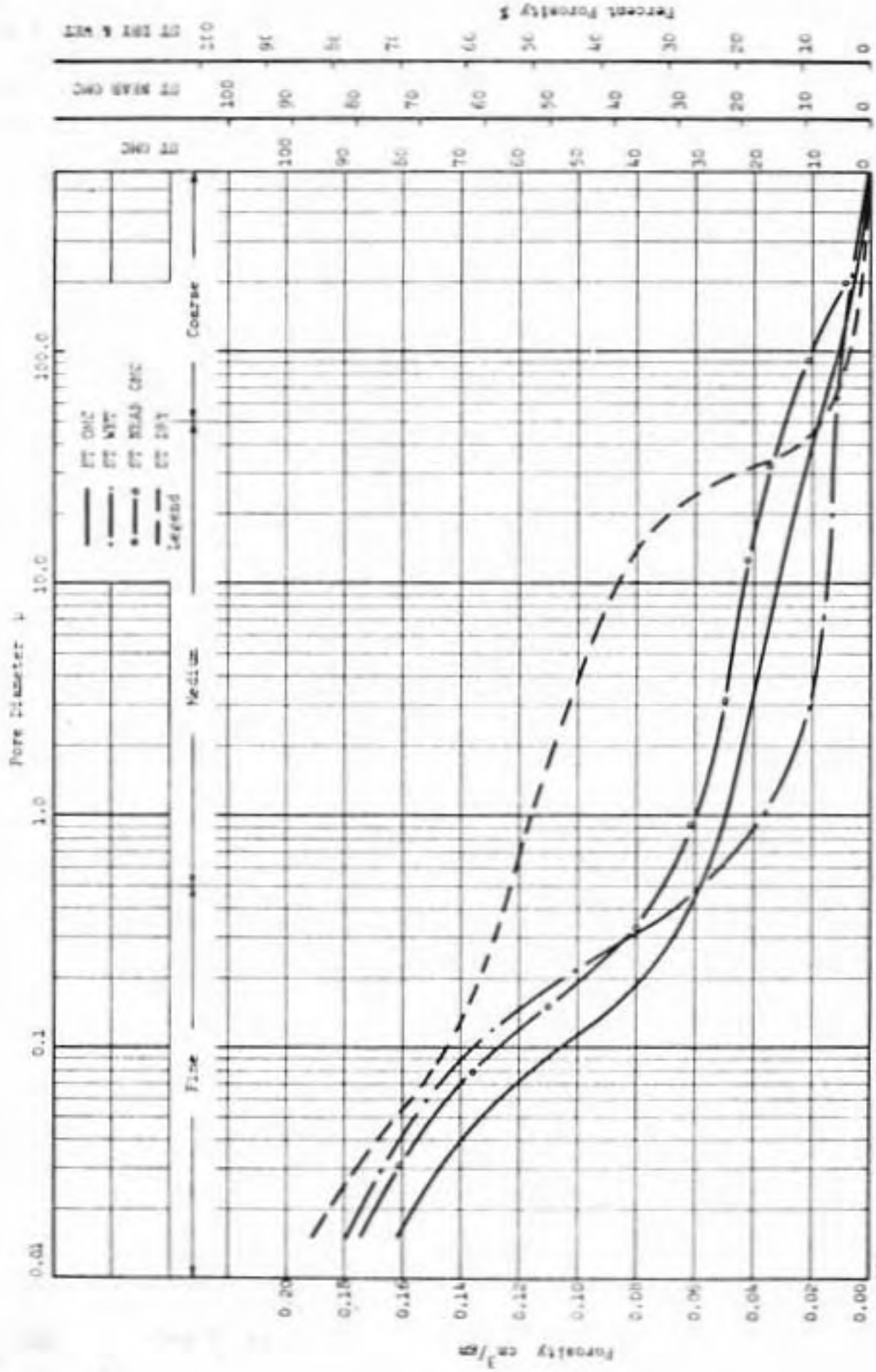

Figure 24 - Pore Size Distributions of Samples Compacted by Static Compaction (ET) at Various Water Contents

follow apply to all the methods of compaction, at given molding water contents.

The pore size distribution curves for the dry side compaction show that only a small percentage of total porosity, of the order of about 7%, is present in the coarse range. These curves take a sharp upturn as they enter the medium pore range. A large amount of total porosity, of the order of 43%, lies in this range. Porosity in the fine range is about 27% of the total porosity.

Pore size distribution curves for the samples compacted near optimum are somewhat different. Although they also show only a small percentage of total porosity (of the order of 13%) in the coarse pores the porosity in the medium range drops to 19% and in the fine range rises to 49% of the total porosity. As the molding water content is increased to optimum quite similar values of 9%, 17%, and 49% of the total porosity are obtained for the coarse, medium and fine ranges of the pore diameters, respectively. To avoid any misconceptions, it should be noted that the percentage of the total porosity which was penetrable at the smallest diameter was slightly different for the different molding water contents, being 78, 81, 76 and 79 for the dry, near optimum, at optimum and wet of optimum, respectively. Only slight differences in molding water content result in measurable changes in the pore size distribution; this sensitivity of the distribution to molding water content is shown by the two different curves for near optimum, and at optimum compaction for every method of compaction used in this study.

In the examination of the pore size distribution curves for the samples compacted wet of optimum, values of the order of 7%, 19% and 53%

of the total porosity are obtained for the coarse, medium and fine ranges of diameter. The percentage for the coarse range is about the same as was obtained for the samples compacted dry of optimum, but the percentage for the medium range is slightly less than half that obtained for the dry side samples, and the percentage for the fine range is about twice that obtained for the dry side samples. As noted before, the samples on the dry and the wet side were compacted to the same porosity, yet the distribution of porosity among the different sizes of the pores is markedly different.

Effects of Compaction Procedure on Pore Size Distribution

For only one of the types of compaction, the Standard Proctor, is the effort level held constant for all water contents. In the kneading and static compaction, the energy level was adjusted in each case so as to obtain the same dry unit weight obtained by Standard Proctor at the same molding moisture content. Thus when the pore size distribution obtained by kneading compaction at 'optimum water content' is discussed, it is the optimum water content of the Standard Proctor and not that for any defined level of kneading compactive effort.

The average cumulative curves of Figures 25, 26 and 27 compare pore size distributions with essentially constant moisture and total porosity, but for different methods of compaction. The effect of the method of compaction is very minor. In fact, the band width of these average cumulative pore size distribution curves for the various methods of compaction at any one water content is comparable to that for replicate samples prepared by the same method of compaction.

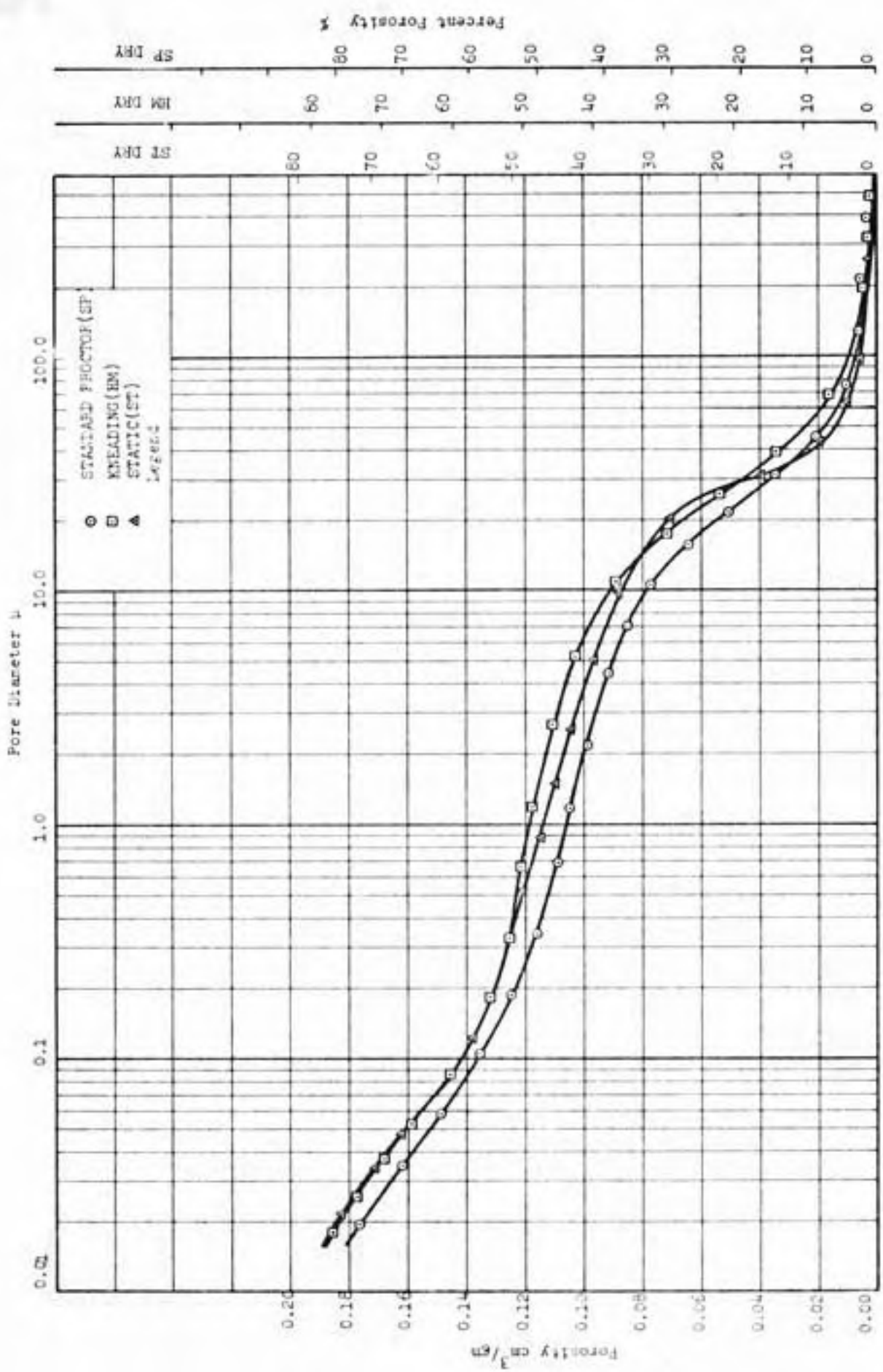

Figure 25 - Pore Size Distributions for Compaction on 'Dry Side' by Different Compaction Methods

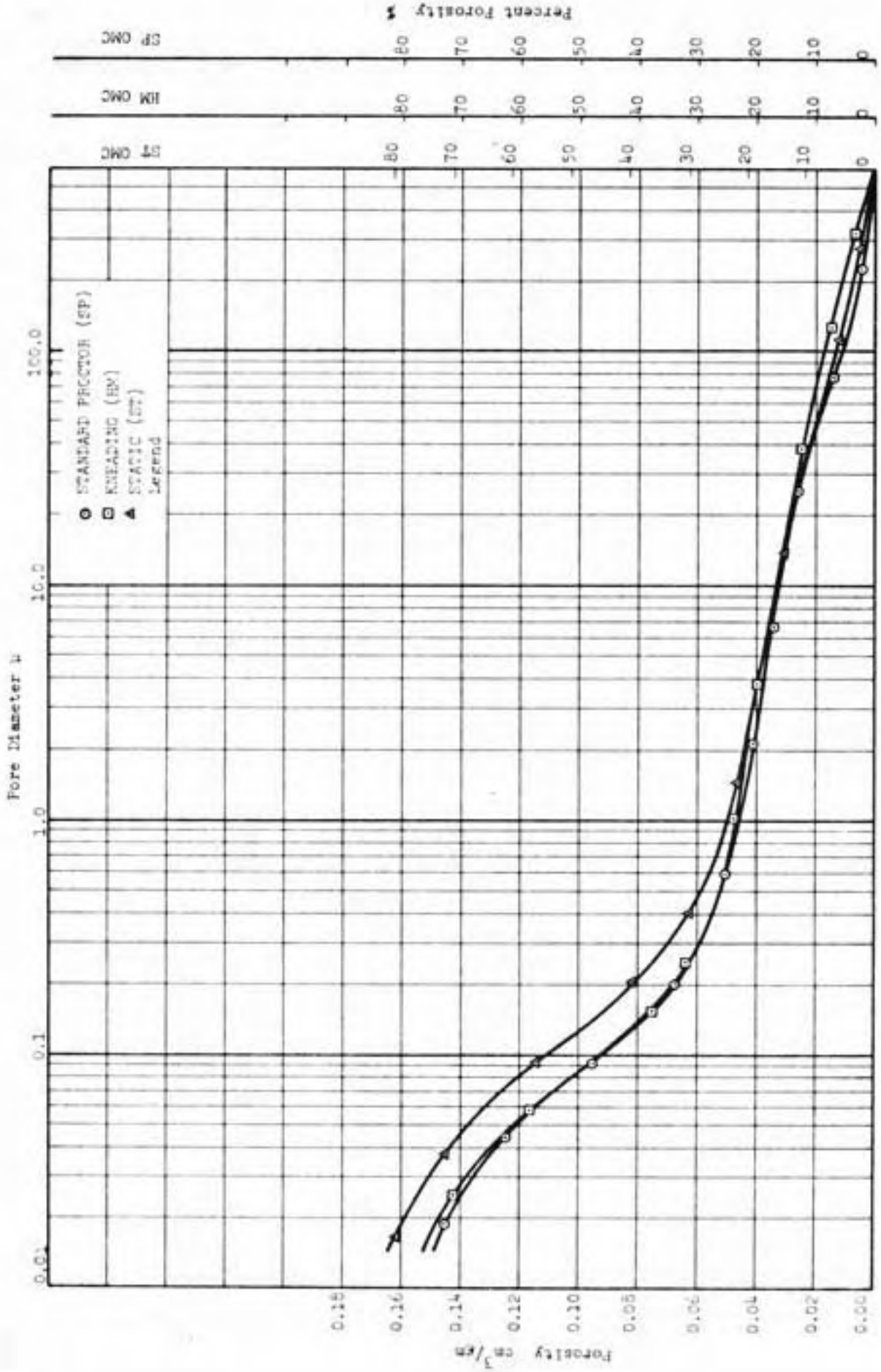

Figure 26 - Pore Size Distributions for Compaction at 'Optimum' by Different Compaction Methods

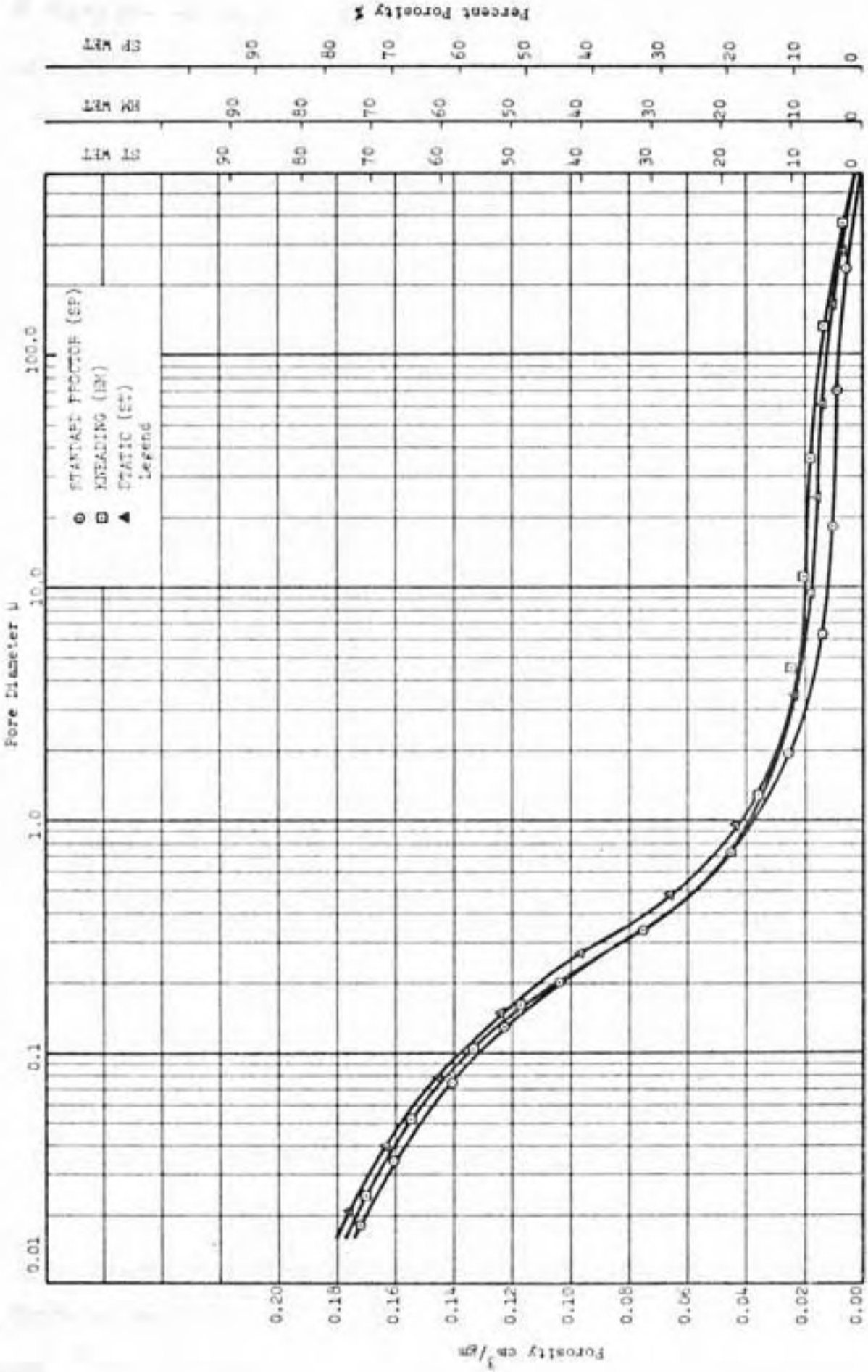

Figure 27 - Pore Size Distributions for Compaction on 'Wet Side' by Different Compaction Methods

Turning now to Table 20, it is observed (last column) that on the dry side kneading compaction provides the largest percentage of the accessible pores, with Standard Proctor closely following. At optimum water content, the static compaction procedure takes the lead with kneading and Standard Proctor following in order. On the wet side static leads by a margin of more than 7% over the Standard Proctor which in turn has a margin of about 5% over kneading compaction. Not only was the percentage of total penetration the highest for the static compaction on the wet side, but also the percentages of total penetration were the highest, compared with the other two methods, for each of the three ranges of diameters (Table 20).

Numerical representations of the cumulative pore size distribution curves are obviously helpful. The simplest of such representations is the mean pore diameter. Mean pore diameters for the various distributions are given in Table 21. An average porosity was obtained from the values of porosity for the different methods of compaction at a particular water content. The mean diameter (D_{50}) was defined as the diameter obtained at 50% of this porosity. The values of D_{50} for the various methods of compaction are close to each other on the wet side and at optimum but are farther apart for dry side compaction. Static compaction gives the highest value of D_{50} for the wet side and at optimum. Relative values of D_{50} are plotted in Figure 28.

Another way of examining the results is to represent them as frequency diagrams (differential distributions). These are plotted in Figures 29, 30 and 31. The whole diameter range was divided into about 25 divisions, histograms were plotted and the median diameters of the divisions were connected to give the frequency diagrams. These diagrams

TABLE 20

Percent of Total Porosity Penetrated

Dry Side

Compaction Method	Diameter Range			Total %
	Coarse (609-50μ)	Medium (50-0.5μ)	Fine (0.5-0.016μ)	
SP*	6.9	45.0	26.4	78.4
HM*	8.3	41.1	26.9	70.5
ST*	6.4	43.1	27.0	76.5
AVG.	7.2	43.1	26.8	77.8

Optimum

Compaction Method	Diameter Range			Total %
	Coarse (609-50μ)	Medium (50-0.5μ)	Fine (0.5-0.016μ)	
SP	8.5	17.5	48.2	74.2
HM	10.5	15.3	49.2	75.0
ST	8.1	18.6	50.8	77.5
AVG.	9.0	17.1	49.4	75.6

Wet Side

Compaction Method	Diameter Range			Total %
	Coarse (609-50μ)	Medium (50-0.5μ)	Fine (0.5-0.016μ)	
SP	7.4	18.2	52.7	78.3
HM	6.7	17.3	49.3	73.4
ST	8.1	21.9	55.6	85.6
AVG.	7.4	19.1	52.5	79.1

*SP = Standard Proctor
HM = Kneading Compaction
ST = Static Compaction

TABLE 21

Pore Diameter at 50% Porosity

Compaction Method		Molding Water Content %	Avg. Porosity n_{PAFD} cm^3/gm	D_{50} μ	$D_{50}/D_{50(SP)}$
SP*	WET	26.05	0.230	0.176	1.00
HM*	WET	26.23	0.230	0.161	0.92
ST*	WET	26.05	0.230	0.189	1.07
SP	OPTIMUM	21.37	0.203	0.078	1.00
HM	OPTIMUM	21.43	0.203	0.078	1.00
ST	OPTIMUM	21.37	0.203	0.111	1.42
SP	DRY	15.64	0.240	0.250	1.00
HM	DRY	16.15	0.240	0.940	3.76
ST	DRY	15.64	0.240	0.740	2.96

*SP: Standard Proctor
HM: Kneading Compaction
ST: Static Compaction

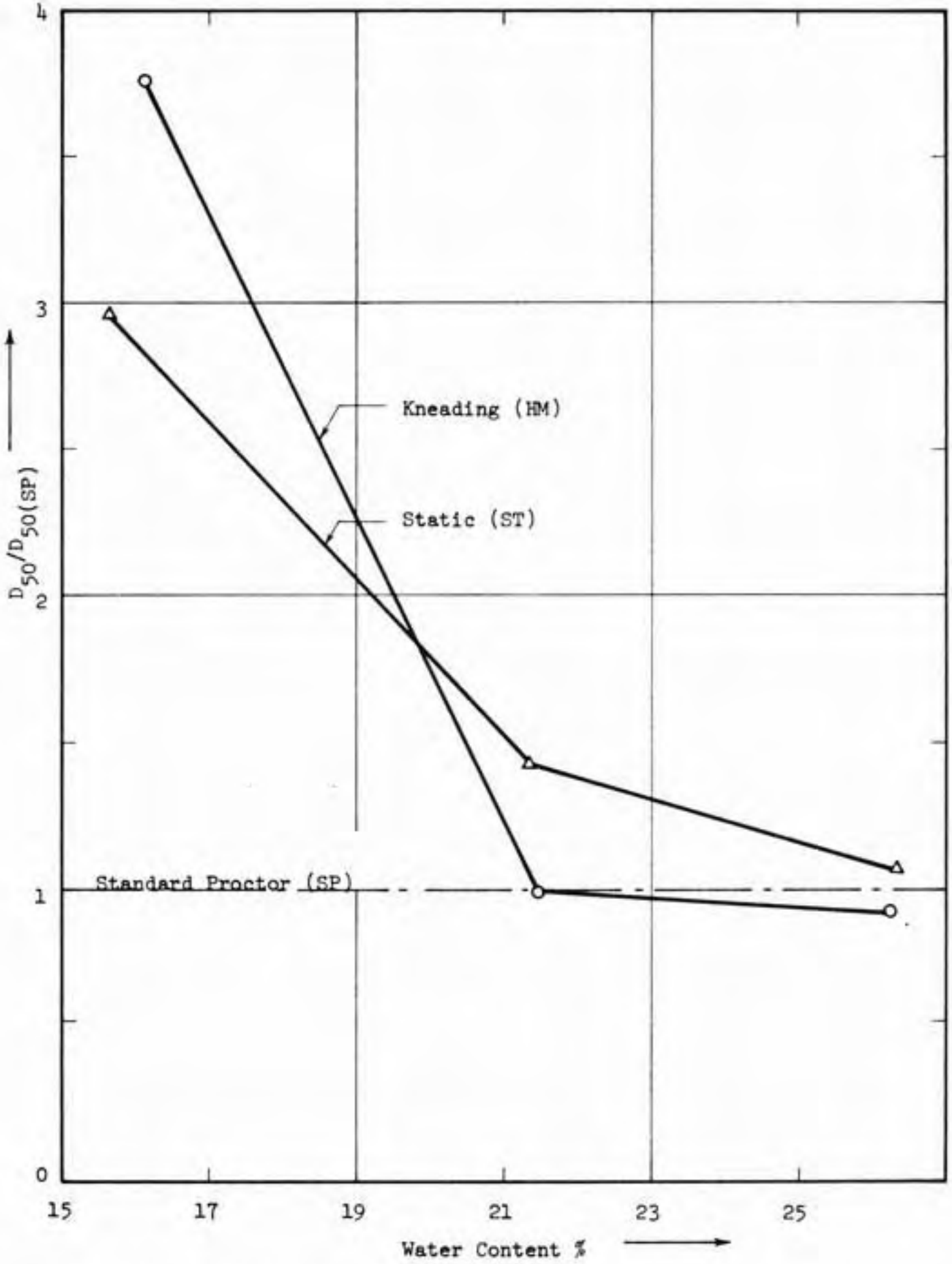

Figure 28 - Relative Values of D_{50} for Different Methods of Compaction

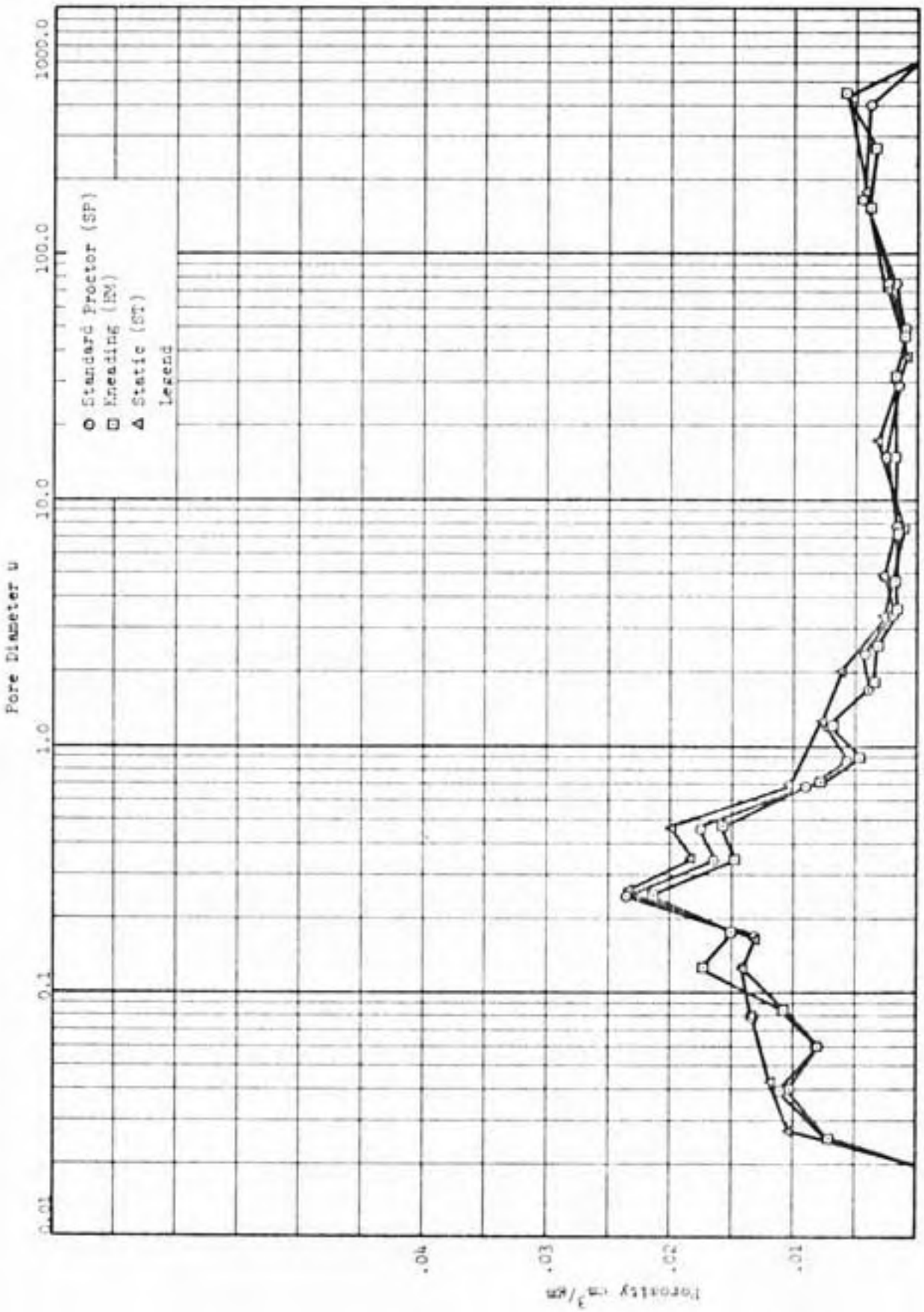

Figure 29 - Frequency Diagrams for Compaction on 'Wet Side' by Different Compaction Methods

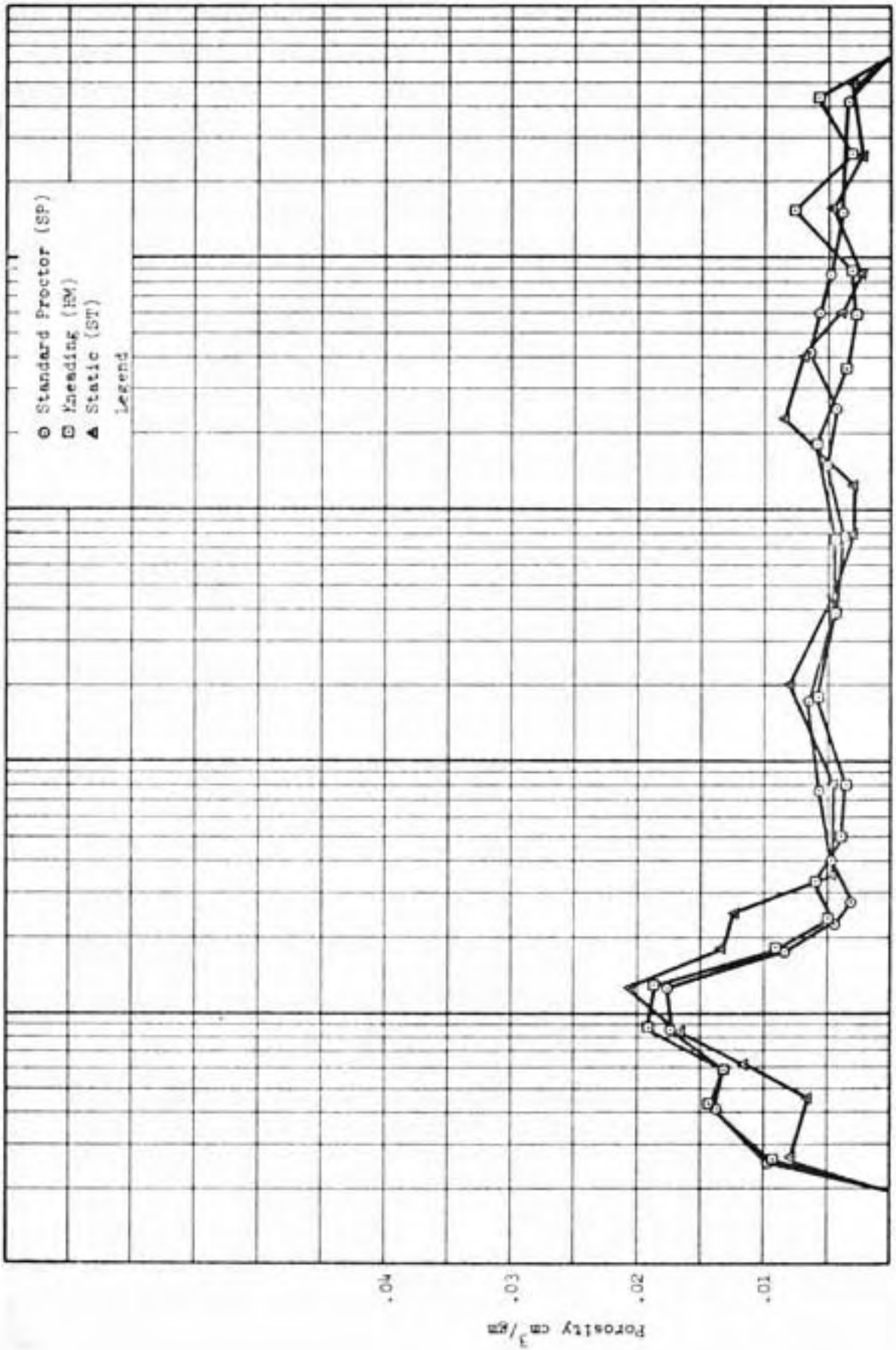

Figure 30 - Frequency Diagrams for Compaction at Optimum by Different Compaction Methods

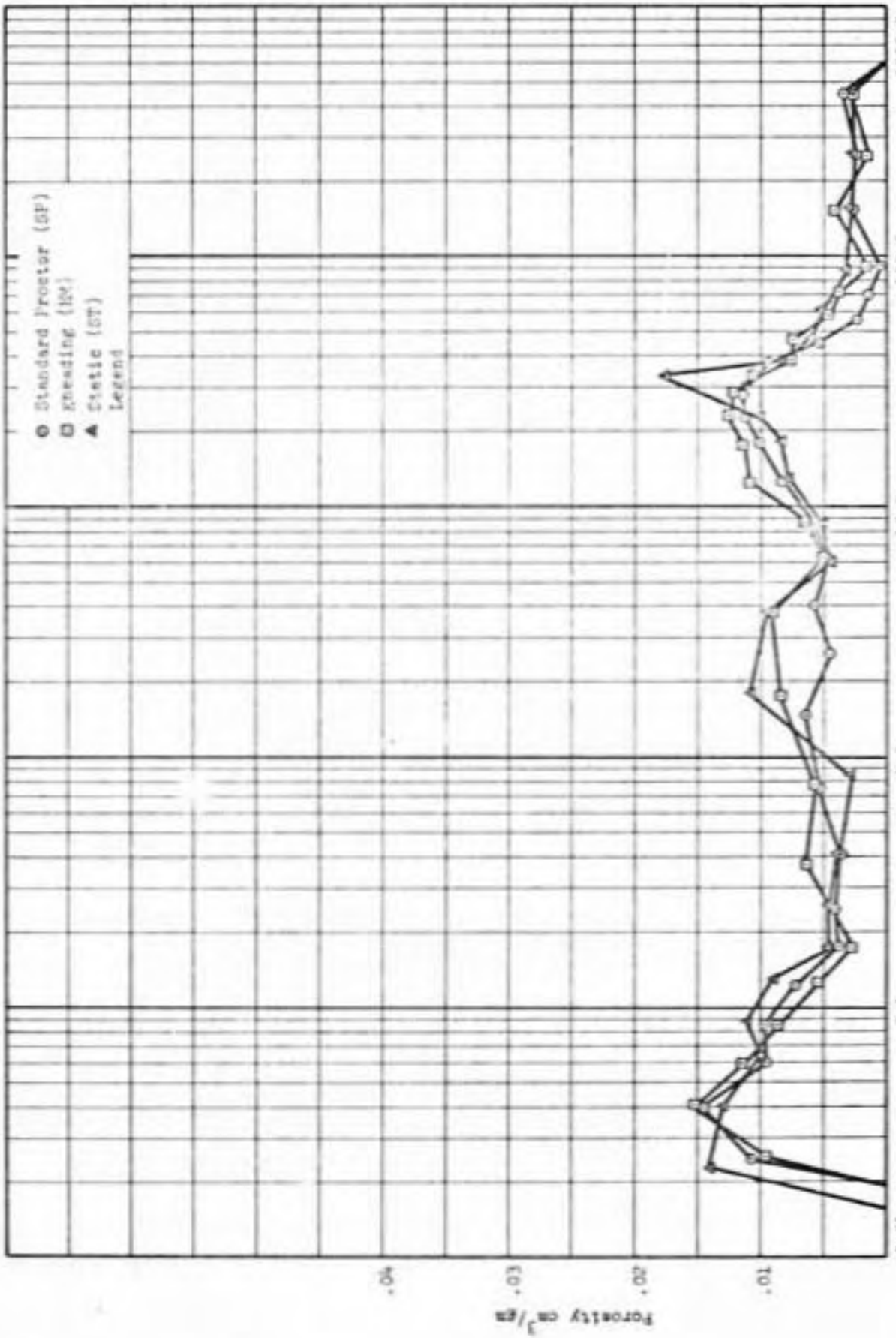

Figure 31 - Frequency Diagrams for Compaction on Dry Side by Different Compaction Methods

show peaks in porosity in the fine range for all the methods of compaction for the wet side compaction. For optimum moisture content the curves still peak in the fine range, but there is more porosity in other diameter ranges. Frequency curves for the dry side show many local peaks.

Effects of Oven Drying on Pore Size Distribution

The solid lines in Figures 32 through 40 were obtained by oven drying the samples. For the purpose of comparison, pore size distribution curves obtained by freeze drying are shown by dashed lines. The porosities of the samples are given in Tables 22 through 30. It appears that the initial molding water content is the most significant variable.

Samples compacted wet of optimum and dried in the oven showed a considerable reduction in the total porosity (see Figures 32, 33, 34 and Tables 22, 23, 24). Pore size distribution curves obtained after oven drying lie much below the curves obtained after freeze drying and become parallel to the latter only in the range of diameters smaller than 0.1 micron. This reduction in porosity is the familiar shrinkage which accompanies oven drying of clays at high degrees of saturation.

Oven dried samples compacted at optimum water content also showed reduced porosity compared to freeze dried samples, but the reduction was less than with samples compacted on the wet side. The pore size distribution curves again lie significantly under the curves obtained after freeze drying. However, there is a distinct effect of the kind of compaction. For kneading and static compaction, the two drying curves are almost parallel, i.e., they show a rather uniform reduction in porosity. In contrast, the oven drying and freeze drying curves for the Standard

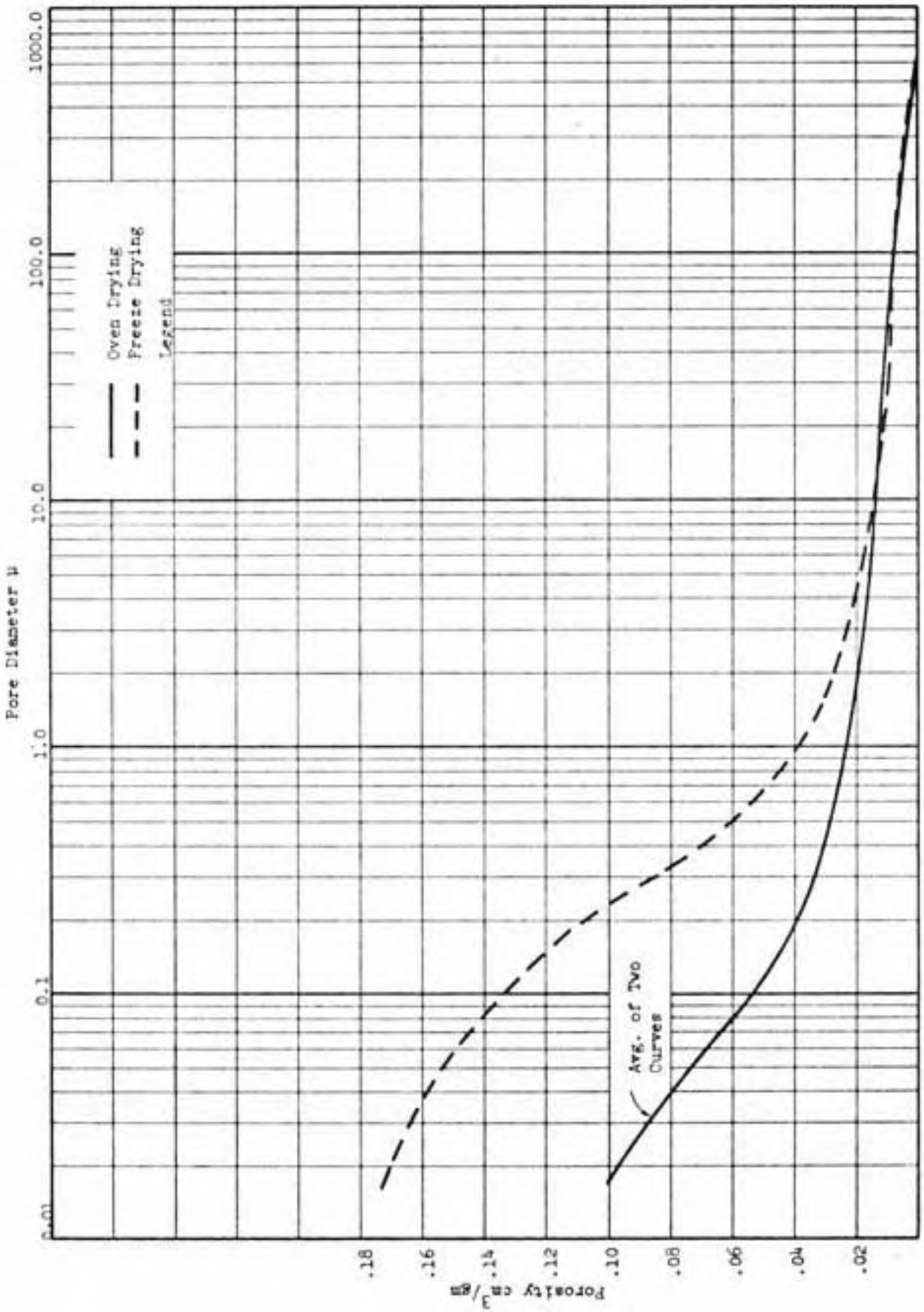

Figure 32 - Pore Size Distribution after Oven Drying - Standard Proctor, 'Wet Side'

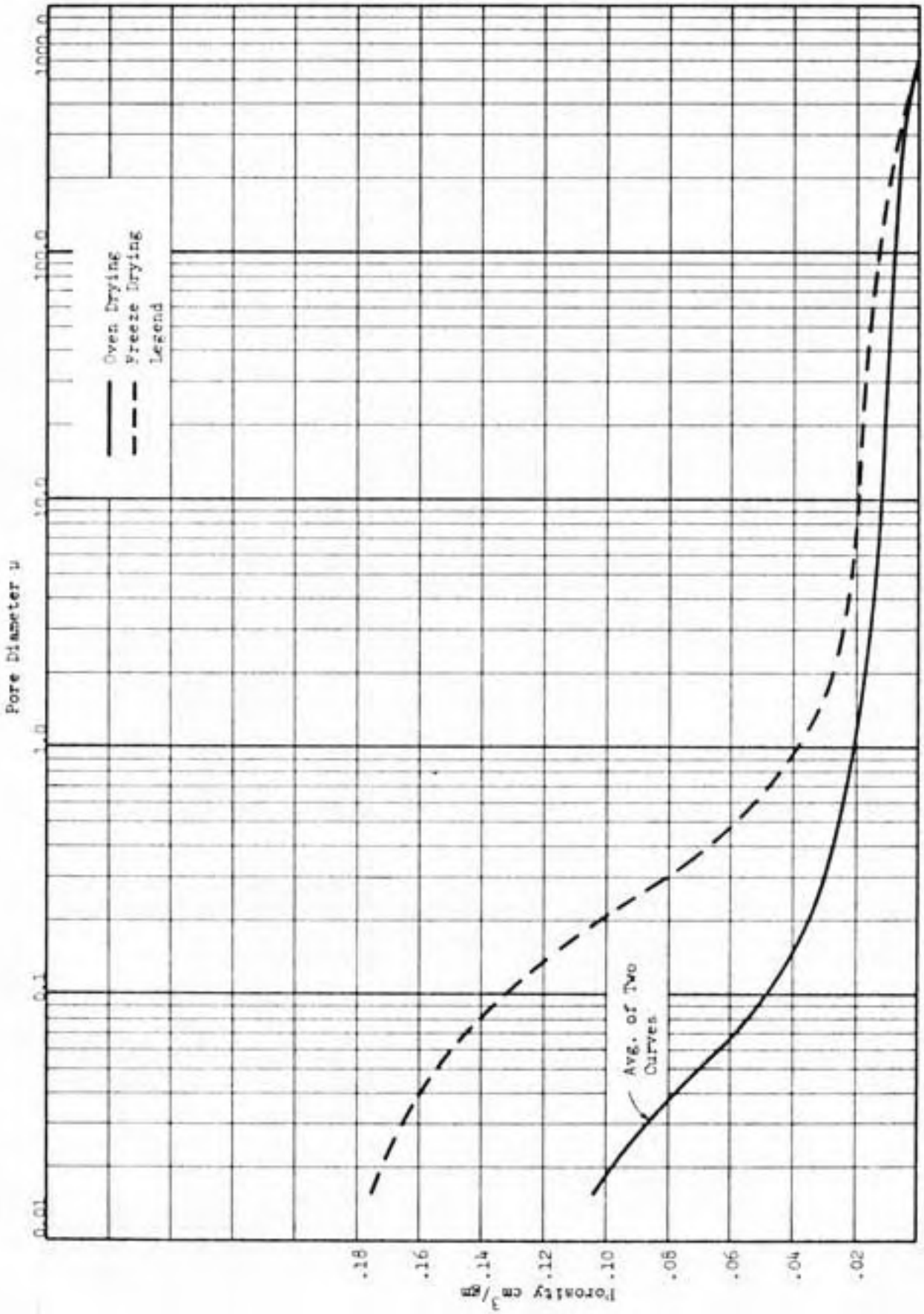

Figure 33 - Pore Size Distribution after Oven Drying - Kneading Compaction, Wet Side

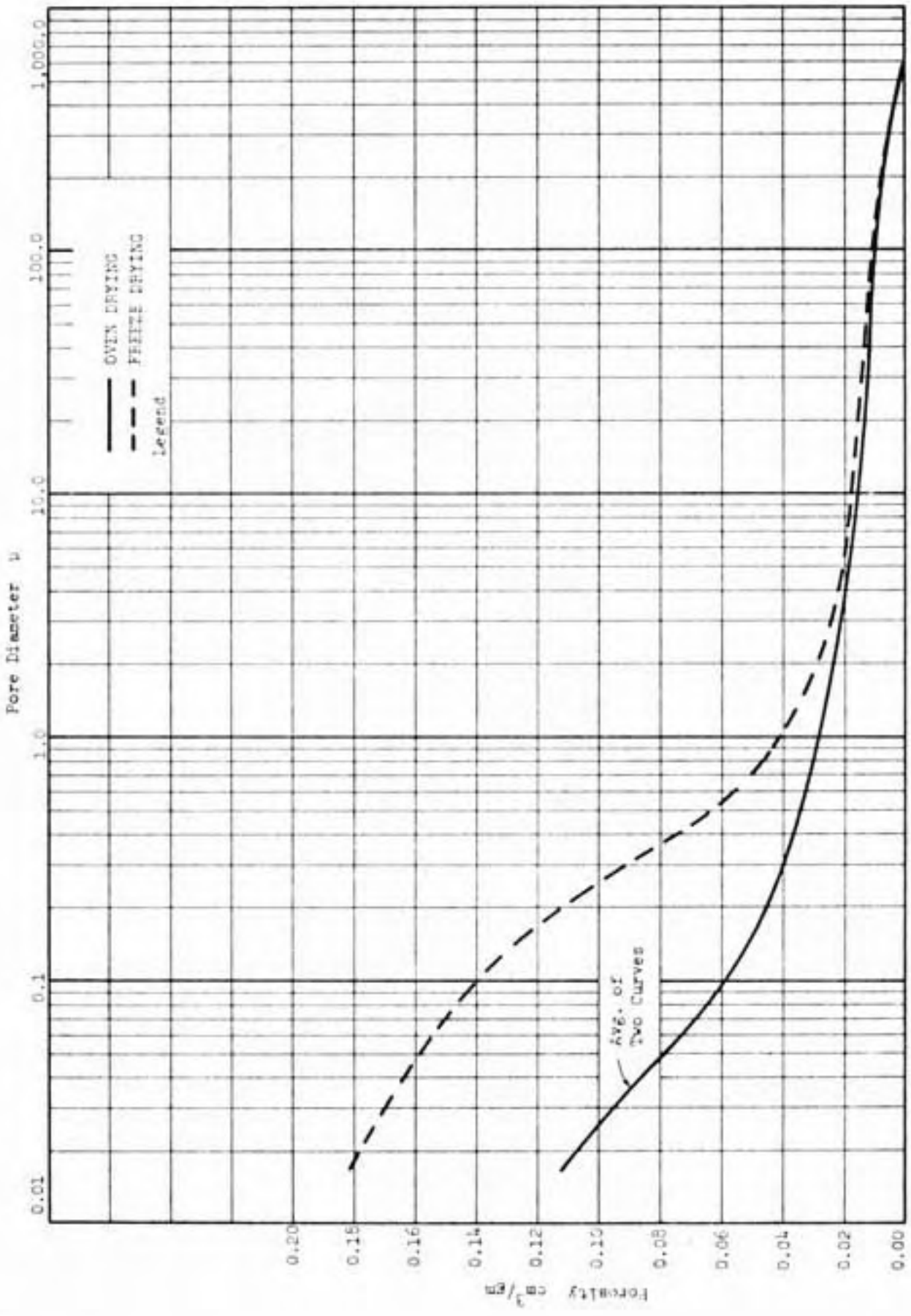

Figure 34 - Pore Size Distribution after Oven Drying - Static Compaction, 'Wet Side'

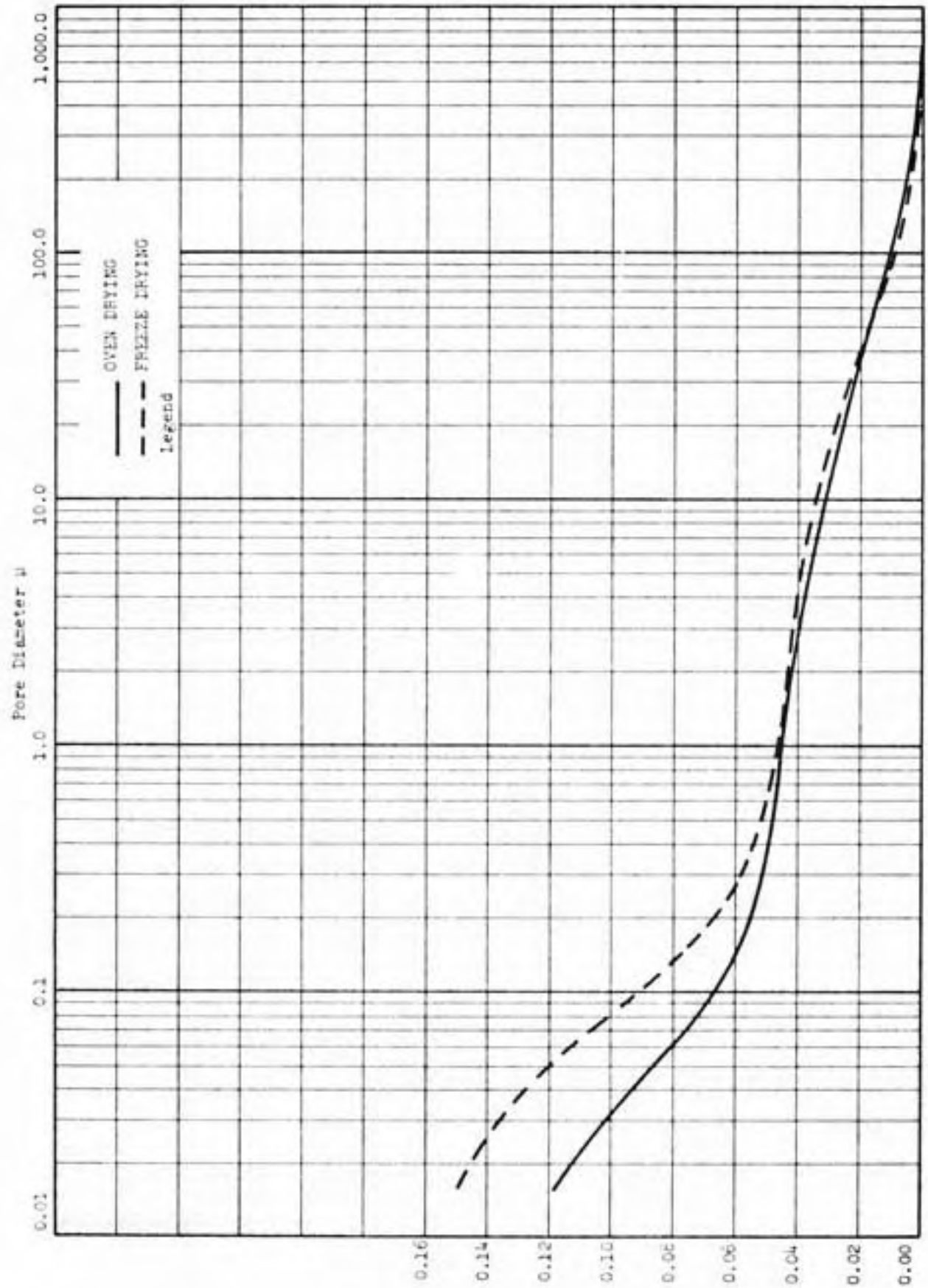

Figure 35 - Pore Size Distribution after Oven Drying - Standard Proctor, Optimum

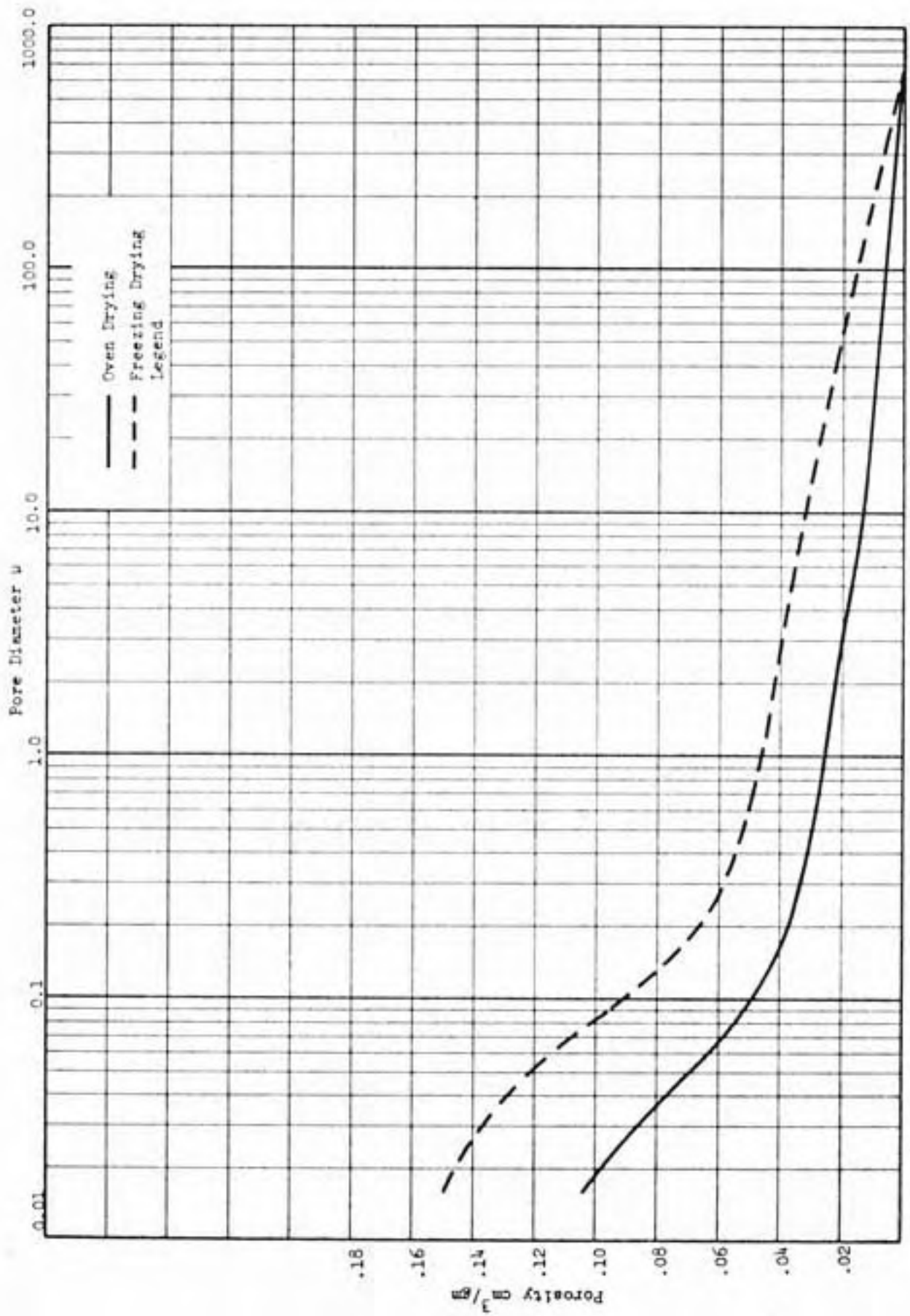

Figure 36 - Pore Size Distribution after Oven Drying - Kneading Compaction, Optimum

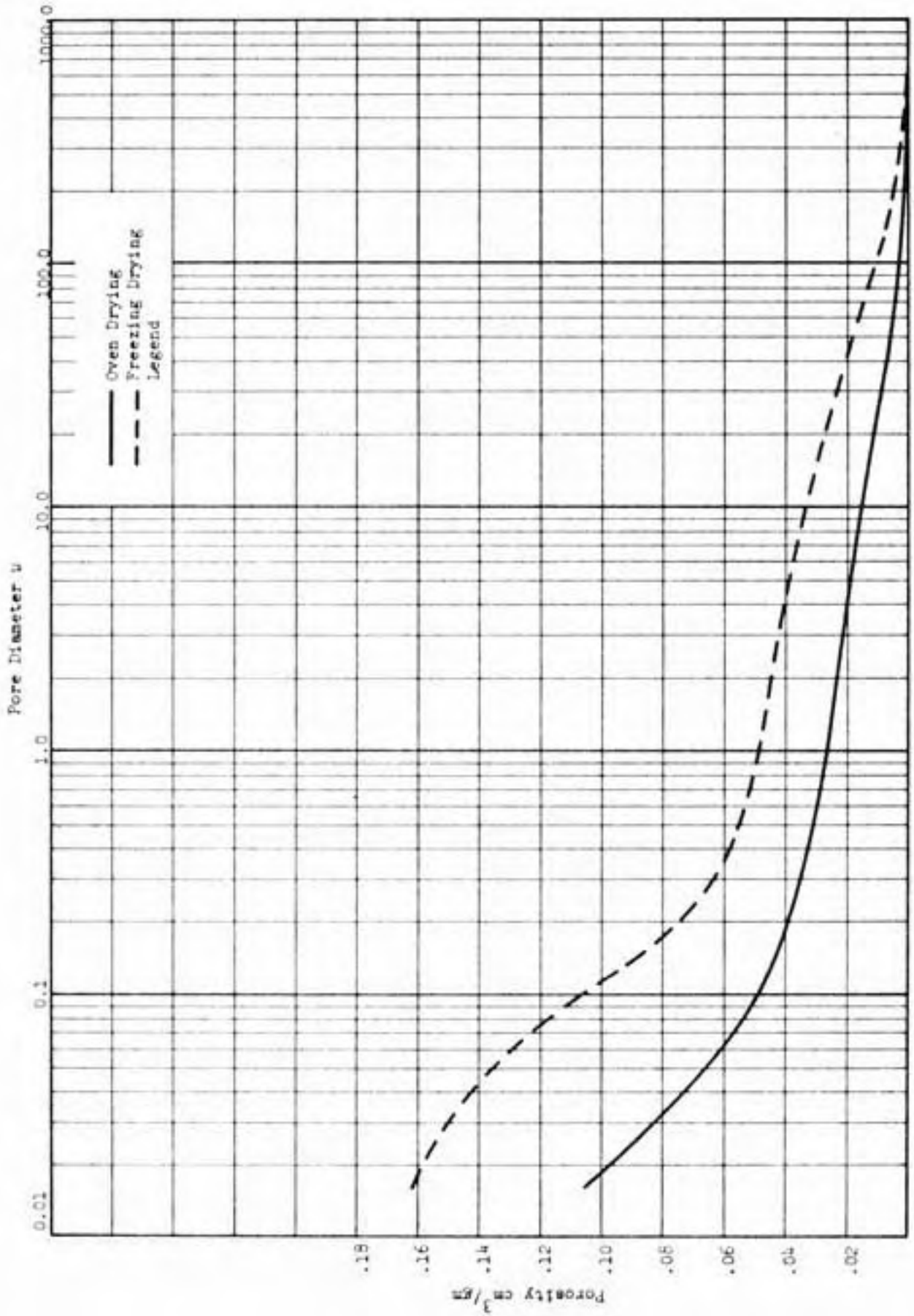

Figure 37 - Pore Size Distribution after Oven Drying - Static Compaction, 'optimum'

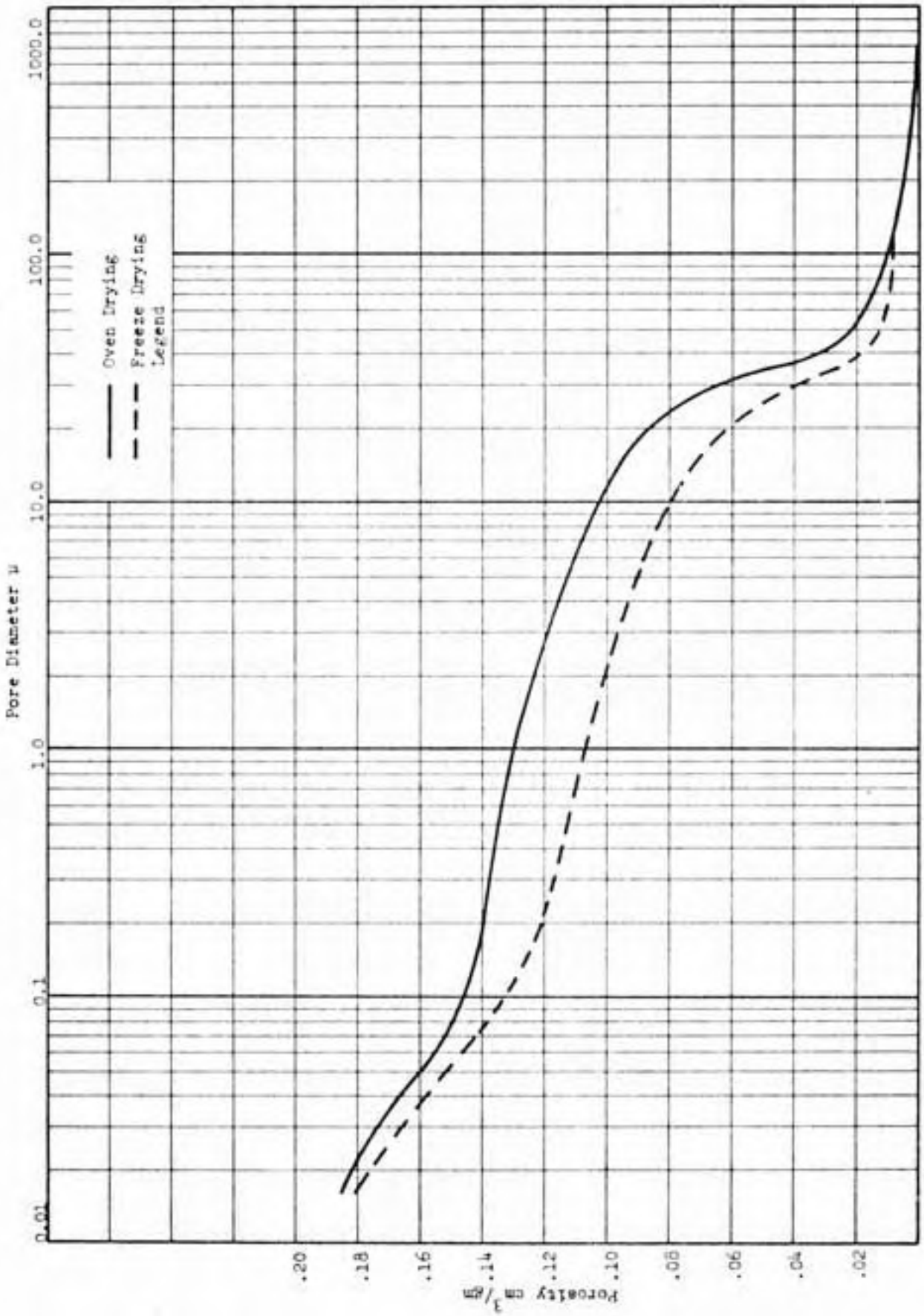

Figure 38 - Pore Size Distribution after Oven Drying - Standard Proctor, Dry Side

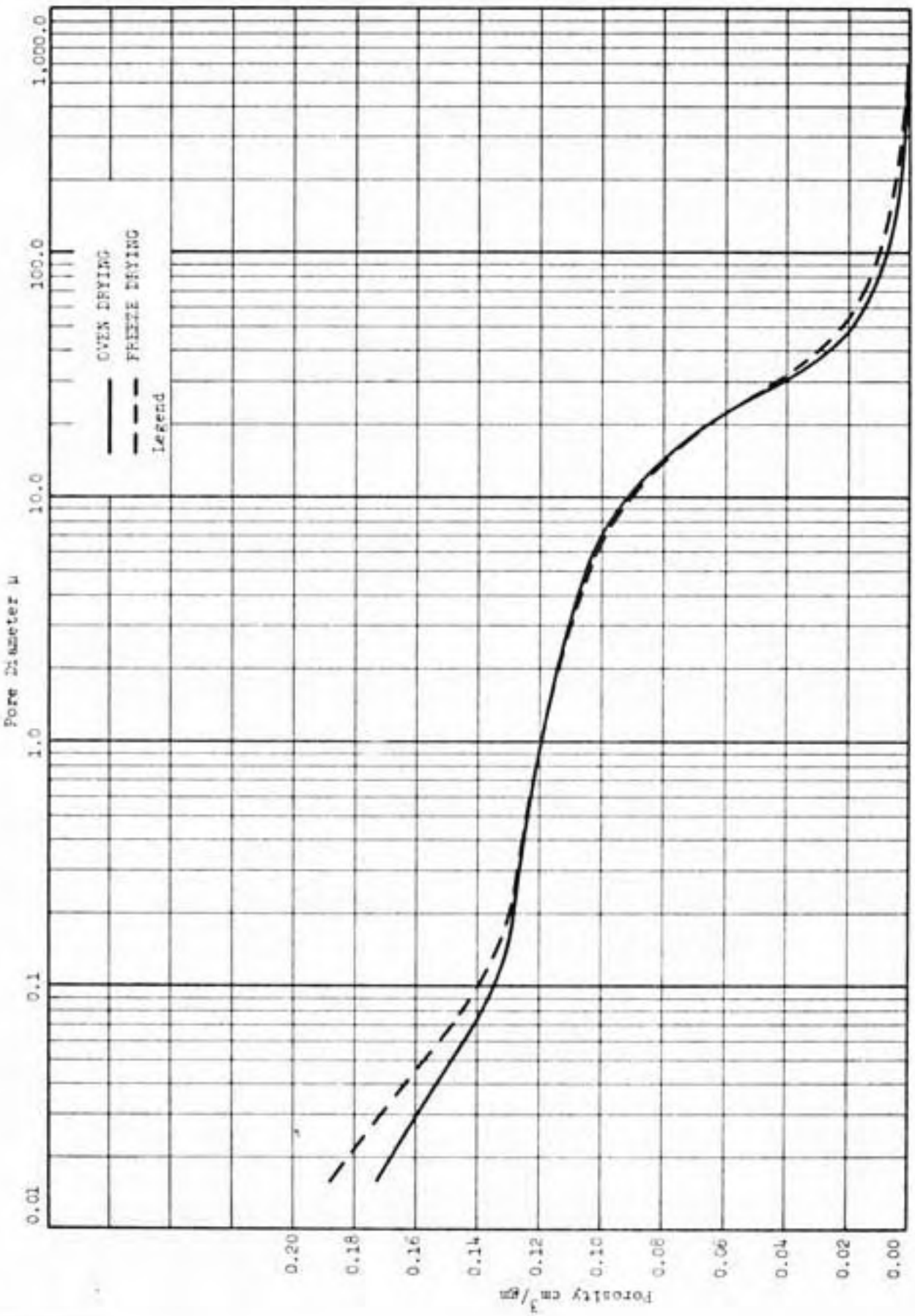

Figure 39 - Pore Size Distribution after Oven Drying - Kneading Compaction, 'Dry Side'

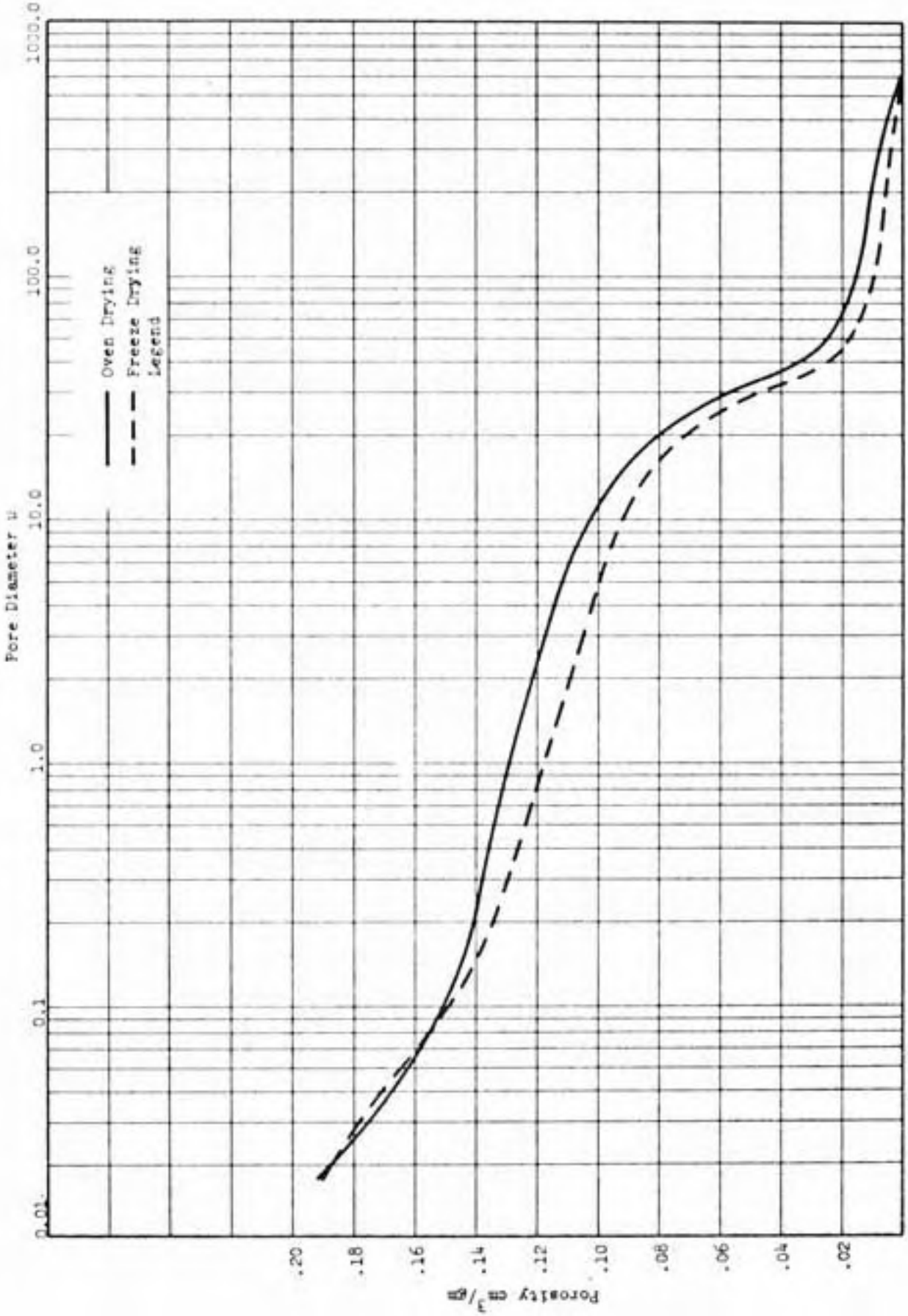

Figure 40 - Pore Size Distribution after Oven Drying - Static Compaction, 'Dry Side'

TABLE 22

Porosity Ratios

Standard Proctor Wet Side

SERIES & RUN NO.	POROSITY (n) MBOD cm^3/gm	MAOD cm^3/gm	PAOD cm^3/gm	MAOD ÷ MBOD %	PAOD ÷ MBOD %
S III R 33	0.26	0.17	0.16	65	62
AVG.	0.26	0.17	0.16	65	62

TABLE 23

Porosity Ratios

Kneading Compaction Wet Side

SERIES & RUN NO.	POROSITY (n) MBOD cm^3/gm	MAOD cm^3/gm	PAOD cm^3/gm	MAOD ÷ MBOD %	PAOD ÷ MBOD %
S III R 35	0.27	0.17	0.15	63	56
S III R 34	0.34	0.18	0.16	53	47
AVG.	0.30	0.17	0.15	58	51

TABLE 24

Porosity Ratios

Static Compaction Wet Side

SERIES & RUN NO.	POROSITY (n) MBOD cm^3/gm	MAOD cm^3/gm	PAOD cm^3/gm	MAOD ÷ MBOD %	PAOD ÷ MBOD %
S III R 28	0.26	0.18	0.16	69	62
S III R 29	0.26	0.16	0.15	62	58
AVG.	0.26	0.17	0.15	65	60

Notes: MBOD = Volume obtained by micrometer measurements before oven drying.
MAOD = Volume obtained by micrometer measurements after oven drying.
PAOD = Volume obtained in penetrometer after oven drying.

TABLE 25

Porosity Ratios

Standard Proctor Optimum

SERIES & RUN NO.	POROSITY (n)				
	MBOD cm^3/gm	MAOD cm^3/gm	PAOD cm^3/gm	MAOD ÷ MBOD %	PAOD ÷ MBOD %
S III R 94	0.27	0.19	0.18	70	67
S III R 97	0.23	-	0.16	-	70
AVG.	0.25	-	0.17	-	68

TABLE 26

Porosity Ratios

Kneading Compaction Optimum

SERIES & RUN NO.	POROSITY (n)				
	MBOD cm^3/gm	MAOD cm^3/gm	PAOD cm^3/gm	MAOD ÷ MBOD %	PAOD ÷ MBOD %
S III R 96	0.23	0.16	0.15	70	65
AVG.	0.23	0.16	0.15	70	65

TABLE 27

Porosity Ratios

Static Compaction, Optimum

SERIES & RUN NO.	POROSITY (n)				
	MBPD cm^3/gm	MAOD cm^3/gm	PAOD cm^3/gm	MAOD ÷ MBOD %	PAOD ÷ MBOD %
S III R 95	0.24	0.17	0.15	71	63
AVG.	0.24	0.17	0.15	71	63

Notes: MBOD = Volume obtained by micrometer measurements before oven drying.
MAOD = Volume obtained by micrometer measurements after oven drying.
PAOD = Volume obtained in penetrometer after ovenr drying.

TABLE 28

Porosity Ratio

Standard Proctor Dry Side

SERIES NO.	RUN NO.	POROSITY (n) PAOD cm^3/g	POROSITY (n) PAOD ÷ AC %
S III	R 92	0.26	90
S III	R 99	0.23	79
AVG.		0.245	84

TABLE 29

Porosity Ratio

Kneading Compaction Dry Side

SERIES NO.	RUN NO.	POROSITY (n) PAOD cm^3/g	POROSITY (n) PAOD ÷ AC %
S III	R 91	0.26	90
S III	R 98	0.22	76
AVG.		0.24	83

TABLE 30

Porosity Ratio

Static Compaction Dry Side

SERIES NO.	RUN NO.	POROSITY (n) PAOD cm^3/g	POROSITY (n) PAOD ÷ AC %
S III	R 100	0.25	86
S III	R 101	0.25	86
AVG.		0.25	86

Notes: PAOD ≡ Volume obtained in penetrometer after oven drying
AC ≡ As compacted porosity

Proctor compaction, do not become parallel until a very small diameter of about 0.05 micron is reached.

The dry side samples had a low degree of saturation (about 46%) and presumably the highest tension in the pore water. As drying takes place, the water tension increases, but also acts over smaller areas. The net result may be a small shrinkage or even a small expansion or relaxation. The resulting oven dry porosity may be compatible with that obtained after freeze drying, or it may be higher than that obtained after freeze drying and nearer to the as compacted porosity. Examination of the pore size distribution curves shows that kneading (KM) and static (ST) fall in the first category and Standard Proctor in the second.

It appears that for low degrees of saturation oven drying is a reasonably reliable procedure for extracting water from compacted samples while preserving the as compacted structure.

Some Observations from Freeze Drying Experiments

In Tables 31 through 36 are presented the gross volumes of all the samples whose pore size distributions have been reported earlier. These volumes were obtained by making measurements of diameter and height of the cylindrical samples with a precision micrometer. All freeze dried samples showed a small decrease in the gross volume, the maximum decrease being slightly over 5% of the original volume. In general shrinkage of this magnitude is not believed to cause any significant disturbance to the clay fabric. Most probably, the shrinkage takes place during sublimation, and may be caused by partial rearrangement of particles due to interparticle tension caused by adsorbed water films, which are the last to be removed. Researchers in this field have observed that clay

Sample Volumes Before and After Freeze Drying

TABLE 31

Standard Proctor (OMC)

SERIES & RUN NO.	SAMPLE VOLUME		
	*MBFD cm^3/gm	MAFD cm^3/gm	MAFD ÷ MBFD %
S III R 43	0.43	0.41	95
S III R 44	0.45	0.43	96
S III R 45	0.43	0.42	98
S III R 46	0.46	0.46	100
S III R 47	0.47	0.46	98
S III R 93	0.59	0.58	98
AVG.	0.47	0.46	97

TABLE 32

Kneading Compaction (OMC)

SERIES & RUN NO.	SAMPLE VOLUME		
	*MBFD cm^3/gm	MAFD cm^3/gm	MAFD : MBFD %
S III R 51	0.54	0.48	89
S III R 53	0.35	0.34	97
S III R 54	0.46	0.44	96
S III R 55	0.39	0.38	97
S III R 56	0.43	0.42	98
S III R 57	0.40	0.38	95
S III R 58	0.50	0.48	96
AVG.	0.37	0.42	95

TABLE 33

Static Compaction (OMC)

SERIES & RUN. NO.	SAMPLE VOLUME		
	*MBFD cm^3/gm	MAFD cm^3/gm	MAFD ÷ MBFD %
S III R 59	0.57	0.56	98
S III R 60	0.49	0.47	96
S III R 61	0.49	0.48	98
S III R 62	0.36	0.35	97
S III R 63	0.46	0.45	97
AVG.	0.46	0.45	97

*MBFD = Micrometer measurements before Freeze Drying
*MAFD = Micrometer measurements after Freeze Drying

Sample Volumes Before and After Freeze Drying

TABLE 34

Standard Proctor (Wet Side)

SERIES & RUN NO.	SAMPLE VOLUME		
	*MBFD	MAFD	MAFD ÷ MBFD
	cm^3/gm	cm^3/gm	%
S III R 6	0.42	0.42	100
S III R 7	0.37	0.35	95
S III R 8	0.30	0.30	100
S III R 9	0.48	0.48	100
S III R 10	0.41	0.40	98
S III R 11	0.36	0.36	100
AVG.	0.39	0.38	99

TABLE 35

Kneading Compaction (Wet Side)

SERIES & RUN NO.	SAMPLE VOLUME		
	*MBFD	MAFD	MAFD ÷ MBFD
	cm^3/gm	cm^3/gm	%
S III R 19	0.34	0.32	94
S III R 20	0.36	0.35	97
S III R 24	0.36	0.34	94
S III R 25	0.41	0.40	98
S III R 26	0.44	0.43	98
AVG.	0.38	0.37	96

TABLE 36

Static Compaction (Wet Side)

SERIES & RUN NO.	SAMPLE VOLUME		
	*MBFD	MAFD	MAFD ÷ MBFD
	cm^3/gm	cm^3/gm	%
S III R 12	0.36	0.35	97
S III R 13	0.33	0.32	97
S III R 14	0.36	0.34	94
S III R 15	0.34	0.33	97
S III R 16	0.34	0.32	94
AVG.	0.35	0.33	96

*MBFD ≡ Micrometer measurements before Freeze Drying
*MAFD ≡ Micrometer measurements after Freeze Drying

particles are separated from ice by a layer of unfrozen, liquid-like water; the presence of such a layer during the freeze drying process would result in attractive forces between particles and particle rearrangement to some unknown but probably limited degree.

In Tables 37 through 45 are given the water contents as determined by freeze drying. Comparisons with the water contents defined by oven drying on companion samples show that, on the average, the freeze drying value is the lesser by a little over one percent. Thus, the samples were judged suitably dried in the freeze drying process.

Unconfined Compression Tests

Unconfined compression tests were done on the compacted samples to study their relative load-deformation characteristics. Pore size distributions for replicate samples had been obtained earlier.

Although the pore size distribution did not vary significantly with type of compaction at a common unit weight and moisture content, the axial stress relations were distinctly influenced by the method of compaction.

In addition to the stress-strain curves, volume change vs. axial strain has also been plotted. The volume reduction, which is the result of the reduction of pore space, follows a general linear trend up to the point of failure.

Stress-Strain Relationships

Stress-strain curves of the samples compacted by the three methods of compaction are presented in Figures 41 through 49 for the molding water contents on the dry side of optimum, at optimum, and on the wet side of optimum of the Standard Proctor procedure. The reduction of

Water Removal on Freeze Drying

TABLE 37

Standard Proctor

Series & Run No.	Sample No.	Layer From Top	Moisture Condition & Compaction Method	Water Lost in Freeze Drying %	Avg. Water Content of Companion Samples by O.D. %
S III R 77	2(C) G	TOP	DRY, SP	13.49	
S III R 78	2(C) F	MIDDLE	DRY, SP	13.81	
S III R 79	4(C) K	BOTTOM	DRY, SP	13.24	14.22
S III R 82	3(E) J	BOTTOM	DRY, SP	9.55	(Avg. of three
S III R 89	1(E) F	MIDDLE	DRY, SP	13.61	samples)
			AVG.	12.88	

TABLE 38

Kneading Compaction

Series & Run. No.	Sample No.	Layer From Top	Moisture Condition & Compaction Method	Water Lost in Freeze Drying %	Avg. Water Content of Companion Samples by O.D. %
S III R 70	1(E) K	1	DRY, HM	13.57	
S III R 71	1(E) A	2	DRY, HM	13.40	
S III R 72	2(E) L	3	DRY, HM	14.07	15.29
S III R 73	2(E) C	4	DRY, HM	14.54	(Average of four
S III R 74	4(E) C	5	DRY, HM	13.92	samples)
S III R 81	1(E) B	5	DRY, HM	14.05	
			AVG.	13.92	

TABLE 39

Static Compaction

Series & Run No.	Sample No.	Layer From Top	Moisture Condition & Compaction Method	Water Lost in Freeze Drying %	Avg. Water Content of Companion Samples by O.D. %
S III R 64	2M	-	DRY, ST	14.66	
S III R 65	1M	-	DRY, ST	14.83	
S III R 66	3F	-	DRY, ST	15.00	15.54
S III R 67	3F	-	DRY, ST	15.00	(One sample)
S III R 68	1F	-	DRY, ST	15.08	
S III R 69	4F	-	DRY, ST	14.84	
			AVG.	14.90	

Water Removal on Freeze Drying

TABLE 40

Standard Proctor

Series & Run No.	Sample No.	Layer From Top	Moisture Condition & Compaction Method	Water Lost in Freeze Drying %	Avg. Water Content of Companion Samples by O.D. %
S III R 43	3(C) 472	3	OMC, SP	18.55	
S III R 44	2(E) 472	3	OMC, SP	18.56	
S III R 45	1(C) 458	2	OMC, SP	16.29	
S III R 46	4(E) 460	2	OMC, SP	16.52	18.63
S III R 47	3(C) 430	1	OMC, SP	16.68	(Avg. of three
S III R 93				17.00	samples)
			AVG.	17.27	

TABLE 41

Kneading Compaction

Series & Run No.	Sample No.	Layer From Top	Moisture Condition & Compaction Method	Water Lost in Freeze Drying %	Avg. Water Content of Companion Samples by O.D. %
S III R 51	2(C) B	2	OMC, HM	17.58	
S III R 53	3(C) 511	3	OMC, HM	17.27	
S III R 54	4(E) 511	3	OMC, HM	17.47	18.55
S III R 55	1(C) 514	4	OMC, HM	16.92	(Avg. of four
S III R 56	2(E) 514	4	OMC, HM	17.74	samples)
S III R 57	1(C) 517	5	OMC, HM	17.56	
S III R 58	3(E) 501	5	OMC, HM	16.92	
			AVG.	17.35	

TABLE 42

Static Compaction

Series & Run No.	Sample No.		Layer From Top	Moisture Condition & Compaction Method	Water Lost in Freeze Drying %	Avg. Water Content of Companion Samples by O.D. %
S III R 59	4	507	-	OMC, ST	17.14	
S III R 60	1	507	-	OMC, ST	17.45	
S III R 61	1	505	-	OMC, ST	17.82	19.1
S III R 62	2	504	-	OMC, ST	18.31	(Avg. of three
S III R 63	4(E)	500	-	OMC, ST	17.46	samples)
				AVG.	17.64	

TABLE 43

Standard Proctor

Series & Run No.	Sample No.	Layer From Top	Moisture Condition & Compaction Method	Water Lost in Freeze Drying %	Avg. Water Content of Companion Samples by O.D. %
S III R 6	2(C)H	Middle	Wet, SP	21.92	
S III R 7	3(C)I	Bottom	Wet, SP	22.38	
S III R 8	2(E)I	Middle	Wet, SP	22.52	23.05%
S III R 9	1(E)E	Bottom	Wet, SP	22.72	(Avg. of three samples)
S III R10	3(C)J	Top	Wet, SP	21.55	
S III R11	2(E)J	Top	Wet, SP	21.19	
			AVG.	22.05	

TABLE 44

Kneading Compaction

Series & Run No.	Sample No.	Layer From Top	Moisture Condition & Compaction Method	Water Lost in Freeze Drying %	Avg. Water Content of Companion Samples by O.D. %
S III R19	1(E)C	4	Wet, HM	21.50	
S III R20	4(E)B	3	Wet, HM	20.72	
S III R24	1(C)D	3	Wet, HM	21.75	22.29%
S III R25	2(C)C	4	Wet, HM	21.24	(Avg. of four)
S III R26	2(C)K	5	Wet, HM	21.60	
			AVG.	21.36	

TABLE 45

Static Compaction

Series & Run No.	Sample No.	Layer From Top	Moisture Condition & Compaction Method	Water Lost in Freeze Drying %	Avg. Water Content of Companion Samples by O.D. %
S III R12	3(E)L	-	Wet, ST	22.57	
S III R13	2 F	-	Wet, ST	22.54	
S III R14	2 W	-	Wet, ST	22.17	24.03%
S III R15	4 F	-	Wet, ST	22.98	(Avg. of three)
S III R16	3 F	-	Wet, ST	22.66	
			AVG.	22.58	

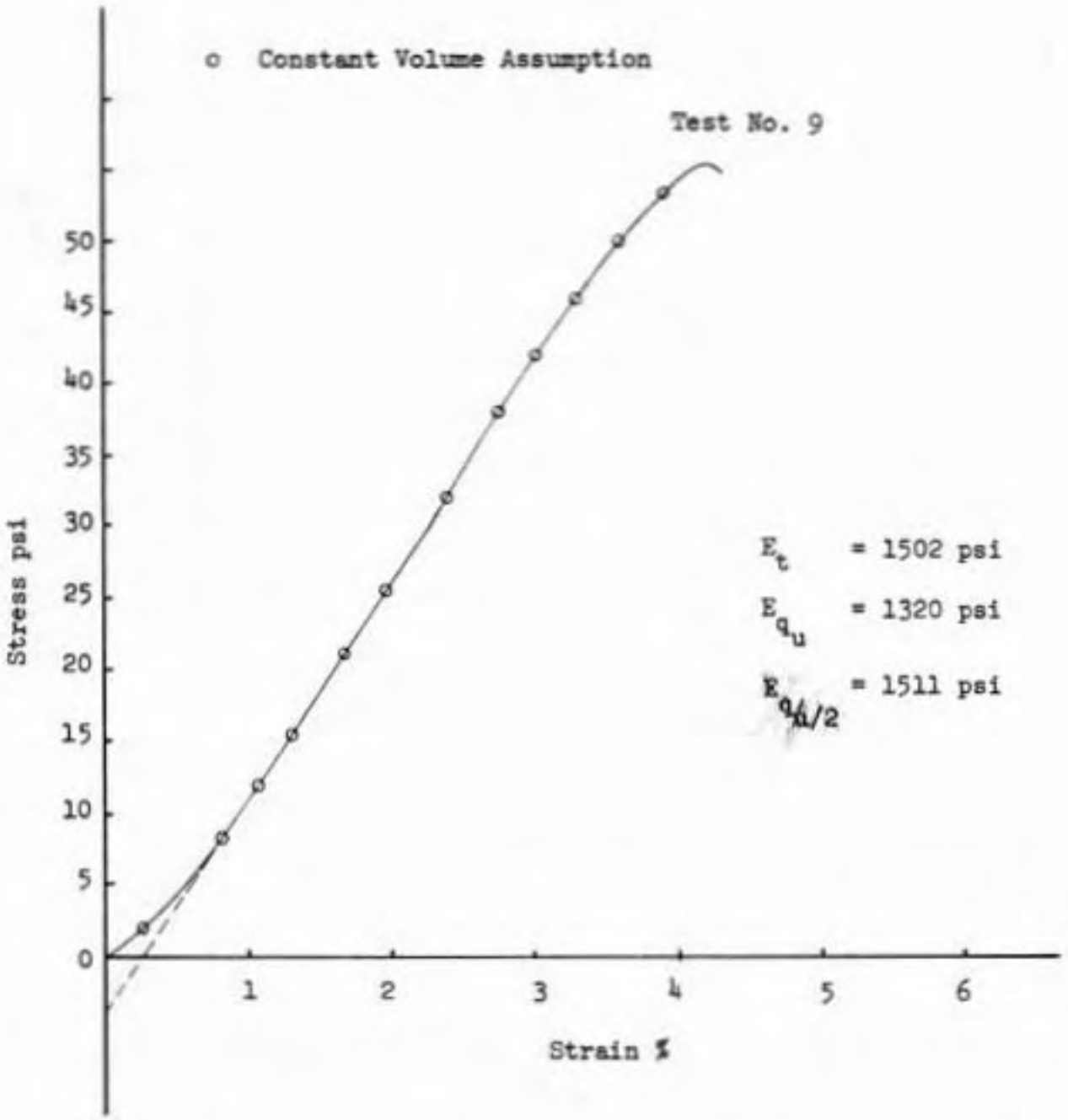

Figure 41 - Stress-Strain Relationship of the Standard Proctor Compaction on the Dry Side

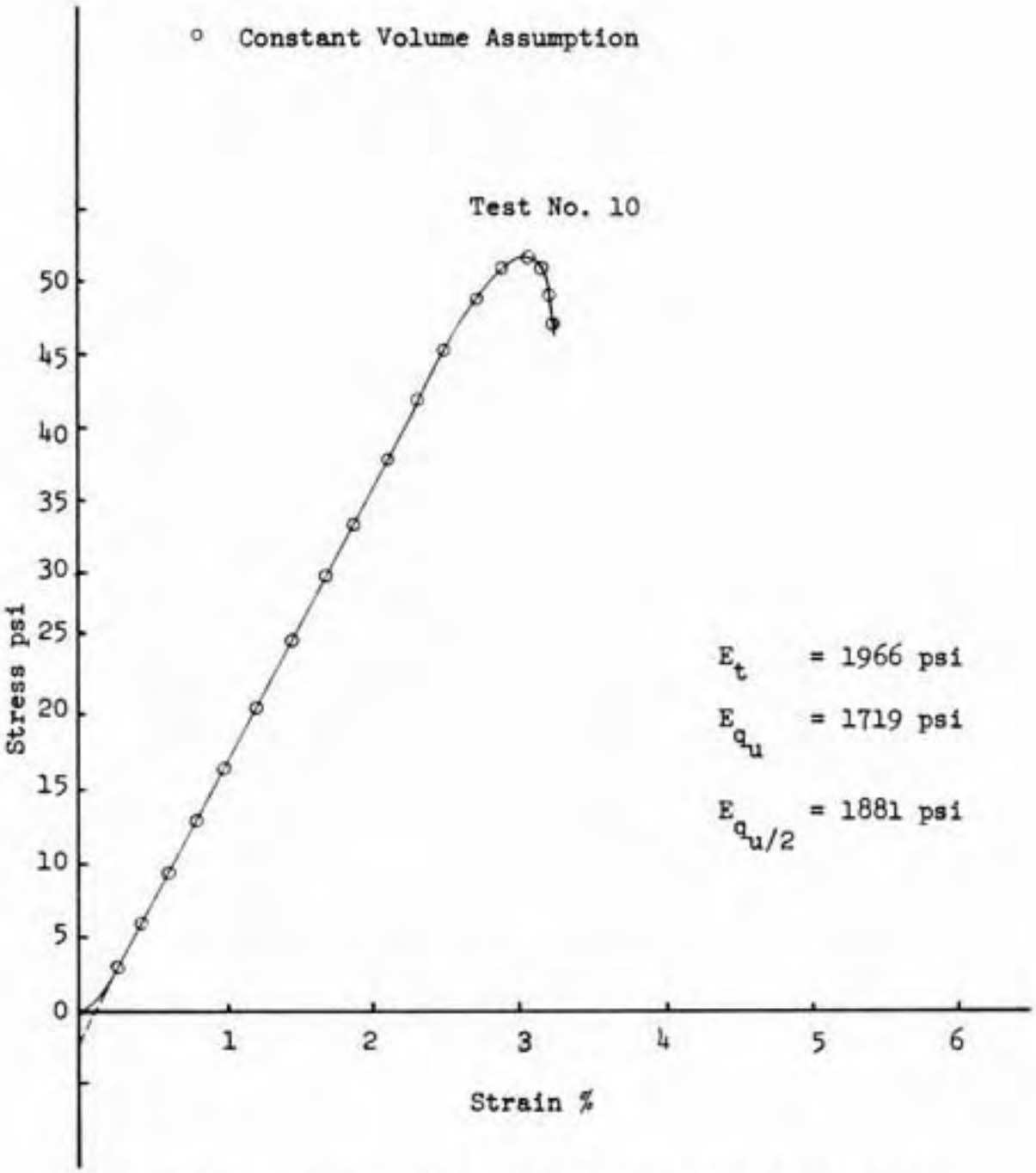

Figure 42 - Stress-Strain Relationship of the Kneading Compaction on the Dry Side

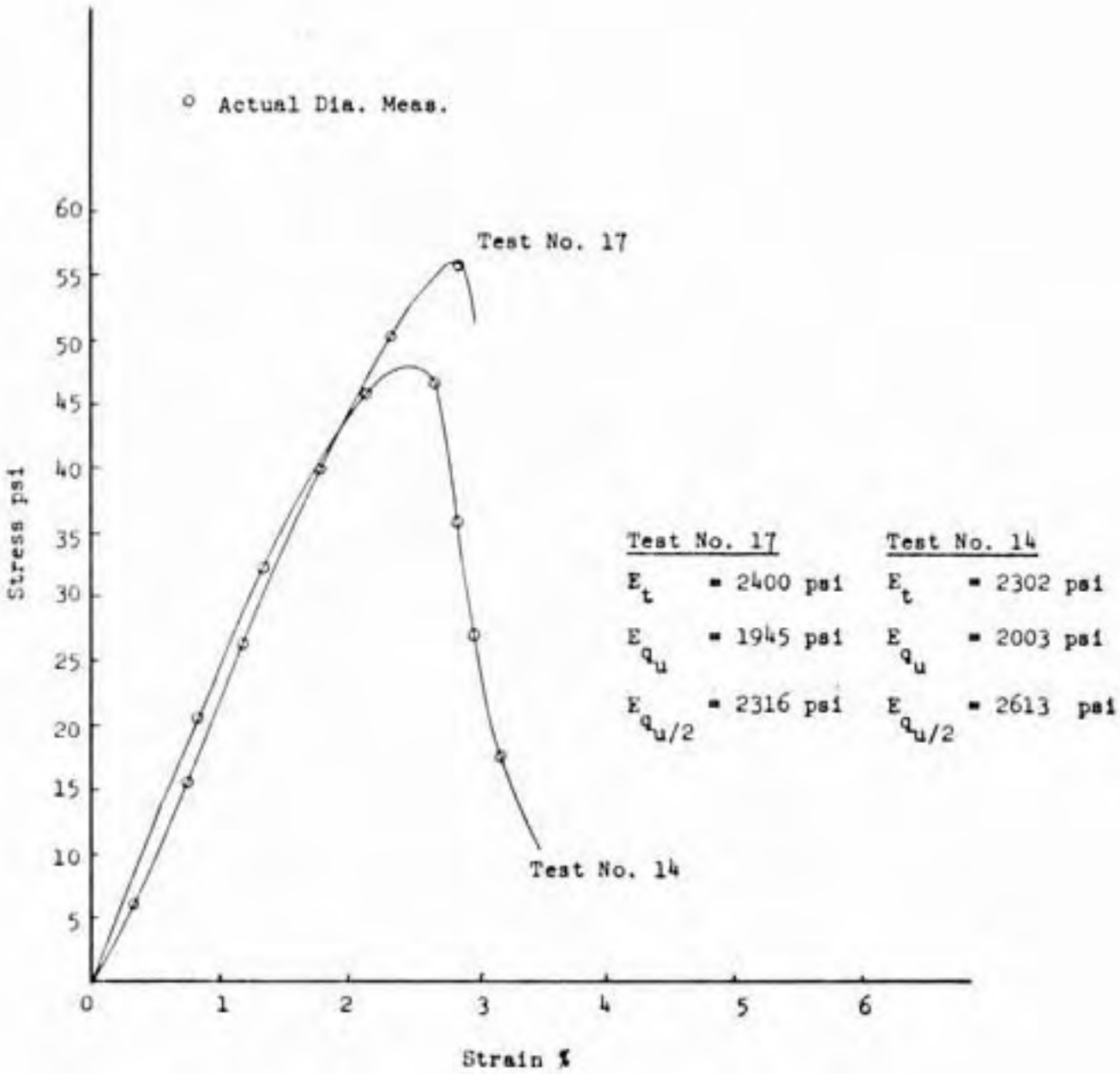

Figure 43(A) - Stress-Strain Relationship of the Static Compaction on the Dry Side

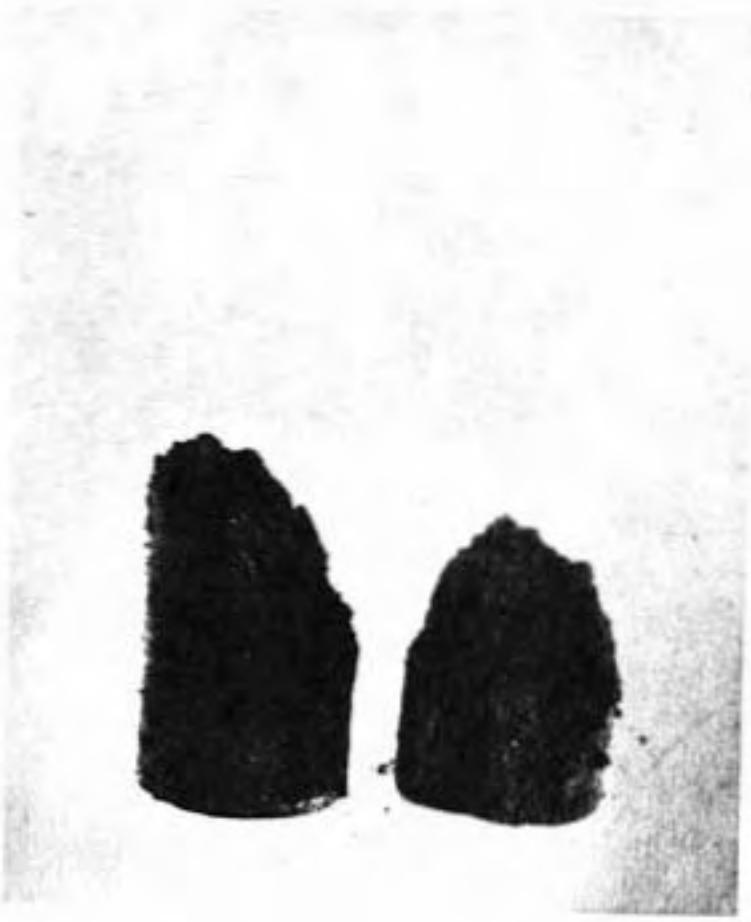

Figure 43(B): Sample after Failure (Test No. 17)

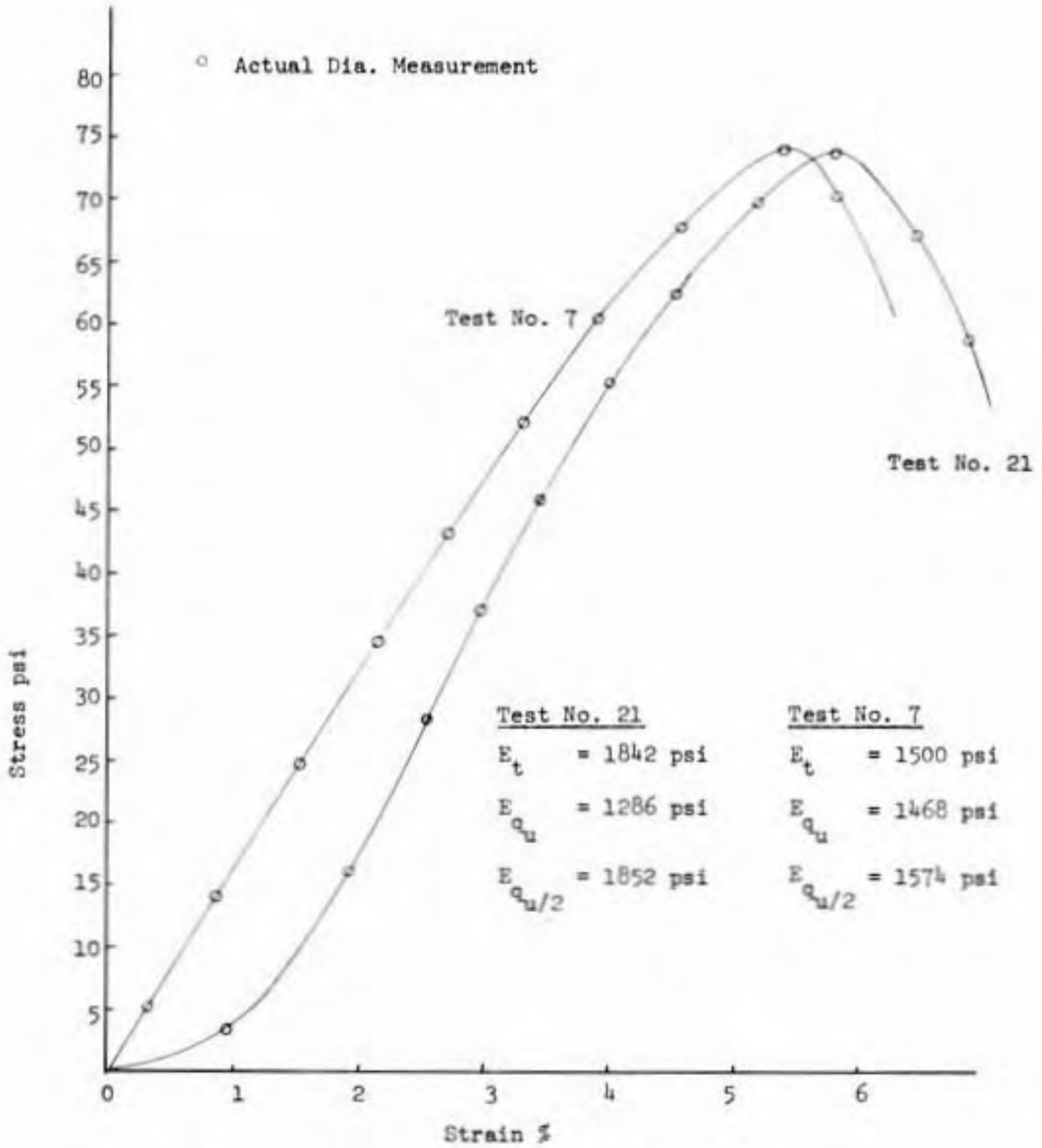

Figure 44(A) - Stress-Strain Relationship of the Standard Proctor Compaction at Optimum

Figure 44(B): Sample After Failure (Test No. 21)

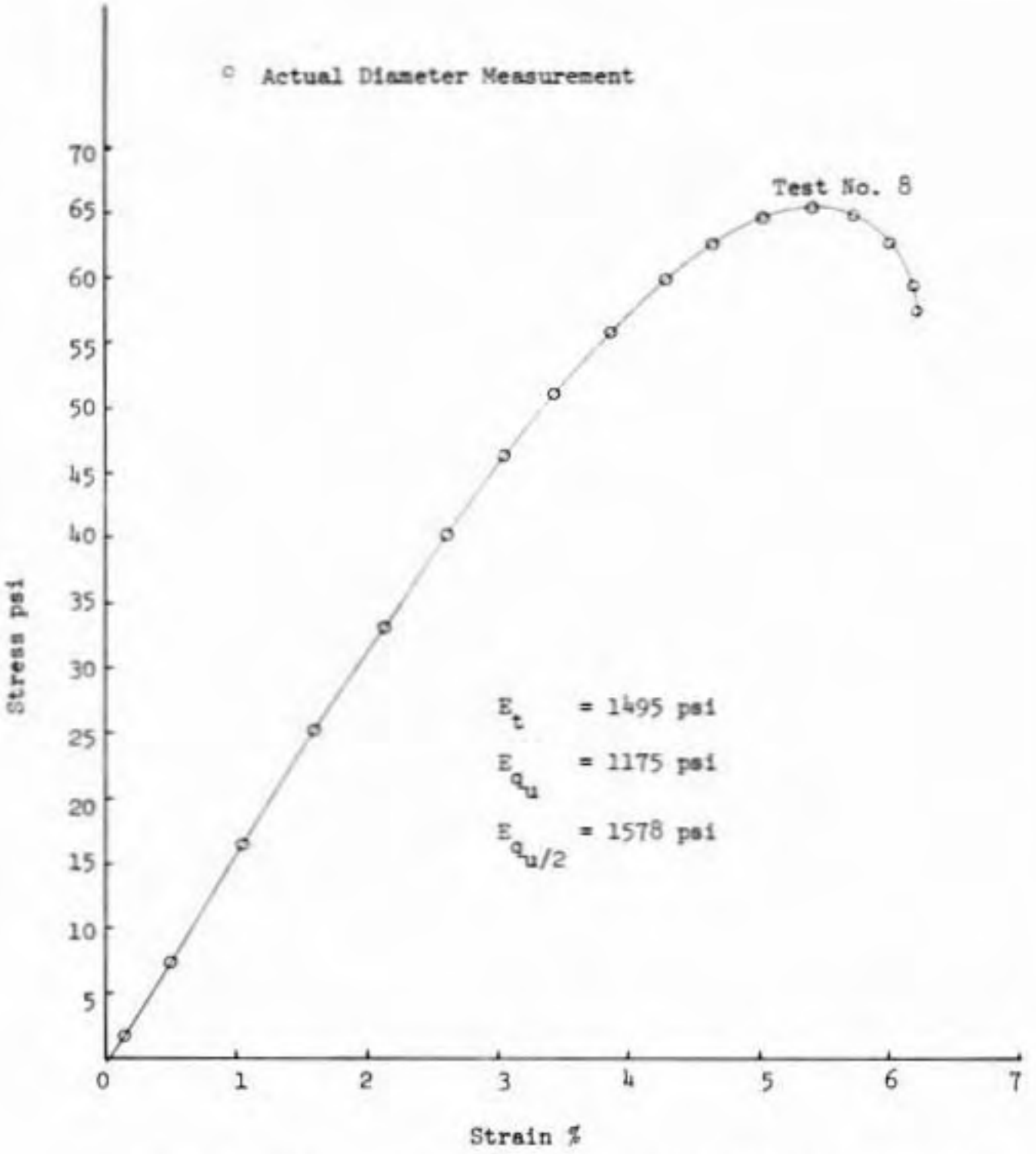

Figure 45 - Stress-Strain Relationship of the Kneading Compaction at Optimum

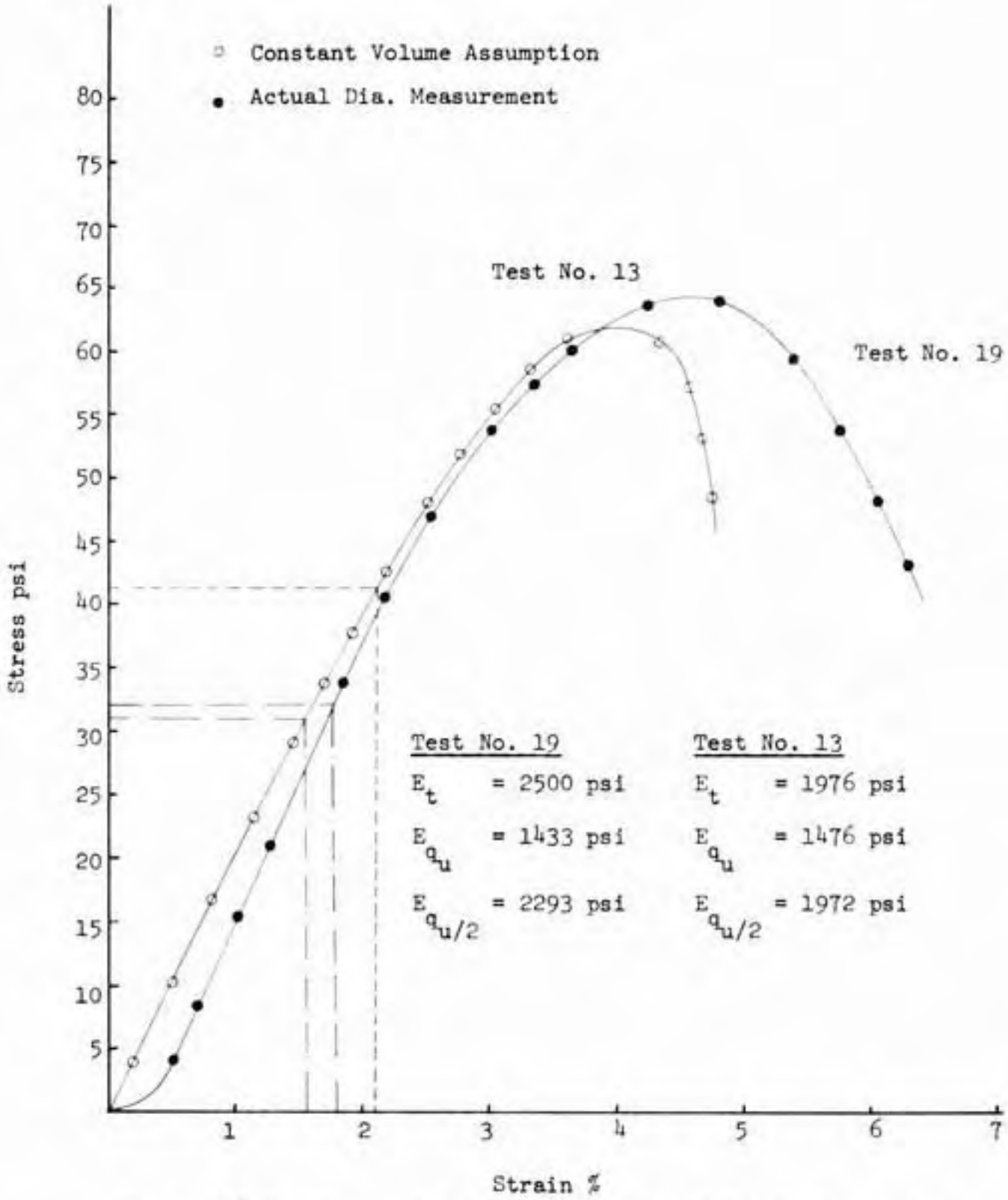

Figure 46(A) - Stress-Strain Relationship of Static Compaction at Optimum

Figure 46(B): Sample After Failure (Test No. 19)

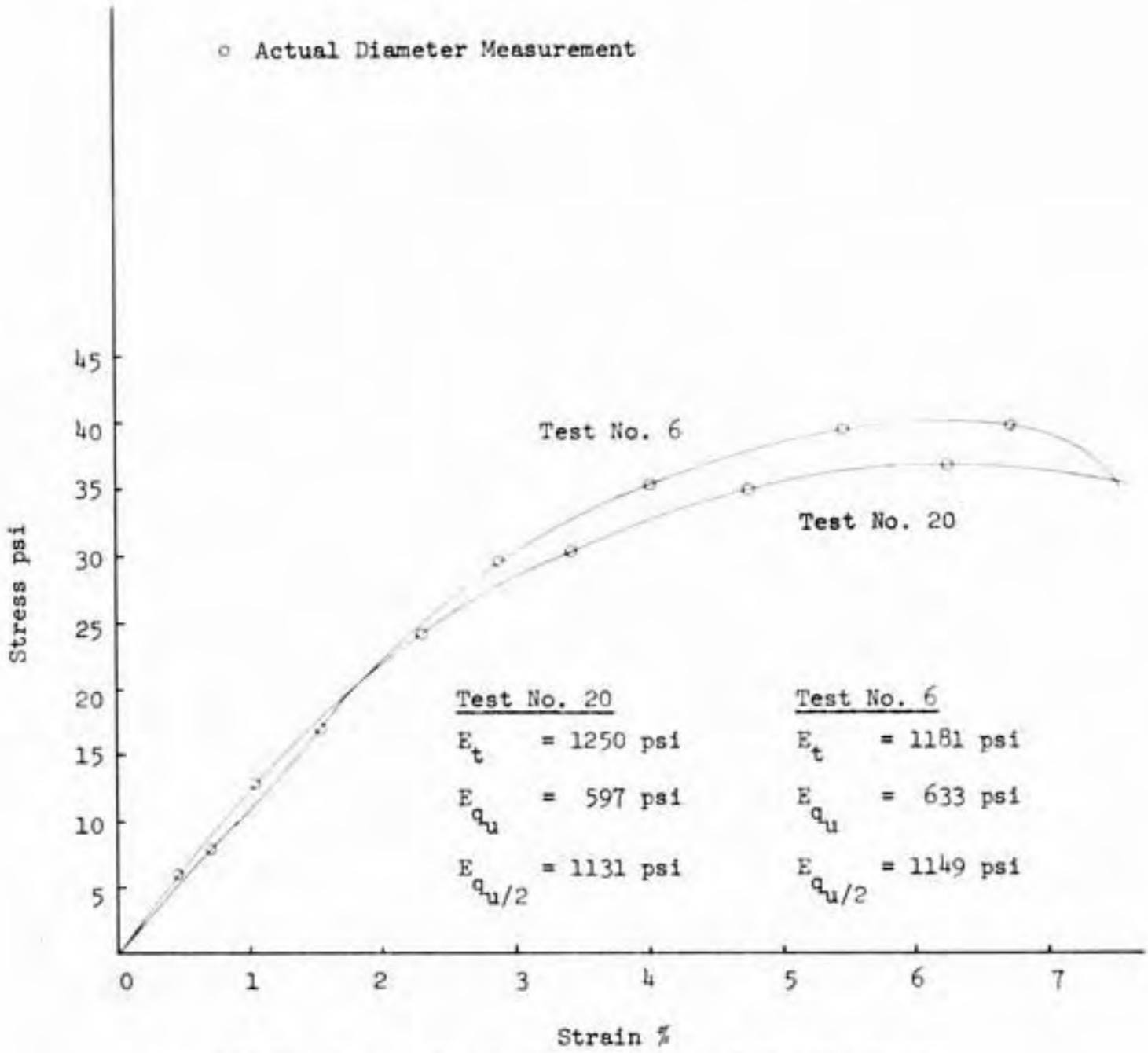

Figure 47(A) - Stress-Strain Relationship of the Standard Proctor Compaction on the Wet Side

Figure 47(B): Sample After Failure (Test No. 20)

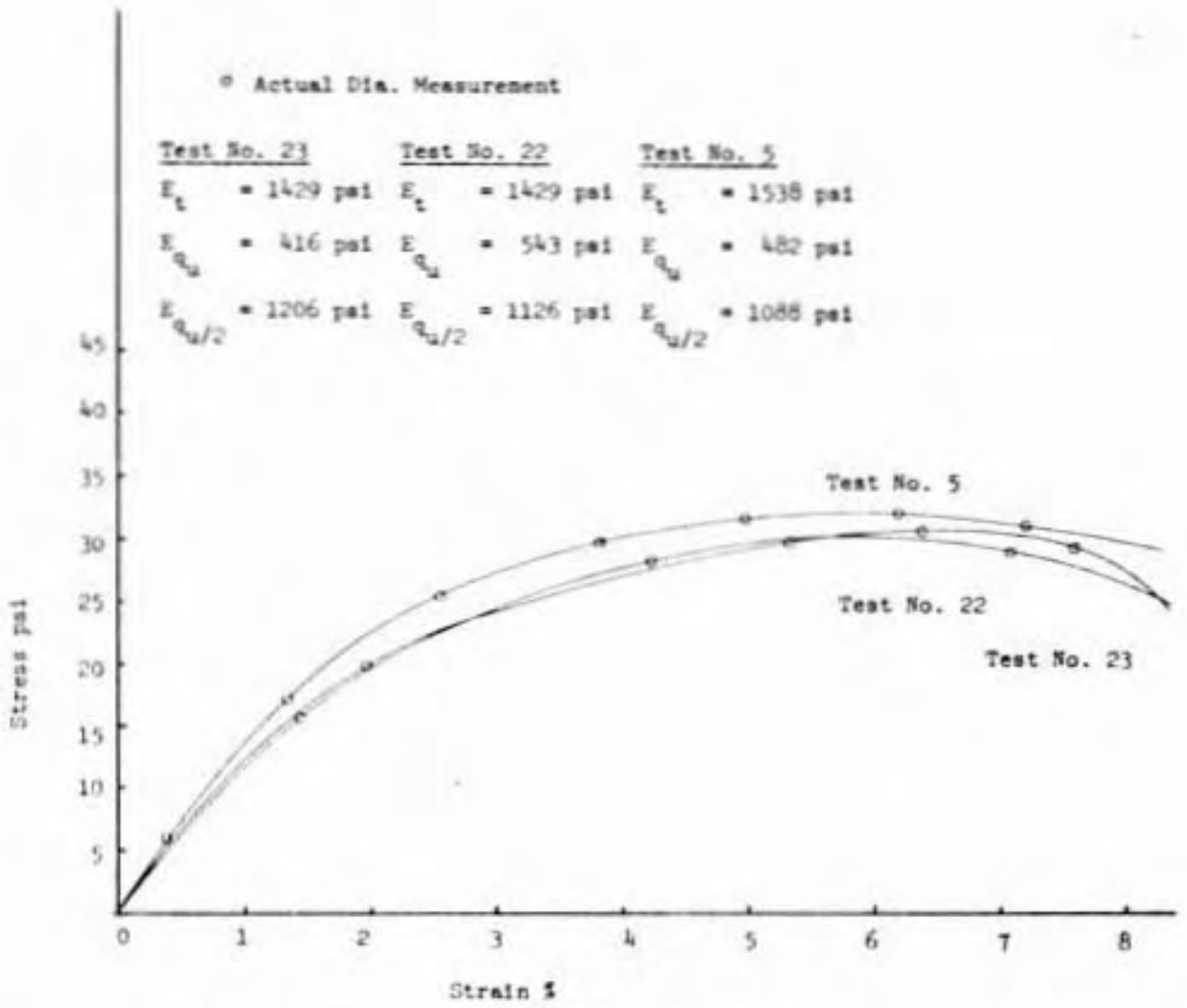

Figure 48 - Stress-Strain Relationship of the Kneading Compaction on the Wet Side

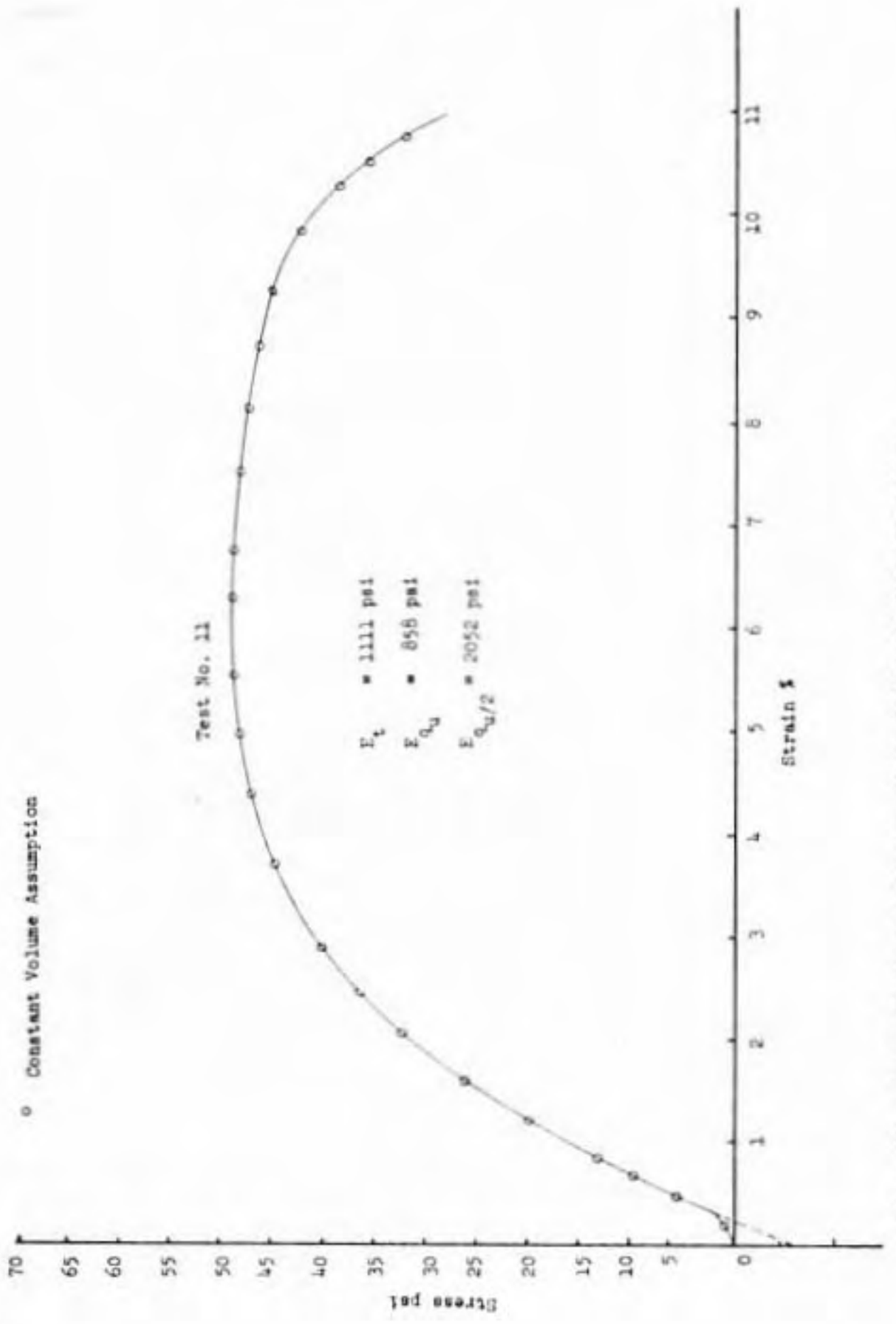

Figure 49 - Stress-Strain Relationship of the Static Wet Side Compaction

axial load to axial stress was based upon the estimated area based on measurement of the sample diameter at mid-height. Wherever actual diameter measurements could not be made, due to experimental difficulties, the stress was obtained by employing the constant volume assumption.

Corrections were applied to those stress-strain curves for which seating difficulties at the start of the test gave rise to upward concavity at the start of the test. These corrections are explained by Figure 41. Table 46 summarizes the values of the peak stresses and the corresponding axial strains for each stress-strain curve.

The stress-strain curves for the dry side compaction are characterized by brittle failure at low strains. Pore size distribution studies of these samples revealed that the largest pore size class (50 - 609 μ in diameter) was dominant. A small amount of movement seems sufficient to break the 'boundaries' of such large pores. Once these large pores collapse, the peak stress is quickly attained, and the sample almost disintegrates (see Figure 43b).

Stress-strain curves for the samples compacted at optimum showed quasi-brittle failures, but the drop in stress past the peak was not very sudden. At optimum water content considerable lubrication between grains can occur; thus, compared with the sample of the dry side, larger deformations were required to mobilize the peak stress.

Samples compacted wet of optimum show a gradual shear failure with peak stress being mobilized at higher strains. In these samples, due to the high water content, mobility of soil grains is easier and the deformations may continue without any significant reduction in the already small sizes of the pores. Although the dry side and the wet side samples

TABLE 46

Peak Stresses & Failure Strains Compared

Test No.	Compaction Type	Water Content %	Dry Unit Weight pcf	Peak Stress (Actual Dia.) psi	Failure Strain (Actual Dia.) %	Peak Stress (Const. Vol.) psi	Failure Strain (Const. Vol.) %
9	SP	15.64 (dry)	95.99	-	-	55.29	4.19
10	HM	16.15 (dry)	95.34	-	-	51.92	3.02
14	ST	15.64 (dry)	95.71	48.07	2.40	47.15	2.40
17	ST	15.64 (dry)	96.20	56.03	2.88	-	-
7	SP	21.37 (optimum)	100.11	73.99	5.41	70.90	5.41
21	SP	21.37 (optimum)	100.11	74.06	5.76	-	-
8	HM	21.43 (optimum)	99.06	66.26	5.64	62.84	5.64
13	ST	21.37 (optimum)	100.24	-	-	62.31	4.22
19	ST	21.37 (optimum)	99.66	64.20	4.48	-	-
6	SP	26.05 (wet)	96.39	39.99	6.40	38.40	6.40
20	SP	26.05 (wet)	96.39	37.32	6.25	-	-
5	HM	26.23 (wet)	96.27	33.07	6.86	32.21	6.36

TABLE 46, continued

Test No.	Compaction Type	Water Content %	Dry Unit Weight pcf	Peak Stress (Actual Dia.) psi	Failure Strain (Actual Dia.) %	Peak Stress (Const. Vol.) psi	Failure Strain (Constant. Vol.) %
22	HM	26.23 (wet)	95.89	30.40	5.60	-	-
23	HM	26.23 (wet)	96.13	30.15	7.24	-	-
11	ST	26.05 (wet)	96.13	-	-	49.23	5.74

Notes: SP: Standard Proctor
HM: Kneading Compaction
ST: Static Compaction

were about the same percentage of water content distant from the optimum, the samples on the wet side showed smaller peak stresses. This is interpreted as being the result of the lesser contribution of the negative pore pressure at the higher degree of saturation of these samples.

It is interesting to compare the average dry unit weight and the average peak stress, obtained by the different methods of compaction at given molding water contents. Average dry unit weight for the dry side compaction was about 95% of the dry unit weight at optimum and that for the wet side compaction was about 96% of the dry unit weight at optimum. On the other hand the peak stresses were about 76% and 54% of the peak stress at optimum, for the dry side and the wet side compactions respectively. The basic reason for such a difference in the peak stresses of dry side and the wet side compaction appears to be related to the differences in the distribution of pore sizes. Since other related factors, such as negative pore pressures, are also of influence, it is not possible to be conclusive with respect to the pore size influence.

It was observed that, in contrast with the other methods of compaction the statically compacted samples mobilized the peak stress at comparatively low strains. The explanation of this differential behavior of statically compacted samples is not apparent.

The initial tangent modulii and secant modulii at peak stress and at half the peak stress were calculated for both stresses evaluated using the constant volume assumption. They are given in Table 47. Values of initial tangent modulii vary from about 1180 psi for Standard Proctor, wet side compaction to 2500 psi for static compaction at optimum. Secant modulii at peak stress vary from about 400 psi for kneading compaction,

TABLE 47

Modulii of Elasticity

Test No.	Compaction Type	Water Content %	Dry Unit Weight pcf	E_t (Actual Dia.) psi	E_{q_u} (Actual Dia.) psi	$E_{q_{u/2}}$ (Actual Dia.) psi	E_t (Const. Vol.) psi	E_{q_u} (Const. Vol.) psi	$E_{q_{u/2}}$ (Const. Vol.) psi
9	SP	15.64 (dry)	95.99	-	-	-	1502	1320	1511
10	HM	16.15 (dry)	95.34	-	-	-	1966	1719	1881
14	ST	15.64 (dry)	95.71	2302	2003	2613	-	-	-
17	ST	15.64 (dry)	96.20	2400	1945	2316	-	-	-
7	SP	21.37 (optimum)	100.11	1500	1468	1574	1500	1311	1477
21	SP	21.37 (optimum)	100.11	1842	1286	1852	-	-	-
8	HM	21.43 (optimum)	99.06	1495	1175	1578	1492	1114	1533
13	ST	21.37 (optimum)	100.24	-	-	-	1976	1476	1972
19	ST	21.37 (optimum)	99.66	2500	1433	2293	-	-	-

TABLE 47, continued

Test No.	Compaction Type	Water Content %	Dry Unit Weight pcf	E_t (Actual Dia.) psi	E_{q_u} (Actual Dia.) psi	$E_{q_{u/2}}$ (Actual Dia.) psi	E_t (Const. Vol.) psi	E_{q_u} (Const. Vol.) psi	$E_{q_{u/2}}$ (Const. Vol.) psi
6	SP	26.05 (wet)	96.39	1181	633	1149	1181	601	1181
20	SP	26.05 (wet)	96.39	1250	597	1131	-	-	-
5	HM	26.23 (wet)	96.27	1538	482	1088	1333	506	1289
22	HM	26.23 (wet)	95.89	1429	543	1126	-	-	-
23	HM	26.23 (wet)	96.13	1429	416	1206	-	-	-
11	ST	26.05 (wet)	96.63	-	-	-	1111	858	2052

Notes: SP: Standard Proctor
HM: Kneading Compaction
ST: Static Compaction

wet side compaction to about 2000 psi for static dry side compaction. At half peak stress secant moduli vary from about 1100 psi for the kneading wet side compaction to about 2600 psi for the static dry side compaction. Due to imperfect seating, the initial portions of some of the stress strain curves showed concavity upwards instead of the usual concavity downward of shear test. For obtaining the moduli the stress scale was corrected by extending the straight line portion of the curve, as shown in Figure 41.

Evaluation of the Constant Volume Assumption

Figures 50 through 54 present stress strain curves, where the area of the sample, at different strain levels was obtained:

(1) by making actual diameter measurements at the mid height of the sample, and

(2) by assuming a constant sample volume. In the latter case the area is calculated as:

$$\text{area} = \frac{\text{initial cross sectional area}}{1 - \text{axial strain}}$$

Table 48 summarizes the values of the peak stresses and of the failure strains.

In general the customary assumption of constant volume tends to overestimate the cross sectional area and thus underestimates the stress. The difference in peak stress obtained by actual diameter measurements and that obtained by the constant volume assumption is a maximum for the samples compacted at optimum and showing the highest peak stress. The discrepancy on the dry side is low because of the small axial strain. It appears that the assumption of constant volume does not greatly

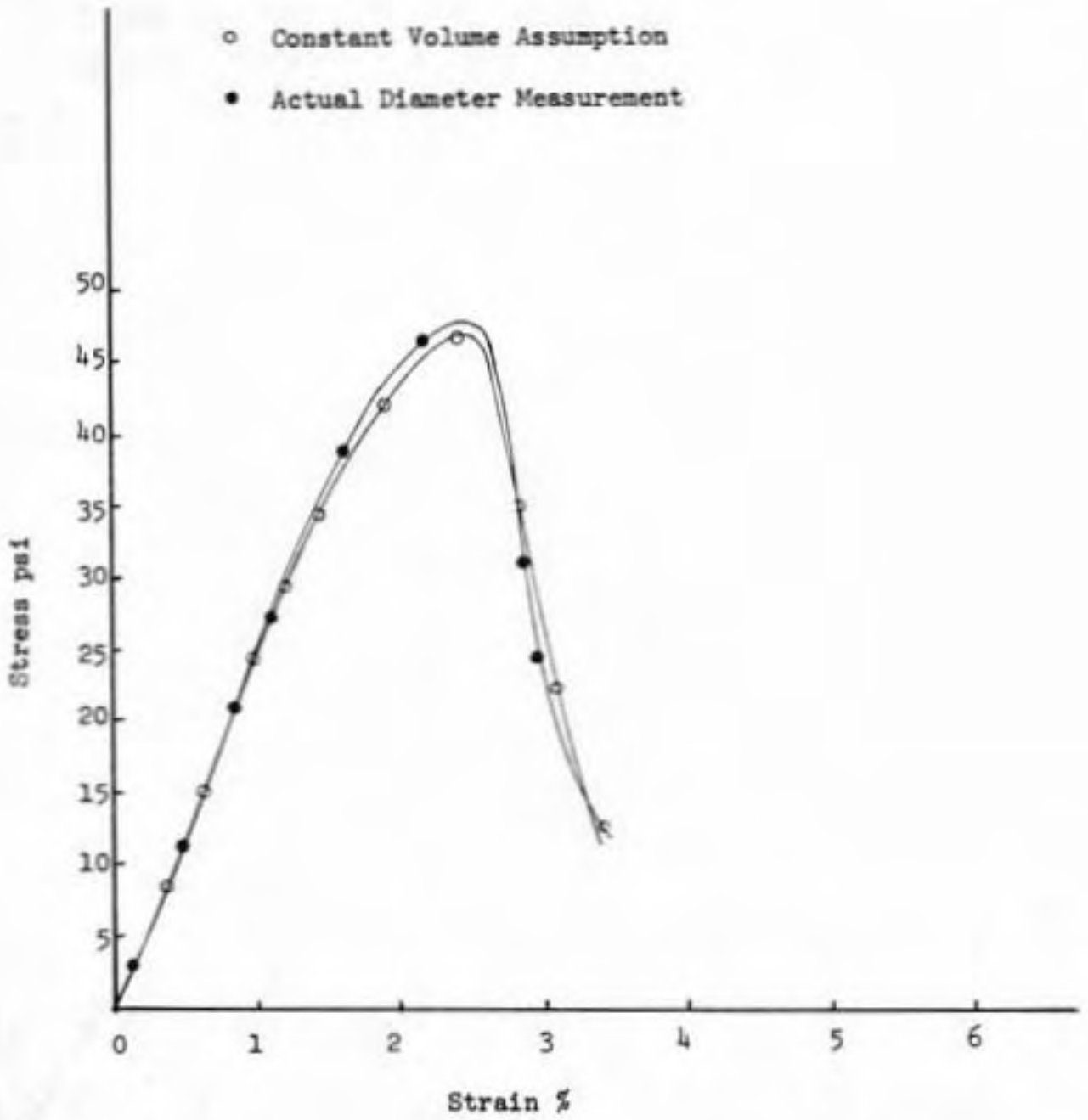

Figure 50 - Comparison of Stress-Strain Relationship of the Static Compaction on the Dry Side.

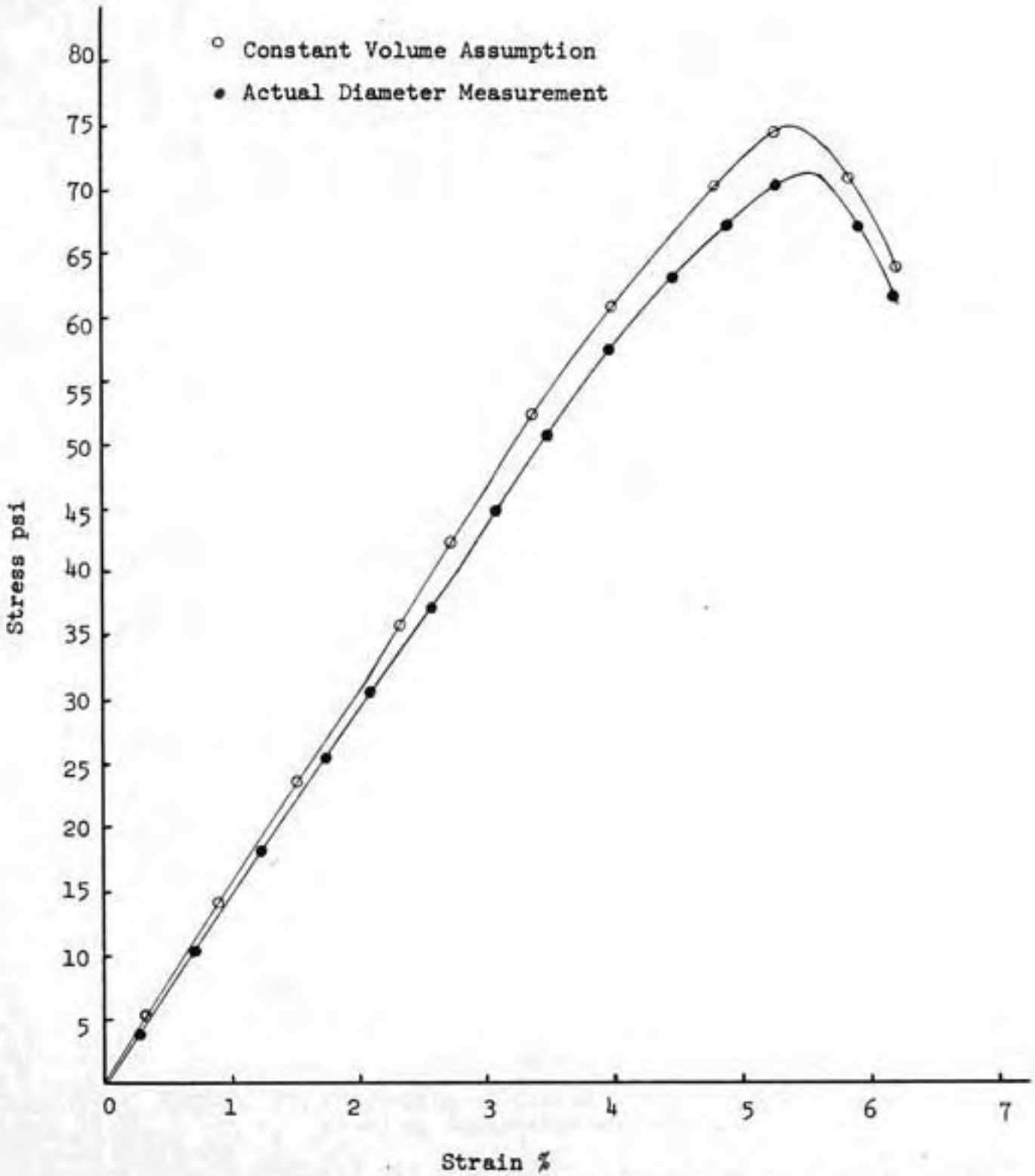

Figure 51 - Comparison of Stress-Strain Relationship of the Standard Proctor Compaction at Optimum

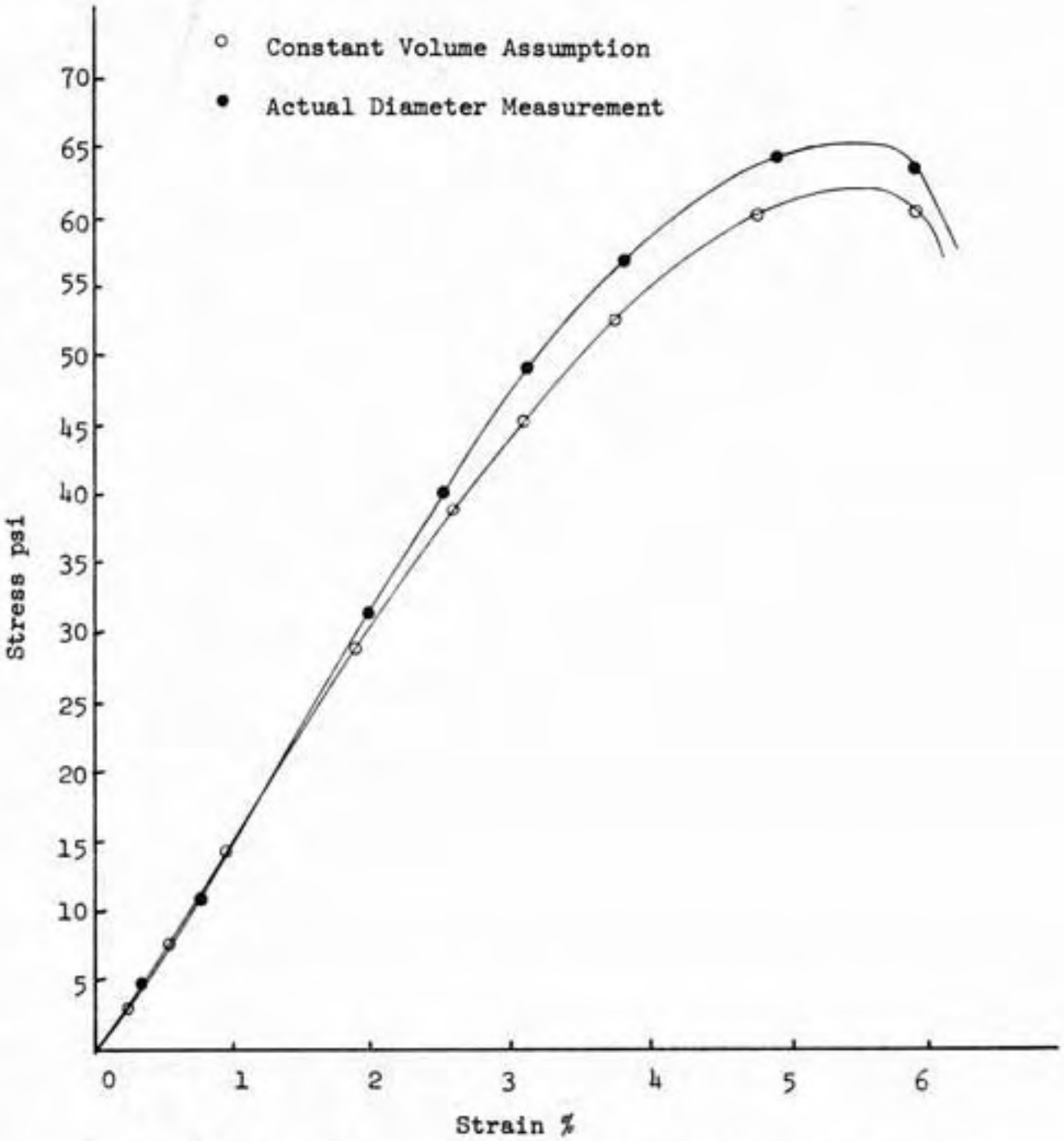

Figure 52 - Comparison of Stress-Strain Relationship of the Kneading Compaction at Optimum

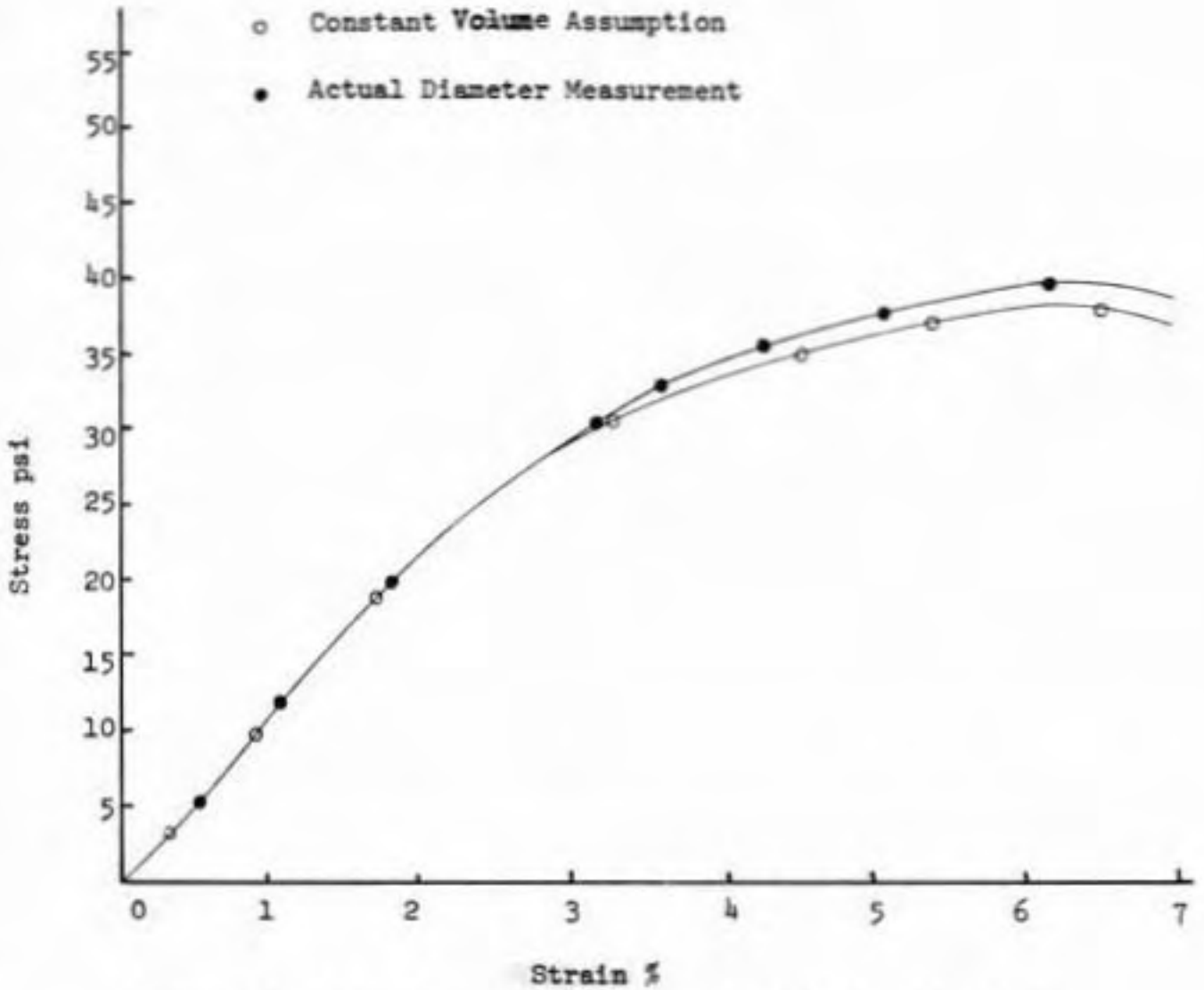

Figure 53 - Comparison of Stress-Strain Relationship of the Standard Proctor Compaction on the Wet Side

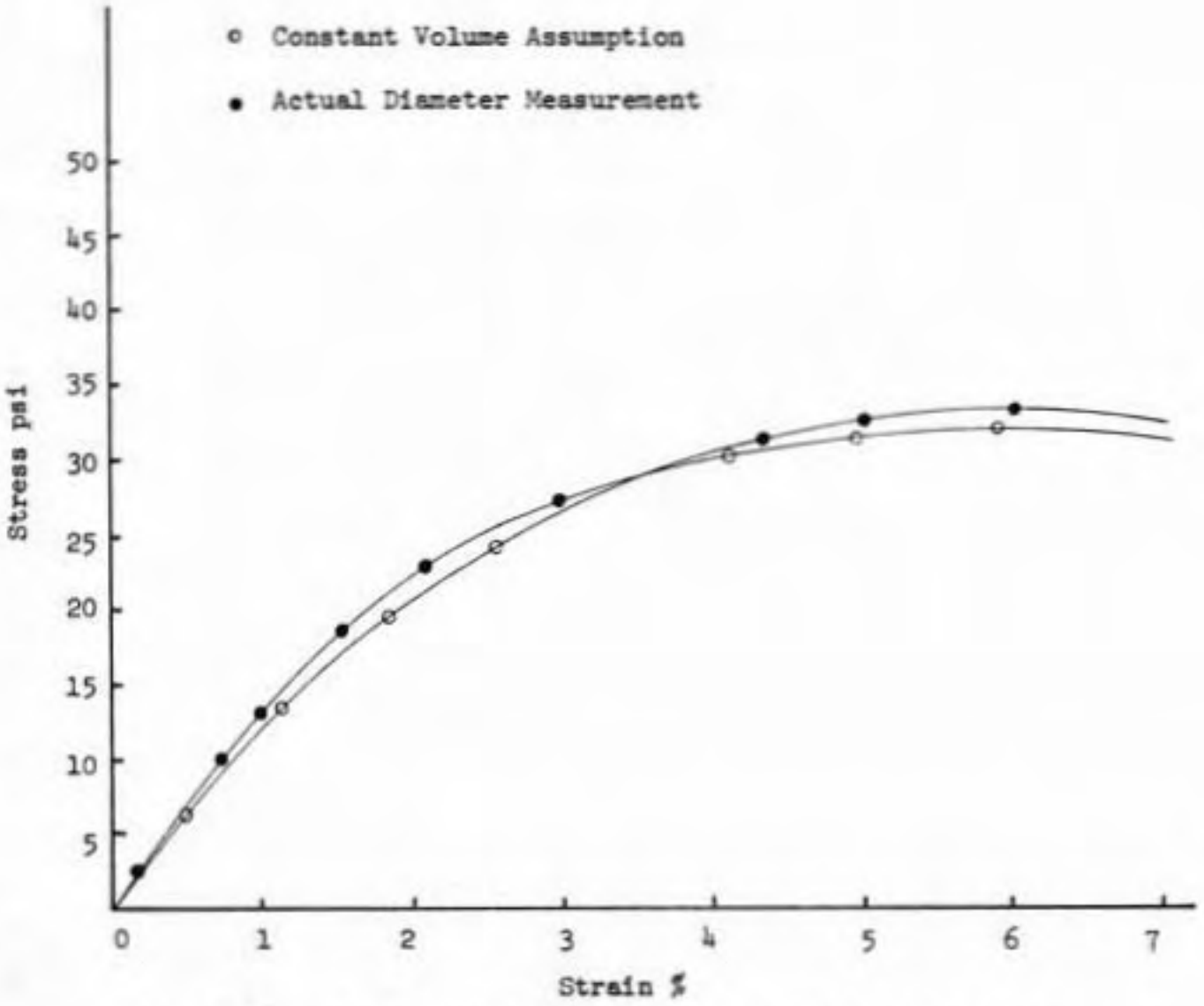

Figure 54 - Comparison of Stress-Strain Relationship of the Kneading Compaction on the Wet Side.

TABLE 48

Peak Stresses and Failure Strains Compared

Test No.	Compaction Type	Water Content %	Dry Unit Weight pcf	Peak Stress (Actual Dia.) psi	Failure Strain (Actual Dia.) %	Peak Stress (Const. Vol.)	Failure Strain (Const. Vol.)
14	ST	15.64 (dry)	95.71	48.07	2.40	47.15	2.40
7	SP	21.37 (optimum)	100.11	73.99	5.41	70.90	5.41
8	HM	21.43 (optimum)	99.06	66.26	5.04	62.84	5.04
6	SP	26.05 (wet)	96.39	39.99	6.40	38.40	6.40
5	HM	26.23 (wet)	96.27	33.07	6.86	32.21	6.36

Notes: SP: Standard Proctor
HM: Kneading Compaction
ST: Static Compaction

overestimate the area for the samples compacted on the wet side.

Examination of Table 47 shows that values of the modulii of elasticity can be significantly in error when the constant volume assumption is used for computing the stress.

Volume Change Characteristics

The volumes of the samples at given states of strain were estimated using the instantaneous measured diameters at mid height and axial lengths, and assuming the samples were cylindrical. Curves of volumetric strain vs. axial strain are shown in Figures 55 through 60. These curves show an almost linear decrease in the volumetric strain up to failure. Past these strains the curves show a positive dilatational trend, and may even assume positive values. The largest volumetric strains (a maximum of 5 1/2%) are observed for the samples compacted at optimum. This finding supports the deduction made earlier, i.e., the error in the values of the stress is the largest for the samples compacted at optimum when the assumption of constant volume is used in computing the stress. Samples compacted by the static compaction procedure showed the least volume change among the three methods of compaction at the optimum water content.

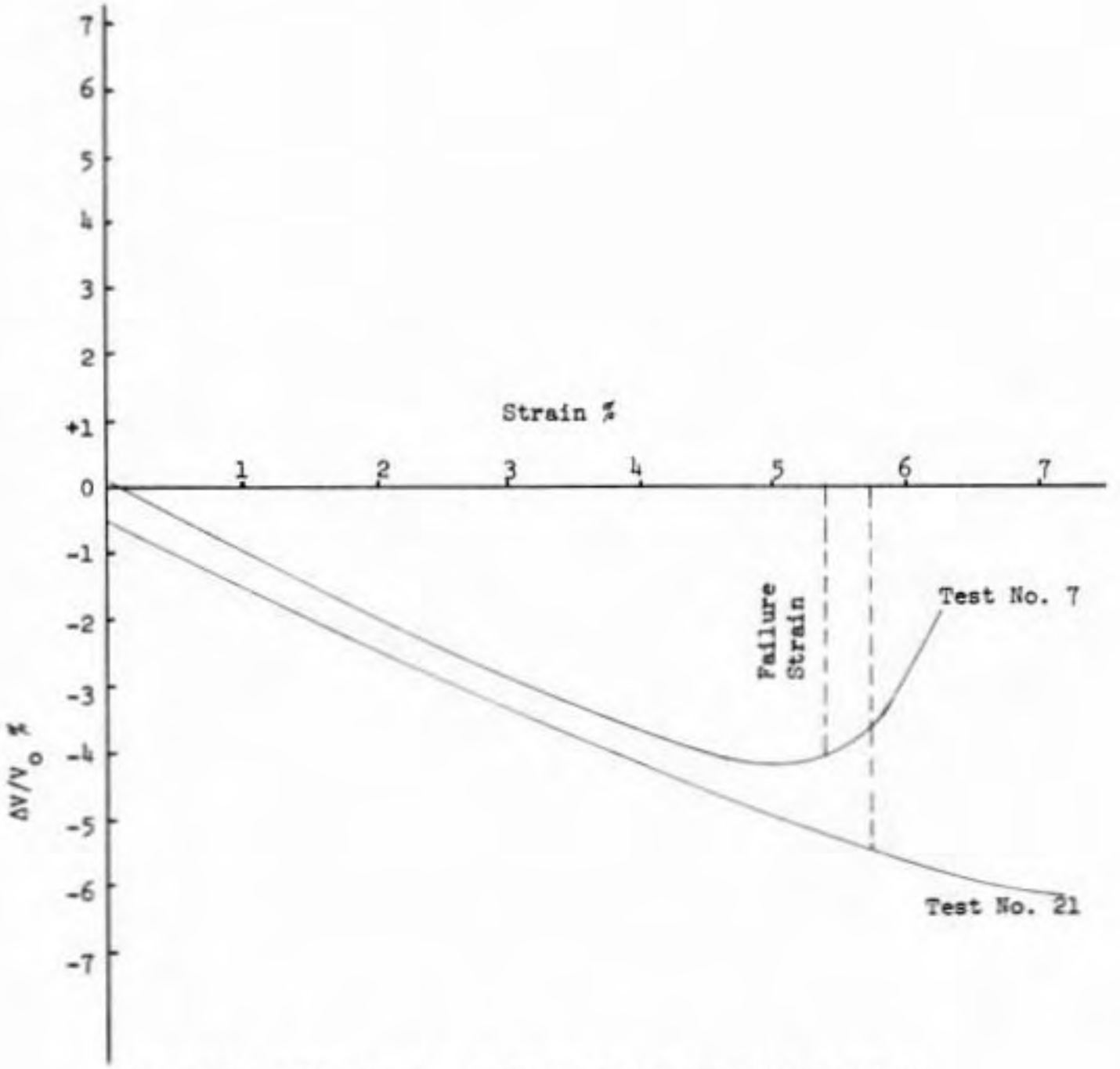

Figure 55 - Volume Change Characteristics of the Standard Proctor Compaction at Optimum

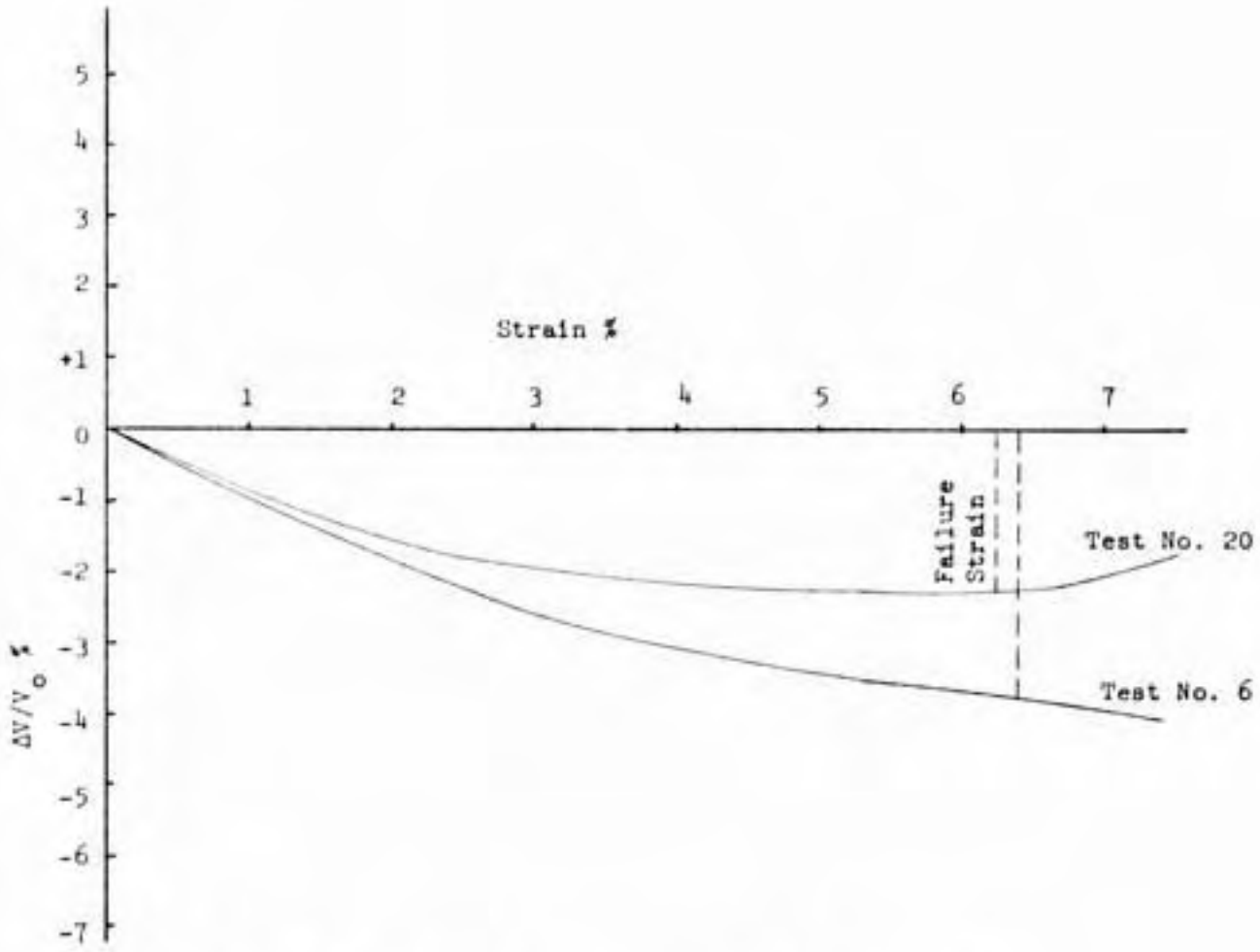

Figure 56 - Volume Change Characteristics of the Standard Proctor Compaction on the Wet Side

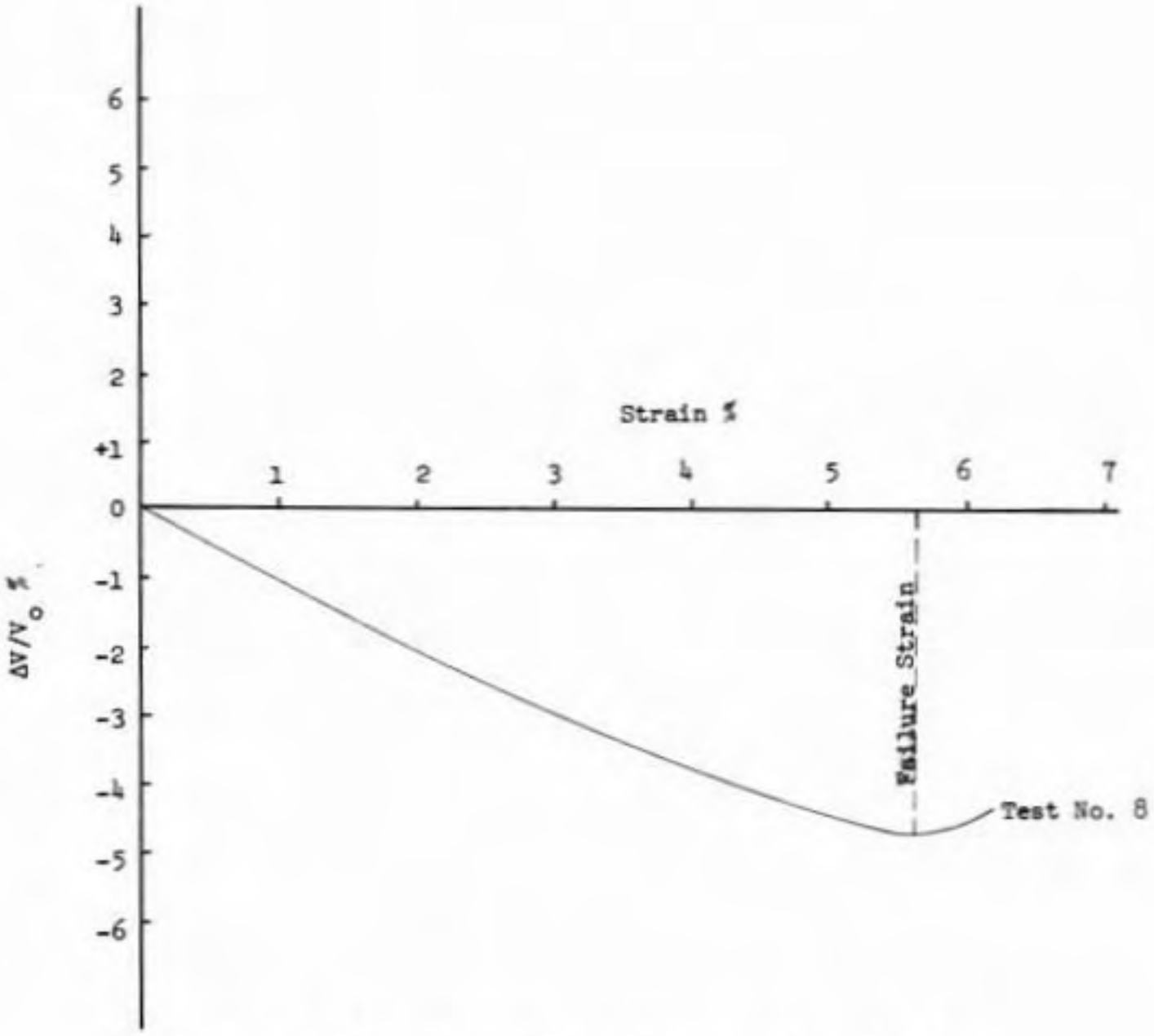

Figure 57 - Volume Change Characteristics of the Kneading Compaction at Optimum

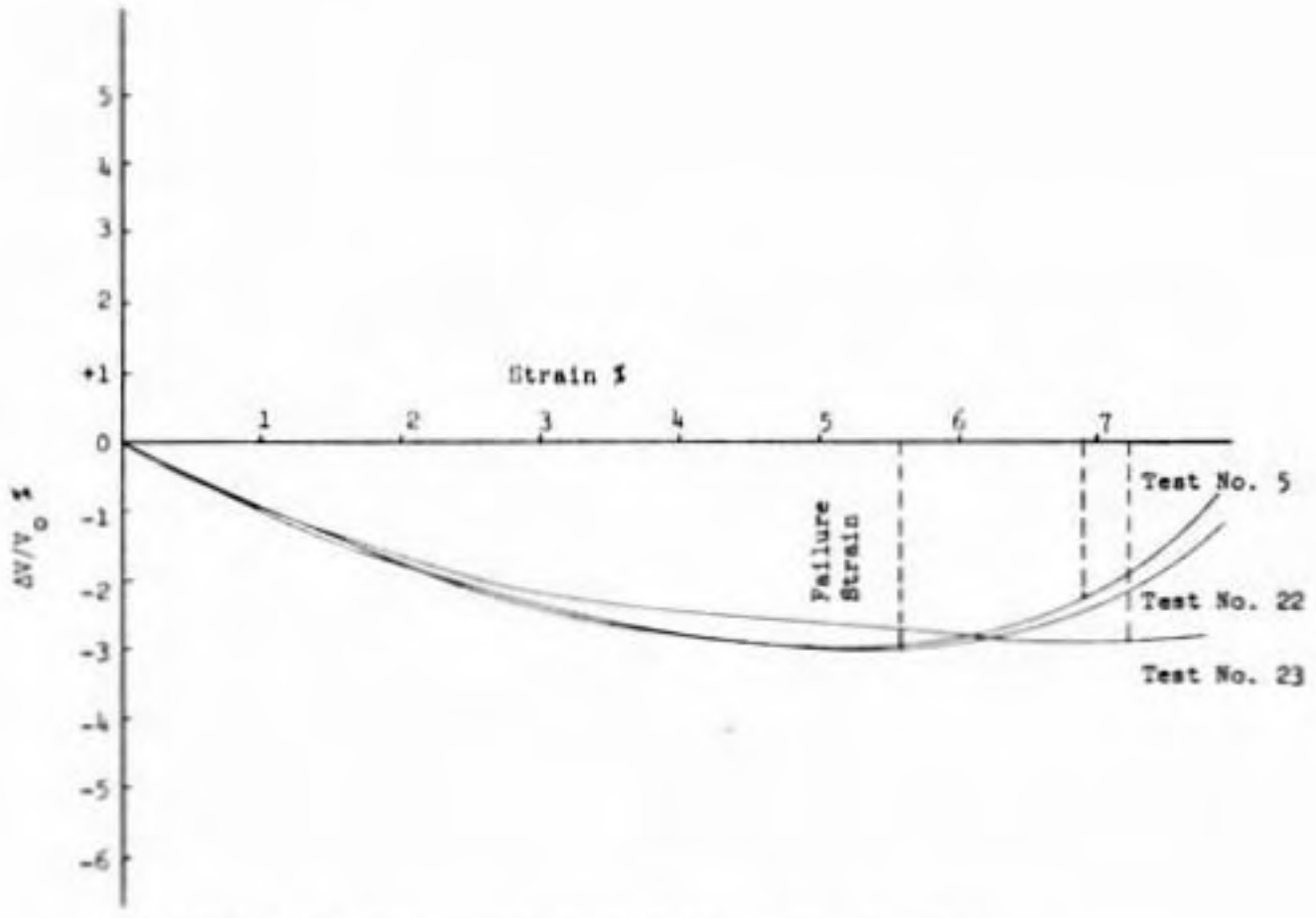

Figure 58 - Volume Change Characteristics of the Kneading Compaction on the Wet Side

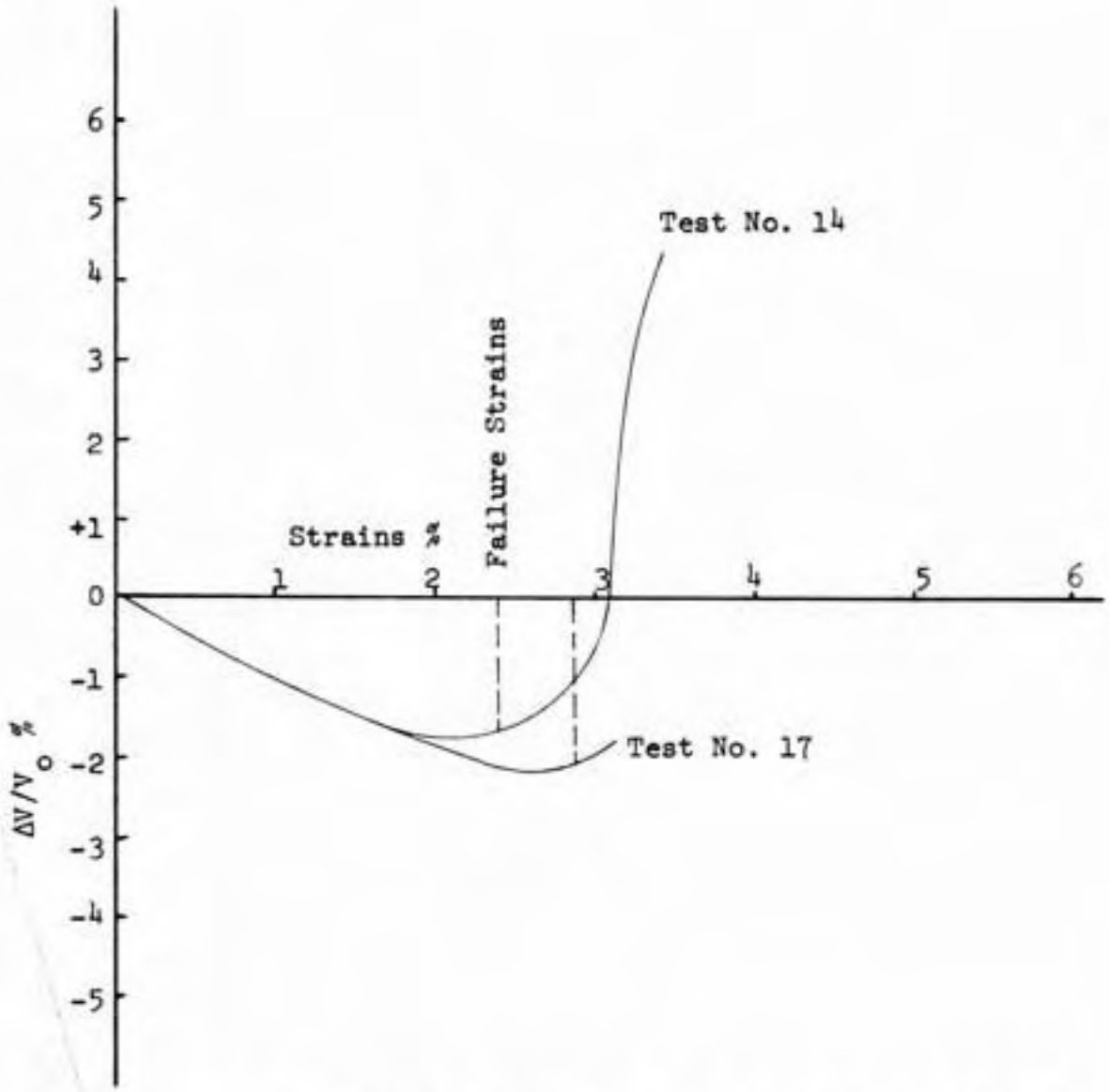

Figure 59 - Volume Change Characteristics of the Static Compaction on the Dry Side

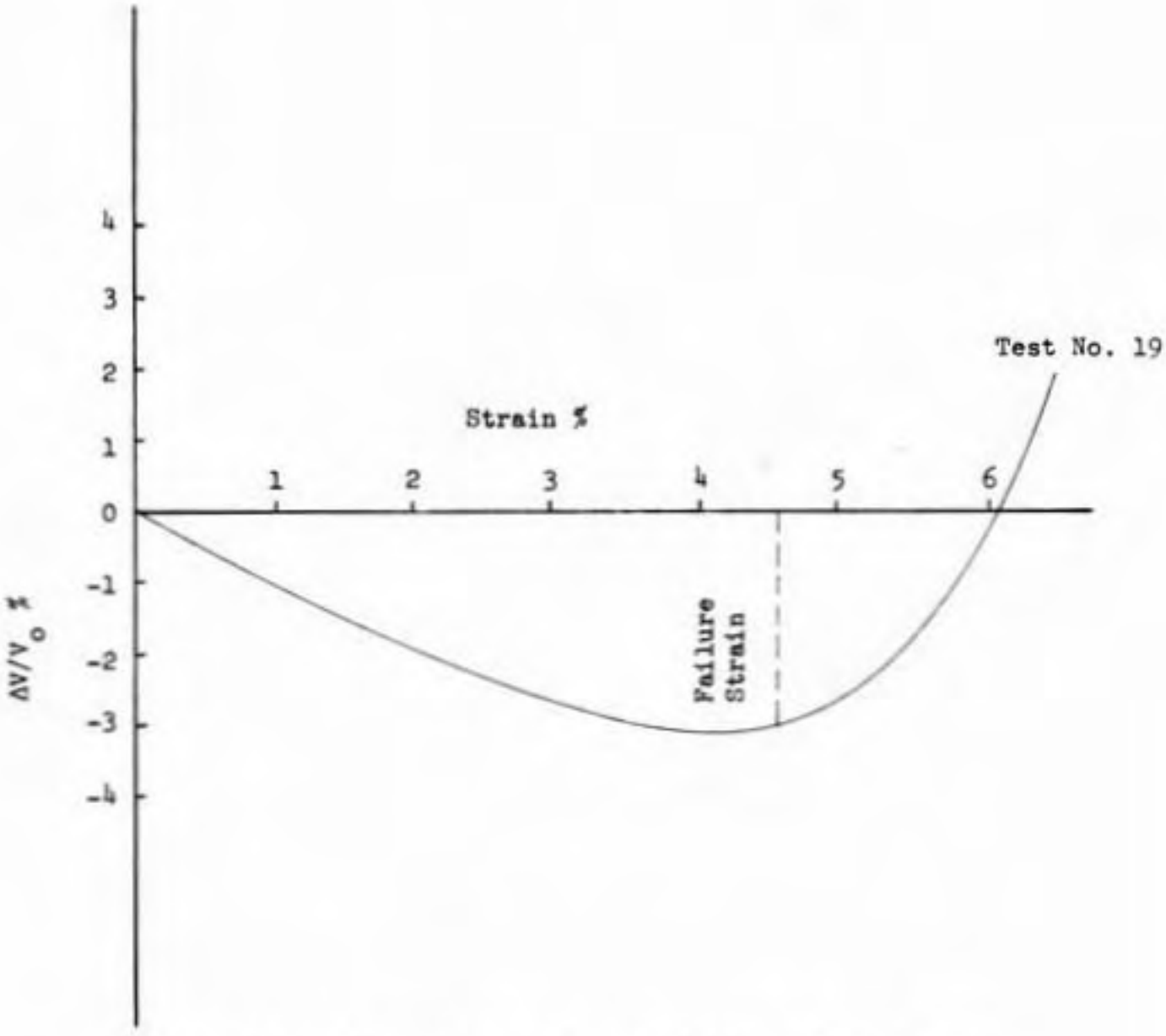

Figure 60 - Volume Change Characteristics of the Static Compaction at Optimum

CONCLUSIONS

1. For all methods of compaction, pore size distribution has been found to be most closely related to the molding water content. Variations exist primarily in the distribution of pores smaller than 50 microns.

The features of pore size distribution become distinct when they are divided into three pore diameter ranges: coarse, from 609 to 50 μ; medium, 50 to 0.5 μ, and fine, 0.5 to 0.016 μ. For all methods of compaction, for moisture contents dry of optimum, very close to 43% of the total intruded porosity is in the medium pore diameter range; whereas, at optimum and wet of optimum the maximum percentages of the total intruded porosity (averaging 49% and 53% respectively) are found in the fine pore diameter range. Samples compacted on the wet side of optimum possess twice as much porosity in the fine pore diameter range as dry side samples with the same total porosity.

2. Pore size distributions were affected very little when samples were compacted to the same moisture-unit weight condition by different methods of compaction.

3. Stress-strain curves in the unconfined compression tests varied systematically with molding water content. Dry of Proctor optimum, brittle failures occurred at low axial strains. Quasi-brittle failures at moderate strains were observed for compactions at Proctor optimum. Gradual shear failure at high strains occurred for the wet side compaction samples. The highest peak strenght (71 psi) was recorded for

samples compacted in the Standard Proctor test to Standard Proctor optimum. Kneading compaction for samples on the wet side of optimum showed the lowest strength (32 psi).

On the average, the peak strength of samples compacted on the wet side of Proctor optimum was about two thirds that for samples compacted on the dry side of Proctor optimum. These comparisons are made at equal unit weights.

4. Samples with similar total porosity values can have entirely different pore size distributions. Therefore, pore size distribution can correlate differently with soil behavior than total porosity.

5. Freeze drying of compacted samples is suitable for this research in that

> (1) essentially the same moisture loss occurs as in oven drying and
>
> (2) the moisture loss produces quite nominal volume changes, e.g., about 5% reduction in volume or less.

It is assumed that only nominal changes in pore size distribution are produced by nominal changes in total porosity.

6. Oven drying, in contrast to freeze drying, induces shrinkage which varies greatly with the degree of saturation. Samples with a high degree of saturation were reduced in volume as much as 20%. At low degrees of saturation the shrinkage was quite small. At a low degree of saturation of about 52%, the pore size distributions determined after oven drying were substantially the same as for freeze drying.

BIBLIOGRAPHY

BIBLIOGRAPHY

1. Ahlrichs, J. L., and White, J. L.: "Freezing and Lyophilizing Alters the Structure of Bentonite Gels", Science, Vol. 136, June 1962, pp. 1116-1117.

2. Anderson, D. M. and Hoekstra, P.: "Crystallization of Clay Adsorbed Water", Science 149, pp. 318-319, (1965).

3. Altschaeffl, A. G., and Lovell, C. W., Jr.: "Compaction Variable and Compaction Specifications", Proceedings of the 54th Annual Purdue Road School, Jan. 1969.

4. Barden, L., and Sides, Geoffery R.: "Engineering Behavior and Structure of Compacted Clay", J. Soil Mech. and Foundations Div., Vol. 96, July 1970.

5. Casagrande, A., and Hirschefeld, R. C.: "Stress Deformation and Strength Characteristics of a Clay Compacted to a Constant Dry Unit Weight", Proc. Research Conf. on Shear Strength of Cohesive Soils, Boulder, Colorado, 1960.

6. Childs, E. C., and Collis-George, N.: "The Permeability of Porous Material", Proceedings Royal Society, Vol. 201, A, 1950.

7. Csathy, Thomas I., and Townsend, D. L.: "Pore Size and Field Frost Performance", Highway Research Board Bulletin No. 331, 1962.

8. Delsemme, A., and Wenger, J.: "Superdense Water Ice", Science Vol. 167, Jan. 1970.

9. Diamond, S.: "Pore Size Distribution in Clays", Clays and Clay Minerals, Vol. 18, 1970, pp. 7-23.

10. Dowell, L. G., and Reinfret, A. P.: "Low Temperature Forms of Ice as Studied by X-Ray Diffraction", Nature, Vol. 188, Dec. 31, 1960, pp. 1144-1148.

11. Drake, L. C.: "Pore Size Distribution in Porous Materials", Journal of Industrial and Engineering Chemistry, Vol. 41, 1949.

12. Drake, L. C., and Ritter, H. L.: "Macropore Size Distributions in Some Typical Porous Substances", Journal of Industrial and Engineering Chemistry, Vol. 17, 1945, pp. 782-786.

13. Hamilton, A. B.: "Freezing Shrinkage in Compacted Clays", Canadian Geotechnical Journal, Vol. II, Number 1, Feb. 1966.

14. Highter, W. H., Altschaeffl, A. G., and Lovell, C. W., Jr.: "Low Temperature Effects on the Compaction and Strength of a Sandy Clay" Highway Research Record No. 304, 1970, pp. 45-51.

15. Hiltrop, C. L., and Lemish, J.: "Relationship of Pore-Size Distribution and Other Rock Properties to Serviceability of Some Carbonate Aggregates", Highway Research Board Bulletin No. 239, 1960.

16. Hill, A.: "An Improved Method of Interpreting Mercury Penetration Data", British Ceramic Society, Transactions, 39(6), 1960, pp. 198-212.

17. Hvorslev, J. M.: "Subsurface Exploration and Sampling of Soils for Civil Engineering Purposes", Waterways Experiment Station, Vicksburg, Mississippi, Nov. 1946.

18. Klock, O. G., and Boersma, L.: "Pore Size Distribution as Measured by the Mercury Intrusion Method and their Use In Predicting Permeability", Soil Science Society of America, Proceedings, 1968.

19. Kun, K. A., and Kunin, R.: "Pore Structure of Some Macroreticular Ion Exchange Resins", Polymer Letters, Vol. 2, 1964, pp. 587-591.

20. Lambe, T. W.: "The Engineering Behavior of Compacted Clay", Jour. Soil Mech. and Foundation Div., Paper No. 1654, May 1958.

21. Lambe, T. W.: "The Engineering Behaviors of Compacted Clay", Jour. Soil Mech. and Foundation Div., Paper No. 1655, May 1958.

22. Lambe, T. W.: "Soil Testing", John Wiley and Sons Inc., New York, 1967.

23. Lange, A. N.: "Handbook of Chemistry", McGraw Hill Book Company, Inc., 1961.

24. Leonards, G. A.: "Strength Characteristics of Compacted Clays", Proc. Amer. Soc. of Civil Engineers, Separate No. 360, Vol. 79, 1953, pp. 1-35.

25. Leonards, G. A. and Altschaeffl, A. G.: "Compressibility of Clay", Jour. Soil Mech. and Foundation Div., Sept., 1964.

26. Leonards, G. A.: "Foundation Engineering", McGraw Hill Book Company, Inc.

27. Lovell, C. W., Jr.: "Temperature Effects on Phase Composition and Strength of Partially Frozen Soil", Highway Research Board Bulletin No. 168, 1957.

28. Luyet, B.: "Recent Developments in Crystobiology and their Significance in the Study of Freezing and Freeze Drying of Bacteria", Proc. Low Temperature Microbiology Symposium, Camden, N. J., 1961.

29. Luyet, B., Tanner, J., and Rapatz, C.: "X-Ray Diffraction Study of the Structure of Rapidly Frozen Gelatin Solutions", Biodynamics, Vol. 9, No. 173, Dec. 1962, pp. 21-46.

30. Luyet, B. J.: "Cytology of the Blood Forming Organs', Besis, M, 216, Grunne and Stratton, N. Y. 1956.

31. M.I.T.: "Engineering Behaviour of Partially Saturated Soils", Research Report R63-26, 1963, pp. 1-66.

32. Merryman, H. T.: "Principles of Freeze Drying," New York Academy of Sciences, Vol. 85, March-May 1960.

33. Merryman, H. T.: "X-Ray Analysis of Rapidly Frozen Gelatin Gels", Biodynamica, Vol. 8, No. 157, Dec. 1958, pp. 69-72.

34. Norrish, K., and Ransell-Colorn, J. A.: "Effect of Freezing on the Swelling of Clay Minerals", Clay Minerals Bulletin No. 5, 1962, pp. 9-16.

35. Orr, C., Jr.: "Application of Mercury Penetration to Materials Analysis", Power Technology 3, pp. 117-121, 1969.

36. Rice, R. U., Kaesberg, P., and Stahmann, M. A.: "Freeze Drying for Electron Microscopy", Archives of Biochemistry and Biophysics 59, 1955, pp. 332-340.

37. Drake, L. C., and Ritter, H. L.: "Pore Size Distribution in Porous Materials", Journal of Industrial and Engineering Chemistry, Vol. 17, 1945, pp. 782-786.

38. Rootare, H. M.: "A Short Literature Review of Mercury Porosimetry as a Method of Measuring Pore-Size Distribution in Porous Materials, and a Discussion of Possible Sources of Errors in This Method", Aminco Lab News, 1969.

39. Rosenqvist, Th. I.: "Physico-Chemical Properties of Soils", Jour. Soil Mech. and Foundation Div., ASCE, April 1959.

40. Rowe, Terence, W. G.: "The Theory and Practice of Freeze Drying", New York Academy of Science Annals, Vol. 85, March-May 1960.

41. Sarakhov, A. I.: "Some Comments on the Accuracy of the Method of Mercury Porosimetry", Russian Journal of Physical Chemistry, Feb. 1963.

42. Seed, H. B., and Chan, C. K.: "Structure and Strength Characteristics of Compacted Clays", Jour. Soil Mech. and Foundation Div., Oct. 1959.

43. Seed, H. B., Mitchell, J. K., and Chan, C. K.: "The Strength of Compacted Cohesive Soils", Research Conference on Shear Strength of Cohesive Soils, Boulder, Colorado, 1960.

44. Sridharan, A., Altschaeffl, A. G., and Diamond, S.: "Pore Size Distribution Studies", Jour. Soil Mech. and Foundation Div., May, 1971.

45. Sridharan, A.: "Some Studies on the Strength of Partially Saturated Clays", Ph.D. thesis, Purdue University, August 1968.

46. Taylor, D. W.: "Fundamentals of Soil Mechanics", Wiley, 1948.

47. Terzaghi, K., and Peck, R. T.: Soil Mechanics in Engineering Practice, Wiley, 1948.

48. Washburn, E. W.: "Note on a Method of Determining the Distribution of Pore Sizes in a Porous Material", Proc. National Academy of Science, Vol. 7, 1921.

49. Watson, A., May, J. O., and Butterworth, B.: "Studies of Pore Size Distribution", Trans. British Ceramic Soc., Vol. 56, 1957.

50. Wilson, S. D.: "Suggested Method of Test for Moisture Density Relations of Soils Using Harvard Compaction Apparatus", Engineering News Record, Nov. 2, 1950.

51. Winslow, N. M. and Shapiro, J. J.: "An Instrument for the Measurement of Pore Size Distribution by Mercury Penetration", ASTM, Feb., 1959.

52. Winslow, N. D. and Diamond, S.: "The Pore Size Distribution of Portland Cement Paste", Journal of Materials, Vol. 5, No. 3, 1970.

APPENDICES

APPENDIX A

PROPERTIES OF GRUNDITE

TABLE A1

Index Properties of Grundite

Liquid Limit	52
Plastic Limit	30
Plasticity Index	22
% finer than 0.002 mm	65
Specific Gravity	2.77

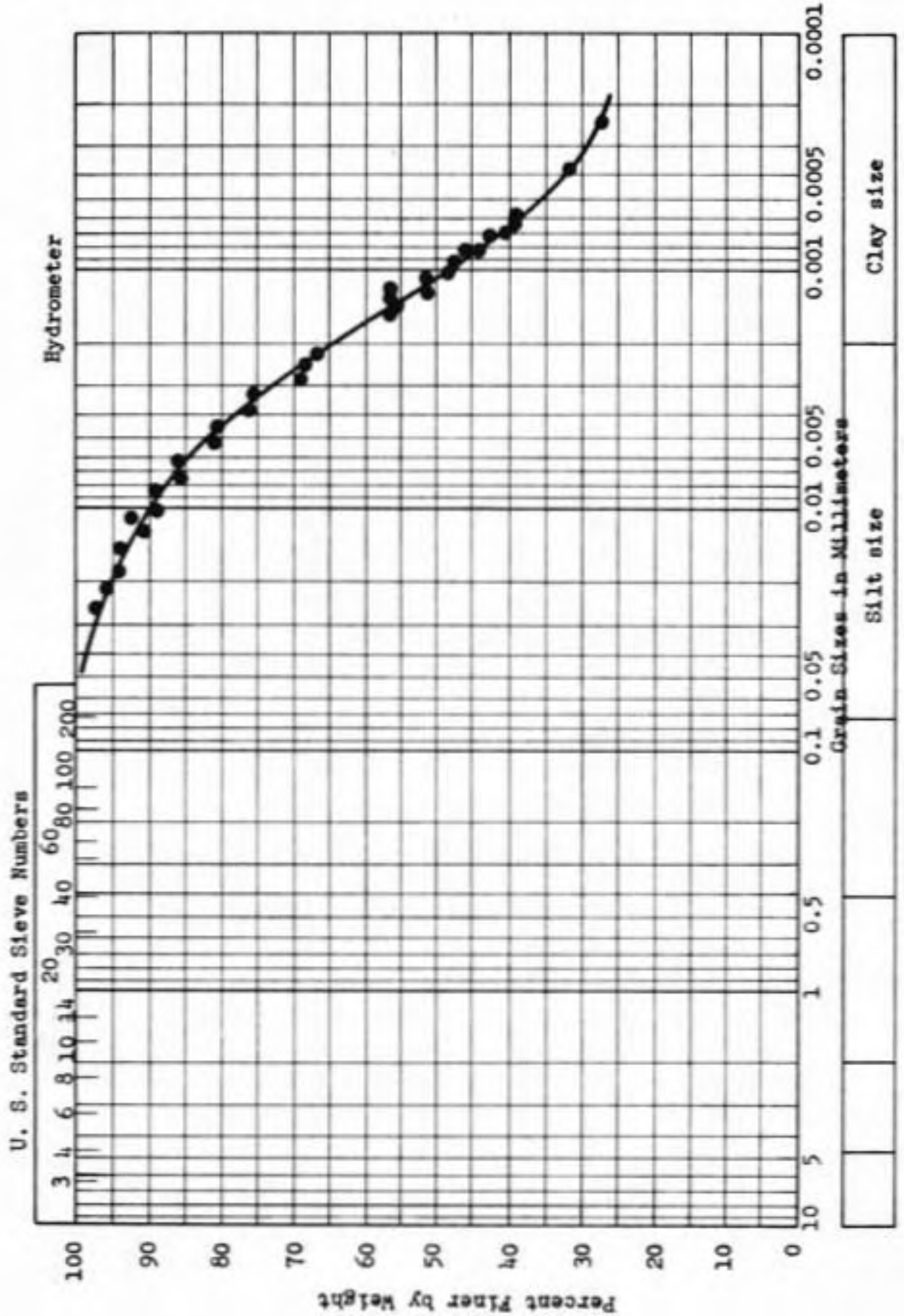

Figure A1 - Grain Size Distribution for Grundite

SCANNING ELECTRON MICROGRAPHS

Scanning electron micrographs of the samples compacted dry of optimum, at optimum, and wet of optimum, by the three methods of compaction are shown in Figures B1 through B8. The molding water contents were: 15.6%, 19.8%, and 26.0% for the dry side, at optimum, and the wet side, respectively.

It is seen from these Figures that the mixing and compaction process results in more less spherical aggregations of clay particles being retained on the dry side of optimum. At optimum and wet of optimum, the aggregations of clay are deformed and broken down in the compaction process to produce a mosaic like appearance. Examination of electron micrographs taken at higher magnifications shows that individual clay particles are bent, twisted and curled in the compaction process. These micrographs give the notion that shear failure, once induced, would cause a rapid collapse of the solid-void packing on the dry side.

It appears that the arrangement and packing of the soil aggregates is related to the molding water content, but it is not significantly influenced by the compactive procedure when the moisture-unit weight condition is held constant.

APPENDIX B

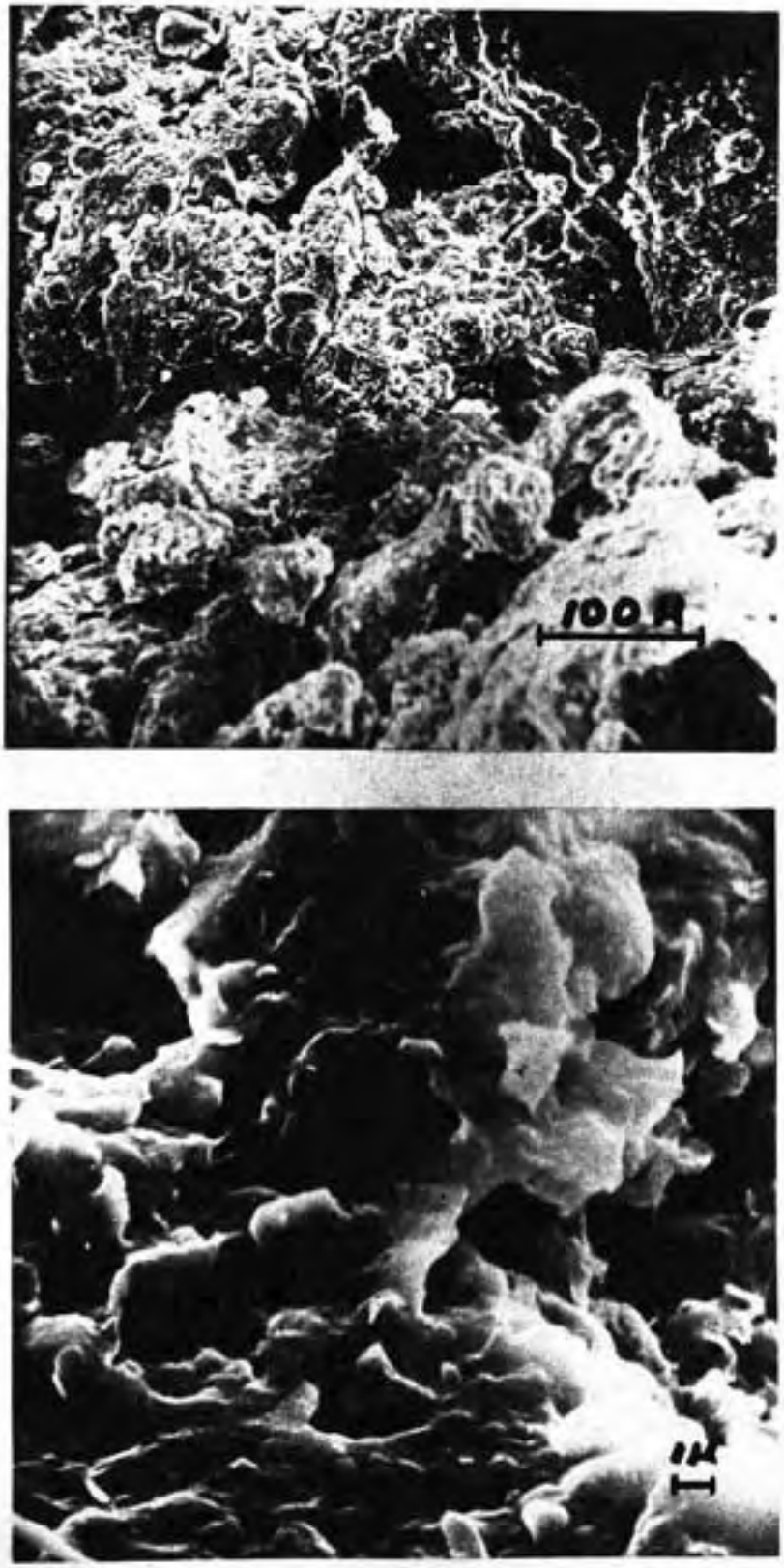

Figure B1 - Electron Micrographs of Samples Compacted by Kneading Compaction on the Dry Side

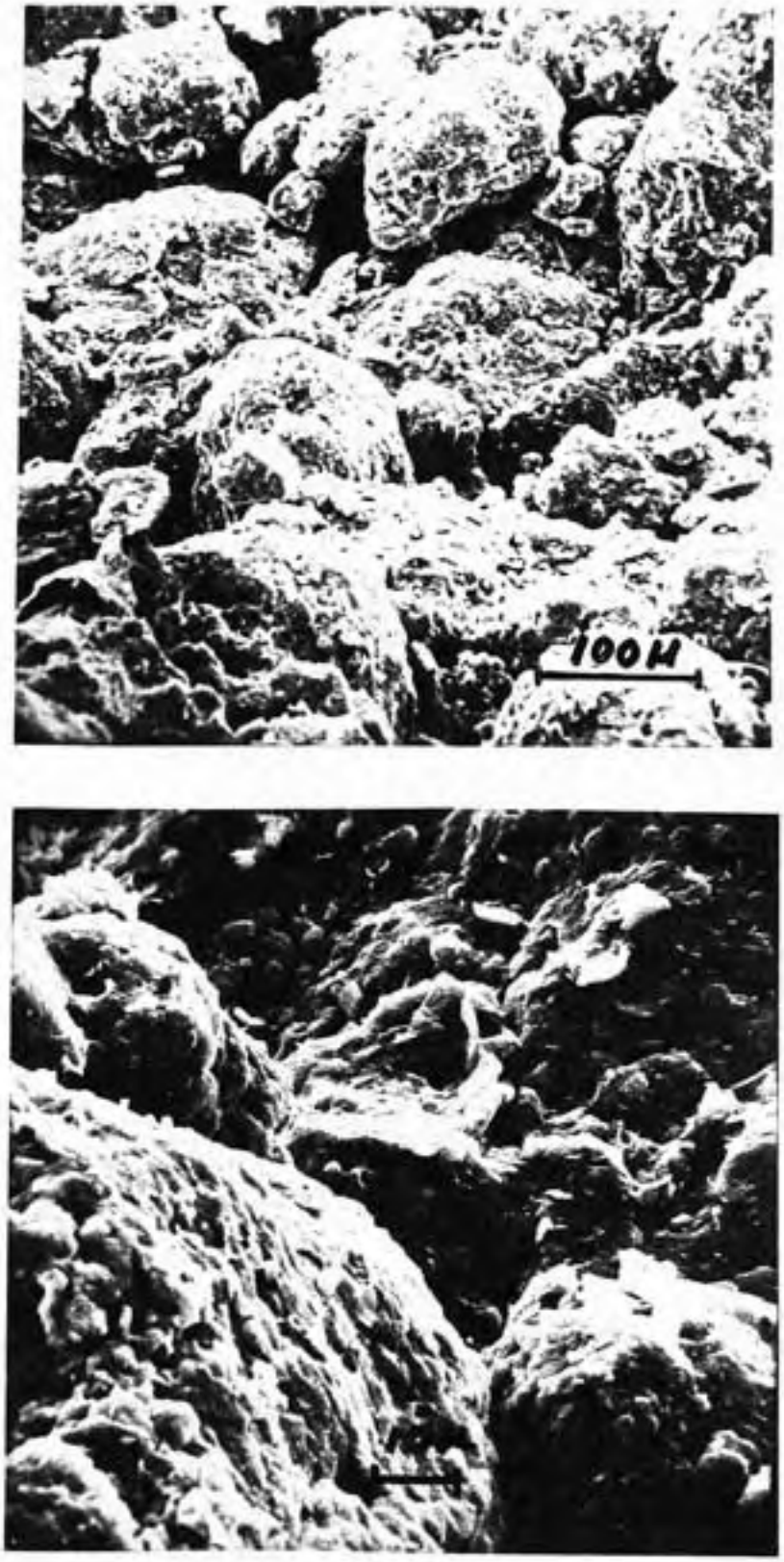

Figure B2 - Electron Micrographs of Samples Compacted by Static Compaction on the 'Dry Side'

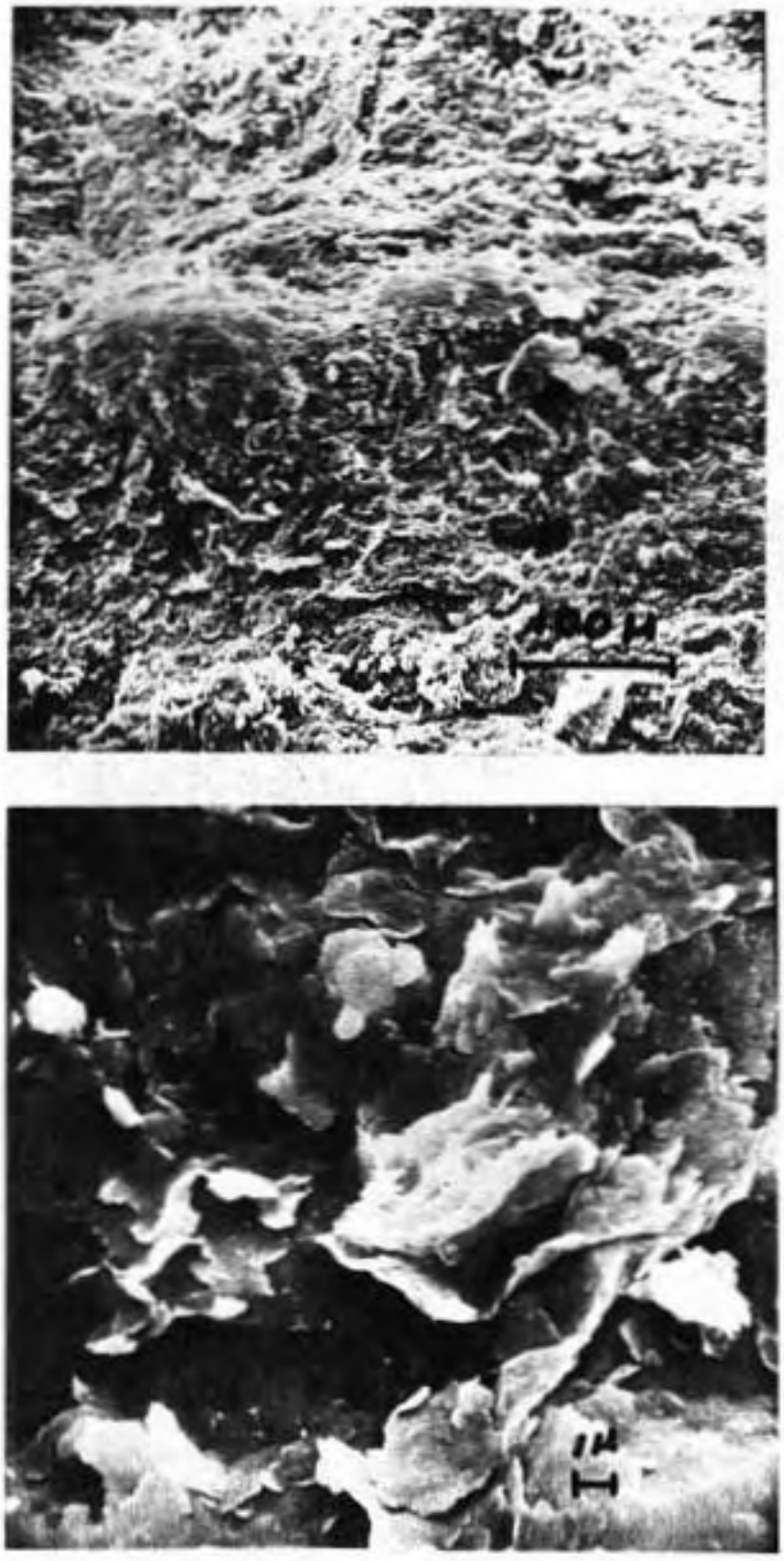

Figure B3 - Electron Micrographs of Samples Compacted by Standard Proctor at 'Optimum'

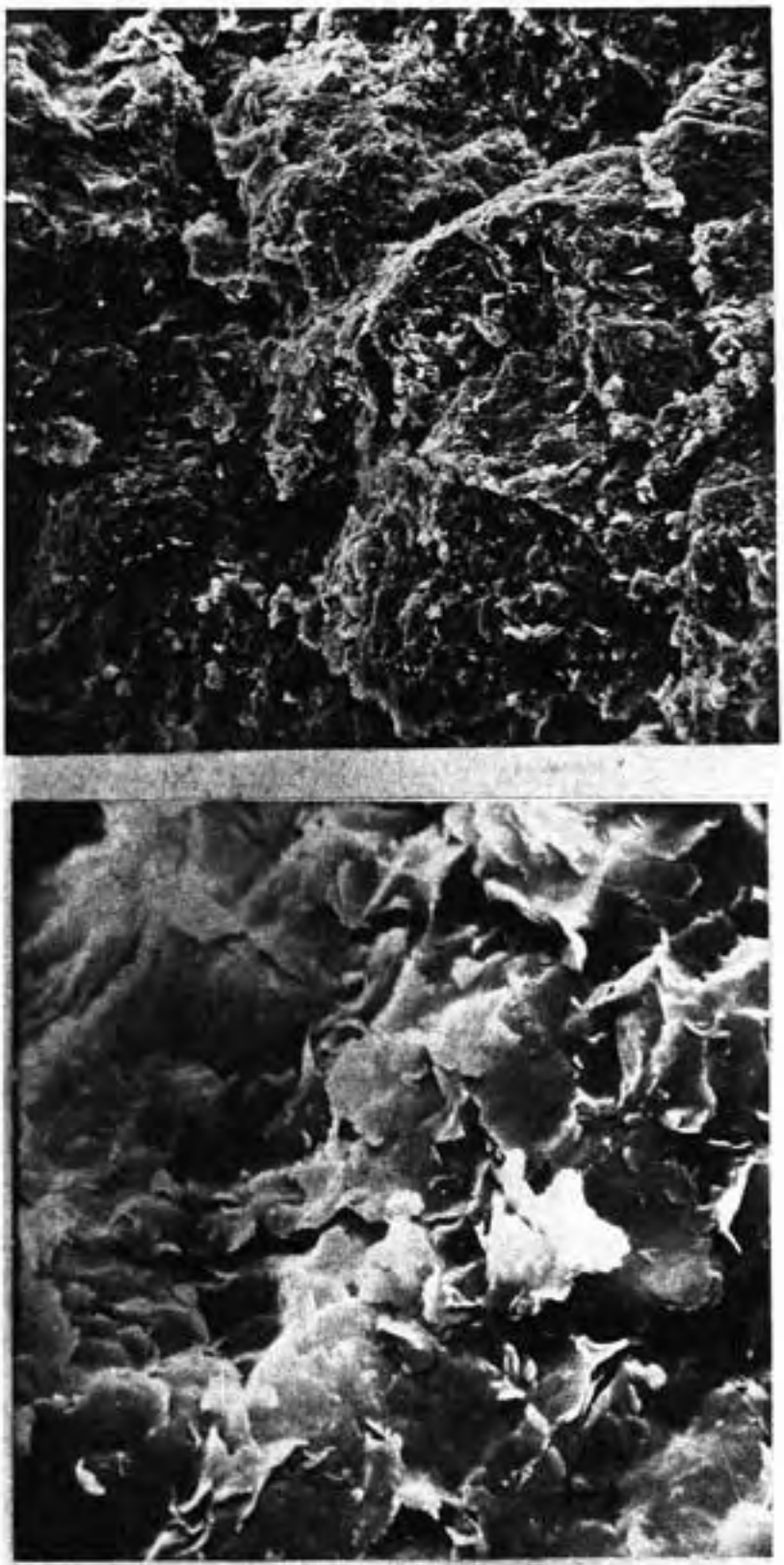

Figure B4 - Electron Micrographs of Samples Compacted by Kneading Compaction at 'Optimum'

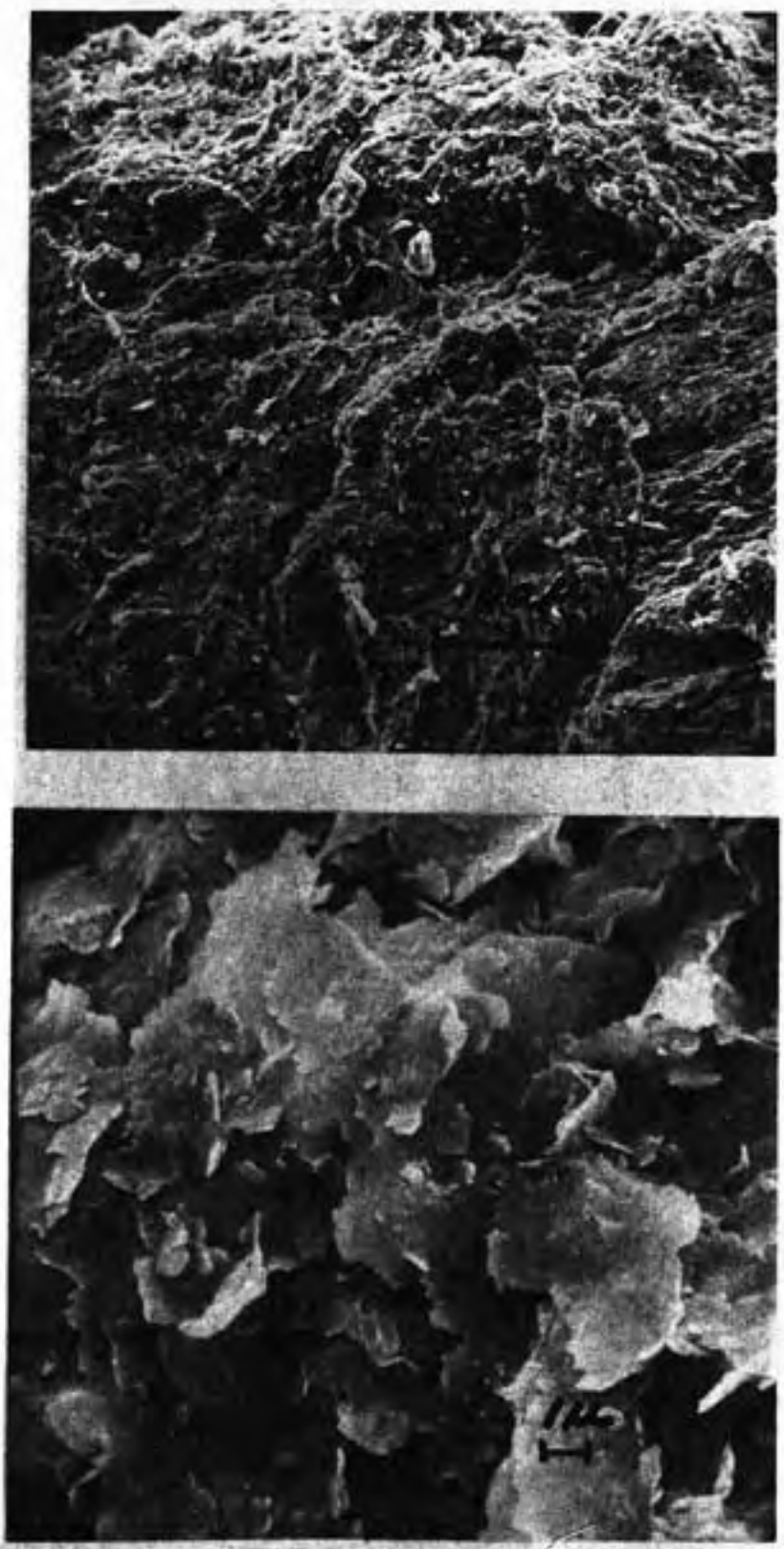

Figure B5 - Electron Micrographs of Samples Compacted by Static Compaction at 'Optimum'

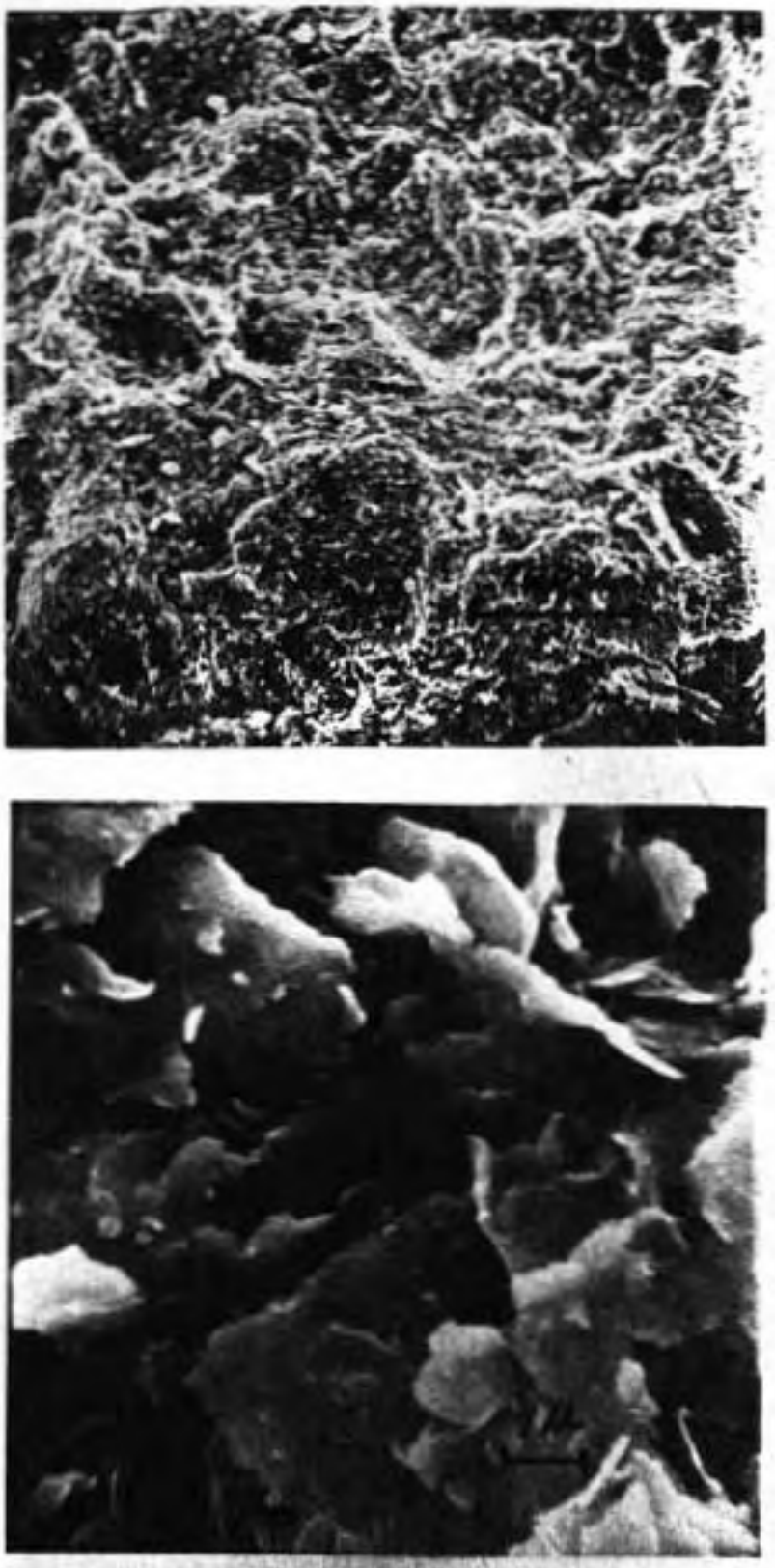

Figure B6 - Electron Micrographs of Samples Compacted by Standard Proctor on the 'Wet Side'

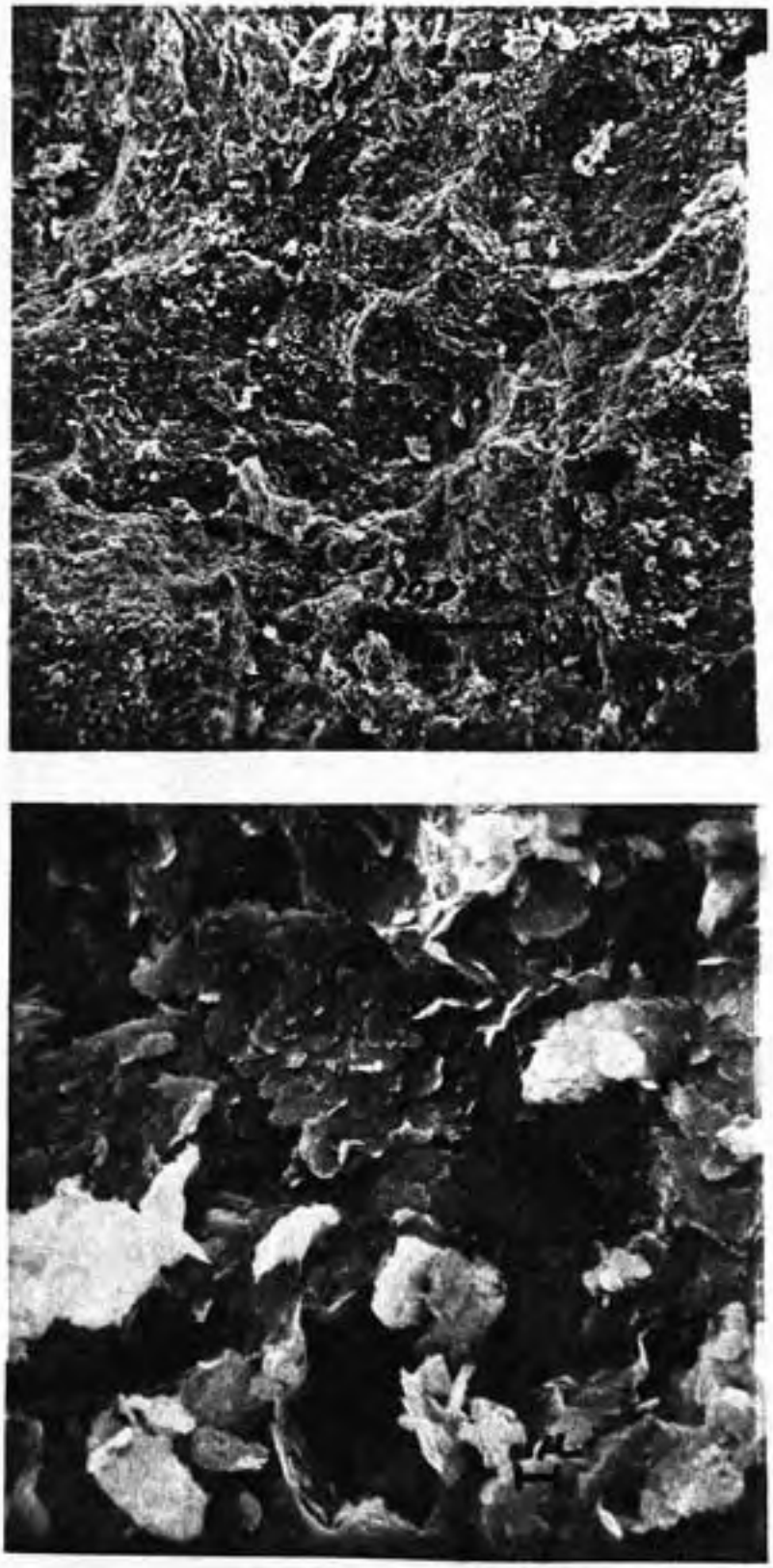

Figure B7 - Electron Micrographs of Samples Compacted by Kneading Compaction on the 'Wet Side'

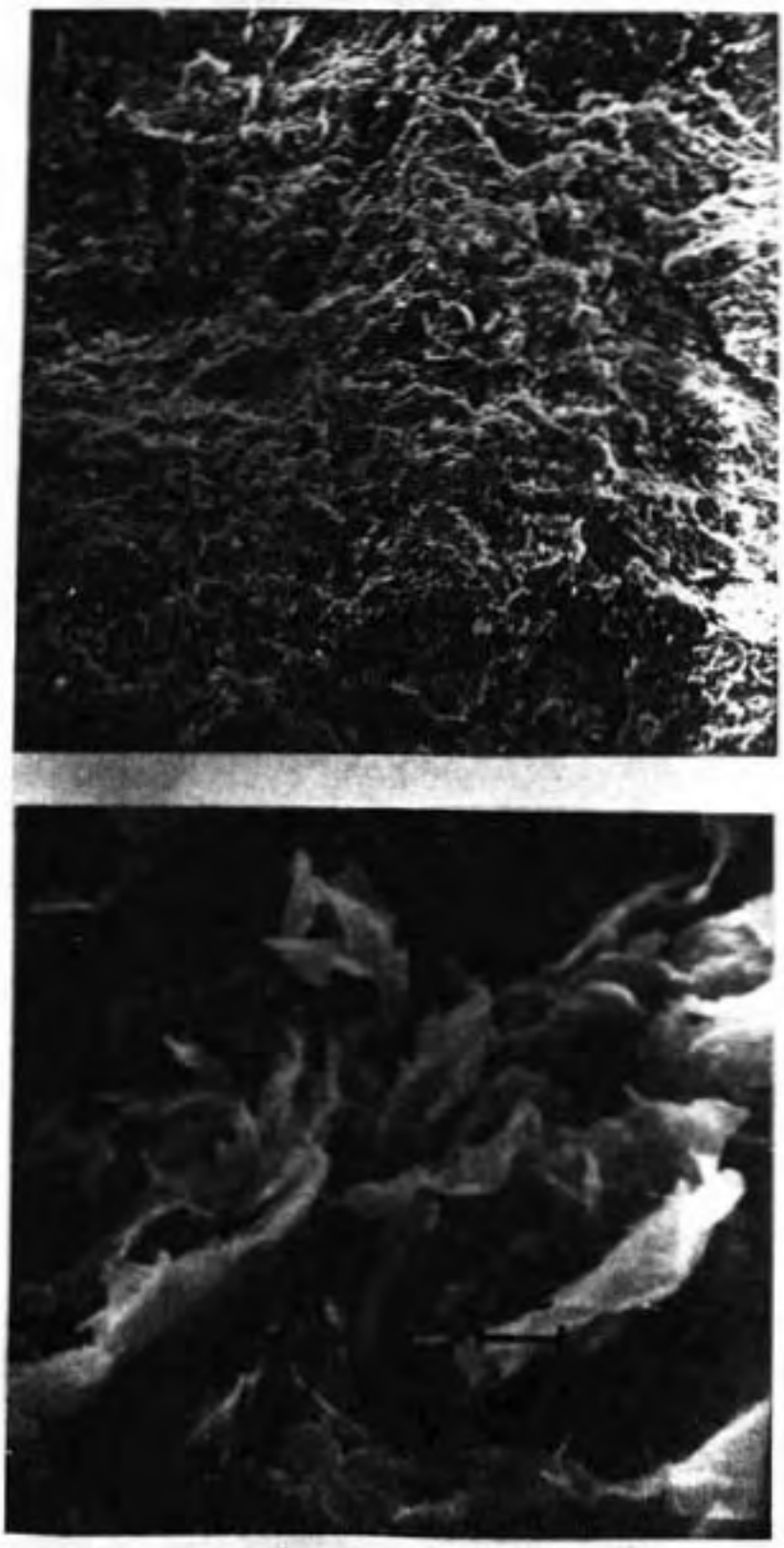

Figure B8 - Electron Micrographs of Samples Compacted by Static Compaction on the 'Wet Side'

APPENDIX C

EXPERIMENTAL DETAILS

Example of Calculations for Matching the Dry Unit Weight of Kneading and Static Compaction with That of Standard Proctor at the Same Water Content

Kneading

Dry Unit Weight at Selected Point of the Standard Proctor curve = 98.89 pcf

Wet Unit Weight at Selected Point of the Standard Proctor curve = 115.50 pcf

Wet weight required to compact the cylinder by kneading compaction of volume 1/454 cf (2.2×10^{-3}) = 115.50 gm. But the compaction extends about one half inch into the collar, therefore the compacted height is 2.816 + 0.5 = 3.316 in. and the volume will be 2.6×10^{-3} cf. Therefore, the actual wet weight required = $115.50 \times \frac{2.6}{2.2} = 136.4$ gm.

Static

Volume of cylinder = 9.1×10^{-4} cf.

Wet weight required for γ_d of 98.89 = $(115.50)(9.10 \times 10^{-4})(453.60)$

= 47.5 gm.

Investigation of Sampling Disturbance for Samples Compacted on the Dry Side of Standard Proctor Optimum

In Table C1 values of heights for the first two samples are those obtained when the sample was still in the cylinder. The last two columns give the expected 'as compacted' porosity and void ratio based on the water contents as mentioned previously. The heights of the cylinders showed shortening due to extrusion. Values of porosities of the first

two samples obtained by using the dimensions after extrusion and water content as given in Col. X below, were obtained and compared with the expected porosity. For the first two samples this ratio was 84.9 and 81.2 percent, respectively. When these ratios are compared with those given in Col. IX for sample No. 1 and 2 a loss of the order of 3% is observed due to extrusion.

The analysis which follows assumes that the soil displaced by the sampler volume is pushed into the sampler causing the densification of the sample.

Outside Area of the Samper = 0.57555 cm^2

Inside area of the Sampler = 0.52544 cm^2

Annular Area of the Sampler = 0.05011 cm^2

TABLE C1

Sampling Disturbance of Samples Compacted on the Dry Side

As Compacted Properties: $e = 0.80$, $n = 0.29\ cm^3/gm$ $w = 15/64\%$ $\gamma_d = 95.99$ pcf

Col. No.	I	II	III	IV	V	VI	VII	VIII	IX	X	XI	XII
Sample No.	Dia. mm	Height mm	Wet Wt. gm	Sample Vol. cm^3	Void Vol. cm^3	Void Ratio (e)	Porosity (n)	$\frac{e}{e_{AC}}$ %	$\frac{n}{n_{AC}}$	Water content obtained by oven drying %	Expected e_{AC}	Expected n_{AC}
1	8.20	9.88	0.9829	0.522	0.216	0.702	0.254	87.74	87.83	13.00	0.76	0.27
2	8.18	9.79	0.9862	0.515	0.207	0.673	0.244	84.13	84.22	13.55	0.77	0.28
3	8.19	11.56	1.2008	0.608	0.233	0.624	0.225	77.90	77.99	14.36	0.77	0.28

Sample No. 1

$V_{metal} = (0.05011) \times (0.98781) = 0.049499\ cm^3$

$V_{corrected} = 0.52226 + 0.049499 = 0.571759\ cm^3$

$V_v = V_{corrected} - V_s = 0.571759 - \frac{0.9829/1.13^*}{2.77} = 0.257749\ cm^3$

$e = \frac{V_v}{V_s} = \frac{0.257749}{0.314010} = 0.82033 = 108\%$ of 'Expected e_{AC}'

$n = \frac{V_v}{W_s} = \frac{0.257749}{0.86982} = 0.26932 = 108\%$ = 'Expected AC'

Sample No. 2

$V_{correct} = 0.515130 + 0.049499 = 0.564196\ cm^3$

$V_v = 0.564196 - 0.313354 = 0.250656\ cm^3$

$e = 0.79945 = 104\%$ of 'Expected e_{AC}'

$n = 0.28860 = 104\%$ of 'Expected n_{AC}'

Sample No. 3

$V_{corrected} = 0.666417$

$V_v = 0.267360$

$e = 0.75808 = 97.20\%$ of 'Expected e_{AC}'

$n = 0.27367 = 97.23\%$ of 'Expected n_{AC}'

Experience with the first two samples showed that about 3% (or more) is the loss due to extrusion. Therefore, actually the ratios of void ratio and porosity are almost exactly the desired or expected values.

---

* $V_s = \frac{W_{wet/1 + w/100}}{G_s} = \frac{W_s}{G_s}$

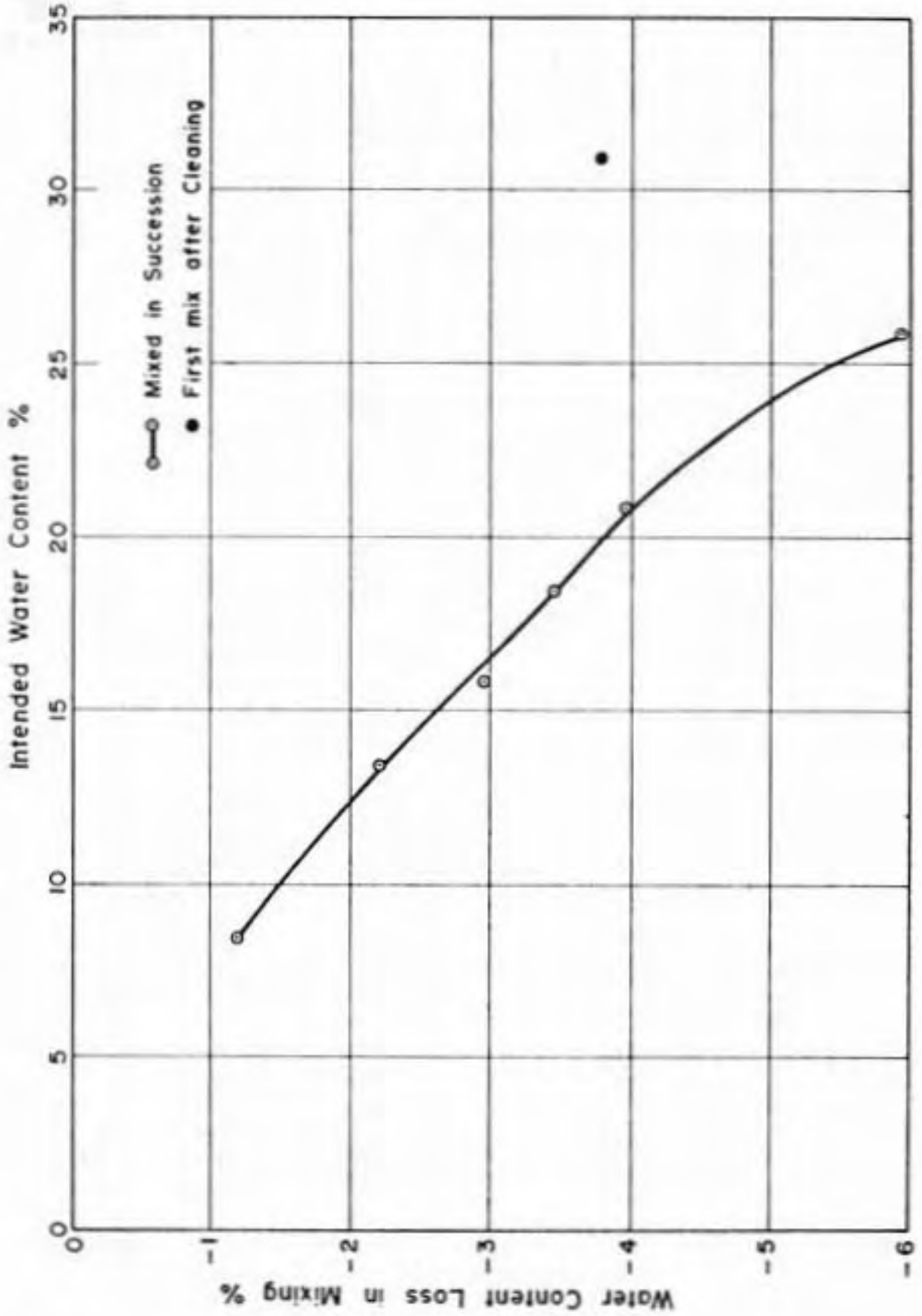

Figure C1 - Loss of Water Content in Liquid Solids Blender

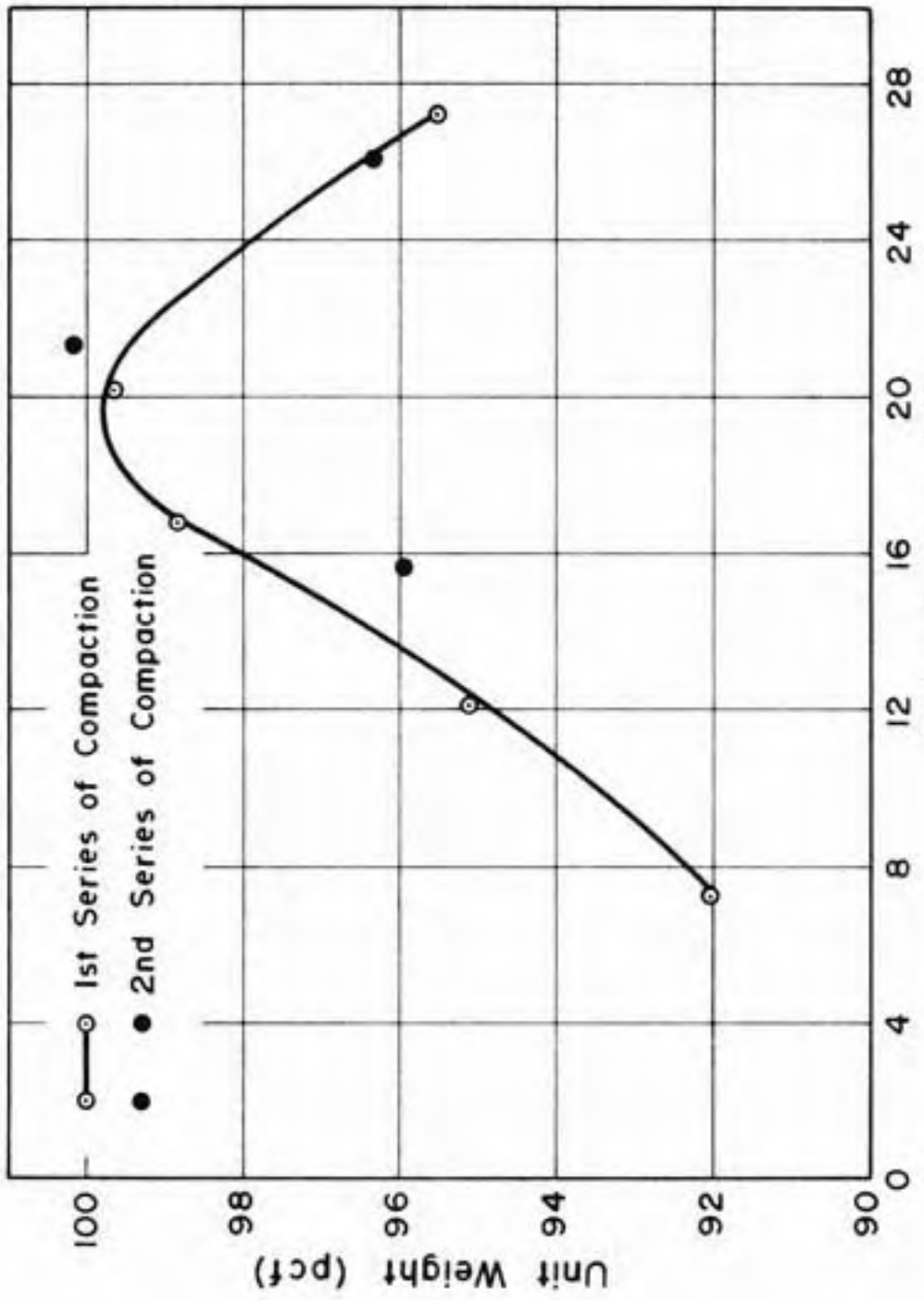

Figure C 2 - Moisture - Unit Weight Relationship of Standard Proctor Compaction

Program for Determining Pore Size Distribution

(Olivetti Underwood Programma 101)

Instructions for Basic Data

AV
S
B† Sample weight
S
C† Sample unit weight
S
D† Penetrometer volume
S
E† Density of mercury
S
b† Weight of sample and penetrometer
S
C† Evacuation pressure
S
d† Filling pressure
S
e† Stem reading at filling pressure
S
f† Wt. of sample + penetrometer + mercury
f+
b-
E:
f
c+
fx
d:
f+
e+
e
B+
C:
C
D+
e-
D
AW
D+
C-
A Void of voids
D
D+
C:
A◊ Void ratio
D+
(continued in the second column)

B-
A◊ Porosity
C+
fx
A◊ P_v x V_v
d:
A◊ Air entrapped at filling pressure
/◊
V

Instructions for Low Pressure Data

AY
S
B↑ Pressure in mm Hg
S
C↑ Stem Reading ml
B↓
bx
A◊ Pressure in PSI
D↓
B÷
C+
f-
E-
C
c↓
B÷
b÷
A◊ Pore Diameter in Microns
C↓
d÷
A◊ Cumulative Voids per Gram
C↓
e÷
A◊ Cumulative Percent Voids
/
Y

Instructions for High Pressure Data

AZ
S
B Absolute Pressure psia
S
C Probe reading 1 x 10^4
S
D Pressure correction on 1 x 10^4
D
C
D
C
c
D-
b-
C
d
B
A◊Pore Diameter Microns
C
E
A◊Cum. Voids per Gram
C
e
A◊Cum. Percent Voids
/
Z

Constants to be stored were:

D $P_v \times V_v$
E Vol. air entrapped
b 0.019337 (for conversion into psi)
C 235.5 (Washburn's Eq. reduces to

$$P = \frac{235.5}{d}$$ by substitution

of appropriate values of σ and θ)
d Sample Weights
e Void Vol. ÷ 100
f Stem Reading at filling pressure

Constants to be stored were:

E Sample Weight
b Transfer correction (obtained by substituting pressure from low pressure data from penetration at 15 psi)
c 10^4
d 235.5
e Void Vol. ÷ 100

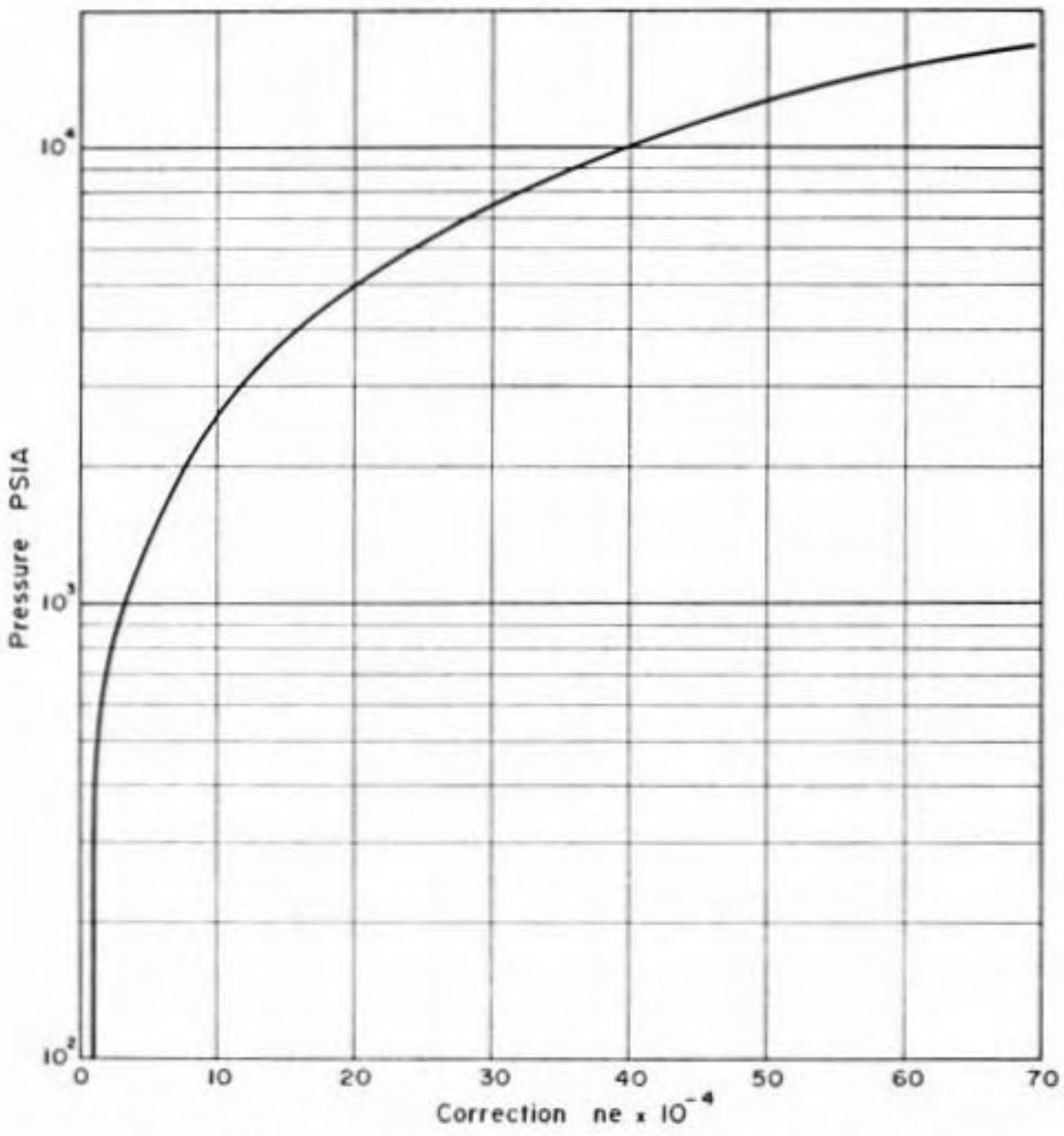

Figure C3 - Correction for Compressibility of Mercury

A Typical Run of Pore Size Distribution Determination

A. Sample No. 472(2) 'E' Type SP, Bottom Layer

Reference P73 Book I

Original Preparation Procedure 0.72658 0.26200 21.37 100.11

Water Removal Method F.D No. 19

B.

1. Sample Weight	0.7184	gm
2. Sample Density (solids only)	2.77	g/cm^3
3. Penetrometer No. C Volume	6.2619	ml
4. Temperature 27°C Density of Mercury	13.5291	g/cm^3
5. Weight of Sample and Penetrometer	47.9161	gm
6. Pressure to which sample evacuated	.0050	mm Hg
7. Pressure at which system filled with mercury	20	mm Hg
8. Stem reading at filling pressure	0000	cm^3
9. Weight of sample and penetrometer and mercury	127.0921	gm

Micrometer Measurements

D	H	V_v	e	n
8.03 mm	8.52 mm			
7.95 mm				
8.03 mm				
8.00	8.52 mm			
Avg. 7.98 mm	8.52 mm	0.16896	0.6514	0.23518 cm^3/gm

C. Compute Basic Data (Program Card Side A)

Program V

Enter B1 on keyboard

Press S

Enter B2 on keyboard

Press S

Press B3 on keyboard

Press S

Press B4 on keyboard

Press S

⋮

Enter B9 on keyboard

Press S

Output

10.	Vol. Voids	0.14882 ml.
11.	Void Ratio	0.57361
12.	Porosity	0.20715 cm /gm
13.	P_e(vac.) x V_e(Vac.)	0.02926
14.	Vol. air trapped at filling pressure	0.00146 ml.

D. LOW PRESSURE DATA (Program Card - Side B)

(a) Store Constants in memory

D PV (C-13) b/ 0.019337

E aur traooed *C-14) c/ 235.5

d/ wt. sample (B-1)

e/ Vol voids - 100 = (C-10) - 100

f/ Stem reading when filled = (b-8)

(b) Program - Y

enter mm Hg.

S

enter stem reading

Output

15. Pressure in PSI
16. Pore Diameter Microns
17. Cumulative Voids/Gram
18. Cumulative % Voids

Pressure mm Hg	Stem Reading ml	Pressure PSI (15)	Pore Dia (16)	Cum Voids /Gram (17)	Cum % Voids (18)
20	.0000	.38674	608.93623	.00000	.00000
60	.0035	1.16022	202.97874	.00350	1.69332
100	.0060	1.93370	121.78724	.00672	3.24553
150	.0140	2.90055	81.19149	.01771	8.55395
200	.0188	3.86740	60.89362	.02433	11.74573
300	.0250	5.80110	40.59574	.03289	15.87824
400	.0275	7.73480	30.44681	.03634	17.54468
500	.0281	9.66850	24.35744	.03950	19.07001
750	.0310	14.50275	16.23829	.04116	19.86964

After computing data for highest pressure press CΦ for cumulative voids penetrated (19) 0.02957 ml

E. High Pressure Data (Program Card Side B)

(a) Compute cumulative void penetration at transfer

Probe reading at 4 psi	0.03350	ml
-(19)	0.02957	ml
Transfer correction	0.00393	ml

(b) Store constants in memory

E - Weight of sample (B-1) d/235.5
b/ transfer correction (ml.) e/ Vol. voids ÷ 100 = (C-10) ÷ 100
c/ 10,000

(c) Program Z

enter absolute pressure - psi
S
enter probe reading - ml x 10^4
S
enter pressure corr. - ml x 10^4

Output
(20) Pore diameter - microns
(21) Cumulative Voids/gram
(22) Cumulative % Voids

Gauge Pressure PSIG	Abs. Pressure PSIA	Probe Rdg. ml x 10^4	Pressure Corr. ml x 10^4	Pore Dia. μ (20)	Cum Voids /gram (21)	Cum % Voids (22)
0	11	334	0.0	21.40909	.04102	19.80244
4	15	335	0.0	15.70000	.04116	19.86964
25	36	370	0.0	6.54166	.04603	22.22147
50	61	398	0.0	3.86065	.04993	24.10294
100	111	424	1.0	2.12162	.05341	25.78282
150	161	441	1.0	1.46273	.05577	26.92514
250	261	466	1.0	.90229	.05925	28.60502
400	411	487	1.2	.57299	.06215	30.00268
600	611	508	1.91	.38543	.06497	31.36675
800	811	525	2.61	.29038	.06724	32.46203
1100	1111	552	3.93	.21197	.07082	34.18895
1500	1511	597	5.55	.15585	.07686	37.10522
2000	2011	673	7.83	.11710	.08712	42.05751
2500	2511	762	9.92	.09378	.09922	47.89678
3000	3011	840	11.93	.07821	.10979	53.00362
3700	3711	912	14.83	.06345	.11941	57.64682
4500	4511	969	18.04	.05220	.12690	61.26192
5500	5511	1022	22.03	.04273	.13372	64.55449
7000	7011	1072	28.14	.03359	.13983	67.50436
8500	8511	1107	34.34	.02767	.14384	69.43959
10,000	10,011	1137	40.04	.02352	.14722	71.07243
12,000	12,011	1176	47.54	.01960	.15161	73.18908
14,150	14,161	1224	55.80	.01662	.15704	75.85673

A Typical Unconfined Compression Test

A: Actual Diameter Measurements

Reference ---------- : #3P73 Book I (SP)
Proving reorg. no. and const.: Const. 0.1282
Dial gauge no. and const.--- : Const. 0.001
Duration of test---------- : 10 mt 27 sec.
Cap size ---------- : 2" dia. oversize

As compacted properties: 0.79321, 0.28603, 96.39, 26.05
Lo ---------- : 2.6250 in.
Do ---------- : 1.3125 in.
Strain rate ---------- : .02"/min. = .00033"/sec.
Failure plane angle--- :
Ao ---------- : 1.353 sq. in.

I Deflection dial	II Deflection = I x Const. "inch"	III Time II ÷ St. rate "sec."	IV Apparent Dia. change "inch"	V Time for IV "sec"
0	0	0	0	0
5	.005	15.15	-.0002	38
10	.010	30.30	-.0002	58
15	.015	45.45	-.0001	78
19	.019	57.58	.0003	118
23	.023	69.70	.0015	158
27	.027	81.82	.0040	198
36	.036	109.09	.0057	218
40	.04	121.21	.0086	258
45	.045	136.36	.0186	338
50	.05	151.52	.0266	398
55	.055	166.67	.0366	458
60	.060	182.82	.0396	478
65	.065	196.97	.0446	518
71	.071	215.15	.0546	578
78	.078	236.36	.0596	618
87	.087	263.64	.0616	628
98	.098	296.96		
104	.104	315.15		
110	.110	333.33		
118	.118	357.58		
128	.128	387.88		
135	.135	409.09		
145	.145	439.39		
154	.154	466.67		
159	.159	481.82		
168	.168	509.09		
175	.175	530.30		
178	.178	539.39		
181	.181	548.48		

(continued on following page)

I Deflection dial	II Deflection = I x Const. "inch"	III Time II ÷ St. Rate "sec."	IV Apparent Dia. Change "inch"	V Time for IV "sec"
183	.183	554.55		
186	.186	563.64		
189	.189	572.73		
192	.192	581.82		
194	.194	587.88		
195	.195	590.91		
196	.196	593.94		
197	.197	596.97		
198	.198	600.00		

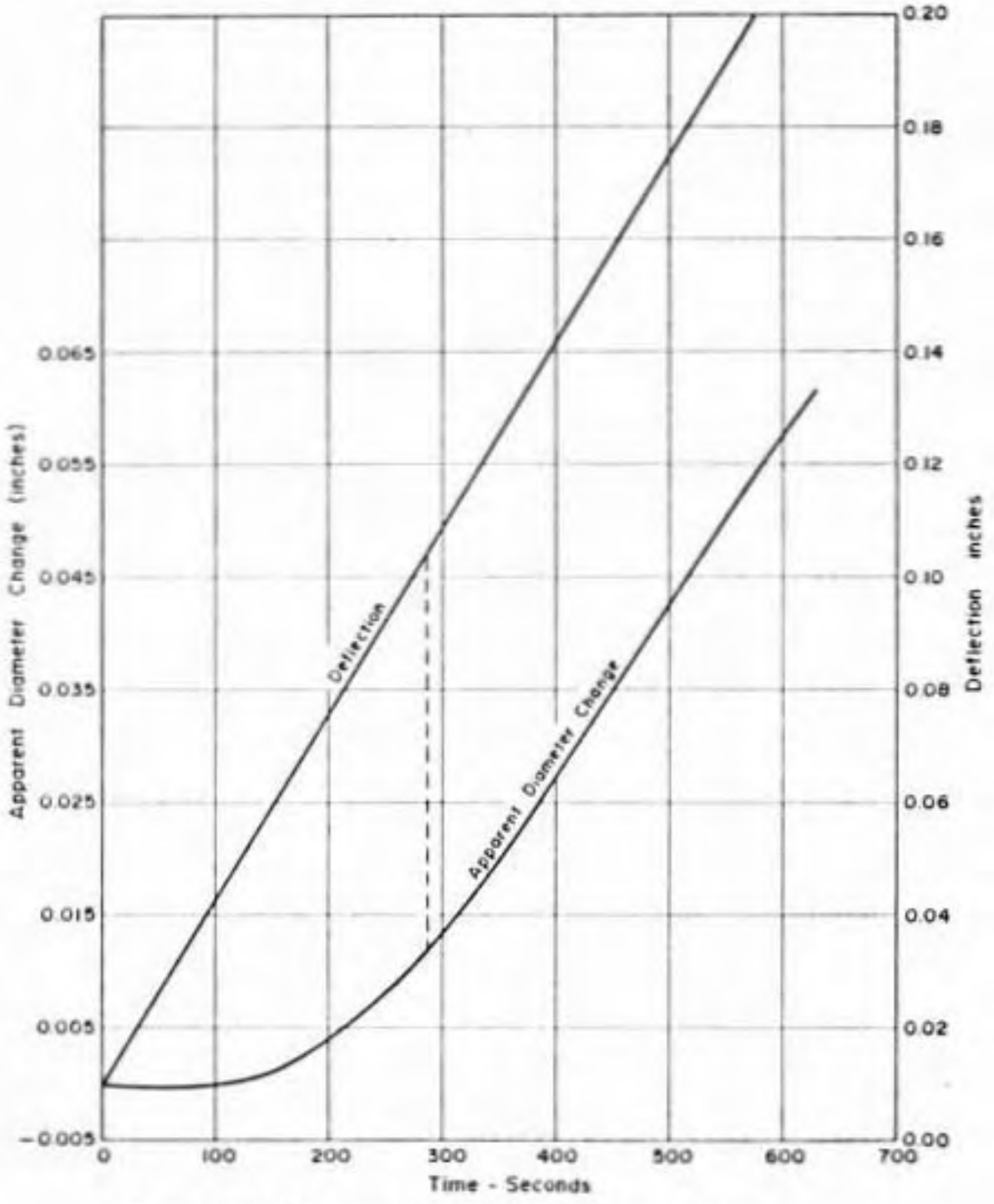

Figure C4 - Calculation of Apparent Diameter Change

VI	VII	VIII	IX	X	XI	XII
Strain =II ÷ Lo "ε"	Actual Dia. change for VI "inch" = XI x 0.4221	Diameter Do ± VII "inch"	Area = 7855 x (VIII)^2 "sq. inch"	Proving ring	Apparent Dia. change "inch"	Stress = "psi"
0	0	1.31250	1.35314	0	0	0
0.190	0	1.31250	1.35314	20	0	1.899
0.381	0	1.31250	1.35314	40	0	3.790
0.571	0	1.31250	1.35314	60	0	5.685
0.724	0	1.31250	1.35314	80	0	7.579
0.876	0	1.31250	1.35314	100	0	9.474
1.029	0	1.31250	1.35314	120	0	11.369
1.371	0	1.31250	1.35314	160	0	15.159
1.524	0.00021	1.31271	1.35357	180	0.0005	17.046
1.714	0.00037	1.31287	1.35390	200	0.0009	18.938
1.905	0.00059	1.31309	1.35435	220	0.0014	20.825
2.095	0.00084	1.31334	1.35487	240	0.0020	22.709
2.286	0.00135	1.31385	1.35593	260	0.0032	24.582
2.476	0.00168	1.31418	1.35660	280	0.0040	26.460
2.705	0.00219	1.31469	1.35765	300	0.0052	28.328
2.971	0.00287	1.31537	1.35906	320	0.0068	30.186
3.314	0.0045	1.31655	1.36150	340	0.0096	32.015
3.628	0.00582	1.31721	1.36362	360	0.0138	33.481
3.962	0.00662	1.31912	1.36682	370	0.0157	34.704
4.190	0.00764	1.32014	1.36893	380	0.0181	35.587
4.495	0.00903	1.32153	1.37182	390	0.0214	36.446
4.876	0.01051	1.32301	1.37489	400	0.0249	37.298
5.143	0.01181	1.32431	1.37760	410	0.0280	38.139
5.524	0.01380	1.32630	1.38174	420	0.0327	38.963
5.867	0.01557	1.32807	1.38543	427	0.0369	39.512
6.057	0.01679	1.32929	1.38798	430	0.0398	39.717
6.400	0.01823	1.33073	1.39099	434	0.0432	39.999
6.667	0.02000	1.33250	1.39469	435	0.0474	39.985
6.781	0.02051	1.33301	1.39576	434	0.0486	39.863
6.895	0.02097	1.3347	1.39672	432	0.0497	39.652
6.971	0.02135	1.33389	1.39752	430	0.0506	39.446
7.086	0.02211	1.33461	1.39911	426	0.0524	39.034
7.200	0.02266	1.33516	1.40027	420	0.0537	38.453
7.314	0.02313	1.33563	1.40125	410	0.0548	37.511
7.390	0.02334	1.33584	1.40169	405	0.0553	37.042
7.428	0.02363	1.33613	1.40230	400	0.0560	36.568
7.467	0.02397	1.33647	1.40302	395	0.0568	36.093
7.505	0.02405	1.33655	1.40318	390	0.0570	35.632
7.543	0.02414	1.33664	1.40337	380	0.0572	34.714

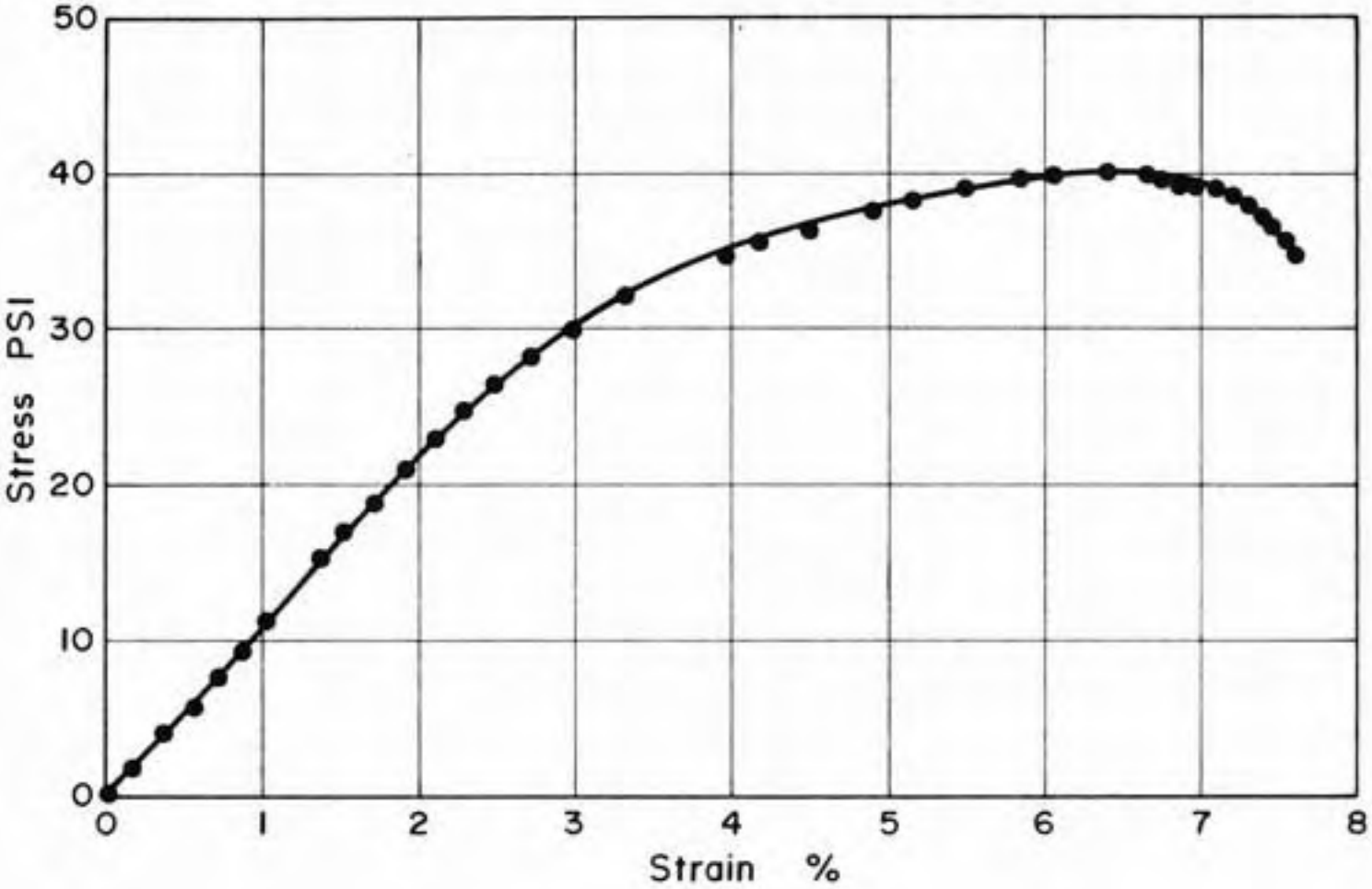

Figure C5 - Stress - Strain Relationship (Actual Diameter Measurement)

B: Constant Volume Assumption

I Deflection dial	II Proving ring	III Deflection "inch"	IV Strain "%"	V Area "sq. inch"	VI Stress "psi"
0	0	0	0	1.353	0
5	20	.005	.190	1.35558	1.891
10	40	.010	.381	1.35817	3.776
15	60	.015	.571	1.36078	5.653
19	80	.019	.724	1.36286	7.525
23	100	.023	.876	1.36496	9.392
27	120	.027	1.029	1.36706	11.253
36	160	.036	1.371	1.37181	14.952
40	180	.040	1.524	1.37394	16.796
45	200	.045	1.714	1.37660	18.626
50	220	.050	1.905	1.37927	20.448
55	240	.055	2.095	1.38195	22.264
60	260	.060	2.286	1.38465	24.072
65	280	.065	2.476	1.38735	25.874
71	300	.071	2.705	1.39061	27.657
78	320	.078	2.971	1.39443	29.420
87	340	.087	3.314	1.39938	31.148
98	360	.098	3.733	1.40547	32.837
104	370	.104	3.962	1.40882	33.669
110	380	.110	4.190	1.41218	34.497
118	390	.118	4.495	1.41668	35.292
128	400	.128	4.876	1.42236	36.053
135	410	.135	5.143	1.42635	36.851
145	420	.145	5.524	1.43211	37.598
154	427	.154	5.867	1.43732	38.086
159	430	.159	6.057	1.44024	38.276
168	434	.168	6.400	1.44551	38.491
175	435	.175	6.667	1.44964	38.470
178	434	.178	6.781	1.45142	38.334
181	432	.181	6.895	1.45320	38.111
183	430	.183	6.971	1.45439	37.903
186	426	.186	7.086	1.45618	37.504
189	420	.189	7.200	1.45797	36.931
192	410	.192	7.314	1.45977	36.007
194	405	.194	7.390	1.46097	35.539
195	400	.195	7.428	1.46157	35.086
196	395	.196	7.467	1.46217	34.633
197	390	.197	7.505	1.46278	34.180
198	380	.198	7.543	1.46338	33.290

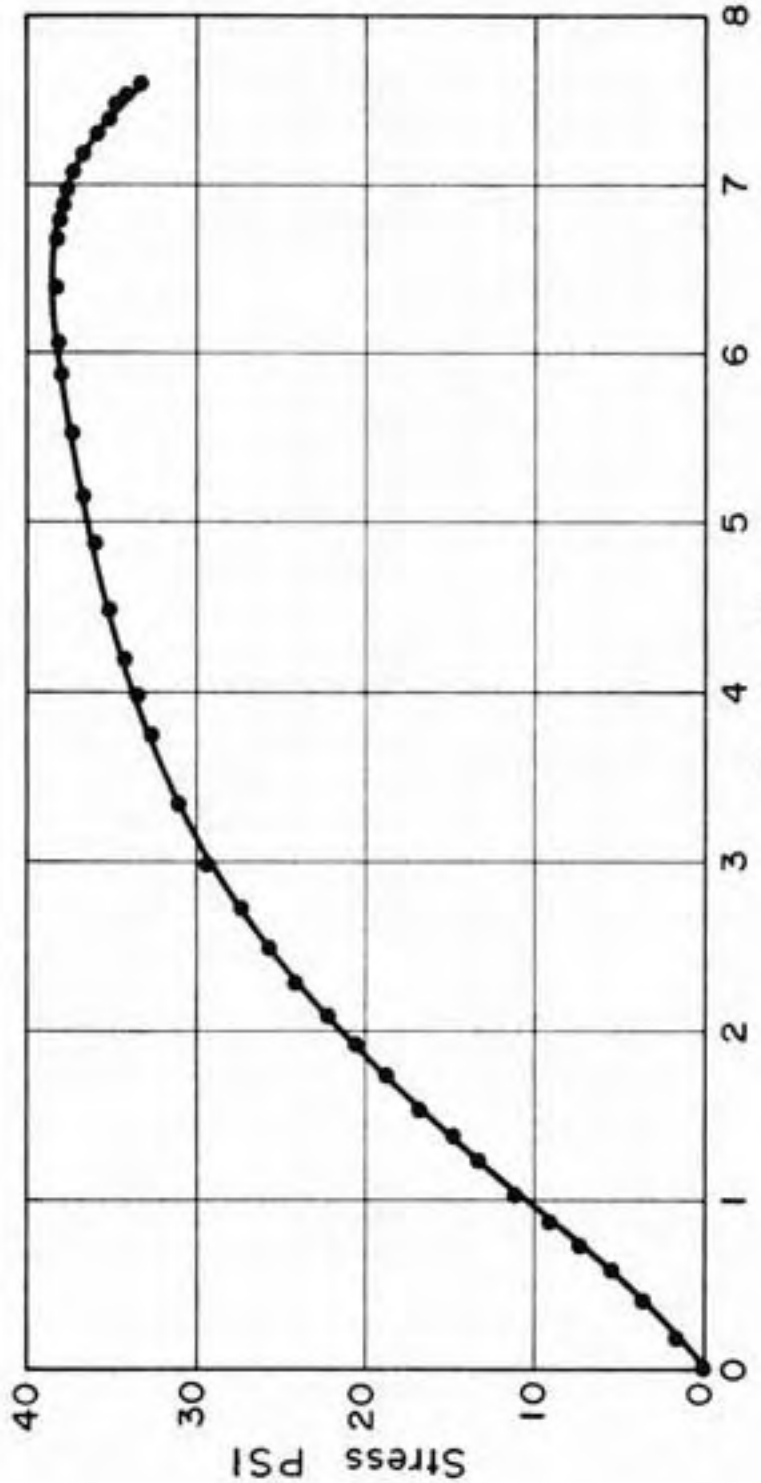

Figure C6 - Stress - Strain Relationship (Constant Volume Assumption)

Volume Change in Unconfined Compression (Typical)

Reference: #3 P73 BOOK I (GP)

As compacted properties: 0.79321 0.28663 96.39 26.05
Lo - - - - - - - - - - - -: 2.6250 in
Do - - - - - - - - - - - -: 1.3125 in
Ao - - - - - - - - - - - -: 1.353142 sq. in
Vo - - - - - - - - - - - -: 3.551992 cc

II	III	IV	I	II	III	IV	V
Poisson's Ratio	Lateral Strain	ΔV cc	Deflection 'inch'	Axial Strain	Diameter 'sq. inch'	ΔV 'c. inch'	ΔV/Vo %
0	0	0	0	0	1.31250	0	0
0	0	-.11096	.005	.190	1.31250	-.00677	-.19000
0	0	-.22175	.010	.381	1.31250	-.01350	-.38000
0	0	-.33271	.015	.571	1.31250	-.02030	-.57100
0	0	-.42138	.019	.724	1.31250	-.02571	-.72300
0	0	-.51005	.023	.876	1.31250	-.03112	-.87500
0	0	-.59889	.027	1.028	1.31250	-.03654	-1.02800
0	0	-.79852	.036	1.371	1.31250	-.04872	-1.37100
.010498	.016000	-.80899	.040	1.524	1.31271	-.05302	-1.49200
.016446	.028190	-.96586	.045	1.714	1.31287	-.05893	-1.65800
.023596	.044952	-1.09781	.050	1.905	1.31309	-.06454	-1.81600
.030548	.064000	-1.14697	.055	2.095	1.31334	-.06998	-1.96900
.044994	.102857	-1.21335	.060	2.286	1.31385	-.07403	-2.08300
.051696	.128000	-1.29644	.065	2.476	1.31418	-.07910	-2.22600
.061684	.166857	-1.38593	.071	2.705	1.31469	-.08456	-2.38000
.073600	.21866	-1.48280	.078	2.971	1.31537	-.09047	-2.54600
.093111	.308571	-1.58179	.087	3.314	1.31655	-.09651	-2.71600
			.098	3.733			
.127304	.504350	-1.74127	.104	3.962	1.31912	-.10624	-2.99000
.138924	.582095	-1.78880	.110	4.190	1.32014	-.10914	-3.07200
.153058	.688000	-1.84944	.118	4.495	1.32153	-.11284	-3.17600
.164224	.800761	-1.94860	.128	4.876	1.32301	-.11889	-3.3460
.174958	.899809	-1.99581	.135	5.143	1.32431	-.12177	-3.4270

Volume Change in Unconfined Compression (Typical), continued

II	III	IV	I	II	III	IV	V
Poisson's Ratio	Lateral Strain	ΔV cc	Deflection 'inch'	Axial Strain	Diameter 'sq. inch'	ΔV 'c. inch'	ΔV/Vo %
.190338	1.051528	-2.05333	.145	5.524	1.32630	-.12528	-3.5260
.202196	1.186285	-2.10775	.154	5.867	1.32807	-.12860	-3.62000
.211199	1.279238	-2.11824	.159	6.057	1.32929	-.12924	-3.63800
.217023	1.388952	-2.20166	.168	6.400	1.33073	-.13433	-3.78100
.228559	1.523809	-2.21265	.175	6.667	1.33250	-.13500	-3.8000
.230447	1.562660	-2.23838	.178	6.781	1.33301	-.13657	-3.8440
.231720	1.597714	-2.16528	.181	6.895	1.3347	-.13211	-3.71900
.233347	1.626666	-2.28230	.183	6.971	1.33385	-.13925	-3.92000
.237732	1.684571	-2.28755	.186	7.086	1.33461	-.13957	-3.9290
.239788	1.726476	-2.31000	.189	7.200	1.33516	-.14094	-3.96700
.240946	1.762285	-2.33967	.192	7.314	1.33563	-.14275	-4.01800
.240633	1.778285	-2.36819	.194	7.390	1.33584	-.14449	-4.06700
.242377	1.800380	-2.36637	.195	7.428	1.33613	-.14441	-4.06500
.244580	1.826285	-2.36114	.196	7.467	1.33647	-.14406	-4.05500
.207607	1.558095	-2.37769	.197	7.505	1.33655	-.14507	-4.08300
.243833	1.839238	-2.39326	.198	7.543	1.33664	-.14602	-4.11000

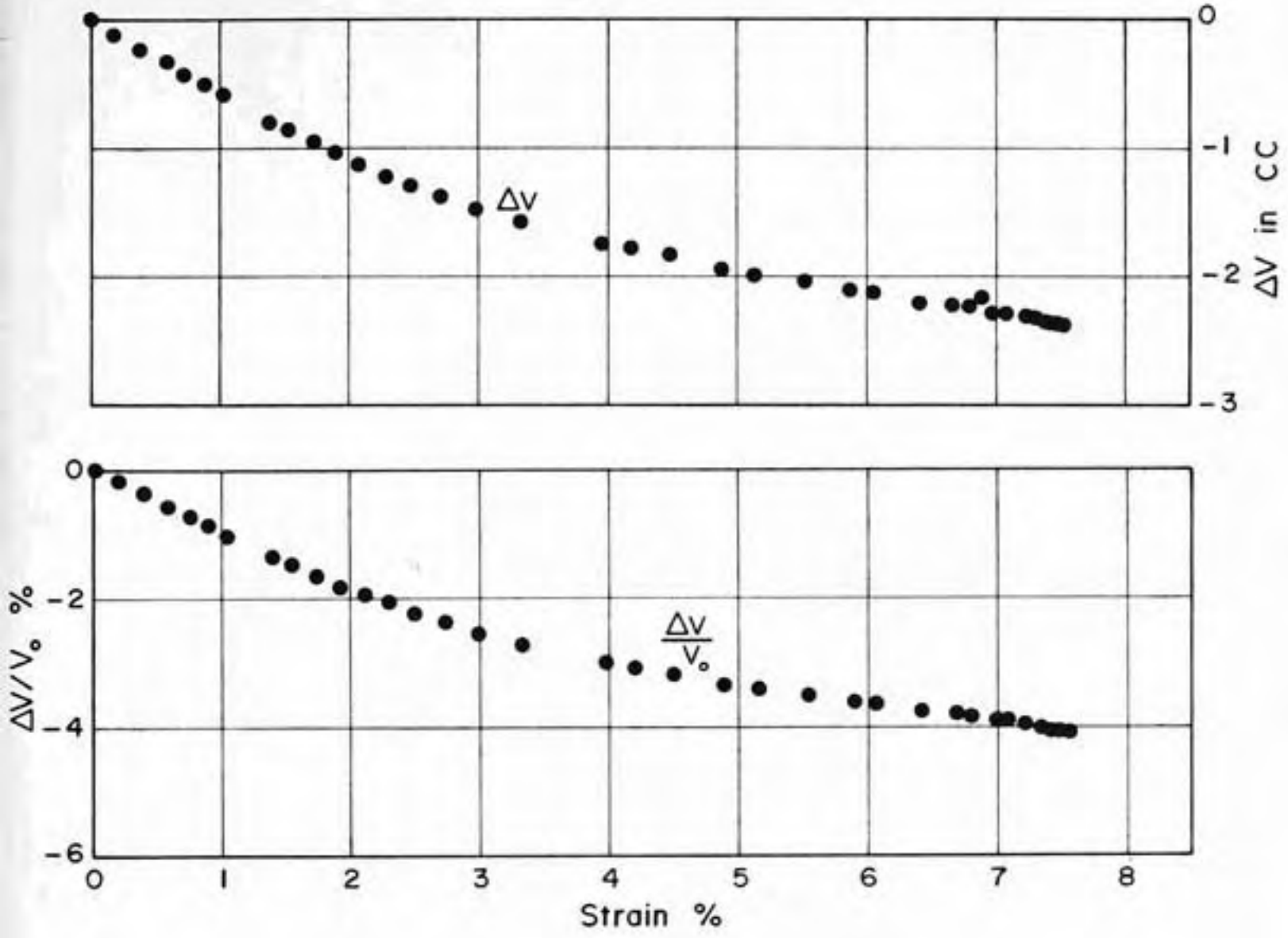

Figure C7 - Volume Change Characteristics